SLAC-R-437
SLAC- 437
SLAC-SSRL 0066
CONF-940250
UC-401, 402, 403, 404
407, 408, 411
(SSRL-M)

WORKSHOP ON SCIENTIFIC APPLICATIONS OF COHERENT X-RAYS

February 12, 1994

ORGANIZATION and PROGRAM

J. Arthur, G. Materlik*, H. Winick
Stanford Linear Accelerator Center
Stanford Synchrotron Radiation Laboratory
Stanford University, Stanford CA 94309

**permanent address*
HASYLAB/DESY
Notkestrasse 85
D-22603 Hamburg, Germany

EXECUTIVE SUMMARY

R.J. Birgeneau**, C.S. Fadley,*** G. Materlik

***Massachusetts Institute of Technology*
Physics, Rm. 13-2114
Cambridge MA 02139

****Lawrence Berkeley Laboratory*
Materials Science Division MS 2-100
Berkeley CA 94720

Prepared for the Department of Energy under contract number DE-AC03-76SF00515

Printed in the United States of America. Available from the National Technical Information Service, U.S. Department of Commerce, 5285 Port Royal Road, Springfield, Virginia 22161

2/80

WORKSHOP ON SCIENTIFIC APPLICATIONS OF COHERENT X-RAYS
Table of Contents

IV. Other Contributions

Appendices

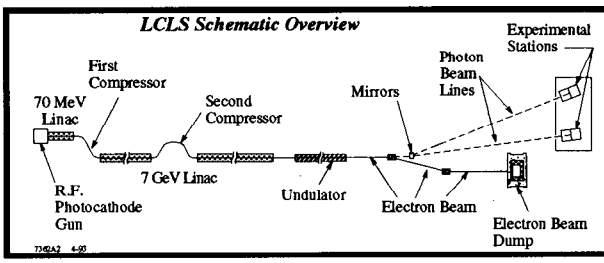

INTRODUCTION

INTRODUCTION

This is a report on a workshop held at SLAC on February 12, 1994 to assess the science that would become possible using high peak power, short pulses of coherent radiation from a Free Electron Laser (FEL) operating in the hard x-ray region, at wavelengths down to about 1 Å. Sixty-three people participated in the workshop. The appendices to this report give a list of participants, the workshop agenda, and the charge to the workshop.

Material describing the performance parameters of several possible sources was made available to the participants along with a graph showing the spectral distribution of the spontaneous as well as the coherent radiation and a note on peak power issues. This material is also included as an appendix to this report.

This report consists of an Executive Summary, brief summaries by the speaker for each of the talks that were given, and copies of some of the viewgraphs that were shown. Also included are important points raised in the discussions that followed each talk. In addition, two contributions from scientists who could not attend the workshop are included, plus one contribution received from a participant after the workshop.

A serious storm on the East coast made it impossible for three speakers and several intended participants to reach Stanford. The talk by Janos Kirz was presented by Malcolm Howells using viewgraphs sent by FAX. The talks by Keith Nelson and Brian Stephenson were not given. We include summaries by them of the talks they would have given, plus copies of some of their viewgraphs, in this report.

BACKGROUND

The initial impetus for this workshop came from technical analysis performed by a group of accelerator scientists from LBL, LLNL, SLAC, and UCLA. Stimulated by presentations and work done at the Workshop on Fourth Generation Light Sources (ref. 1), this group began two years ago to consider the possibility of using the SLAC linac to drive a short wavelength Linac Coherent Light Source (LCLS), based on Self-Amplified-Spontaneous-Emission (SASE). This is a process by which very high coherent power can be achieved in a free-electron laser in a single pass of a high brightness electron beam through a long undulator, without the need for an optical cavity.

Based on the current state of technology of RF photocathode injectors and precision undulators, and also based on the understanding of linac beam dynamics and pulse compression that has been developed as part of the SLAC Linear Collider project, analysis shows that it should be possible using existing technology to construct an FEL device that would operate at wavelengths down to about 30 Å (ref. 2,3). Such a device would use electrons accelerated to about 7 GeV.

With improvements in components, and with the higher energies available at the SLAC linac, the operating wavelength could be reduced towards 1 Angstrom. Recent reports of improved RF photocathode guns give encouragement that an LCLS can indeed be made to operate at SLAC down to such a wavelength. The prospects for short wavelength laser sources was the subject of a workshop on May 21-22, 1993 at Brookhaven National Laboratory, attended by 60 accelerator scientists (ref. 4).

The workshop gratefully acknowledges support from both the Basic Energy Sciences and High Energy Physics Divisions of the Department of Energy and from the National Institutes of Health.

In three areas, the characteristics of the light produced by such a source would exceed by many

orders of magnitude those of any existing or planned source operating in this wavelength range. These areas are peak power and peak brightness, coherence, and shortness of the light pulse. Such a tremendous potential advance in source capability invites a wide-ranging discussion of the possible scientific applications. The workshop described in this report is the second that SLAC has sponsored on the scientific applications of a linac-based free-electron laser. An earlier workshop, held at SLAC on October 21, 1992 (ref. 5), concentrated on scientific applications in the wavelength region 20 - 200 Å.

The timing of this latest workshop was selected so that ideas generated could be used by the National Academy of Sciences Panel on the Scientific Applications of FELs and Other Coherent Light Sources. This panel is now conducting its study and expects to complete a report by summer, 1994.

WORKSHOP ORGANIZERS

John Arthur *(SSRL/SLAC)*, Gerdhard Materlik *(DESY/HASYLAB)* and Herman Winick *(SSRL/SLAC)*.

Michelle Kearney and Carreen Jensen of the SSRL administrative staff are thanked for their organization of the logistical aspects of the workshop. Todd Slater and Lisa Dunn provided assistance in preparation for the workshop and assembling this report. Katherine Cantwell provided invaluable guidance on all aspects of the workshop and is particularly thanked for her efforts to have this report ready for printing two weeks after the workshop.

References:

1. M. Cornacchia and H. Winick (editors), "Report on the Workshop on Fourth Generation Light Sources", SLAC, Feb. 24-27, 1992, *SSRL Report 92/02*.

2. C. Pellegrini, J. Rosenzweig, H.-D. Nuhn, P. Pianetta, R. Tatchyn, H. Winick, K. Bane, P. Morton, T. Raubenheimer, J. Seeman, K. Halbach, K.-J. Kim and J. Kirz, "A 2 to 4 nm High Power FEL on the SLAC Linac," International FEL Conference, Kobe, Japan, August 24-28, 1992, and *Nucl. Instrum .Methods A* **331**, 227 (1993).

3. H. Winick, K. Bane, R. Boyce, G. Loew, P. Morton, H.-D. Nuhn, J. Paterson, P. Pianetta, T. Raubenheimer, J. Seeman, R. Tatchyn, V. Vylet, C. Pellegrini, J. Rosenzweig, G. Travish, D. Prosnitz, E.T. Scharlemann, K. Halbach, K.-J. Kim and M. Xie, "A 2-4 nm Linac Coherent Light Source (LCLS) Using the SLAC Linac", Proceedings of the IEEE 1993 Particle Accelerator Conference, Washington, D.C., May 17-20, 1993, pp. 1445-7. IEEE Catalog Number 93CH3279

4. I. Ben-Zvi and H. Winick (editors), Report on the Workshop "Towards Short Wavelength Free Electron Lasers", Brookhaven National Laboratory, May 21-22, 1993; *BNL Report 49651*.

5. W. Spicer, J. Arthur and H. Winick, "Workshop on Scientific Applications of Short Wavelength Coherent Light Sources", *SLAC Report 414*.

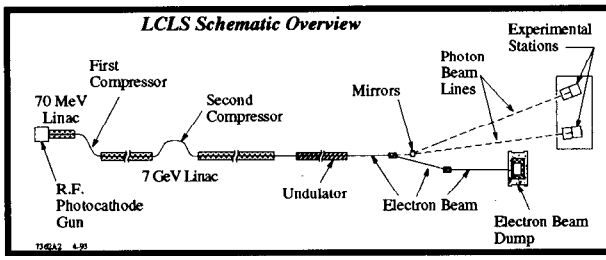

EXECUTIVE SUMMARY

EXECUTIVE SUMMARY

R.J. Birgeneau, C.S. Fadley and G. Materlik

Although a source of coherent x-rays with true x-ray laser properties would have many applications and the search for such a device has occupied many scientists, a practical solution to this problem has not yet been found. To be an efficient research tool, such a source would have to provide stable intensities with short pulses and with repetition frequencies similar to what is found in optical lasers. This workshop dealt with a promising new proposal for creating such coherent x-rays, and the possible applications of such a device. It complements an earlier workshop held at SSRL in October, 1992, and this summary will draw on both of these workshops to present the most complete picture of this x-ray laser and its uses.

As a result of recent advances in electron guns and linear accelerator technology, the means of constructing a true x-ray laser seems now to be within our reach. The proposed Linac Coherent Light Source (LCLS) should provide x-rays at wavelengths down to 1.5 Å in pulses of 150 fs width and with at least a 120 Hz repetition frequency. This source is fundamentally different from an undulator in that the emitted radiation causes oscillatory bunching within each electron bunch, and leads to true stimulated emission and full transverse coherence. The time-averaged spectral brightness of the LCLS would exceed by 10^2 - 10^3 those undulators at the new third-generation synchrotron radiation sources such as APS, ESRF and SPring 8. In fact, the spectral brightness *of each pulse* would exceed the spectral brightness *per second* at the new sources. In addition, the peak brightness within each 150 fs pulse would be greater by more than *10 orders of magnitude* than that in third generation pulses of more than 30-50 ps duration. The proposed source, with a circular focal shape, could be as small as 20 μm in diameter and with an opening angle as little as 5 μrads. At the APS the corresponding values of a third-generation undulator will typically be 150x600 μm^2 with a divergence of 30x50 μrad^2. For the LCLS this means that even at 100 m distance the beam will have opened up to only 0.5 mm. These properties are so significantly different from all other current x-ray sources that the present workshop was organized to discuss the scientific opportunities with such a beam.

The talks and discussions centered mostly on three properties: brightness, coherence, and timing reaching into the fs regime. The use of linear polarization (inherent in the simplest design of an LCLS), circular polarization (possible with a special magnetic structure) and wavelength tunability (possible from harmonics and electron energy variation) were also considered and are clearly additional attractive characteristics of such a source. The high thermal power loads were identified as a technical problem which needs further consideration, although going to shorter wavelengths in the 1-4 Å range would significantly reduce the degree of radiation damage relative to a source at 20-40 Å (in the so-called water window attractive for biological applications) due to the lower absorption coefficients involved. Nonetheless, with time-averaged brightnesses that can be about 100 times those of present undulators, the development of new beam line components and perhaps also special sample configurations (*e.g.*, continuously-replenished solid surfaces, flowing liquids, or free beams of molecules or nanoclusters) would be necessary to fully take advantage of such a source.

The high brilliance per pulse is certainly the most outstanding feature of x-rays from the LCLS. It is the prerequisite for all methods which in addition use other properties such as coherence and time structure, and it permits thinking of doing various scattering and spectroscopic measurements with only a single pulse.

Coherence plays a fundamental role in imaging. However, it was pointed out that it is not desirable in all microscopy methods to increase the degree of coherence. Among the methods which would make the best use of coherence are Fresnel zone plate microscopy and holography. The gain in the latter methods is expected to result from both increased coherence and sharpened timing. The imaging instruments suggested so far are mostly designed for the water window, since great progress has been made in this area over the past ten years in zone plate technology combined with undulator radiation. However, ideas such as angle dispersing diffraction structures seem very well matched to the special characteristics of the LCLS, and the challenge would be to transfer these concepts to the 1-4 Å range.

Measurements of the pump-probe type and making use of the time domain are also excellent examples of longer wavelength techniques that should be exciting to explore at Ångstrom wavelengths. X-ray time correlation spectroscopy based upon the measurement of speckle patterns should make it possible to study the dynamics of atomic scale fluctuations and individual vibrational modes. A great impact on many important problems in statistical physics is anticipated. Specifically, it should be possible to explore the dynamics of condensed matter materials at Å length scales and at time scales between 10^{-3} and 10^{3} seconds. This could have a revolutionary effect on our understanding of the microscopic dynamics of systems as varied as free-standing smectic liquid crystal films, dipolar glasses, lamellar materials absorbed into aerogels and both thin film and disordered magnets. The latter would typically require in addition the exploitation of resonance techniques and/or the use of circularly polarized radiation for excitation. Experiments making use of speckle patterns would greatly benefit from the increased coherence of an LCLS.

It was mentioned that all interferometric methods are also expected to benefit strongly from the gain in coherence. These could be used to generate interference patterns with Å periodicities so as to both create and analyze periodic structures. X-ray interferometry should therefore become a routine method with an LCLS. These patterns might even be used to manipulate structures, and it was suggested that coherent lattice motions could be used to drive specific structural rearrangements. Again by exploiting resonance techniques or circular polarization, standing spin waves or crystal field waves could be established and their time decays measured. Thus, the dynamics of both structural and magnetic order at short distances could be explored. This might be particularly effective in incommensurate systems including, for example, a myriad of intercalated materials; the latter are barely characterized at present primarily due to small sample sizes. Indeed one can comment quite generally that because of the fine focus of the LCLS beam, many materials which can only be prepared in the 0.1 mm size scale would then be readily available for study. It is currently impossible to study the dynamics of 10^{-3} mm^3 crystals using neutron scattering techniques.

Strong emphasis was put on time resolution. The 150 fs pulse will make it possible to study structural changes in small and macro molecules. It is essential for these problems to be able to do x-ray diffraction and follow the electron density changes with time by measuring a diffraction peak or many reflections. The scientific questions related to reactions in chemistry and biology are evident and well formulated. Many new methodologies are proposed and are waiting to be explored further. Their development today is curtailed by the lack of sources with such high peak brightness.

Various spectroscopic aspects of using an LCLS were covered in the earlier workshop emphasizing longer-wavelength applications. Similar spectroscopic advances are possible at shorter wavelengths, but there are also complementary aspects, including being able to study higher energy absorption edges and reducing the degree of beam damage to the specimen (as mentioned previously). Pump-probe experiments with an optical laser and the x-ray laser, or with different harmonics or time-delayed components of the x-ray laser, would open up the ability to follow pump-induced structural changes in the fs regime. For example, following the time development of

individual vibrational modes should be possible. Additional spectroscopic studies of photodesorption and photoelectron emission would be possible in a single-shot or few-shot mode.

Another major advance possible is associated with various types of non-linear x-ray scattering and absorption. So far, even with the new synchrotron radiation sources, only simple feasibility experiments can be carried out. With the LCLS the x-ray study of optically induced charge density modifications should become a routine tool. This will open the door to a real microscopic understanding of light induced polarization of matter. With circular polarization for excitation, spin-dependent charge densities could also be probed. The coupling of two well established scientific fields such as fs laser spectroscopy and x-ray diffraction offers a very special opportunity to broaden our understanding of matter.

Several new ideas for using such an LCLS were also proposed at the workshop. Among these were using the broadband "background" of the LCLS due to spontaneous emission (which is still very bright compared to present x-ray sources) as a short continuum pulse for white beam applications such as Laue crystallography. Also, the satellite peak produced by nonlinear mixing with an optical laser pulse would have a duration in the fs range, and would still be intense enough to serve as a primary x-ray beam with the same time resolution.

We know of only one other proposal that is presently being pursued for producing 1 Å x-rays with fs duration: the Thomson scattering of laser radiation from a relativistic electron beam in the ALS linac discussed in the first workshop. This is clearly a pioneering attempt, but the proposed LCLS would be significantly brighter per pulse and in time averaged brightness, and also would have a much higher degree of coherence.

Finally a comment on the economic aspects of the proposed project is appropriate. The chance to build this source at SLAC seems to be unique worldwide. A section of the operational linac and existing buildings can be used. This would probably reduce the capital investment by about 80% of the total cost as compared to building such a source from scratch. Machine experts have pointed out that additional R&D efforts would be needed to get from the original 40 Å project study (feasible with present electron gun and linac technology) to a 1.5 Å LCLS; however, no insurmountable problems are foreseen with this.

This workshop and its predecessor have thus shown that a wide variety of new and exciting experimental possibilities in physics, chemistry, materials science, and biology would be opened up by an LCLS. Such an x-ray laser should in fact lead to the same sort of revolutionary developments in x-ray studies of matter that was produced in optical studies by the introduction of the visible/UV laser.

Properties of Short Wavelength FELs Using the SLAC Linac

Claudio Pellegrini, UCLA and Herman Winick, SSRL/SLAC

AN FEL ON THE SLAC LINAC

or

A LINAC COHERENT LIGHT SOURCE (LCLS)

Presentation at the Workshop on Scientific Applications of Coherent X-rays

February 12, 1994

Claudio Pellegrini (UCLA)
Herman Winick (SLAC)

SLAC LCLS

A MULTI-INSTITUTIONAL STUDY

SLAC: **J. Arthur, K. Bane, J. Cobb, G. Loew, G. Materlik, P. Morton, H.-D. Nuhn, E. Paterson, P. Pianetta, T. Raubenheimer, J. Seeman, W. Spicer, R. Tatchyn, V. Vylet, H. Winick**

UCLA: **C. Pellegrini, J. Rosenzweig, G. Travish**

LBL: **K. Halbach, K.-J. Kim, M. Xie**

LLNL: **D. Prosnitz, T. Scharlemann**

Univ. of Milano: **R. Bonifacio, L. De Salvo, P. Pierini**

SLAC LCLS

WHAT IS IT?

- **A short wavelength FEL; single pass**
- **Self- Amplified-Spontaneous-Emission (SASE) or Harmonic Generation**
- **A 4th Generation light source**
- **Orders of magnitude higher brightness, peak power, and coherence than any other source.**
- **> 3 nm wavelength in the near future**
- **Shorter wavelength later (~1Å?)**

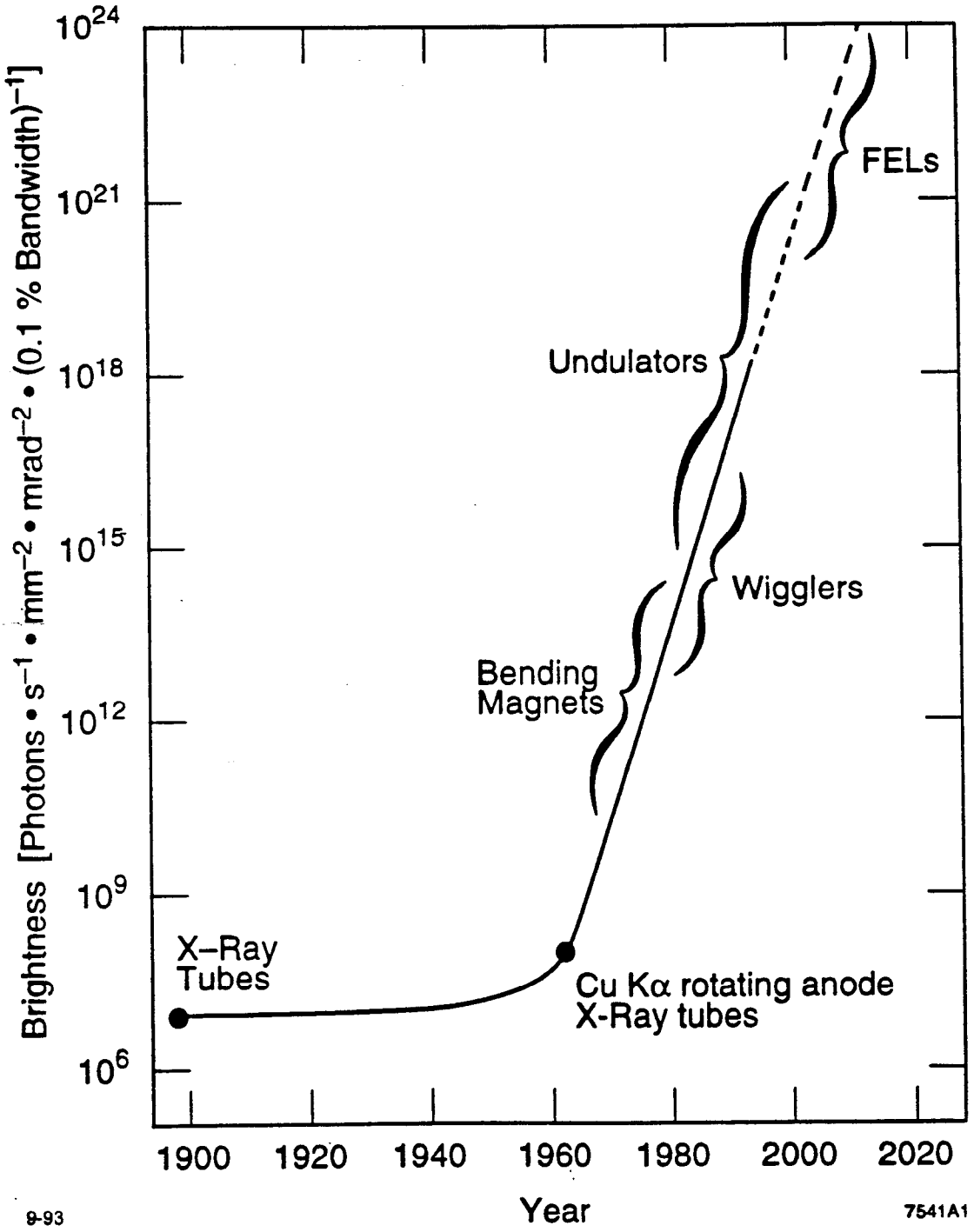
Brightness [Photons • s^{-1} • mm^{-2} • mrad^{-2} • (0.1 % Bandwidth)$^{-1}$]
10^{24}
10^{21}
10^{18}
10^{15}
10^{12}
10^{9}
10^{6}
FELs
Undulators
Wigglers
Bending Magnets
X–Ray Tubes
Cu Kα rotating anode X-Ray tubes
1900
1920
1940
1960
1980
2000
2020
Year
9-93
7541A1

PARAMETERS FOR VARIOUS LCLS CASES

Wavelength (Angstroms)	**40**	**40**	**4.5**	**1.5**
Norm. emittance (mm-mrad)	**3.5**	**1**	**1**	**1**
Peak current (kA)	**2.5**	**5**	**5**	**5**
E (GeV)	**7**	**5**	**15**	**25**
sigmaE/E (%)	**0.02**	**0.02**	**0.02**	**0.02**
Pulse duration (fs,rms)	**130**	**65**	**65**	**65**
Repetition rate (Hz)	**120**	**120**	**120**	**120**
Undulator period (cm)	**8.3**	**4**	**4**	**4**
Peak field (T)	**0.76**	**1.6**	**1.6**	**1.6**
Gain length (m)	**5.8**	**1.5**	**4**	**7**
Saturation length (m)	**60**	**15**	**40**	**70**
Peak power (GW)	**10**	**40**	**100**	**40**
Average power (W)	**0.4**	**0.6**	**1.4**	**0.6**
Energy/pulse (mJ)	**3**	**5**	**12**	**5**
Coherent Ph/pulse (10^{13})	**6.6**	**13**	**3.3**	**0.5**
Bandwidth (%)	**0.1**	**0.1**	**0.1**	**0.1**
Peak Brightness (10^{31})*	**5**	**20**	**500**	**540**
Average Brightness (10^{21})*	**2**	**4**	**100**	**100**
Trans. Size (microns,rms)**	**35**	**20**	**12**	**9**
Trans. Diverg. (urad,rms)**	**10**	**6**	**4**	**2**

* ph/(s,mm^2,mrad^2,0.1% BW) **at exit of undulator 1/25/94

See Appendix D for comments on these examples

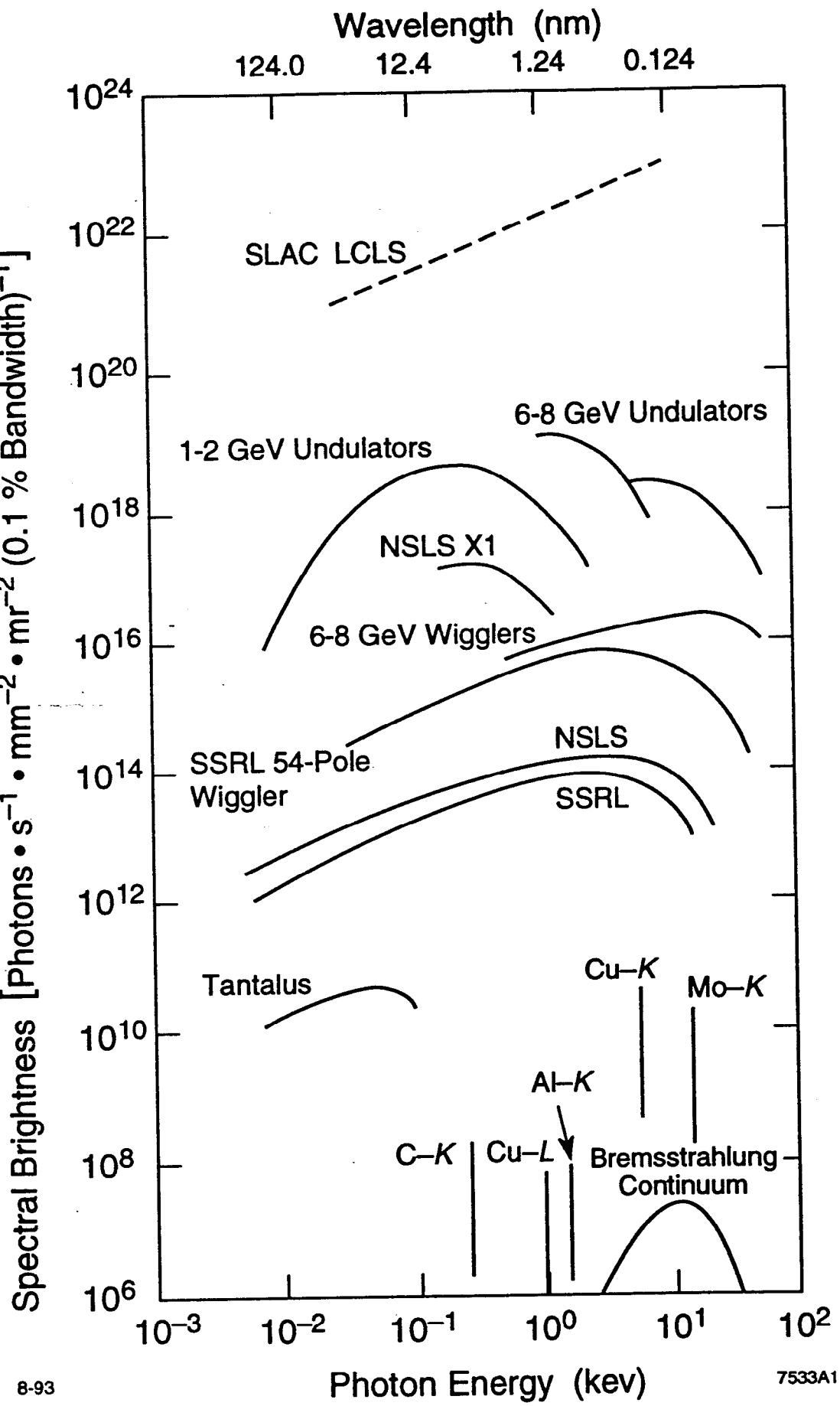
Wavelength (nm)
124.0
12.4
1.24
0.124
10^{24}
10^{22}
10^{20}
10^{18}
10^{16}
10^{14}
10^{12}
10^{10}
10^{8}
10^{6}
Spectral Brightness [Photons • s^{-1} • mm^{-2} • mr^{-2} (0.1 % Bandwidth)$^{-1}$]
SLAC LCLS
6-8 GeV Undulators
1-2 GeV Undulators
NSLS X1
6-8 GeV Wigglers
NSLS
SSRL 54-Pole Wiggler
SSRL
Tantalus
Cu–K
Mo–K
Al–K
C–K
Cu–L
Bremsstrahlung Continuum
10^{-3}
10^{-2}
10^{-1}
10^{0}
10^{1}
10^{2}
Photon Energy (kev)
8-93
7533A1

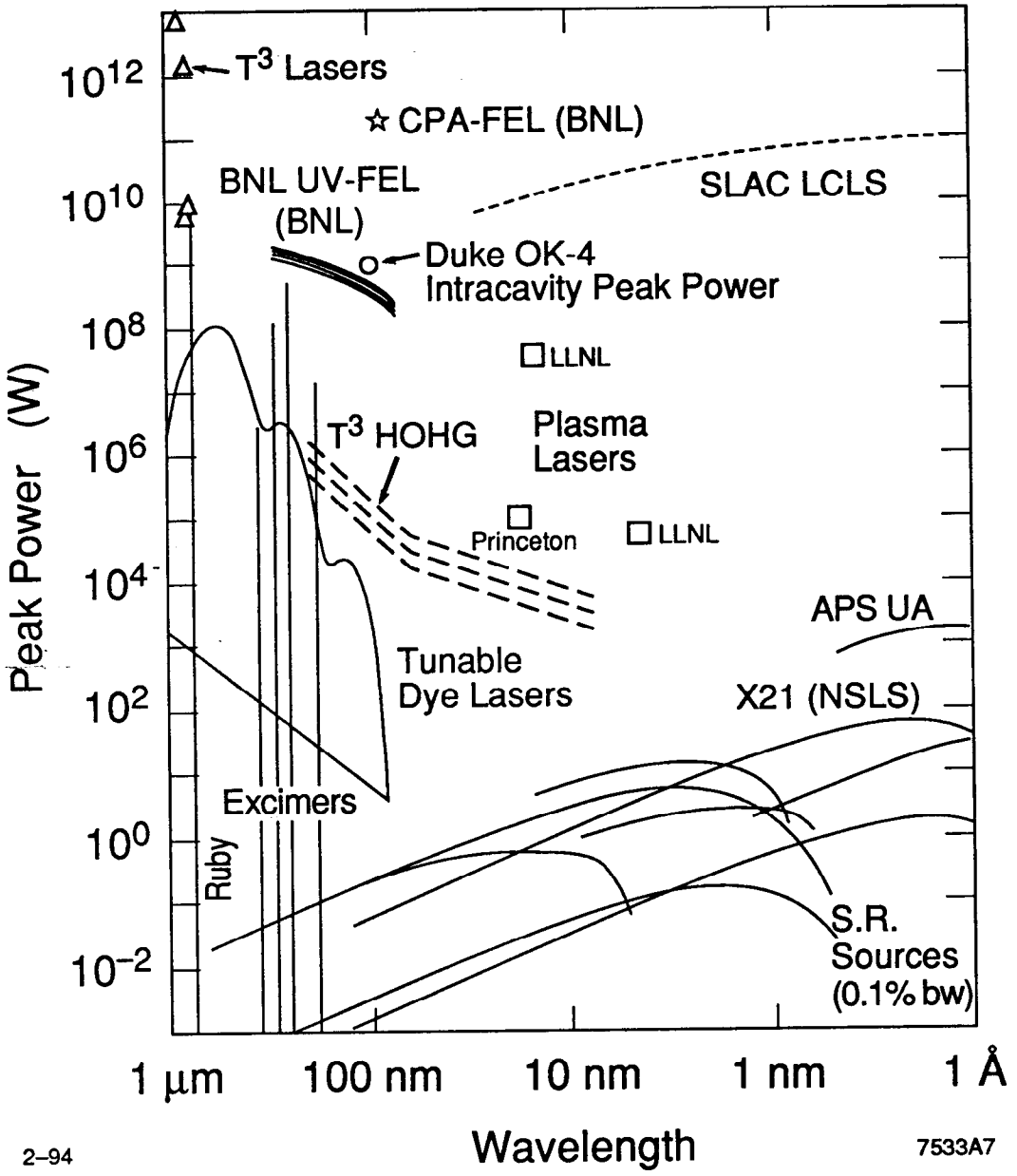
10^{12}
10^{10}
10^{8}
10^{6}
10^{4}
10^{2}
10^{0}
10^{-2}
Peak Power (W)
T3 Lasers
CPA-FEL (BNL)
BNL UV-FEL (BNL)
SLAC LCLS
Duke OK-4 Intracavity Peak Power
LLNL
T3 HOHG
Plasma Lasers
Princeton
LLNL
APS UA
Tunable Dye Lasers
X21 (NSLS)
Excimers
Ruby
S.R. Sources (0.1% bw)
1 μm
100 nm
10 nm
1 nm
1 Å
Wavelength
2-94
7533A7

RECENT DEVELOPMENTS OPEN NEW OPPORTUNITIES FOR LINAC-BASED SHORT WAVELENGTH FELs

1. *RF PHOTOCATHODE ELECTRON GUNS*

   Provide the High Brightness, Low Emittance e^- beams Necessary for Short Wavelength FELs

2. *THE SLC PROJECT & LINEAR COLLIDER R&D*

   Provide the Tools & Understanding to Transport, Accelerate, & Compress e^- bunches without diluting phase space density

3. *PRECISION UNDULATORS*

   As developed at third generation and other light sources

ELECTRON BEAM REQUIREMENTS FOR SHORT WAVELENGTH FELs

1. Diffraction Limited Electron Beam Emittance (ε = Wavelength/4π)

For a 4.0 nm FEL; $\varepsilon = 3.2 \times 10^{-10}$ m-rad
For a 0.4 nm FEL; $\varepsilon = 3.2 \times 10^{-11}$ m-rad

In a linac, $\varepsilon \sim \gamma^{-1} = mc^2/E$
Define normalized emittance: $\varepsilon = \varepsilon_n/\gamma$

RF guns now have $\varepsilon_n = 3 \times 10^{-6}$ m-rad
at 5 GeV; $\gamma = 10{,}000$
$\varepsilon = \varepsilon_n/\gamma = 3\text{x}10^{-6}/10^4 = 3\text{x}10^{-10}$ m-rad

Expect RF guns with $\varepsilon_n = 1 \times 10^{-6}$ soon
at 25 GeV; $\gamma = 50{,}000$ $\varepsilon = 2 \times 10^{-11}$ m-rad

2. High Peak Current (Kilo amperes)
achieved by compression to very short bunch length (<0.2 ps)
(e.g.; 1 nanocoul/ps = 1,000 Amperes)

3. Small Energy Spread (~0.05%)

$$\text{Coherent Fraction} = F_c = \frac{\lambda^2}{(4\pi)^2 \sigma_{Tx} \sigma_{Ty} \sigma_{Tx'} \sigma_{Ty'}}$$

$$\sigma_{Tx} = \left[\sigma_r^2 + \sigma_x^2\right]^{1/2}$$

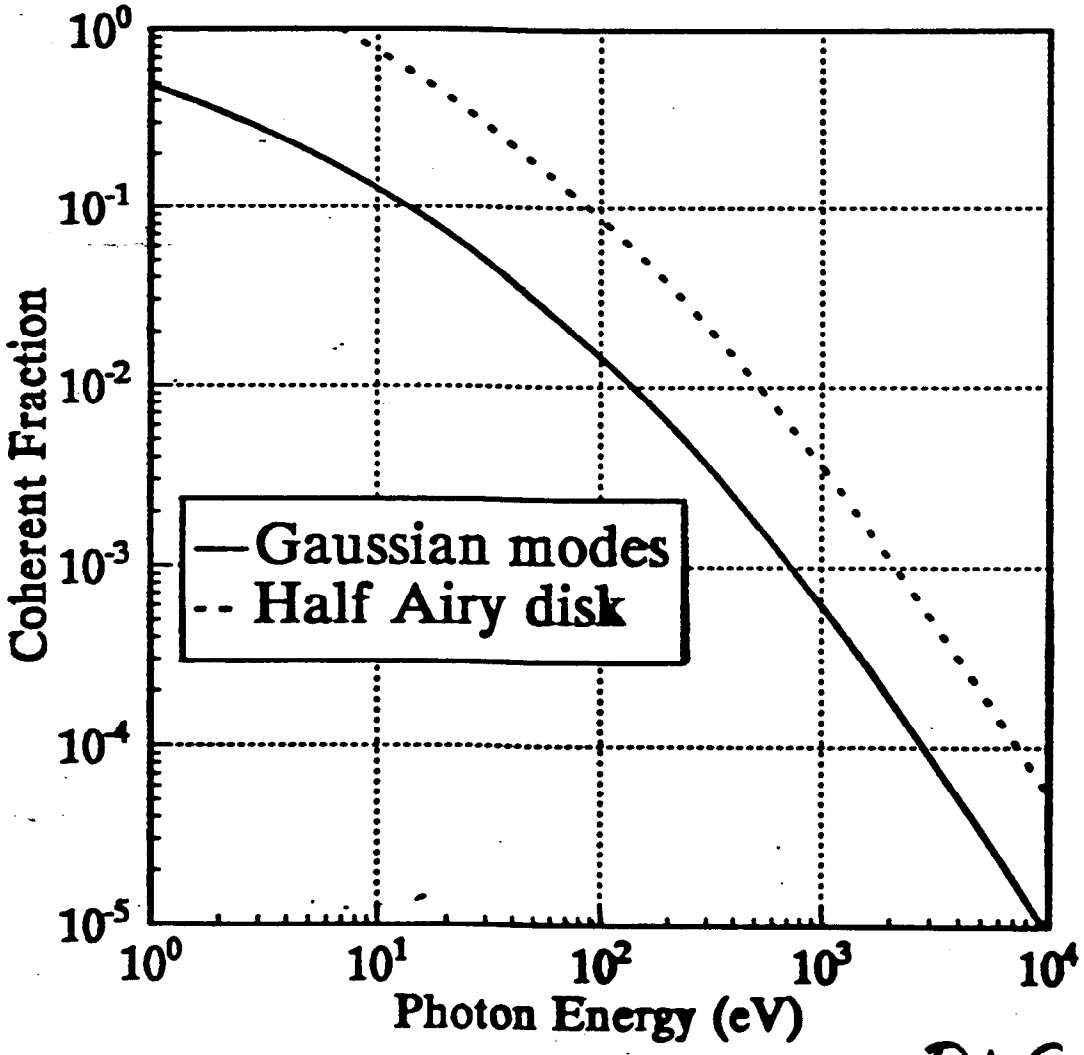

ALS
Brian Kincaid

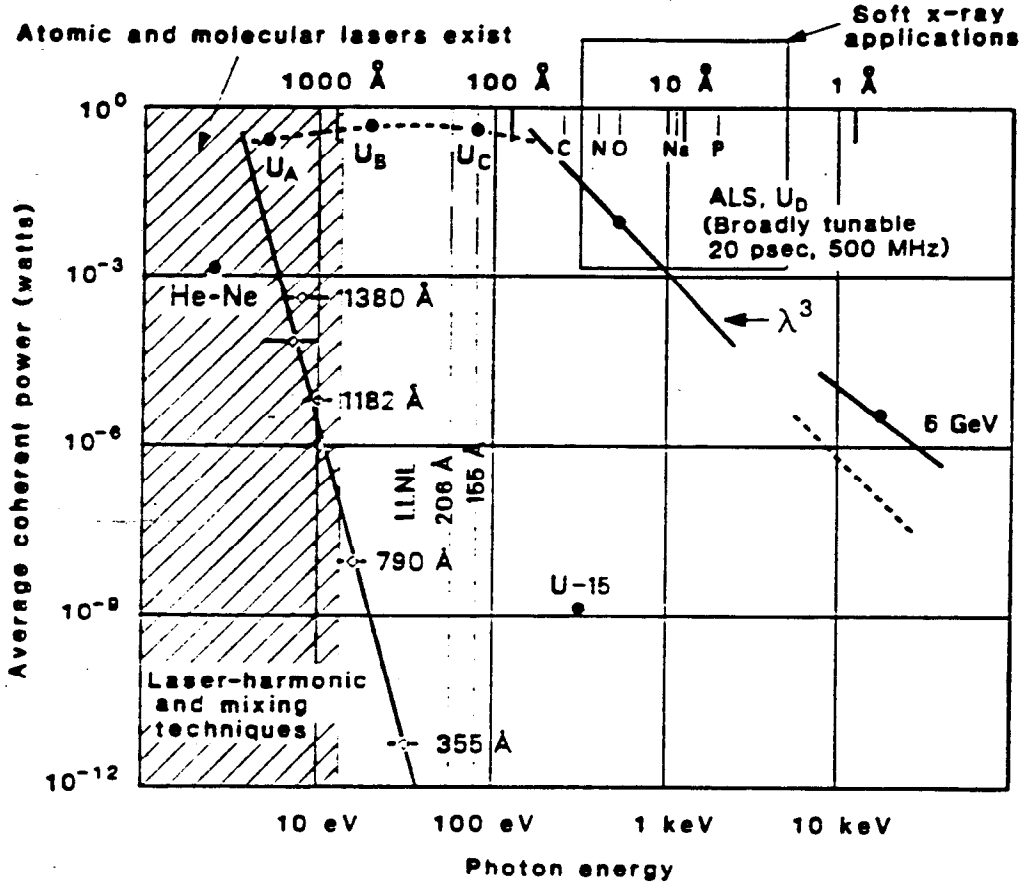

Fig. 4. Broadly tunable coherent power is achievable, in the soft x-ray region, with long magnetic undulators in a specially designed low-emittance storage ring. Undulators U_A, U_B, and U_C provide continuous coverage throughout the vacuum ultraviolet region. Undulator U_D of the ALS would provide continuous coverage through the soft x-ray region. U-15 denotes a bending magnet source at NSLS. The shaded area to the left shows the domain of atomic and molecular lasers, which is constrained primarily to wavelengths of about 1000 Å and longer. Recent laser results at 206 Å and 155 Å driven by the Novette laser at LLNL are indicated. The range of radiation produced by laser-harmonic and mixing techniques is also shown. In the soft x-ray spectral region, which includes the important K-absorption edges of carbon, nitrogen, and oxygen, only undulators could provide significant coherent power in the near term. Coherent power is defined here as radiation having full spatial coherence and a longitudinal coherence length of 1 μm.

D. Attwood, K. Halbach, K.-J. Kim
Science 228 (1985) 1265-72

SLAC LCLS

WHO MIGHT USE IT?

R&D in FELs and accelerator physics

Potential applications include biological imaging, chemical dynamics, electronic and structural properties of materials

Synchrotron radiation community of Users

Workshops on scientific applications

The National Academy of Sciences is conducting a study of the scientific uses of FELs.

SLAC LCLS

WHY AT SLAC?

1. **Multi-GeV linac and FFTB enclosure**
   > $100M savings

2. **Expertise in accelerator and light source technologies**

3. **Compatible with PEP-II B-factory**

4. **LCLS and NLC accelerator physics**

- **Emittance growth during acceleration**
- **Emittance growth during transport**
- **Energy spread control**
- **Multiple bunches**
- **Bunch compression at high energy**

5. **Pump/probe studies; LCLS & SPEAR**

LCLS Schematic Overview

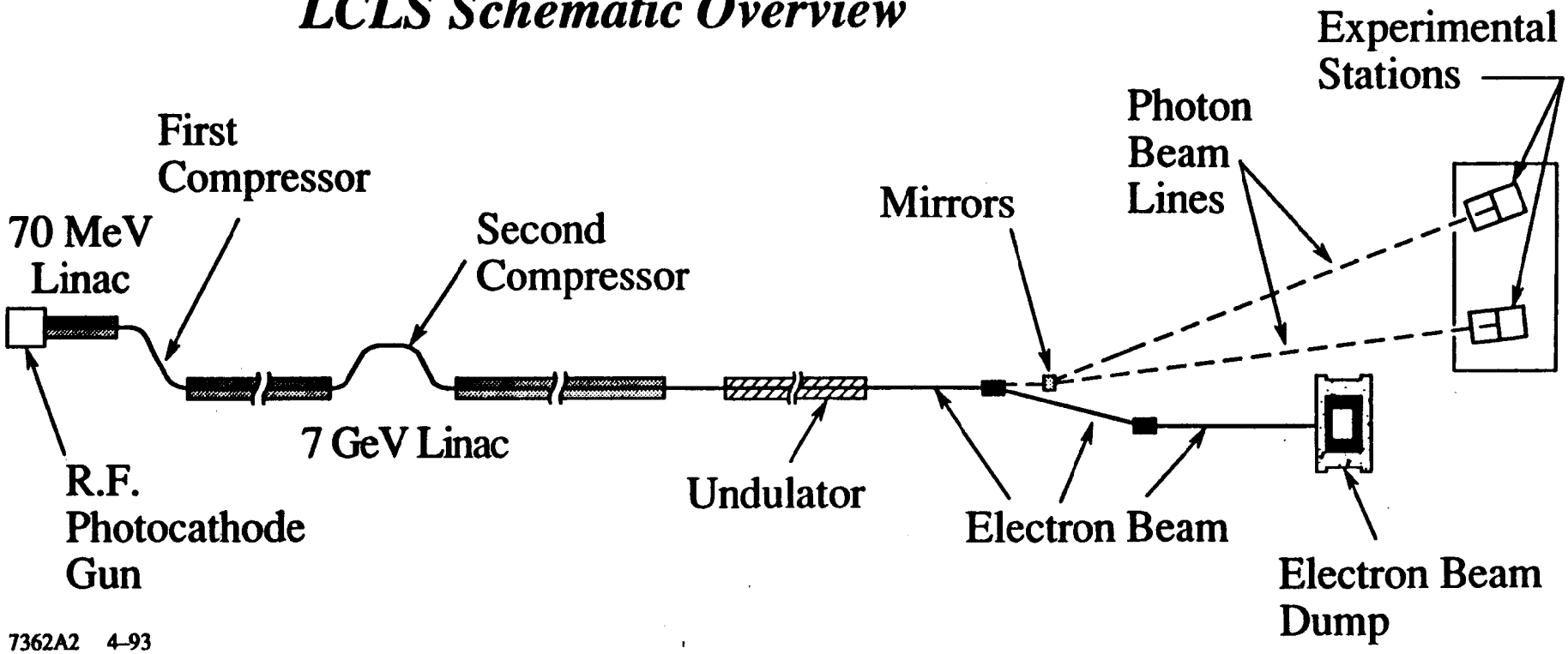

7362A2 4-93

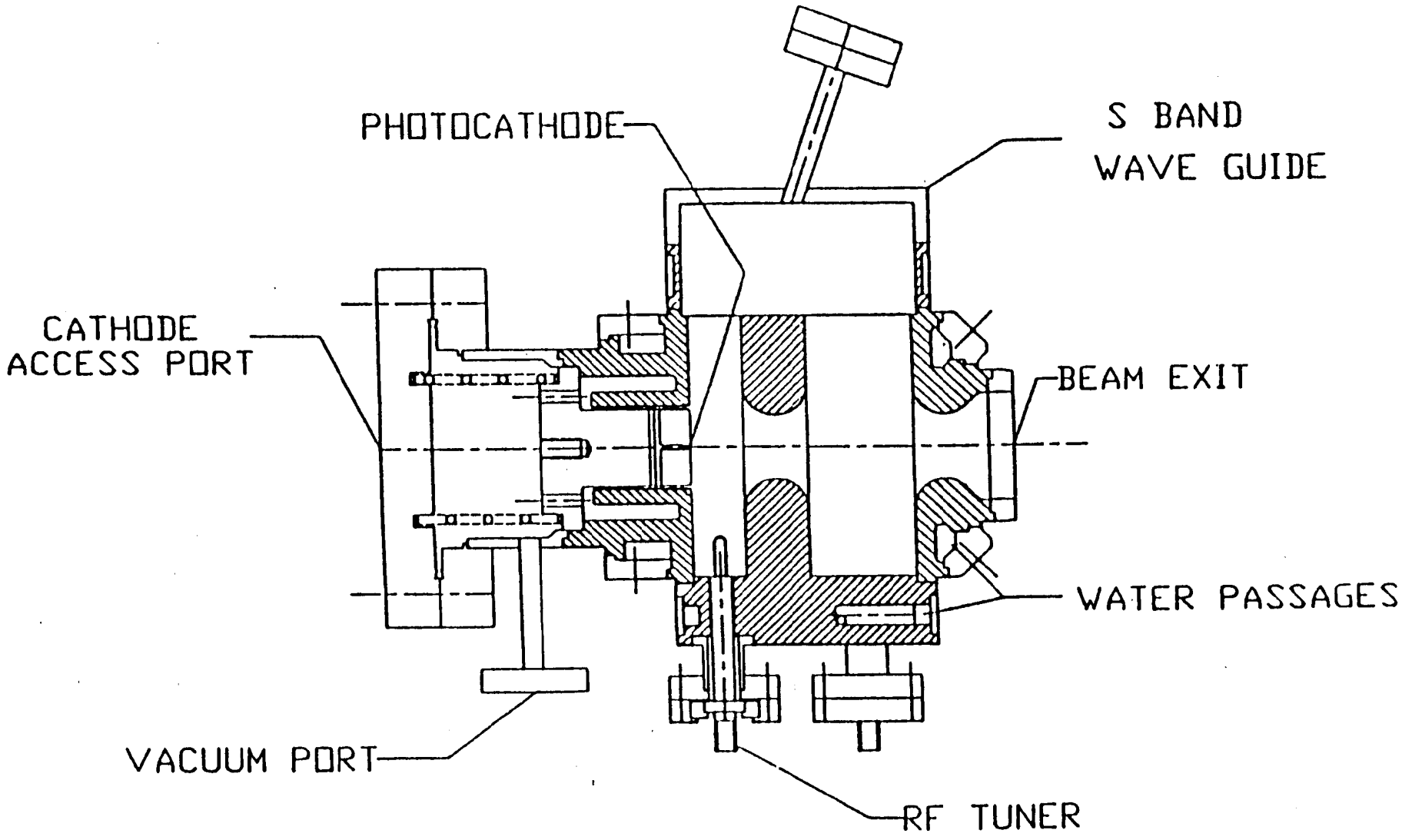

Fig. 6. BNL rf gun cavity (from ref. [21]).

LCLS Undulator (1.6 meter Module)

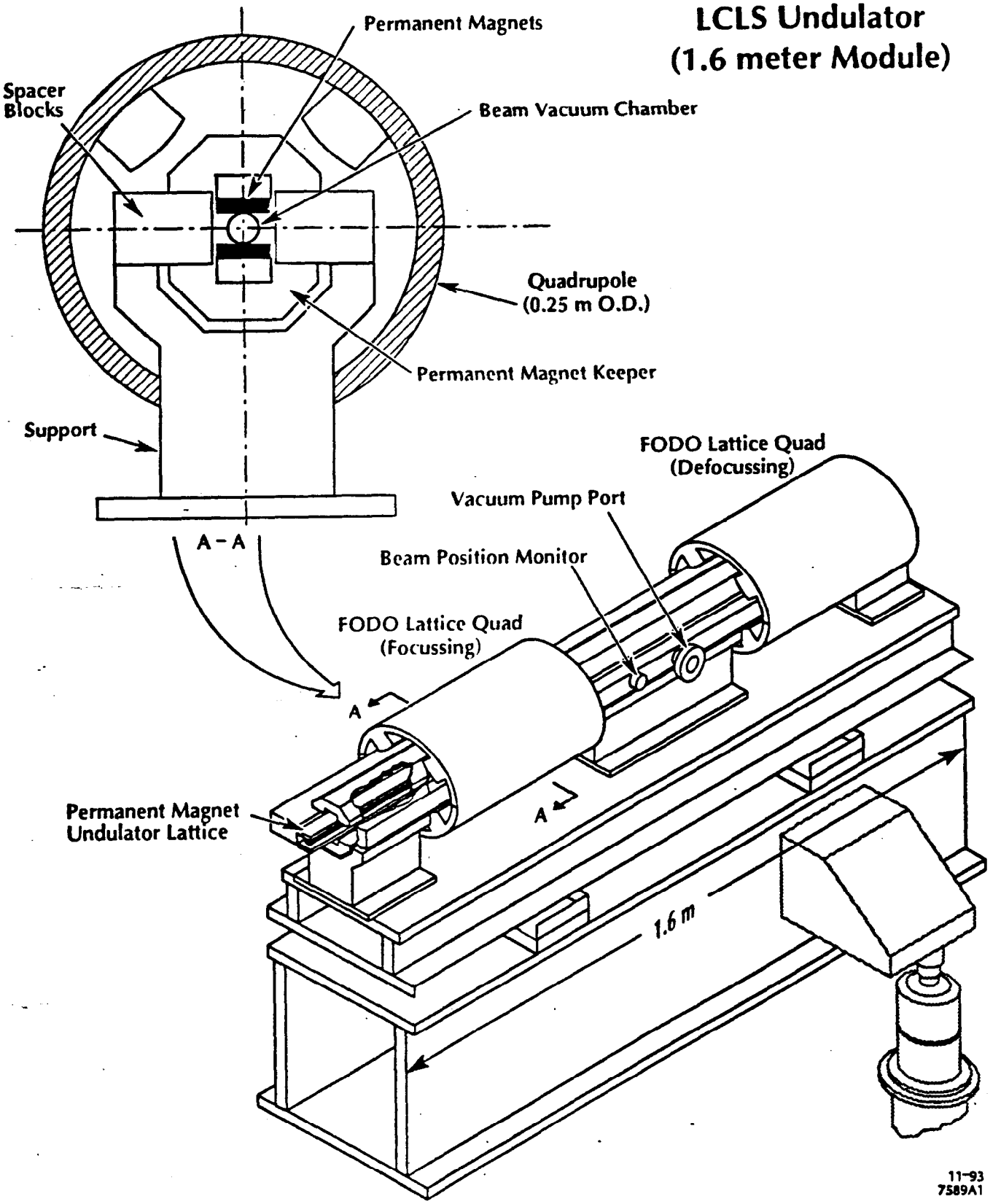

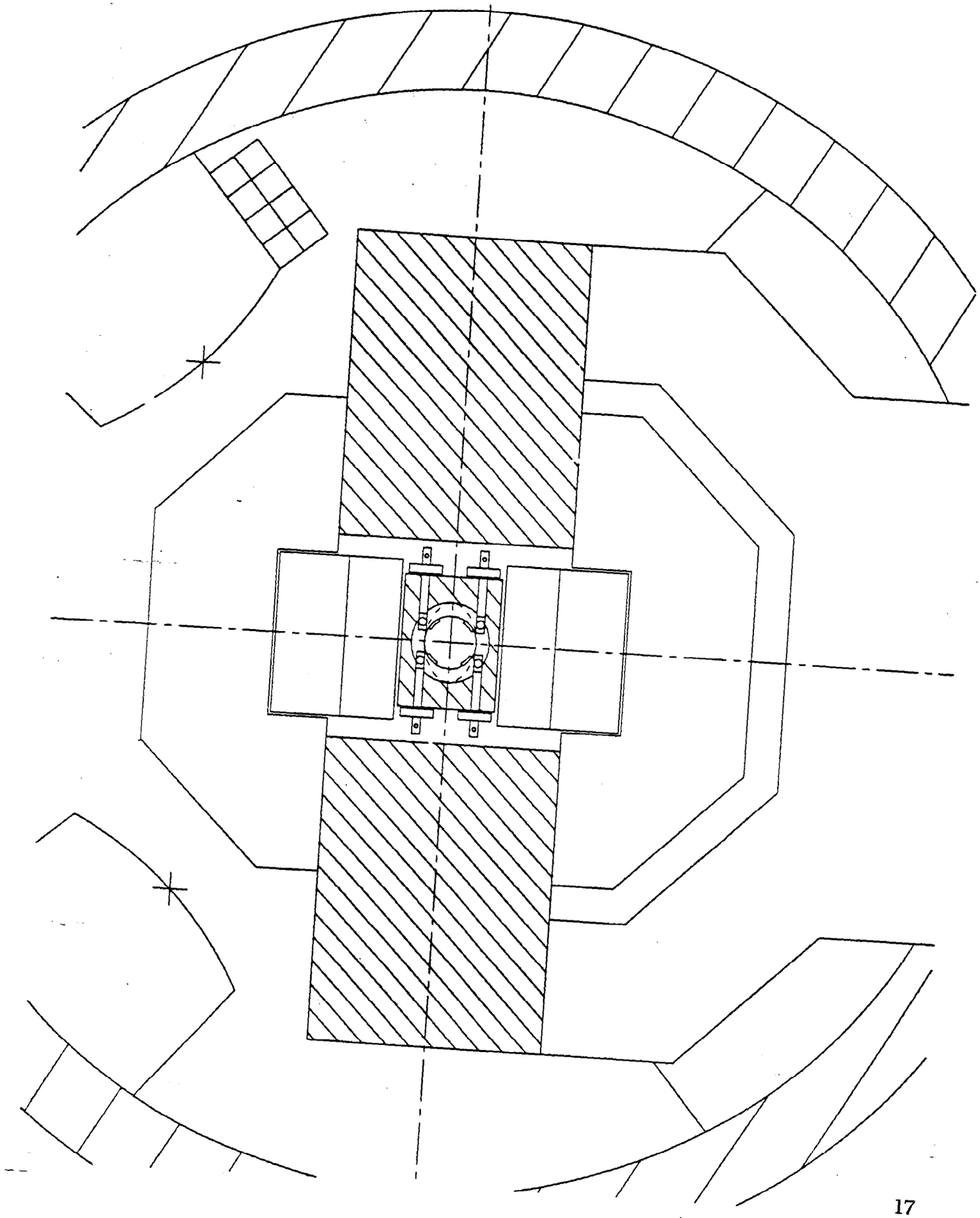

LCLS BEAM LINES MIRROR STATION

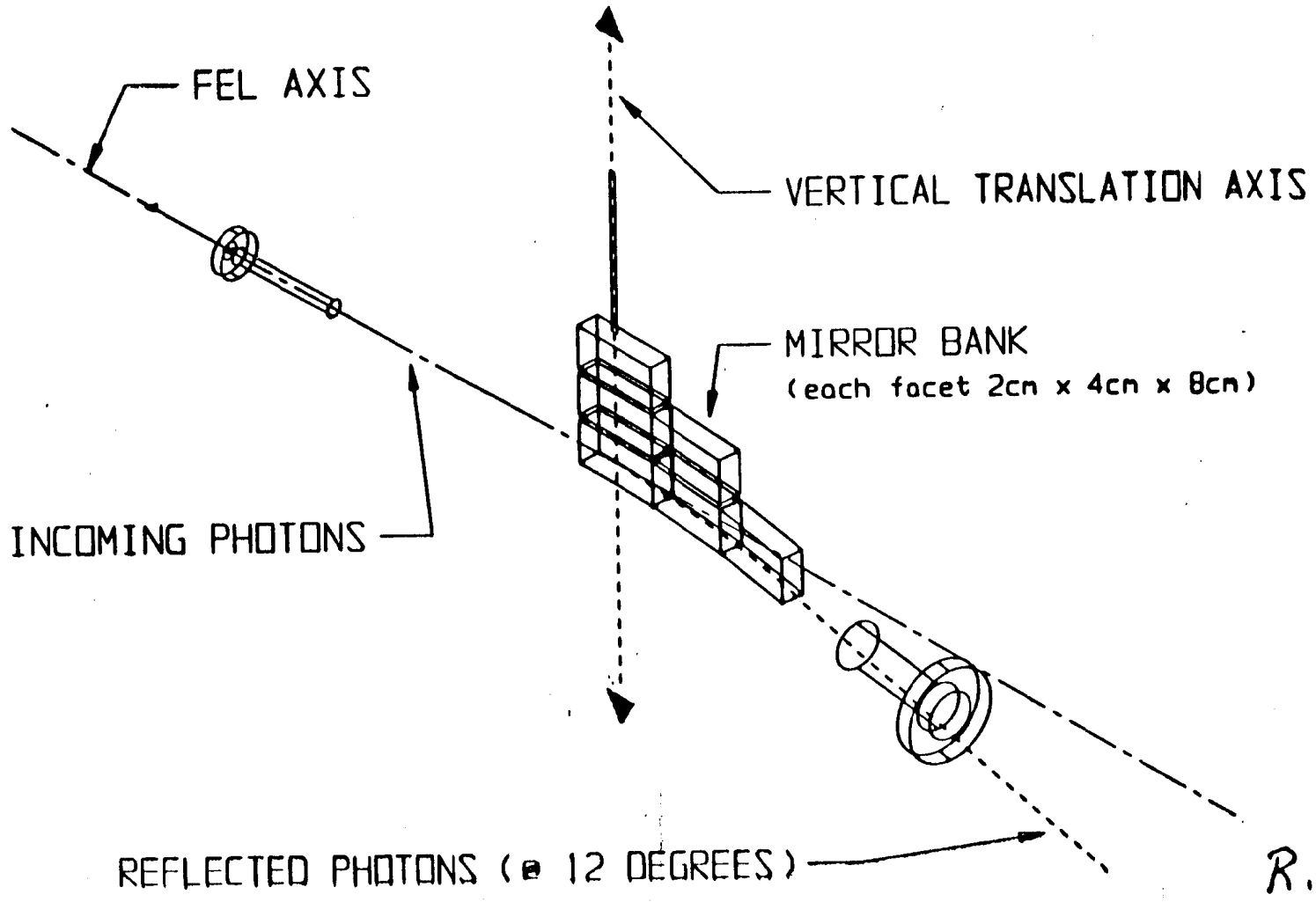

R. Tatchyn

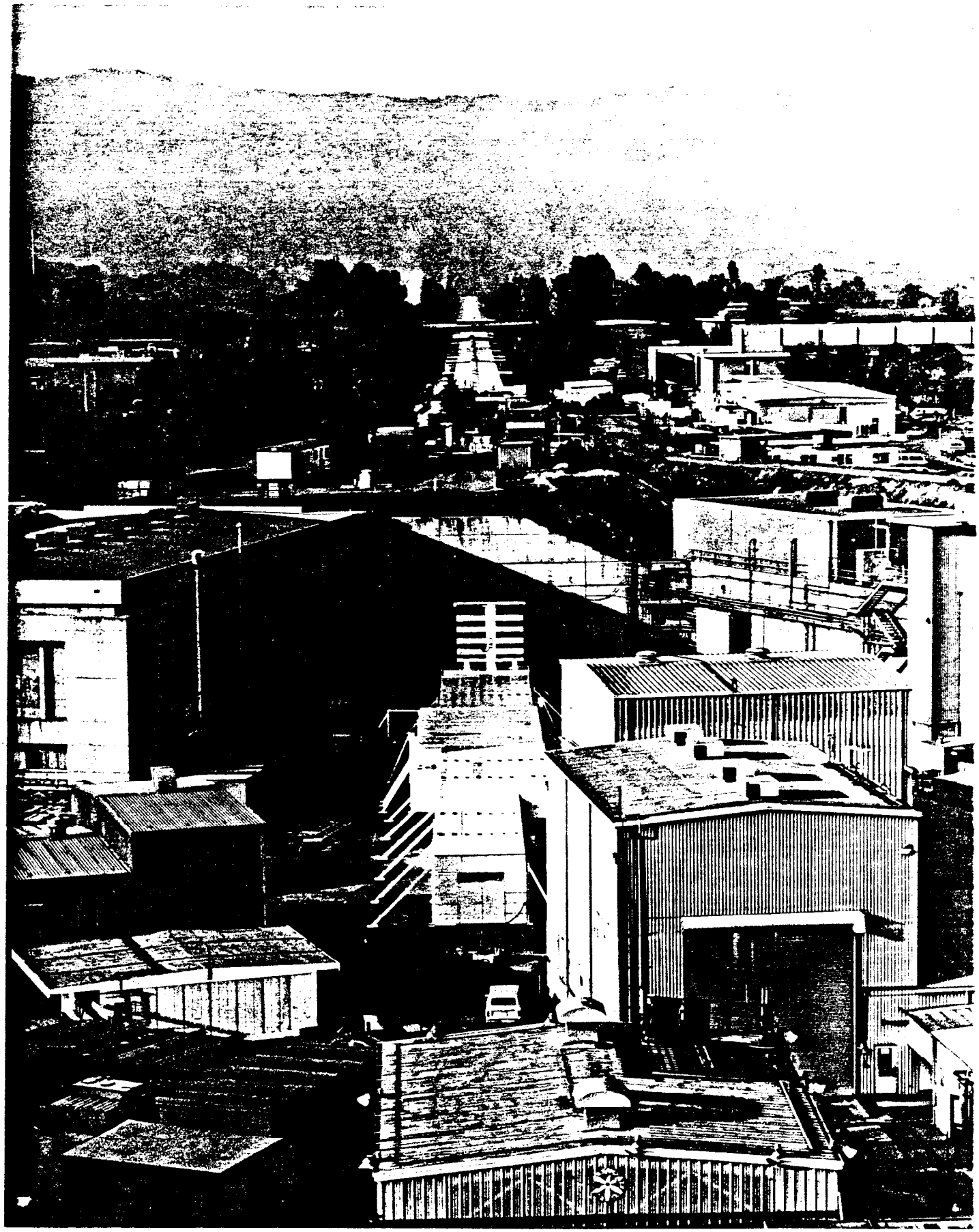

The SLAC/LBL/LLNL B Factory

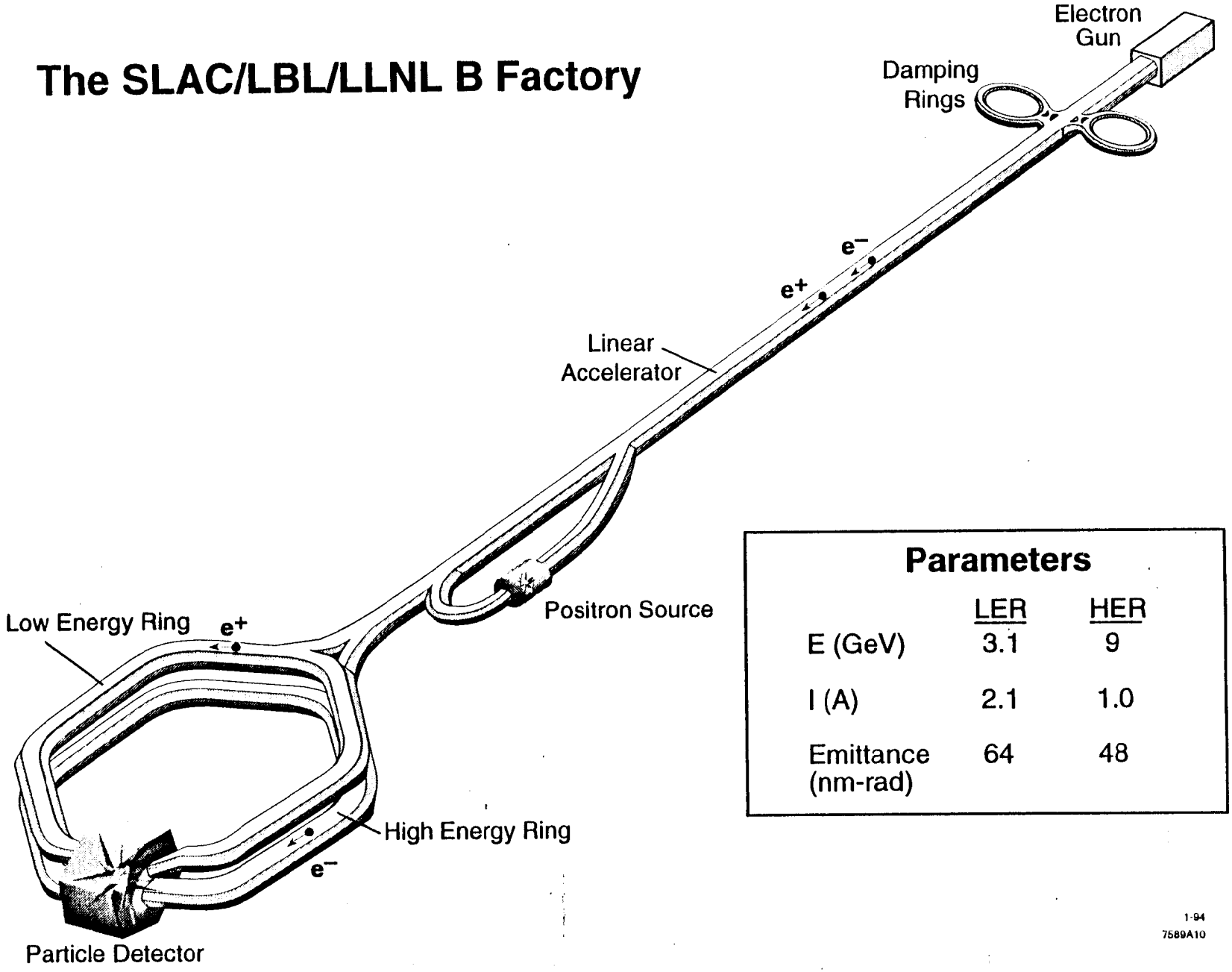

Parameters

	LER	HER
E (GeV)	3.1	9
I (A)	2.1	1.0
Emittance (nm-rad)	64	48

1-94
7589A10

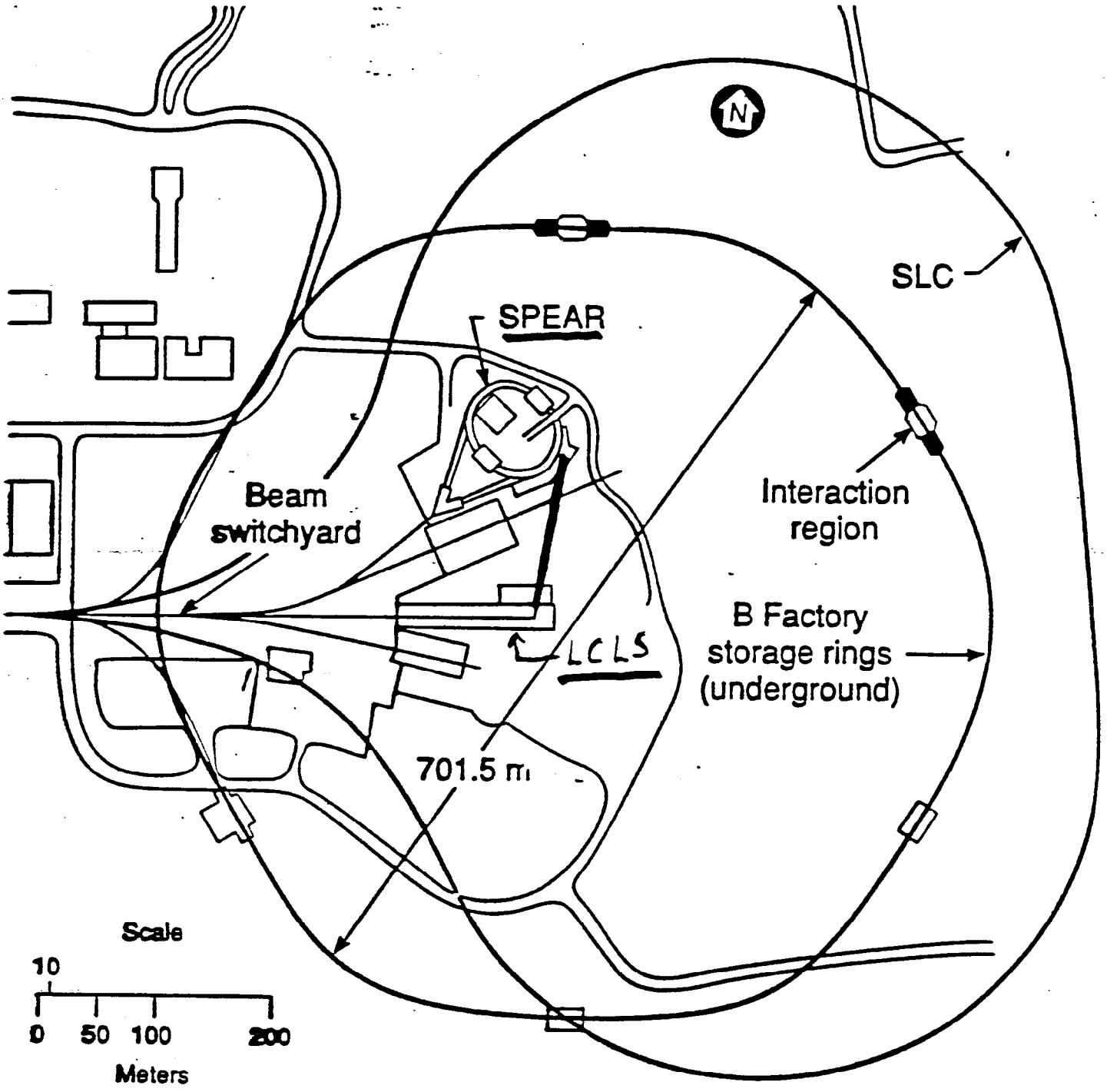
N
SLC
SPEAR
Beam
switchyard
Interaction
region
B Factory
storage rings
(underground)
LCLS
701.5 m
Scale
10
0
50
100
200
Meters

FELs

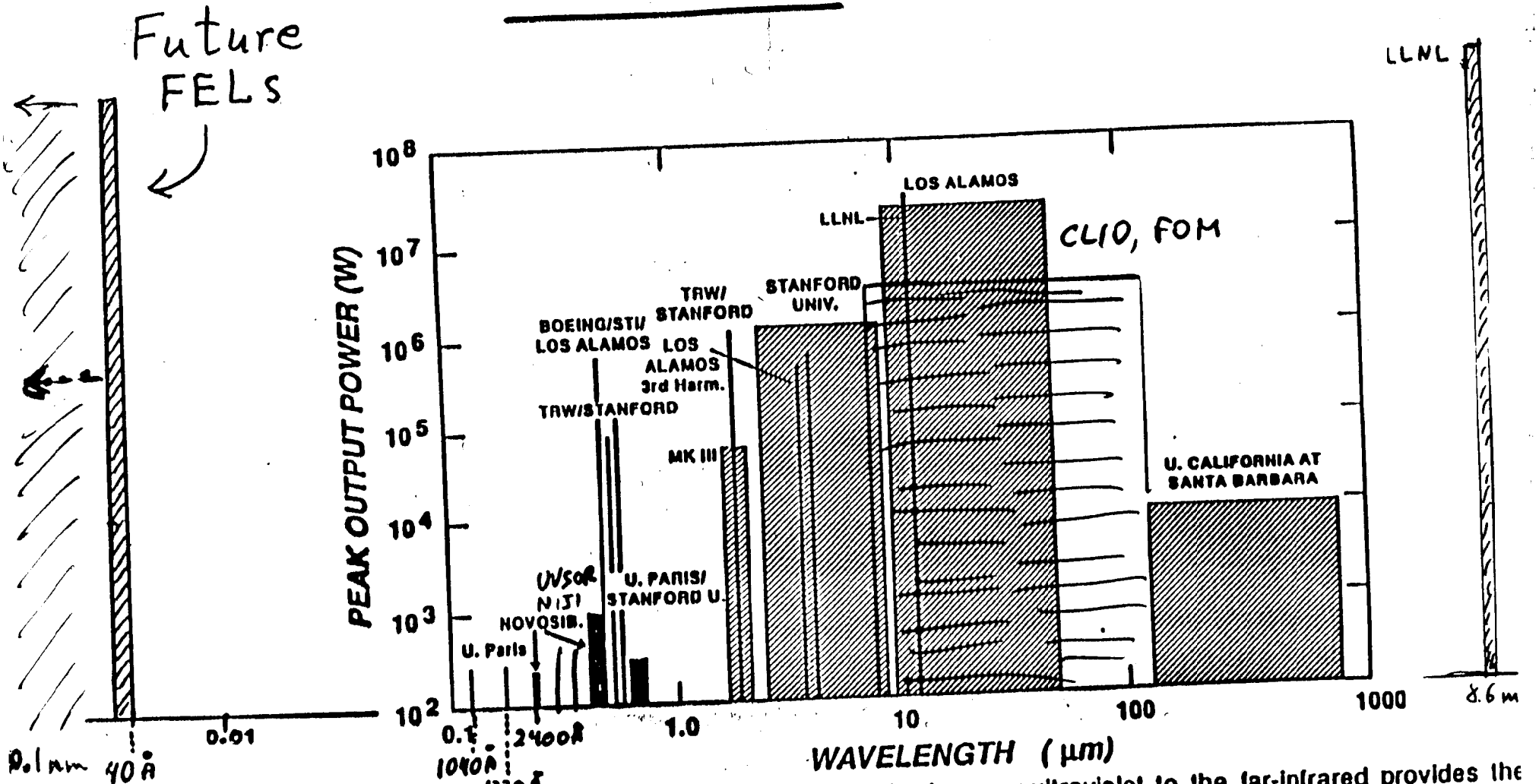

Figure 1. Successful free-electron laser operation in the near-ultraviolet to the far-infrared provides the experience base for extension below 0.1 μm. (The weak output at the two VUV wavelengths was coherent spontaneous emission from electrons bunched within an undulator by an external 532-nm laser.[48])

Courtesy of Brian Newnam, Los Alamos

- Radiation from a single electron.

The coherent radiation from a single electron can be characterized as the radiation from an effective source, positioned in the middle of the undulator.

$B_y = B_0 (\sin 2\pi z/\lambda_u)$

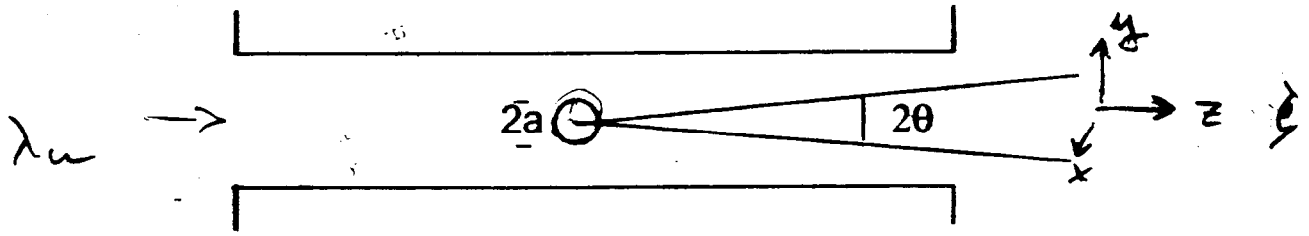

$E = mc^2\gamma$

$$\lambda=\lambda_u(1+k^2)/2\gamma^2 \qquad K = \frac{eB_0\lambda_u}{2\pi mc^2}$$

$$a=(\lambda N\lambda_u)^{1/2}/4\pi \qquad \theta=(\lambda/N\lambda_u)^{1/2} \longrightarrow \theta a = \frac{\lambda}{4\pi}$$

$$\Delta\omega/\omega=1/2N \longrightarrow \frac{\Delta\gamma}{\gamma} < \frac{1}{4N}$$

$$N_{photons}\sim\alpha\,(N_u\Delta\omega/\omega)\sim 10^{-3} \qquad \left(N_{ph} = \frac{\pi\alpha}{2}\frac{K^2}{1+K^2}N_u\frac{\Delta\omega}{\omega}\right)$$

$$\downarrow$$

if $K\sim 1$, $N_u\frac{\Delta\omega}{\omega}\sim 0.1$

NOTICE $\frac{E_{ph}}{E_e}\sim\frac{10^2\,eV}{10^9\,eV}\sim 10^{-7}$, $\mathcal{E}_{eff} = \frac{N_{ph}E_{ph}}{N_e E_e}\sim 10^{-10}$

FROM THE EFFICIENCY WE CAN OBTAIN THE FLUX

$$\dot{N}_p = N_p\left(\frac{I}{e}\right) \quad \text{photons/sec}$$

$\Delta\Omega$ AND $\Delta\omega/\omega$ ARE DETERMINED BY THE ELECTRON BEAM, LASER PULSE (UNDULATO

THE OTHER IMPORTANT QUANTITY IS THE BRIGHTNESS

$$B = \dot{N}_p / (\text{X-RAY PHASE SPACE AREA})^2$$

PHASE SPACE AREA

$$A \simeq \frac{\lambda}{4\pi}$$

FOR A COHERENT, DIFFRACTI LIMITED X-RAY BEAM A IF $\varepsilon < \lambda/4\pi$

$$A \simeq \varepsilon$$

IF $\varepsilon > \lambda/4\pi$

Principle of operation b.) COLLECTIVE INSTABILITY, FEL.

How do we increase the number of photons emitted per electron?

We take advantage of a collective instability of the electron beam- EM radiation field-undulator system:

E-beam+EM Field -> electron energy modulation, scale λ

electron energy modulation + undulator -> electron bunching at scale λ

bunched electrons emit in phase -> larger EM field intensity (limit $I \sim N_e^2$)

---

* UNDULATOR RADIATION IS BEAM NOISE, $I \sim N_e$

* ORGANIZING, INTRODUCING ORDER IN THE BEAM (BUNCHING), WE INCREASE INTENSITY, $I \sim N_e^2$.

The collective instability occurs if some conditions are satisfied. These conditions depend on a single parameter, the FEL parameter ρ:

a. beam emittance < $\lambda/4\pi$

b. energy spread < ρ

If a & b are satisfied the EM field grows exponentially with a characteristic length, the Gain Length,

$$L_G=\lambda_u/4\pi\rho$$

$E = E_0 e^{z/L_G}$

Ω_p = BEAM PLASMA FRE.

$\omega_u = 2\pi c/\lambda_w$

What is ρ?

$$\rho=\left(\frac{K\,\Omega_p}{4\gamma\,\omega_u}\right)^{2/3}$$

- **Saturation power: $P_L \sim \rho\, P_{beam} = \rho\, I\, E$**
- **Saturation length: $L_{sat} \sim 10\, L_G$ or $N_{sat} \sim 10/4\pi\rho \sim 1/\rho$**

To keep the undulator length to less than 1000 period, we need to have $\rho > 10^{-3}$, which implies a large beam peak current >1kA.

The number of photons per electron is

$$N_{ph} \sim \rho \frac{E}{E_{ph}}.$$

For E_{ph}~10eV, E~3GeV, ρ~10-3 we have N_{ph}~10^4.

<u>At saturation we have about 10^4 photons/electron, a gain of about 7 orders of magnitude.</u>

NOTICE : IT IS POSSIBLE TO GO ABOVE SATURATION UP TO $P_L \sim 0.1\, E_B I_B$ CORRESPONDING TO ABOUT 10^6 pl/el.

4 nm FEL : perfect wiggler & steering

$\lambda = 4\,nm$

$\gamma = 14,000$ $(E = 7\,GeV)$

$\lambda_u = 8.3\,cm$

$B_u = 0.76\,T$

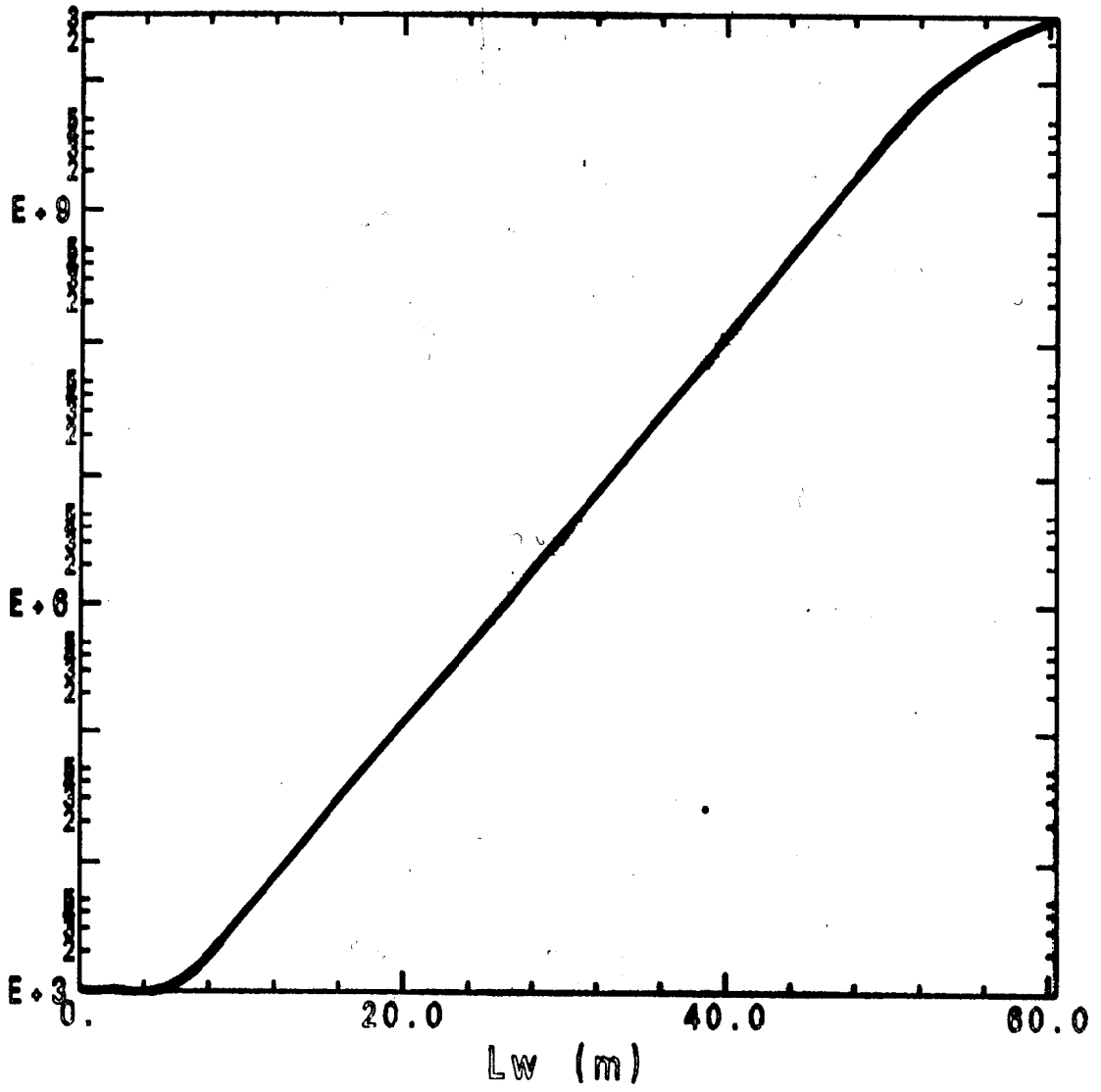

NOTICE:

$\varepsilon < \frac{\lambda}{4\pi}$

$\sigma_E \ll \rho$

$\int \rho \sim 2 \times 10^{-3}$

$P_{in} = 1\,kW$

$P_{out} = 30\,GW$

$L_G = 5.8\,m$

FR3D run : 10-15-92 11:21:02 sl3u7 ; rbeam = 5.493e-03; Bw = 7.536e+00 kG (peak); wavelength = 4.000e-09 m

Present status of short wavelenth FELs

Shortest wavelength produced ~240nm, at Novosibirsk, on a storage ring; peak power in the kW range.

Projects

- KEK, UV, storage ring
- Duke University, UV, storage ring
- Dortmund University, UV, storage ring
- BNL, UV, linac
- Los Alamos, UV to soft X-ray, linac
- SLAC/SSRL, soft x-ray to x-ray, linac

The UV projects have λ~50-200nm; SLAC, LANL λ~1-4nm. with extension to λ~1Å.

What limits the wavelength of an FEL?

FELs are very successful in the visible to infrared and microwave regions; several users facility in the infrared are in operation (Vanderbilt, Stanford, FOM). The wavelength and power limitations at short wavelength are due to electron beam and opticl cavity characteristics.

Electron beam requirements

a. Beam emittance $< \lambda/4\pi$
b. FEL parameter $\rho > 0.001$

Large ρ requires large electron density, large peak current.
Scaling of ρ with wavelength: $\rho \sim (\text{Beam current } \lambda)^{1/2}$ if a &b are satisfied.
The electron beam requirements are more stringent at short wavelength.

Optical cavity problems

Most FELs are run as oscillator, using an optical cavity, and with an undulator shorter than one gain length. The effect of the optical cavity is to effectively increase the undulator length, so that one can reach saturation even with a short undulator. This technique is very convenient at wavelength in the visible or infrared, where mirror reflectivity is very large, and the optical cavity losses are small.

Mirror reflectivity becomes small at short wavelength, resulting in large cavity losses; to compensate for these losses we need a large FEL gain, which requires higher electron beam density.

In addition the mirrors have thermal problems, and suffer from hard X-ray radiation produced from undulators.

An optical cavity for an FEL in the soft X-ray wavelength region is not available today.

Because of the electron beam and mirror problems until now it has not been possible to build a Soft X-ray FEL.

Why is the situation changing?

- avoid mirror problems by operating the laser in Self Amplified Spontaneous Emission (SASE)
- use RF photoinjector to produce better quality electron beams (developments at LANL, BNL, UCLA)
- use linear collider accelerator physics and technology to accelerate and compress electron pulses
- *Result of all these innovations: X-Ray FEL.*

SASE

SOFT X-RAY FEL

(LCLS) Schematic Overview : 4 nm case.

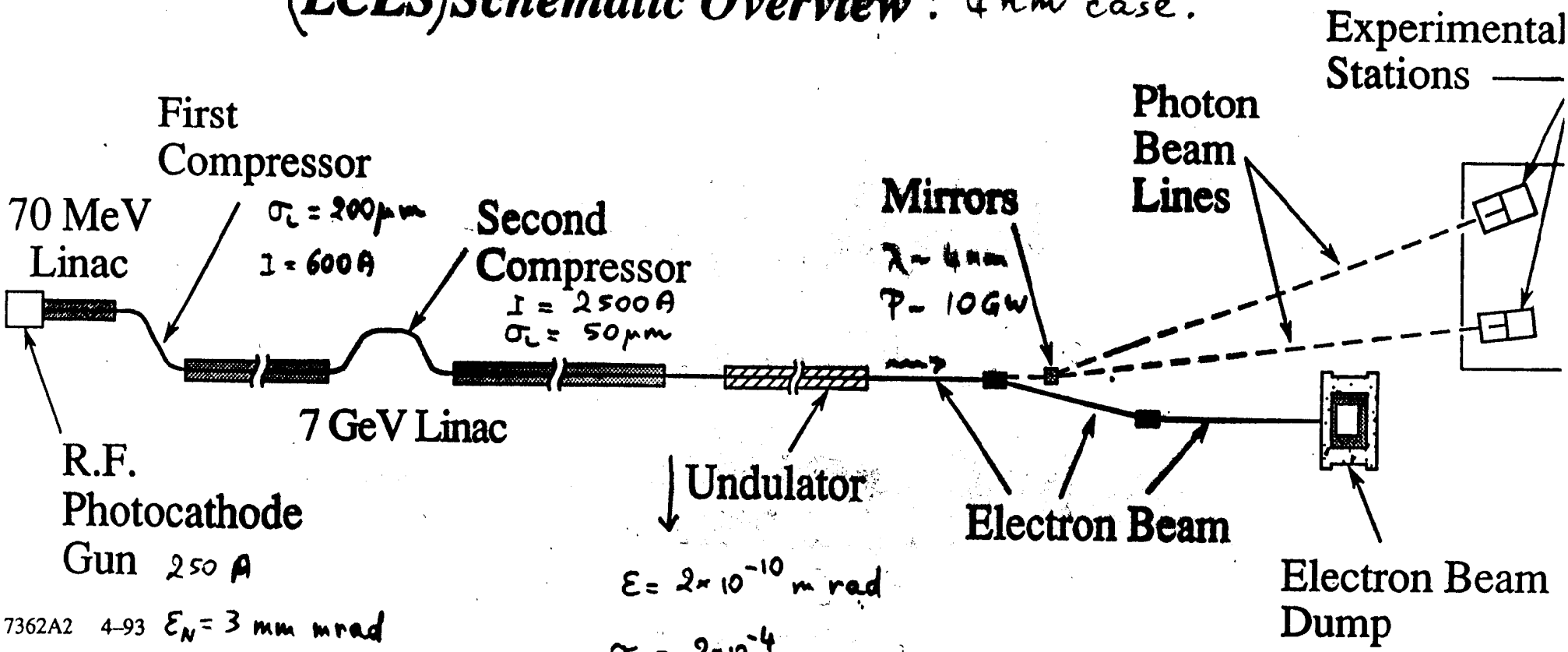

NOTICE : PEAK CURRENT AND EMITTANCE (IN ONE PLANE)

DEMONSTRATED IN STANFORD LINEAR COLLIDER

The AFEL is compact and modular.

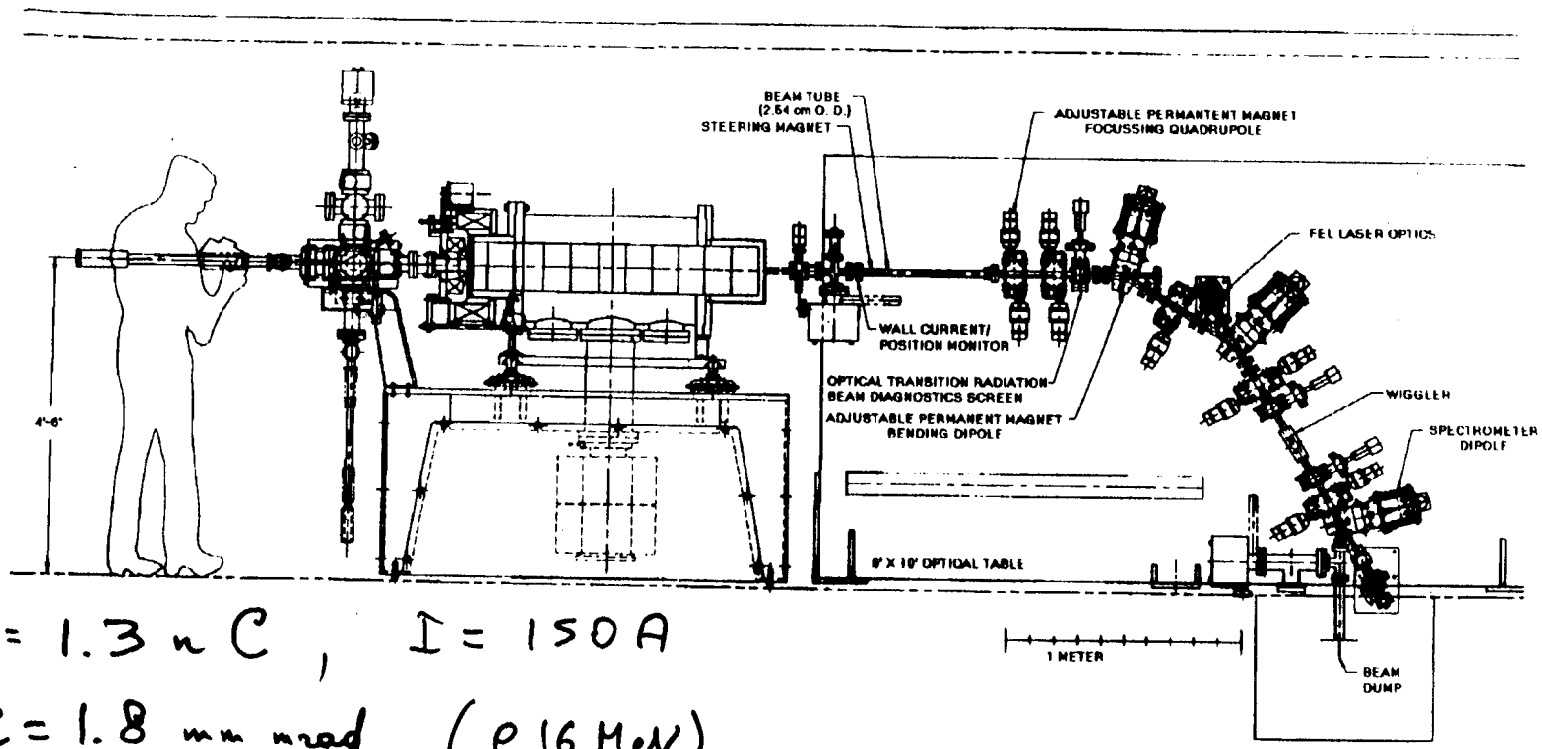

$Q = 1.3\ nC$, $I = 150\ A$

$\varepsilon = 1.8$ mm mrad (@ 16 MeV)

Wavelength, nm	4
Field gain length, m	5.8
Undulator saturation length, m	60
Peak power at saturation, GW	9
Pulse duration, rms, ps	0.16
Line width	0.0015
Photons per pulse	10^{14}
Energy per pulse, mJ	3.6
Repetition rate, Hz	120
Average power, W	0.4
Average brightness, *photons/sec/*(mmmrad)^2/0.1%bandwidth	5 x 10^{21}

Table 4.2: Soft X-ray FEL Properties at 4 nm

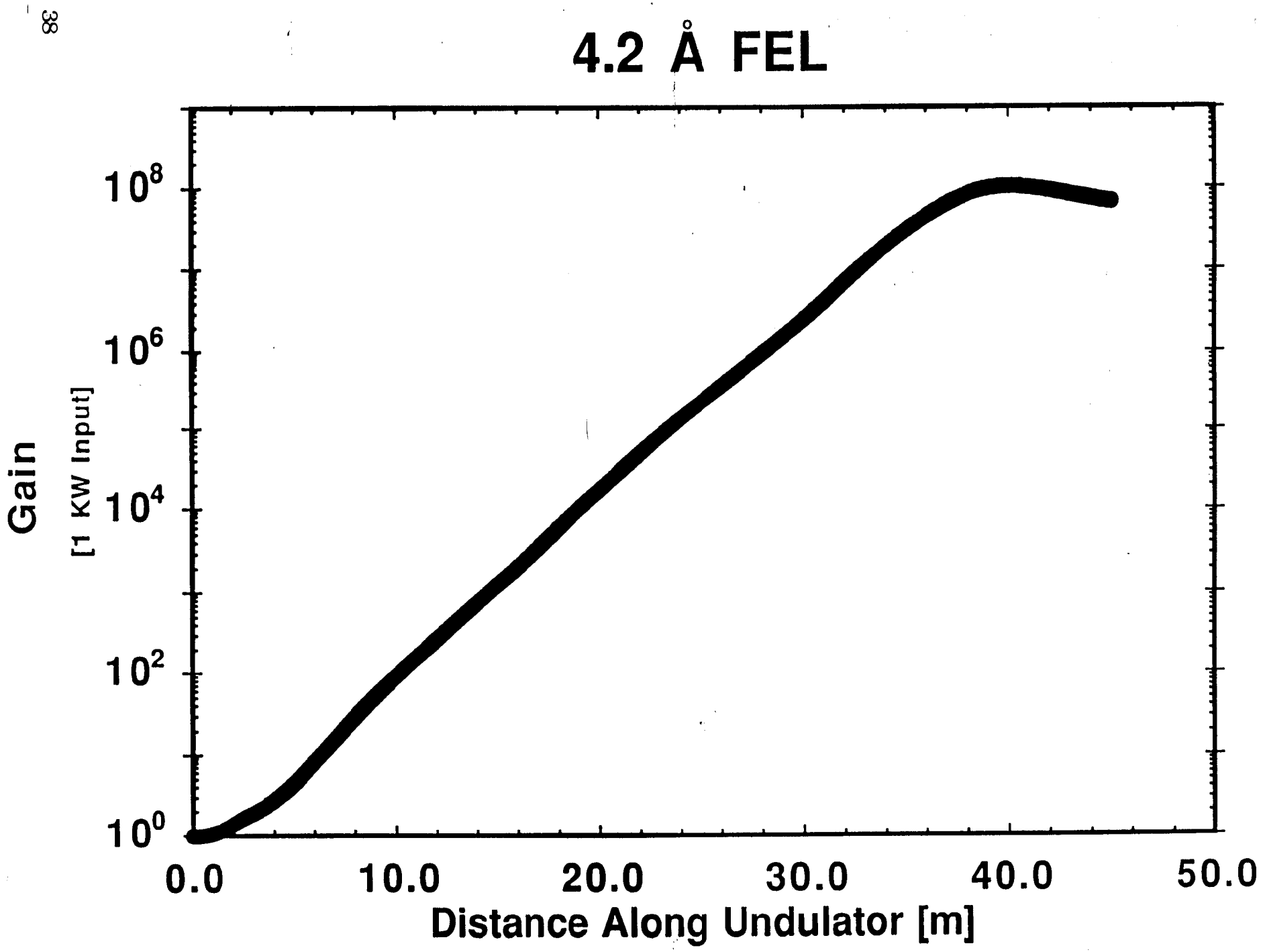
4.2 Å FEL
Gain
[1 KW Input]
10^8
10^6
10^4
10^2
10^0
0.0
10.0
20.0
30.0
40.0
50.0
Distance Along Undulator [m]

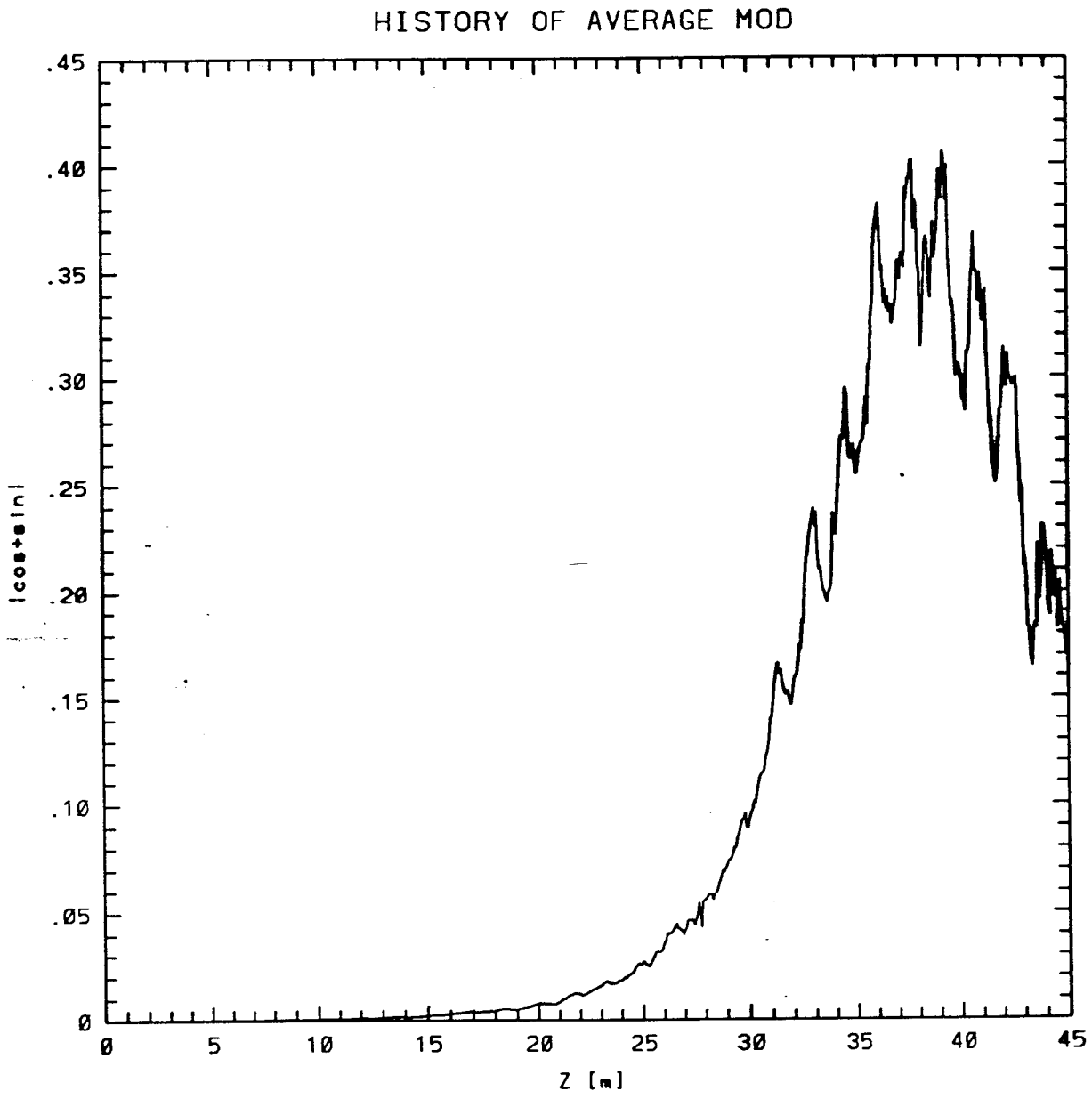
HISTORY OF AVERAGE MOD
.45
.40
.35
.30
.25
.20
.15
.10
.05
0
|cos•sin|
0
5
10
15
20
25
30
35
40
45
Z [m]

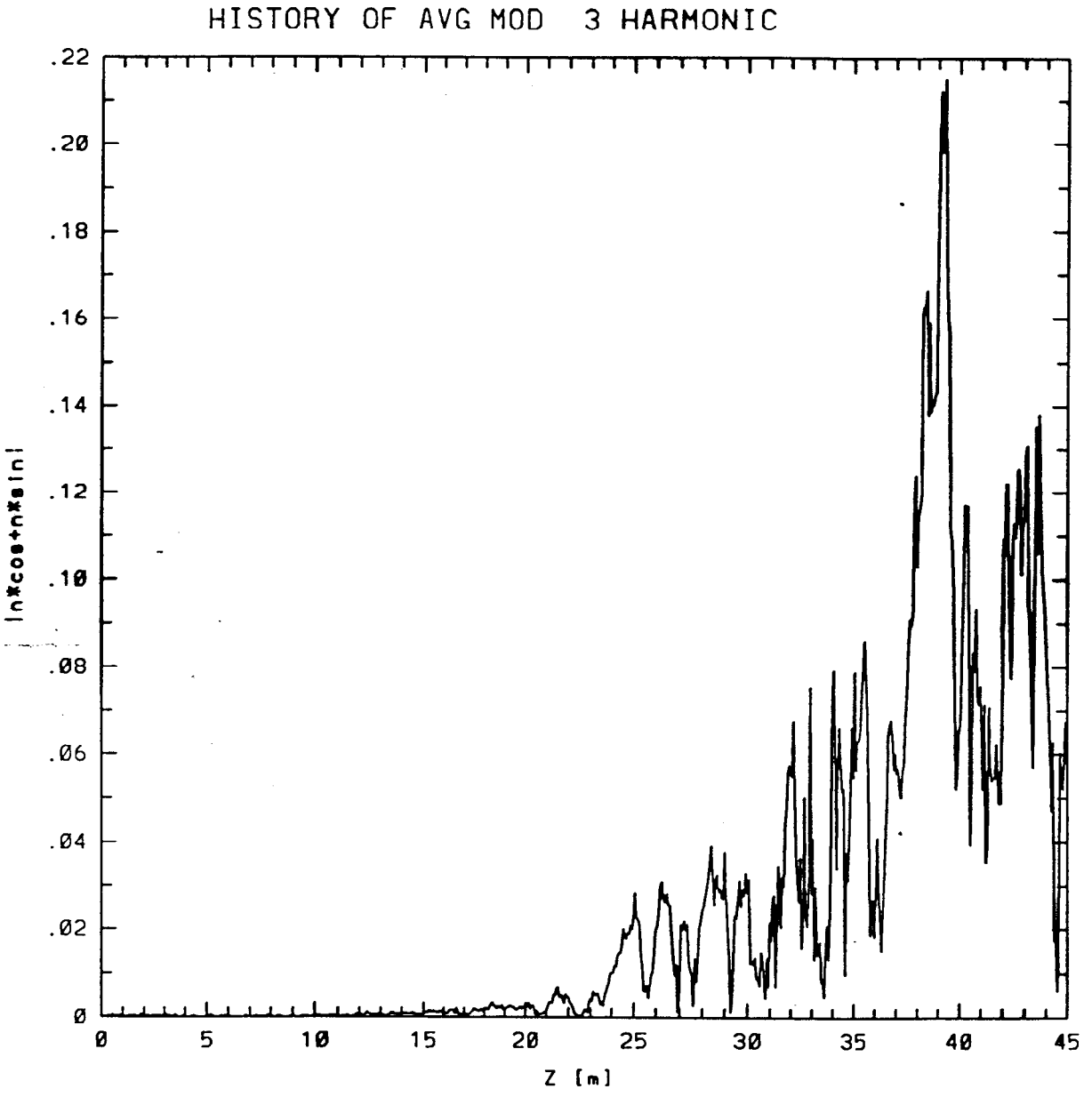
HISTORY OF AVG MOD 3 HARMONIC
.22
.20
.18
.16
.14
.12
.10
.08
.06
.04
.02
0
|n*cos+n*sin|
0
5
10
15
20
25
30
35
40
45
Z [m]

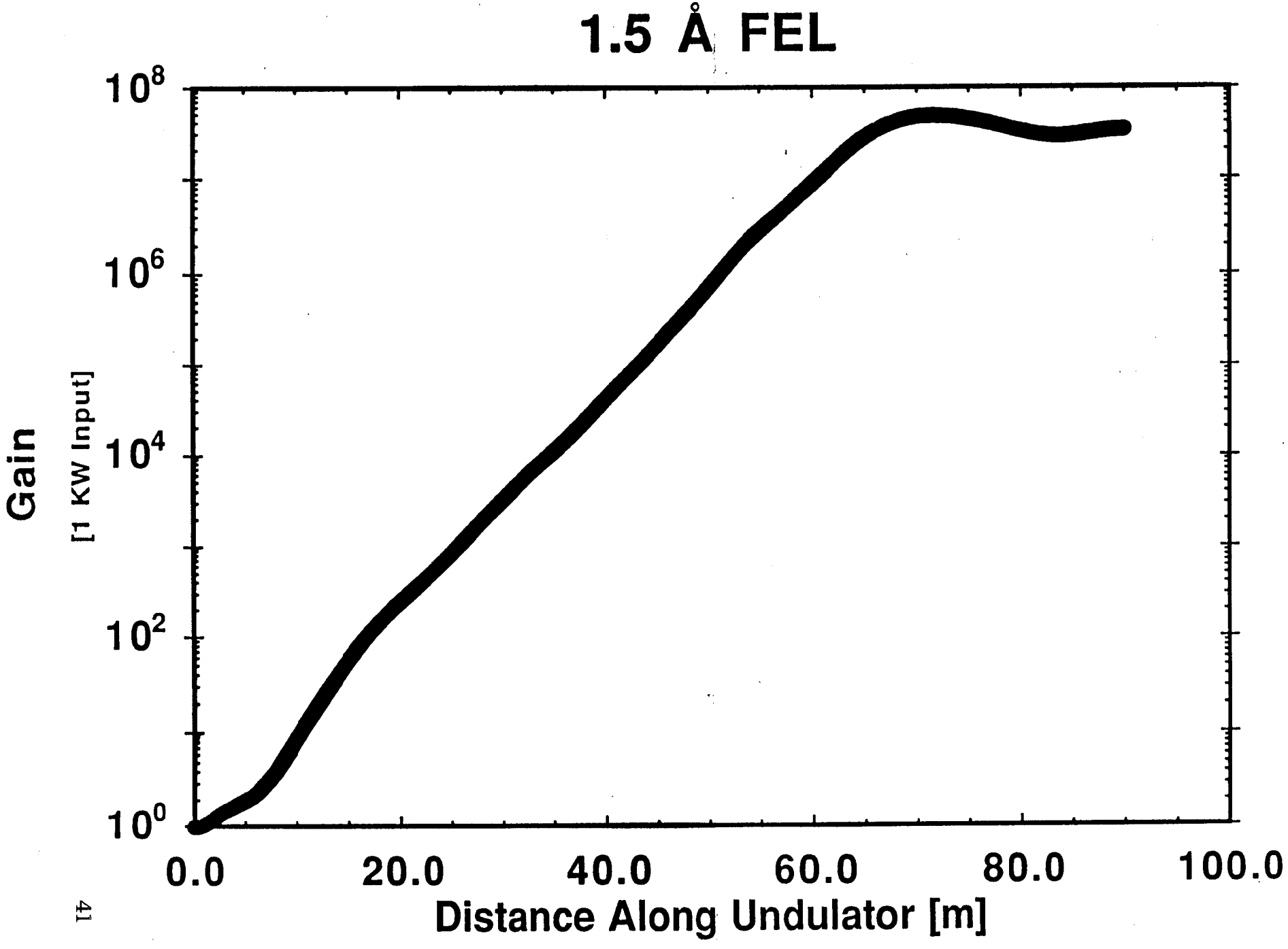
1.5 Å FEL
Gain
[1 KW Input]
10^8
10^6
10^4
10^2
10^0
0.0
20.0
40.0
60.0
80.0
100.0
Distance Along Undulator [m]

CONCLUSIONS

- We are now convinced that the Soft X-Ray FEL that we have designed is feasible, and that an appropriate R&D program will lead to a user friendly system.

- The FEL has been optimized for X-ray microscopy, to be able to take an hologram of a living biological sample in a single subpicosecond shot:

  $N_{photons} \sim 10^{14}$/pulse, $\tau < 1$ ps, $\lambda \sim 2\text{-}4$nm;

- other experiments might use a different optimization, for example shorter pulses; given your inputs we can study other options and make the system flexible enough to make it unique in many areas of research.

- With some further improvements in electron beam quality we can foresee an extension of the X-ray FEL to 0.1 nm. The 2 to 4 nm FELwill also be an R&D tool for the 0.1nm system.

Summary of Discussion

Pellegrini/Winick talks:

Fadley complained that, though the length of the LCLS radiation pulse was expected to be 200 fs or less, the expected uncertainty in pulse arrival time was 500 fs. Better synchronization will be needed for some experiments, such as non-linear studies. Pellegrini explained that this 500 fs value was a rough guess at what level of synchronization might be achievable at a practical cost. One option is to use the laser driving the photocathode as a system clock. There was general discussion, and agreement that time synchronization at the level of the pulse length would be extremely valuable for some timing experiments, and that some research effort should go into seeing how to make this possible.

Chu asked about the dimensional tolerances for the undulator used in the LCLS, as compared with the tolerances for an undulator at a low-emittance storage ring such as the Advanced Light Source. Pellegrini replied that high tolerances are required over one gain length, about 3-5 m in the LCLS. The tolerances that must be met over this length are similar to those achieved in existing ALS undulators, which are of similar length.

A question was raised about the cost of the LCLS. Winick explained that an LCLS producing 40 Å radiation in the fundamental mode from a 60 m undulator was estimated to cost $29M, of which $13M would be the cost of the undulator. With recent improvements in electron gun technology, it now seems that a significantly shorter undulator could be used to give a 40 Å fundamental, reducing the cost. No careful estimate has yet been made for a 1 Å LCLS.

Introductory Comments on Spatial and Temporal Coherence

David Attwood, CXRO/LBL

Introductory Comments on Spatial and Temporal Coherence

David Attwood
Center for X-ray Optics
Lawrence Berkeley Laboratory

and

Department of Electrical Engineering and Computer Science
University of California, Berkeley

Measures of spatial and temporal coherence are obtained based on Heisenberg's Uncertainty Principle. Scaling of coherent power with wavelength, for fixed phase-space, decays to first order as $1/\lambda^3$. Values for undulater radiation are given. Improved temporal coherence and peak power, possible with free electron lasers, is discussed.

Work supported by the Department of Energy's Office of Basic Energy Sciences.

Coherent Radiation

Electromagnetic radiation propagating in such a manner that the wave nature is simply described and interrelated over large distances of space and time, e.g., a spherical wave in which the phase at one point (P_1) is well correlated with the phase elsewhere (P_2)

Mutual Coherence Function:

$$\Gamma(P_1P_2;\tau) \equiv \langle E_1(t+\tau)\, E_2^*(t)\rangle$$

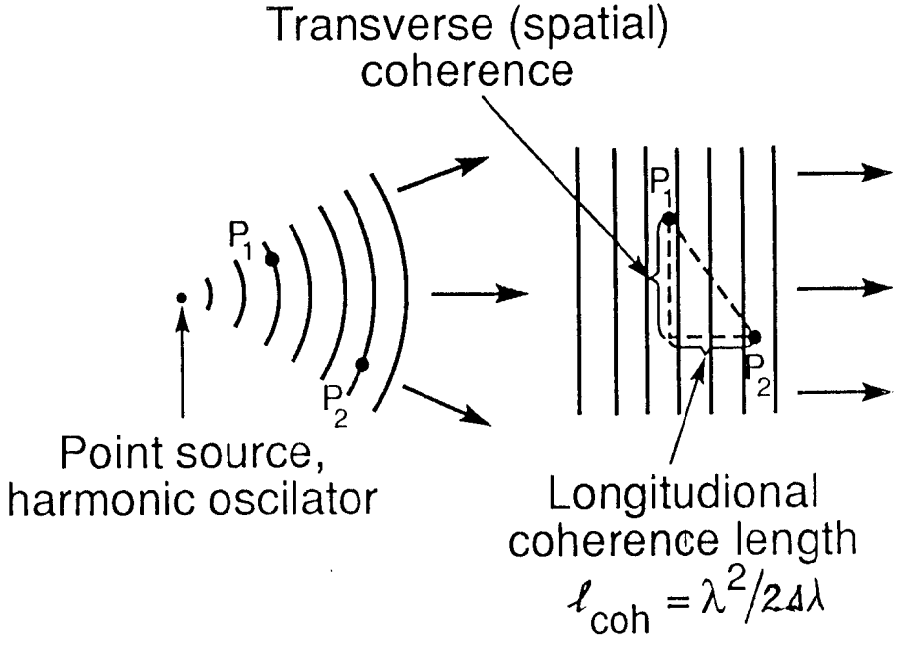

XBL 896-6245

Partial Coherence

Full coherence requires a point source oscillating with a single frequency for all time ($-\infty \leq t \leq \infty$):

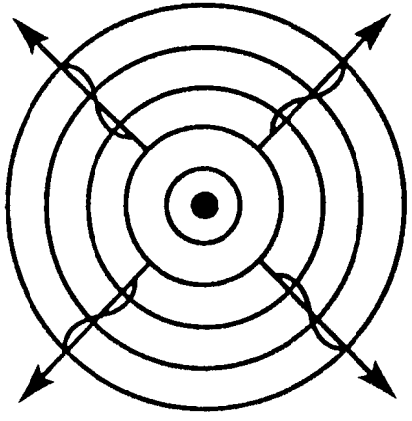

Laboratory sources are finite in both spatial extent and duration and thus are partially coherent:

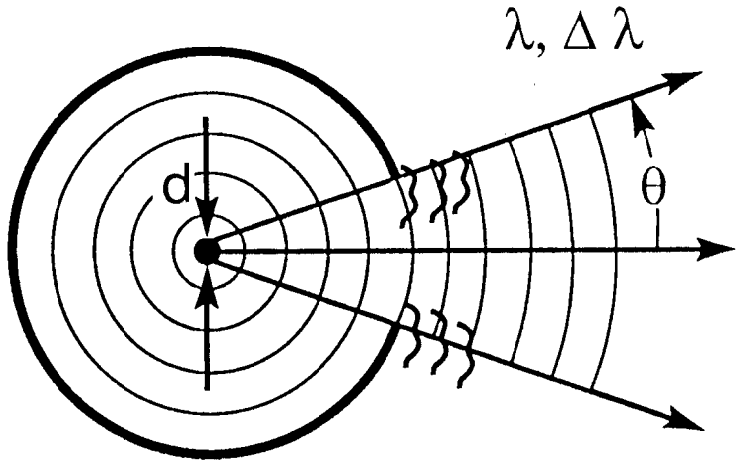

$$\text{"d"} \cdot \theta \simeq \lambda / 2\pi$$

$$\ell_{coh} = \lambda^2 / 2\Delta\lambda$$

XBL 896-6247

A Practical Interpretation of Spatial Coherence

- Associate spatial coherence with a spherical wavefront.
- A spherical wavefront implies a point source.
- How small is a "point source"?

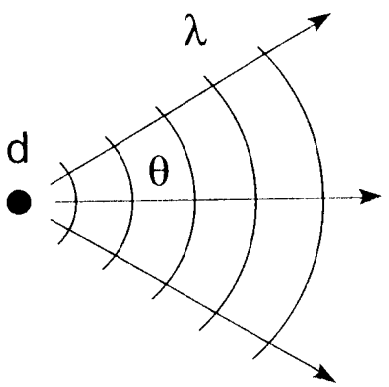

From Heisenberg's Uncertainty Principle ($\Delta x \cdot \Delta p \geq \frac{\hbar}{2}$), the smallest source size "d" you can resolve, with wavelength λ and half angle θ, is

$$d \cdot \theta = \frac{\lambda}{2\pi}$$

XBL 915-6740A

Partially Coherent Radiation Approaches Uncertainty Principle Limits

$$\Delta x \cdot \Delta p \geq \frac{1}{2}\hbar$$

$$\Delta x \cdot \Delta k \geq \frac{1}{2}$$

$$2\Delta x \cdot \Delta\theta \geq \frac{\lambda}{2\pi}$$

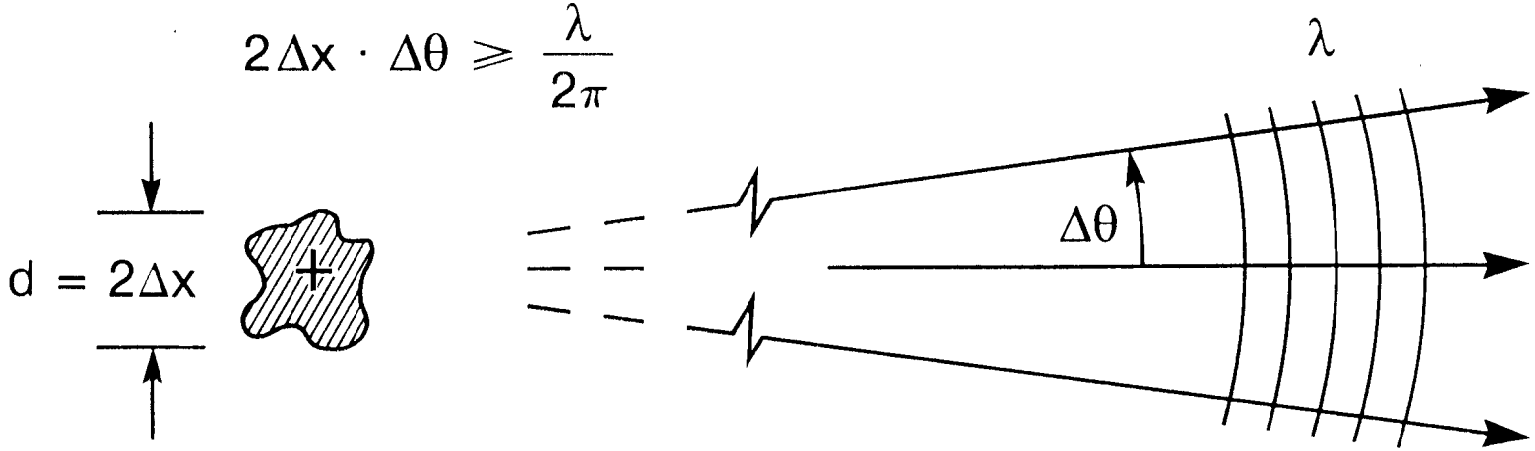

Spherical wavefronts occur in the limiting case

$$\boxed{d \cdot \theta = \frac{\lambda}{2\pi}}$$

(spatially coherent)

XBL 883-8849

Propagation of a Spherical Gaussian Beam

(Following Siegman, Lasers, 1986)

$$\frac{I}{I_0} = e^{-r^2/2r_0^2}, \text{ where } r(z) = r_0\sqrt{1 + \left(\frac{\lambda z}{4\pi r_0^2}\right)^2}$$

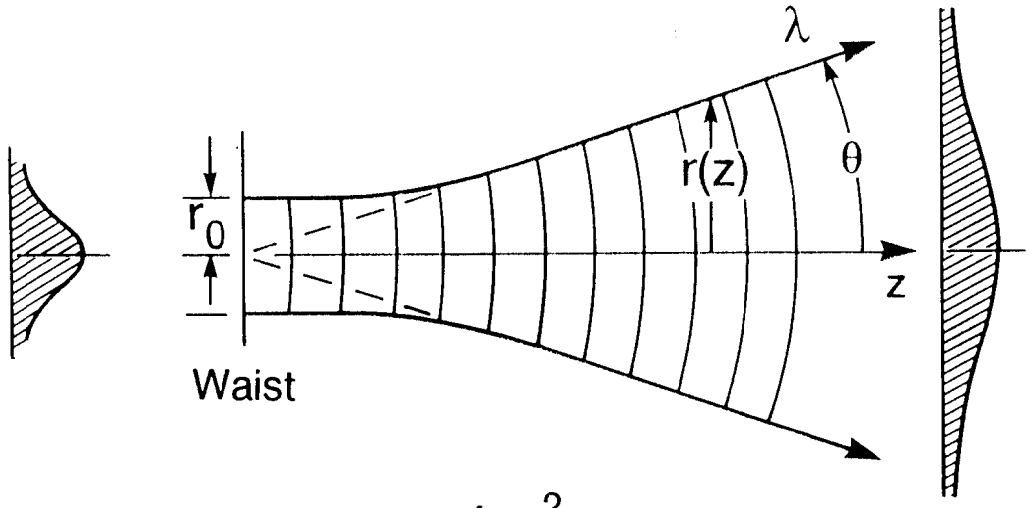

Spherically propagating wave with a Gaussian intensity distribution

In the far field, $z >> \frac{4\pi r_0^2}{\lambda}$

we define $\theta \equiv \frac{r(z)}{z} = \frac{\lambda}{4\pi r_0}$

if $d \equiv 2r_0$, then

$$\boxed{d \cdot \theta \doteq \frac{\lambda}{2\pi}}$$

(Spatially coherent)

rms or $1/\sqrt{e}$ quantities

XBL 883-8848A

Random angular motion (σ') within the electron beam is constrained by storage ring optics to be within the central cone of undulator radiation ($1 / \gamma \sqrt{N}$)

Spatially coherent radiation further requires that the apparent beam size (2σ) be limited to that which yields diffraction limited radiation:

$$d \cdot \theta = \frac{\lambda}{2\pi}$$

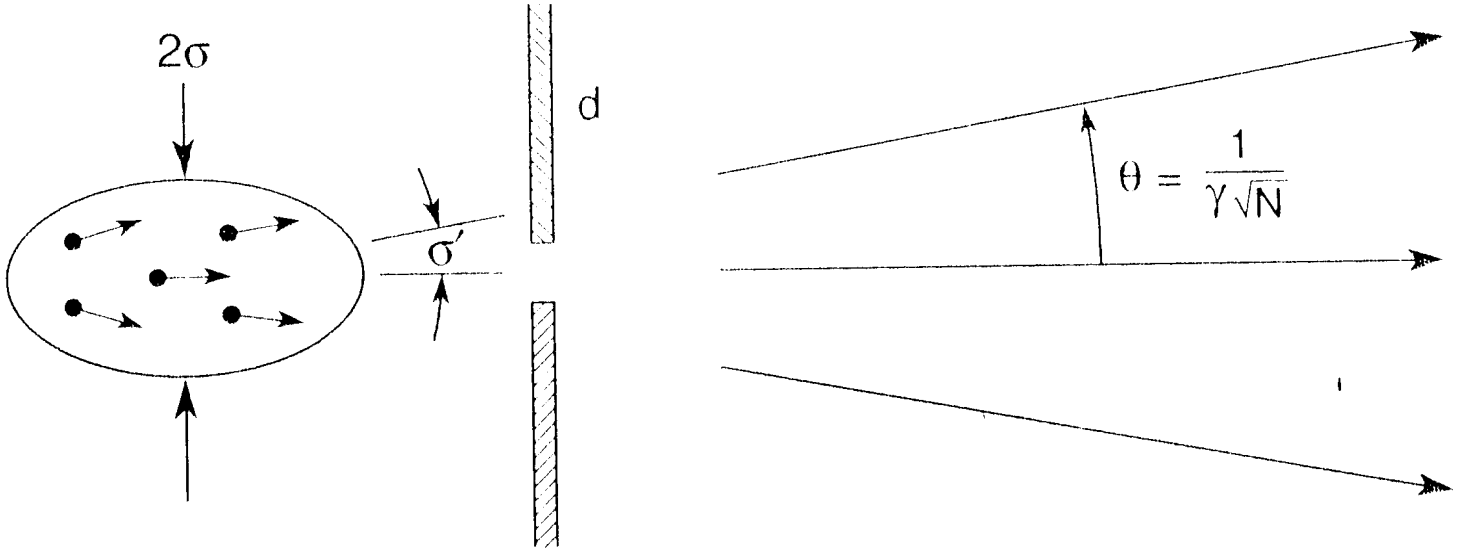

Coherence Length: destructive interference due to finite bandwidth

- not dependent on cause of $\Delta\lambda$
- important in phase-sensitive experiments

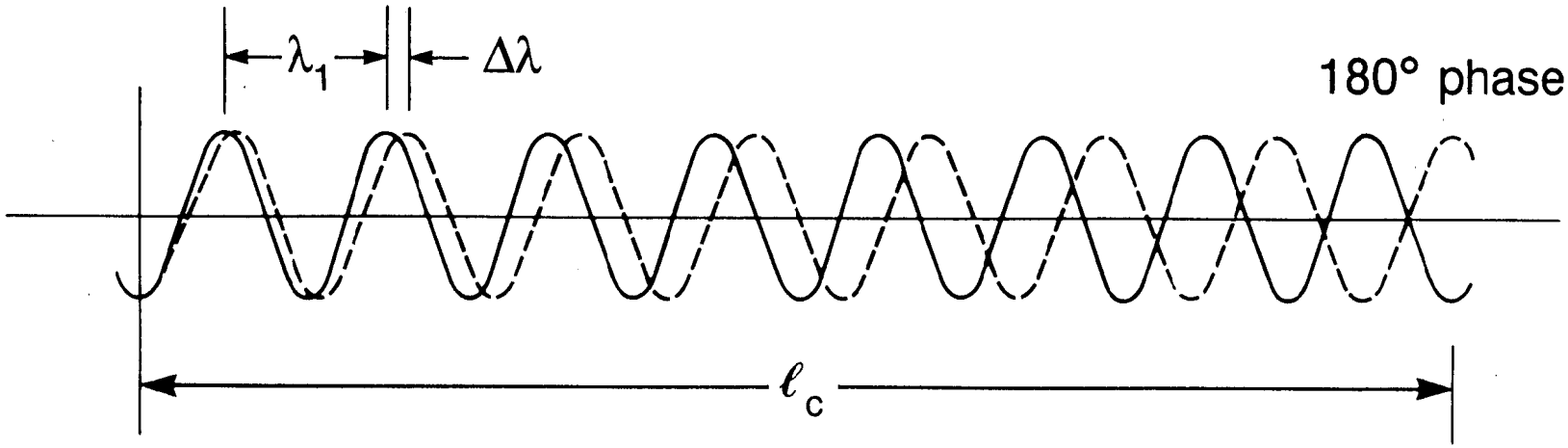

Definition: $\ell_c = N\lambda_1 = (N - \frac{1}{2})\lambda_2$

$$N = \frac{1}{2}\,\frac{\lambda_2}{\Delta\lambda}$$

$$\ell_c = N\lambda_1 \simeq \frac{1}{2}\,\frac{\lambda^2}{\Delta\lambda}$$

XBL 883-8850

Brightness is a Conserved Quantity

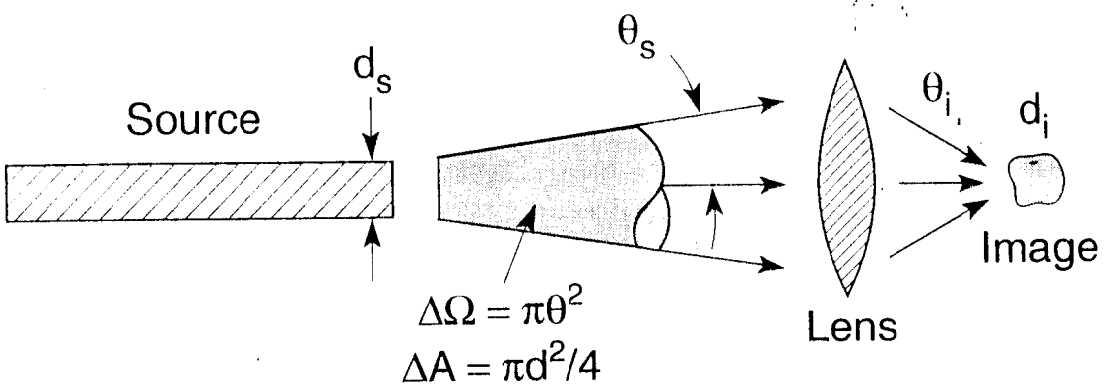

$$B = \frac{\text{Photons/sec}}{\Delta A \cdot \Delta\Omega}$$

$$B_{\Delta\omega/\omega} = \frac{\text{Photons/sec}}{\Delta A \cdot \underbrace{\Delta\Omega}_{\text{Focusability (transverse coherence)}} \cdot \underbrace{\Delta\lambda/\lambda}_{\text{Spectral purity (longitudinal coherence)}}}$$

With spatial filtering,

$$P \rightarrow P_{coh} \quad \text{as} \quad d \cdot \theta \rightarrow \frac{\lambda}{2\pi}$$

yielding

$$P_{coh} = \frac{\lambda^2 B_{\Delta\omega/\omega}}{16\left(\frac{\lambda}{\Delta\lambda}\right)} \cdot \frac{hc/\lambda}{\text{photon}}$$

or

$$P_{coh} = \frac{\lambda^2 B_{\Delta\omega/\omega}}{32\ell_{coh}} \cdot \frac{hc}{\text{photon}} \quad , \qquad \text{where } \ell_{coh} \equiv \frac{\lambda^2}{2\Delta\lambda}$$

XBL 8810-9087

Spectral Brightness and Partial Coherence

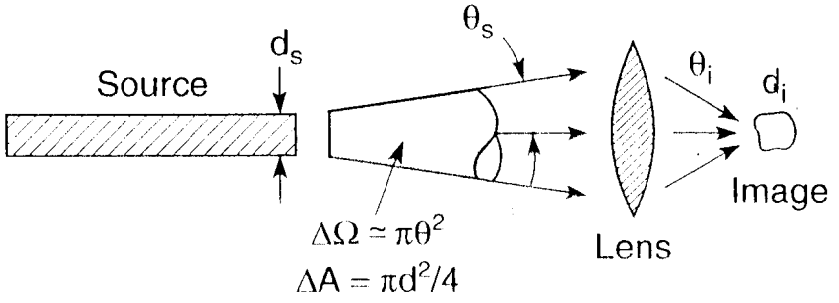

$$B = \frac{\text{Photons/sec}}{\Delta A \cdot \Delta\Omega}$$

$$B_{\Delta\omega/\omega} = \frac{\text{Photons/sec}}{\Delta A \cdot \Delta\Omega \cdot \Delta\lambda/\lambda}$$

Focusability (transverse coherence)

Spectral purity (longitudinal coherence)

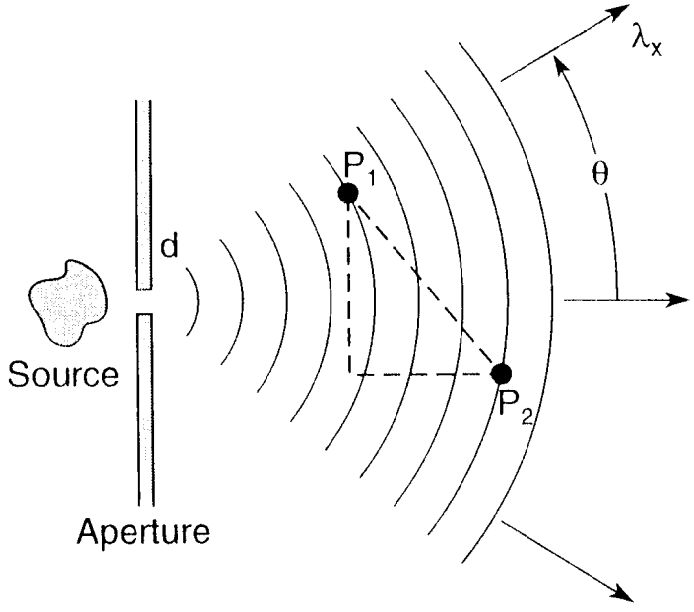

Transverse (spatial) coherence

$d \cdot \theta = \lambda/2\pi$

Longitudinal coherence length

$\ell_{coh} = \lambda^2/2\Delta\lambda$

XBL 924-5677

A Practical Interpretation of Spatial Coherence

- Spatial coherence requires a spherical wavefront.
- A spherical wavefront implies a point source.
- How small is a "point source"?

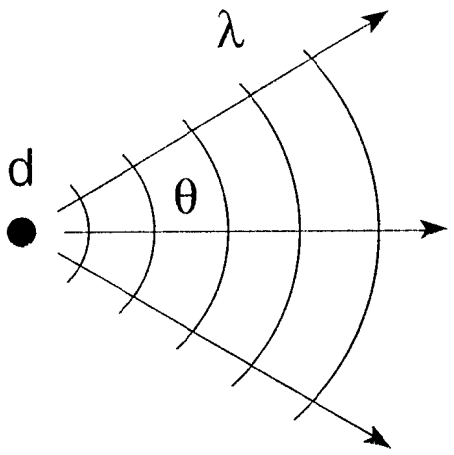

From Heisenberg's Uncertainty Principle ($\Delta x \cdot \Delta p \geq \frac{\hbar}{2}$), the smallest source size "d" you can resolve, with wavelength λ and half angle θ, is

$$d \cdot \theta = \frac{\lambda}{2\pi}$$

XBL 915-6740A

Bandwidth and Coherence Length for Undulator Radiation

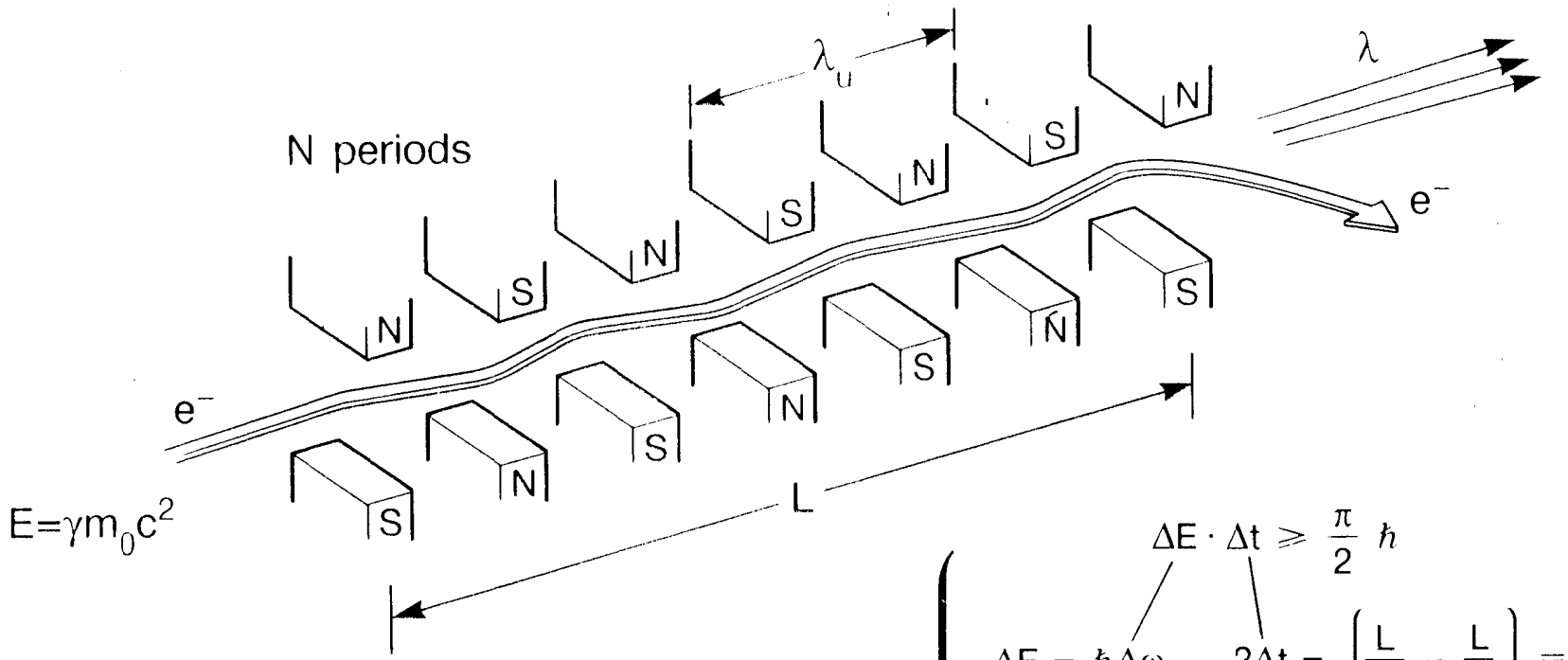

Uncertainty Principle

$$\Delta E \cdot \Delta t \geq \frac{\pi}{2}\hbar$$

$$\Delta E = \hbar\Delta\omega \qquad 2\Delta t = \left(\frac{L}{\bar{v}_z} - \frac{L}{c}\right) = \frac{N\lambda}{c}$$

$$\hbar\Delta\omega \cdot \frac{N\lambda}{c} \geq \pi\hbar$$

$$\frac{2\Delta\omega}{\omega} \cdot N \geq 1$$

$$\frac{\lambda}{2\Delta\lambda} \leq N$$

Coherence length definition: $\ell_c = \dfrac{\lambda^2}{2\Delta\lambda} \leq N\lambda$

XBL 883-8847

Evolution of Synchrotron Radiation

Todays Synchrotrons:

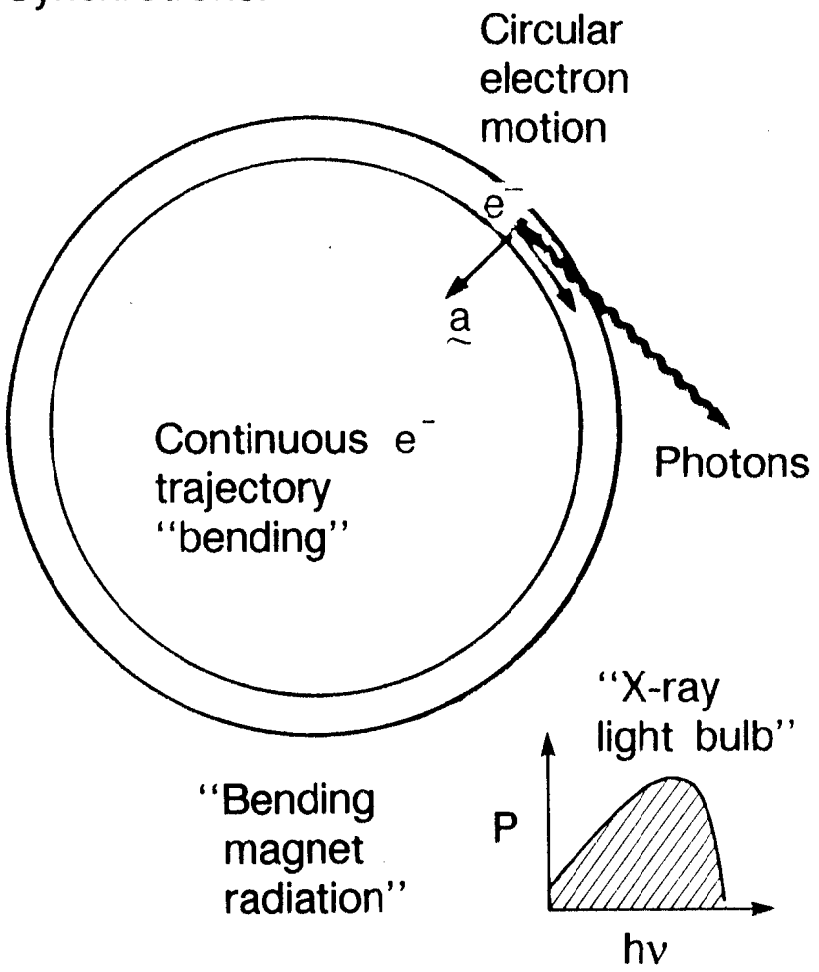

Tomorrows Synchrotrons:

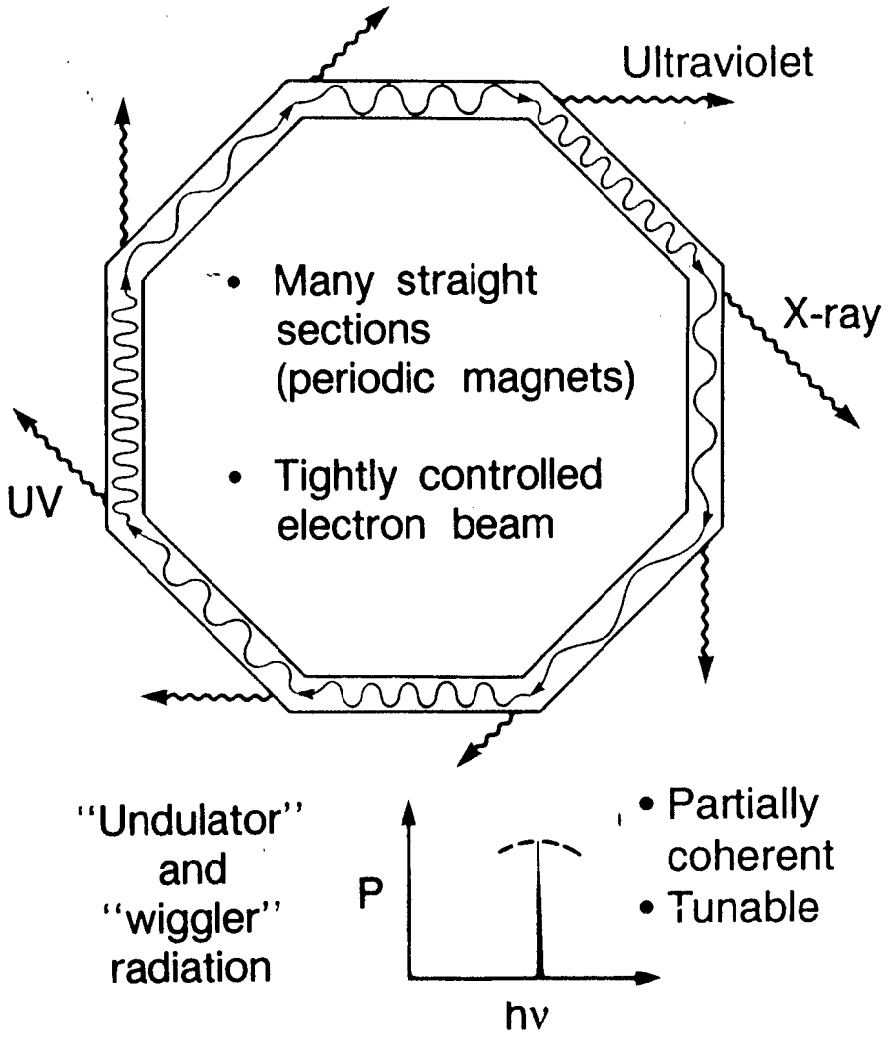

XBL 888-8937A

Coherent X-Rays, Tuneable Across A Broad Spectral Region, are Generated.

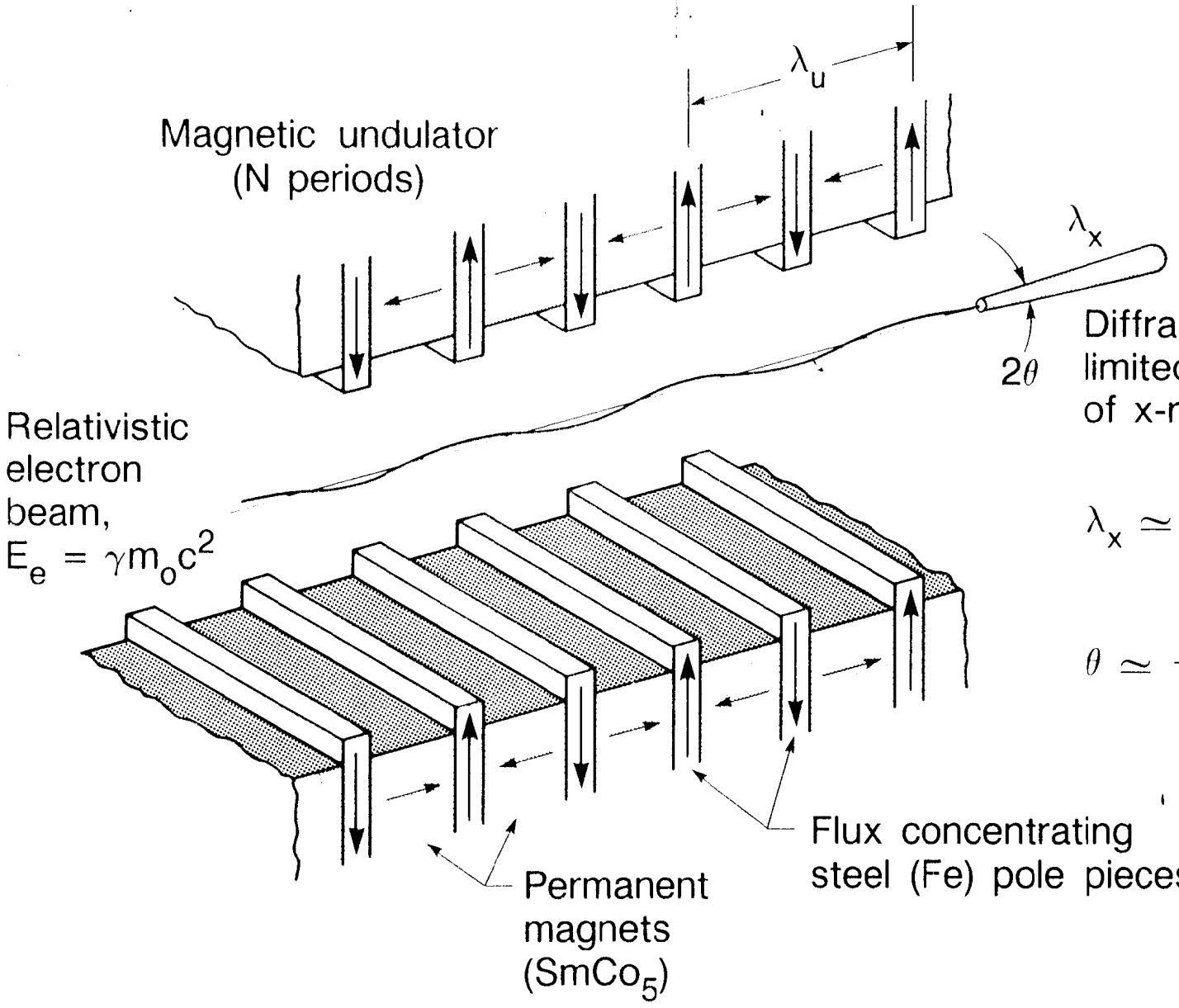

$$\lambda_x \simeq \frac{\lambda_u}{2\gamma^2}$$

$$\theta \simeq \frac{1}{\gamma\sqrt{N}}$$

XBL 831-7589B

Undulator Radiation

Laboratory Frame of Reference

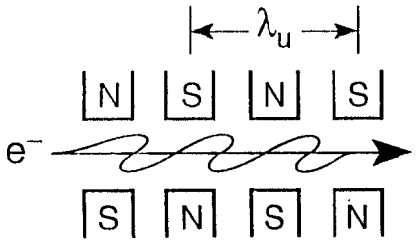

$E = \gamma m_0 c^2$

$$\gamma = \frac{1}{\sqrt{1 - \frac{v^2}{c^2}}}$$

N = # periods

Frame of Moving e^-

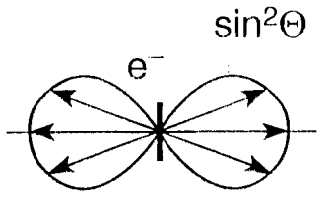

e^- radiates at the Lorentz contracted wavelength:

$$\lambda' = \frac{\lambda_u}{\gamma}$$

Bandwidth:

$$\frac{\lambda'}{\Delta\lambda'} \simeq N$$

Frame of Observer

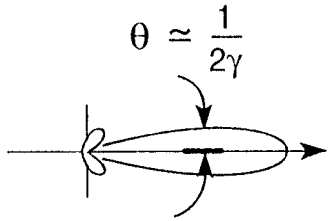

Doppler shortened wavelength on axis:

$$\lambda = \lambda'\gamma(1 - \beta\cos\theta)$$

$$\lambda = \frac{\lambda_u}{2\gamma^2}(1 + \gamma^2\theta^2)$$

More generally:

$$\lambda = \frac{\lambda_u}{2\gamma^2}\left(1 + \frac{K^2}{2} + \gamma^2\theta^2\right)$$

where $K = 0.93\, B_0\,(T)\, \lambda_u\,(cm)$

Following Monochromator

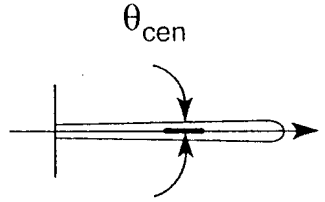

For $\frac{\Delta\lambda}{\lambda} \simeq \frac{1}{N}$

$$\theta_{cen} \simeq \frac{1}{\gamma\sqrt{N}}$$

typically

$\theta_{cen} \simeq 40\ \mu rad$

XBL 884-8870B

High Brightness Radiation Requires a High Brightness Electron Beam

- Many electrons
- ... all contained within a small divergence angle, $< \frac{1}{\gamma\sqrt{N}}$
- ... contained within a spatially small bunch
- ... passing through a long undulator

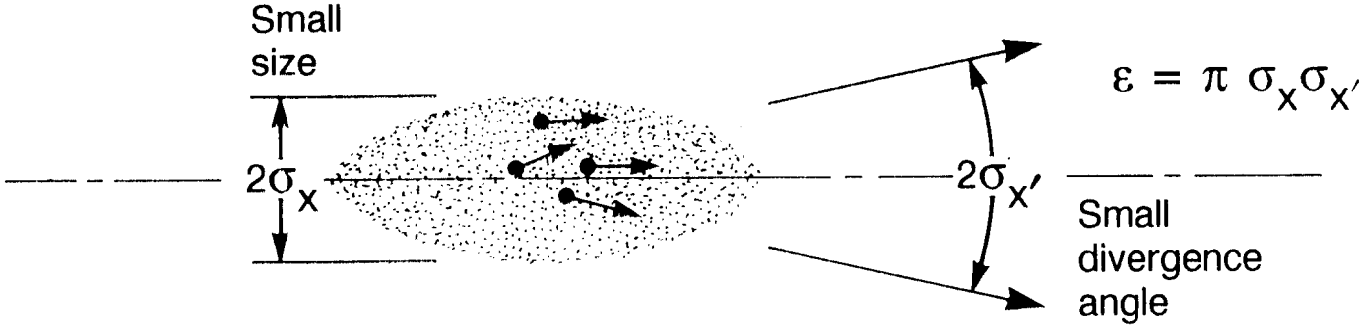

- The ALS is the first facility to be fully optimized for such radiation.

XBL 884-8871

Power in the Central Cone

$$\bar{P}_{cen} = \frac{\pi e K^2 \gamma^2 I}{\varepsilon_0 \lambda_u (1 + \frac{K^2}{2})^2} \qquad \begin{cases} K \leq 1 \\ n = 1 \end{cases}$$

where $K = \frac{eB_0\lambda_u}{2\pi m_0 c}$, $\left(\frac{\Delta\lambda}{\lambda}\right)_{cen} = \frac{1}{N}$, $\theta_{cen} = \frac{1}{\gamma\sqrt{N}}$

$$\gamma^* = \gamma / \sqrt{1 + \frac{K^2}{2}}$$

example: $\lambda_u = 3.65$ cm, $N = 123$,
$\gamma = 2936$, $I = 0.4$ Amp
$K = 0.52$, $B_0 = 0.15$ Tesla

$\lambda = 24$ Å (516 eV)
$\frac{\Delta\lambda}{\lambda} \simeq 1\%$
$\theta_{cen} = 33$ μrad
$P_{cen} = 1.1$ Watts

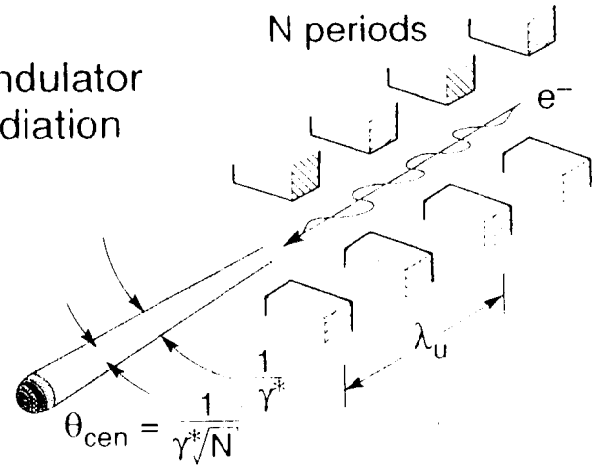

$$\lambda_x = \frac{\lambda_u}{2\gamma^2}(1 + \frac{K^2}{2} + \gamma^2\theta^2)$$

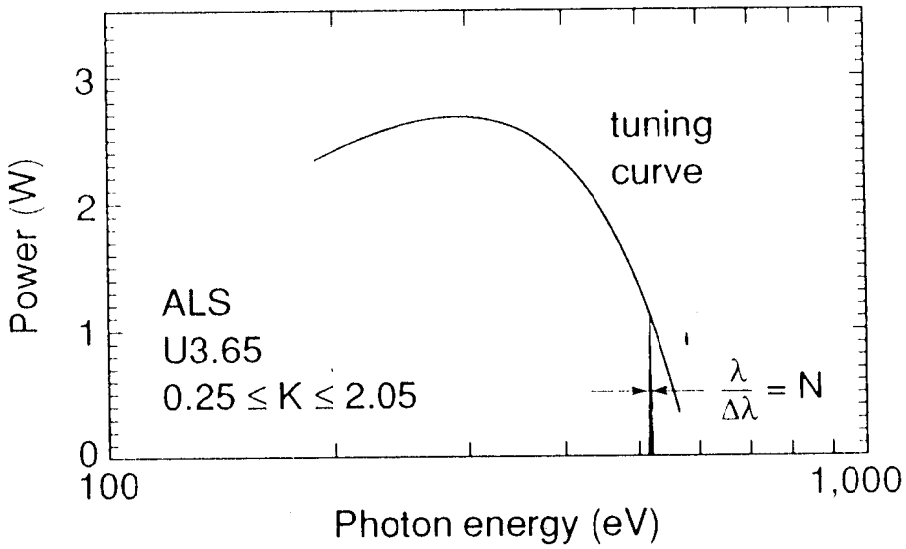

Coherent Power

Ratio of spatially coherent phase-space to total phase-space:

$$P_{coh} = P_{cen} \frac{(\lambda/2\pi)^2}{(d_x\theta_x)(d_y\theta_y)}$$

with a temporal coherence length $\ell_{coh} = \frac{\lambda^2}{2\Delta\lambda}$

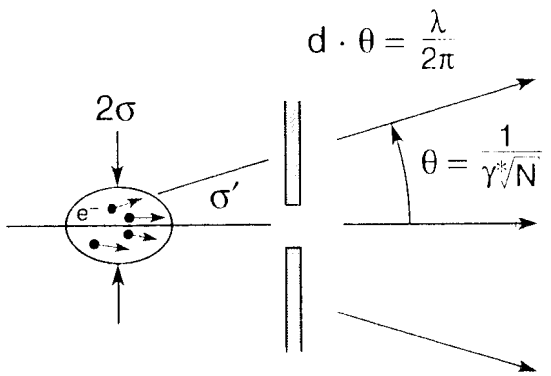

example:

λ_u = 3.65 cm, N = 123,
γ = 2936, I = 0.4 Amp
K = 0.52, B_0 = 0.15 Tesla

λ = 24 Å (516 eV)
$\frac{\Delta\lambda}{\lambda} \simeq 1\%$

θ_{cen} = 33 μrad
P_{cen} = 1.1 Watts
P_{coh} = 1.2 mW
ℓ_{coh} = 0.15 μm

With a monochromator for longer coherence length:

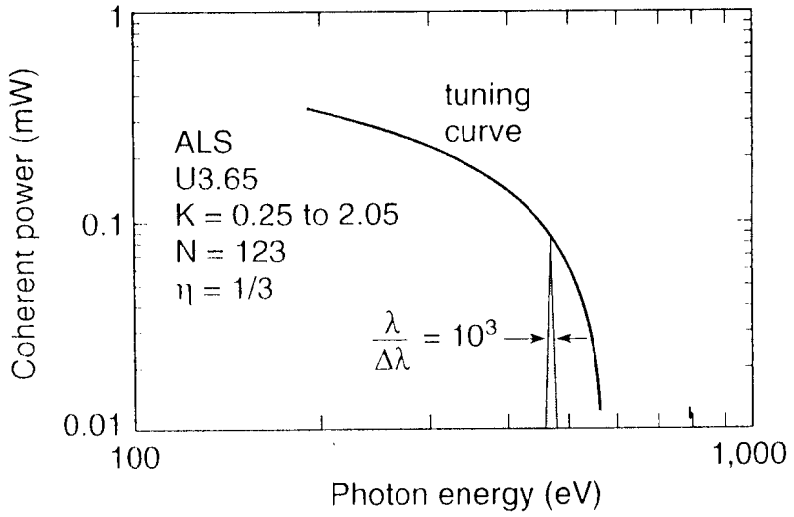

XBL 939-4835

Coherent Radiation at X-Ray and VUV Wavelengths

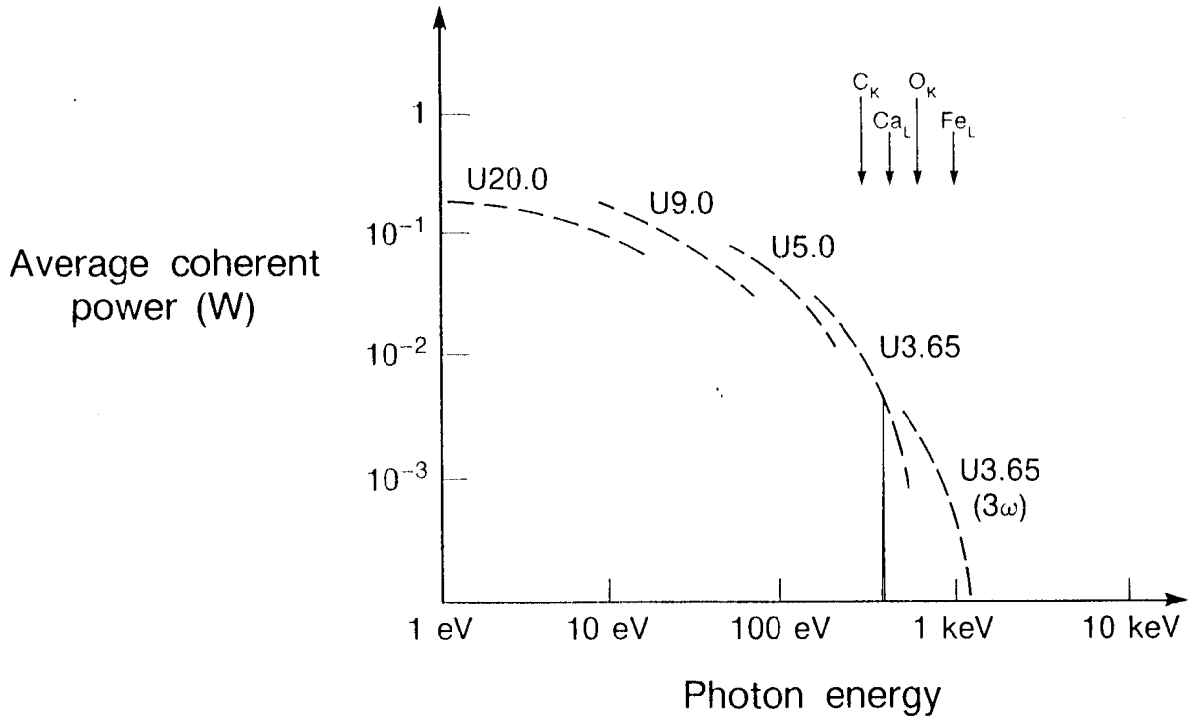

XBL 874-9024

ALS
@1.5GeV

14 June 1985, Volume 228, Number 4705 SCIENCE

Tunable Coherent X-rays

David Attwood, Klaus Halbach, Kwang-Je Kim

Summary. A modern 1- to 2-billion-electron-volt synchrotron radiation facility (based on high-brightness electron beams and magnetic undulators) would generate coherent (laser-like) soft x-rays of wavelengths as short as 10 angstroms. The radiation would also be broadly tunable and subject to full polarization control. Radiation with these properties could be used for phase- and element-sensitive microprobing of biological assemblies and material interfaces as well as research on the production of electronic microstructures with features smaller than 1000 angstroms. These short wavelength capabilities, which extend to the K-absorption edges of carbon, nitrogen, and oxygen, are neither available nor projected for laboratory XUV lasers. Higher energy storage rings (5 to 6 billion electron volts) would generate significantly less coherent radiation and would be further compromised by additional x-ray thermal loading of optical components.

The spectral region referred to as the XUV includes soft x-rays and ultraviolet radiation. Photon energies in this region extend from several electron volts (eV) to several thousand electron volts (keV). The primary atomic resonances of elements such as carbon, oxygen, nitrogen, and sodium, as well as resonances from many molecular transitions, appear in this region. In addition, the photon wavelengths in this region match important spatial scales such as the pitch and diameter of biochemical helices, the microstructural features of materials, and the dimensions of the next generation of electronic microcircuits.

The XUV spectral region has not been exploited to the degree warranted by these spectral and spatial features. In many ways it is a difficult region in which to perform experiments. Present XUV radiation sources are far more limited in intensity, tunability, and directionality than lasers, masers, and klystrons, which emit radiation of longer wavelengths. Optical techniques, including reflection, dispersion, and imaging, suffer from photoelectric absorptive effects in this region. Between the wavelengths of about 10 and 1000 angstroms (Å) there are no materials that are both transmissive and capable of supporting an atmosphere of pressure over macroscopic dimensions.

The authors are at the Center for X-ray Optics, Lawrence Berkeley Laboratory, Berkeley, California 94720

Substantial progress in the development of x-ray optical techniques has been made recently (*1–6*), largely as the result of the need for ever smaller microfabrication capabilities in the electronics industry, research on x-ray emitting, hot dense plasmas for nuclear fusion, and studies of interface formation in materials. For instance, imaging has been demonstrated with normal-incidence x-ray mirrors made with multilayer interference coatings (*1*). X-ray microscopes with diffractive Fresnel zone-plate lenses have produced element-sensitive images of biological systems, in some cases resolved to better than 1000 Å (*2, 8*). X-ray recording instruments with picosecond resolution, initially developed to study energy transport in hot dense plasmas (*9*), are now commercially available.

In order to extend scientific and technological opportunities, a bright source of tunable, partially coherent, XUV radiation is needed. Coherence, in the limited sense used here, refers to the ability to form interference patterns when wave fronts are separated and recombined. Partially coherent radiation is capable of producing clear interference patterns (fringes), but only within limited transverse or longitudinal displacement (*10*). The longitudinal displacement within which fringes can be formed is called the coherence length ℓ_c (*11*), which is given by the wavelength λ times the number of waves of coherence $\lambda/\Delta\lambda$ (spectral purity): $\ell_c = \lambda^2/\Delta\lambda$.

For experiments that utilize phase-sensitive techniques, such as x-ray interferometry and x-ray microholography, a radiation field with full spatial coherence and several micrometers (μm) of longitudinal coherence is often satisfactory. This corresponds to only a few hundred waves of coherence at a wavelength of 100 Å. Radiation with these properties is now attainable as a result of advances in accelerator physics and the development of permanent magnet undulators, structures that produce periodic magnetic fields. In the undulator a narrow beam of relativistic electrons, typically 200 μm in diameter and 50 microradians (μrad) in angular spread, interacts with periodic magnetic fields of precise phase variation to produce directed, tunable radiation, which has narrow spectral features and is nearly diffraction limited, at wavelengths throughout the XUV region (*12*).

Coherence Properties of Radiation from an Undulator

The interaction between an electron beam and a magnetic undulator is illustrated in Fig. 1. A narrowly confined beam of relativistic electrons (or positrons) with an energy equal to γ times the electron rest energy passes between magnets of alternating polarity in a high-fidelity undulator of periodicity λ_u. Ex-

NEW OPPORTUNITIES AT SOFT-X-RAY WAVELENGTHS

Advances in synchrotron radiation, x-ray lasers and x-ray optics permit new studies in the life and physical sciences at spatial resolutions of hundreds of angstroms.

David Attwood

A once dark region of the electromagnetic spectrum is now becoming very bright. The soft-x-ray spectral region, nominally extending from wavelengths of several angstroms to several hundred angstroms and including photon energies from tens of electron volts to several thousand electron volts, is providing many new research and development opportunities in the physical and life sciences and in industry. The move toward shorter wavelengths is driven in part by the desire to see and write smaller features. But the numerous and distinct atomic resonances in this region of the spectrum also provide for elemental identification and, in some cases, chemical sensitivity. (See the article by Bernd Crasemann and François Wuilleumier in PHYSICS TODAY, June 1984, page 34.) Developments in x-ray optics and new sources of high-brightness, partially coherent radiation make it possible to study materials and biological samples with feature sizes of several hundred angstroms.

With soft-x-ray microscopes, biologists can hope to see, in a near-native aqueous environment, structural features far beyond the resolving power of the visible-light microscope, and perhaps even motion. With recent soft-x-ray images discerning features as small as 300 Å in gold test patterns, we can envision the day when we gain new insights into the expression of genetic information encoded in DNA through observations of the higher-order packing and dynamics of chromatin in a near-native environment.[1] Figure 1a shows a chromosome image with 600-Å resolution, obtained at a wavelength of 24 Å.

In the physical sciences, new opportunities are arising in areas such as materials science, solid-state physics, electronic device physics and the industrial pursuit of nanoelectronic integrated circuits. X-ray photoemission microscopes are just becoming available to study elemental distributions and chemical states at material interfaces.[2] The possibility of studying quantum-confined transport in atomically defined channels with focused, spatially resonant excitation is just over the horizon. As the microelectronics industry moves toward faster, more compact electronic structures with feature sizes below 2000 Å, the need for shorter wavelengths is obvious. Nanoelectronic devices that have gate regions on the order of 1000 Å wide and 50 Å deep and whose charge transport depends on small quantities of both dopants and impurities will surely require new analytic tools combining spatial resolutions of several hundred angstroms and high chemical sensitivity. (See the article by Henry I. Smith and Harold G. Craighead in PHYSICS TODAY, February 1990, page 24.)

Optics and undulators

How has the soft-x-ray spectral region become so fertile for scientific and technological endeavors? The answer is that the requisite tools—thin windows, high-resolution lenses, optical coatings, lasers and undulators that generate x rays of high brightness and interesting coherence properties—are now becoming available.[3]

Advances in fabrication technology now make it possible to build the soft-x-ray equivalent of an early visible-light microscope. Materials scientists have contributed an ever improving capability to produce optical coatings comprising alternating layers of materials with

David Attwood is director of the Center for X-Ray Optics at Lawrence Berkeley Laboratory and professor in residence in the college of engineering at the University of California, Berkeley.

JOURNAL DE PHYSIQUE,
Colloque C6, supplément au n° 10, Tome 47, octobre 1986

PARTIALLY COHERENT RADIATION AT X-RAY WAVELENGTHS

D. ATTWOOD, K.J. KIM, N. WANG and N. ISKANDER

Center for X-Ray Optics, Lawrence Berkeley Laboratory, University of California, Berkeley, CA 94720, U.S.A.

Résumé - Dans le document, nous discutons les attributs du rayonnement cohérent partiel produit par les lasers de produits par lasers. Nous discutons les propriétés de cohérence spatiale et temporelle, les expériences liées à la microscopie de rayons-X et à la microholographie qui profitent de degrés variés de cohérence. Nous illustrons, pour les valeurs de crête et de moyenne, le rendement radiatif en fonction de la puissance cohérente et de la luminosité spectrale.

Abstract - In this paper we discuss the properties of partially coherent radiation generated by X-ray lasers, undulators, and laser produced plasmas. We discuss spatial and temporal coherence properties, experiments involving X-ray microscopy and microholography which benefit from varying degrees of coherence, and we illustrate radiative performance in terms of both coherent power and spectral brightness, for both peak and average values.

Introduction

In recent years we have seen a significant advance in the ability to generate coherent radiation at ever shorter wavelengths - now extending throughout the ultraviolet and into the x-ray region of the electromagnetic spectrum. These are particularly interesting spectral regions for applications in many scientific and technological disciplines. Because the wavelength is short, the radiation can be used to both "see" and "write" patterns of small feature size. Thus one can form high spatial resolution x-ray microscopes and microprobes and can fabricate yet more powerful integrated circuits. The photon energy is particularly interesting as it coincides with the many atomic and molecular transition resonances which pervade this region of the spectrum. The new accessibility of this region, provided both high brightness sources and requisite x-ray optics are available, will permit the utilization of many exciting techniques. Element specific bio-dynamics, site specific photochemical processing, polarization sensitive scattering studies of chiral structures, element specific studies of surface state formation, and dynamical studies of thin film and lattice structure formation are, to name a few, fields which would benefit from the unique capabilities of elemental sensitivity and high space-time resolution.

Coherence Requirements

An example of an experimental technique which would benefit many of the above cited sciences is that of an x-ray microprobe. As illustrated in figure 1, a Fresnel zone plate might be used to concentrate radiation in a small

focal spot area. The radiation could be used to probe, stimulate or scan any of a variety of chemically, physically or biologically interesting systems. The size of the focal region is dependent upon both the spatial and temporal properties of the incident radiation. For spatially coherent radiation a focal spot diameter (waist) of $2.4\Delta r$ will be obtained with a zone plate of outer zone width Δr. Resolution, as defined by Rayleigh, would be $1.2\Delta r$. A zone plate of outer zone width of 500 Å would give a focal spot diameter of approximately 1200 Å. To achieve this diffraction limited focusing it is necessary that the zone plate be perfect to a fraction of a wavelength, and that the radiation emanate from an uncertainty limited phase space characterized by $d \cdot \theta \simeq \lambda/2$. If the radiation is characterized by a larger phase space, the resulting focal spot will be proportionally larger and the resolution proportionally degraded. The zone plate microprobe also requires a degree of temporal (longitudinal) coherence, albeit modest. In order to avoid blurring of the focal region by chromatic aberration, the radiation must possess a coherence length (distance over which interference effects are significant) $\ell_c = \lambda^2/\Delta\lambda$, at least as large as the coherence requirements of the zone plate, $N\lambda/2$, where N is the number of Fresnel zones. Generally this is a modest requirement: with $N \simeq 500$ and $\lambda \simeq 30$ Å, one requires $\ell_c \simeq 1\mu m$.

A somewhat more demanding experiment is that of off-axis x-ray microholography, as illustrated in figure 2. In this case the ZP does not form an image in the recording plane, but rather it gathers the high frequency (large angle) scattered radiation (containing details of the smaller sample features) and directs it back toward the recording medium where it is encoded through interference with a plane or spherical reference wave generated by the nearby diffraction grating. The scattered radiation is thus heterodyned by the reference wave, with a carrier spatial frequency roughly that of the grating, allowing use of a lower resolution but more sensitive recorder (perhaps x-ray film) than would otherwise be possible. Both spatial and temporal coherence requirements are more demanding in the holographic case, requiring spatially coherent illumination over a field wider by some factor, and a temporal coherence length increased by that factor squared, e.g. if the grating extends laterally to a distance of five ZP radii, then the temporal coherence must be increased by a factor of twenty-five. Thus one would require full spatial coherence and a longitudinal coherence of 20 μm.

Radiation Sources

The generation of partially coherent radiation, combined with requisite spatial and temporal filtering, can be achieved in several ways. Figures 3-5 illustrate an atomic laser, a magnetic undulator, and a laser-produced, hot-dense plasma emitting x-rays into 2π steradians. All three can generate radiation at XUV wavelengths, and perhaps it can be said that all are partially coherent - certainly all could be used as the source of radiation in figures 1 and 2. The differences are the degree of coherence, determining the amount of spatial and temporal filtering required for a particular application; the average and peak power produced; and the shortness of the wavelength and its nearness to the atomic and molecular resonances of interest.

Radiative Performance

In figures 6-8 we show generated coherent power and spectral brightness, for both average and peak values, and for a variety of spectral widths (coherence lengths). In the estimates of coherent power, only that portion of the radiation within $d \cdot \theta \simeq \lambda/2$ is accepted, such that full spatial coherence would result. In addition, perfect optics are assumed - no aberrations, 100% efficiency. The need for several illustrations is due to the wide variety of applications one can envision, some requiring minimal coherence, others requiring substantial coherence. Upon inspection one readily sees that each of the radiation sources has its own advantages.

Summary of Discussion

Attwood talk:

Moffat asked about extending the longitudinal coherence length by using a monochromator. Attwood stressed that one can always (in principal) increase the coherence length with monochromatization, but one does so at the expense of flux. In planning an experiment, one should try not to use more coherence than is necessary.

Carr asked whether, in x-ray microscopy, the resolution is limited by the size of the pinhole or the size of the zone plate. Attwood replied that in most practical systems, the size of the zone plate limits the resolution.

Remarks on Coherence

Kwong-Je Kim, LBL

COHERENCE PROPERTIES OF THE LCLS RADIATION

Kwang-Je Kim
Lawrence Berkeley Laboratory

In LCLS, the radiation is generated by bright electron beams passing through a long undulator. Initially, the radiation characteristics are the same as the usual undulator radiation, and the intensity is proportional to the number of electrons. As the beam propagates further down the undulator, the radiation field interacts with the beam, causing modulation in the beam density. The density-modulated beams radiate more strongly, and the higher radiation intensity, in turn, causes stronger modulation, and so on. Thus, the radiation intensity increases exponentially, eventually saturating at a level which is many orders of magnitude higher than that expected from usual undulators. Such a radiation is called the Self-Amplified-Spontaneous Emission (SASE).

The coherent properties of SASE can be discussed in two parts, the temporal coherence and the transverse coherence. The temporal coherence can be summarized by saying that the relative bandwidth of the SASE is about ρ; the dimensionless FEL-strength parameter for LCLS is about 10^{-3}. Thus, the coherence length is about 1000λ, where λ is the SASE wavelength. A packet of SASE radiation consists of many wave trains, each of which is about one coherence length long. The wave trains are randomly distributed within the length of the electron bunch.

The transverse coherence properties depend on the relation between the electron beam emittance $\varepsilon_x = \sigma_x \sigma_{x'}$, where σ_x and $\sigma_{x'}$ are, respectively, the rms size and angle of the electron beam and the radiation wavelength. In general, it is necessary to require $\varepsilon_x \leq \lambda/4\pi$ in order to ensure high gain. If this condition is satisfied, the SASE radiation is completely coherent transversely; it consists of a single transverse mode. High-gain SASE is also possible, even if the above condition is not satisfied, so that $\varepsilon_x > \lambda/4\pi$. In that case, there may be several transverse modes present with random phase with respect to each other. For the parameters of LCLS, the calculation shows that the SASE is completely dominated by a single mode for wavelengths in the water window range. Even in wavelengths as short as a few Angstroms, it is expected that the radiation is still highly coherent transversely.

Evolution of SASE

Kim 6

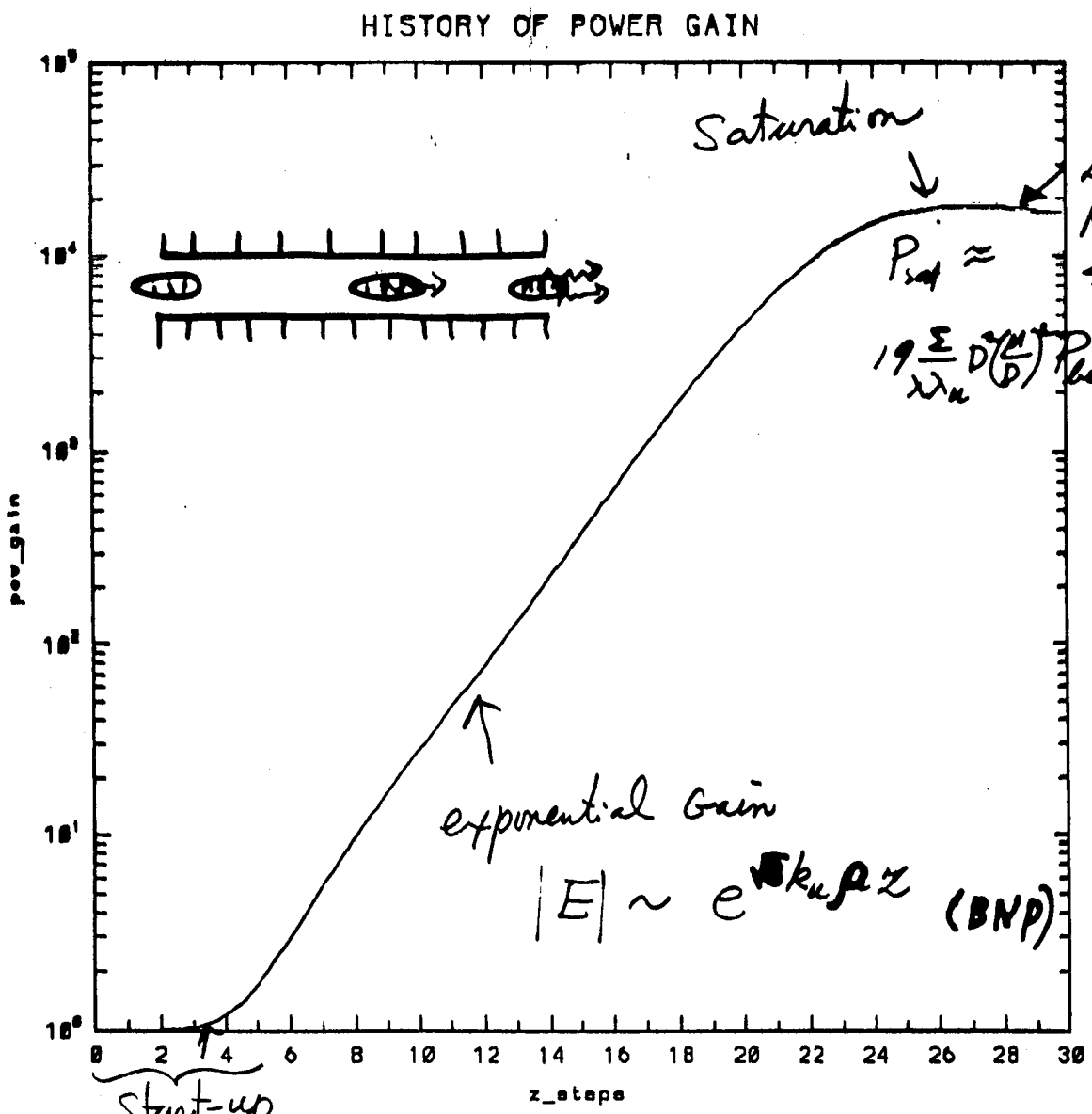

Self-Amplified-Spontaneous-Emission (SASE)

- **Power amplification along the undulator in exponential gain regime:**

  e^{z/L_G} z = length along the undulator

  L_G = power gain length.

- **Total amplification up to 10^8**

→ **Initial noise will amplify to intense, coherent radiation**

$$\frac{dP}{d\omega} = \left(\frac{dP}{d\omega}\right)_{noise} e^{z/L_G}\, S(\omega)$$

$\left(\frac{dP}{d\omega}\right)_{noise}$ = spontaneous solution emitted in one gain length (L_G)

$S(\omega)$ = spectral shape

10 - 50 GW!

Temporal mode profile

Coherence length l_c

$\approx \frac{\lambda}{\rho} \sim 1000\lambda$

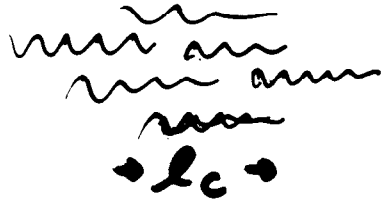

Electron Beam Evolution

(I) Undulator Regime

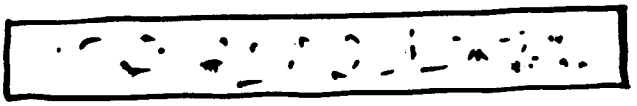

$\longleftarrow \ell \longrightarrow$

N_e electrons randomly distributed

$$\left| \sum_{\text{all } e_s} e^{i\theta_i} \right|^2 \approx N_e$$

(II) AT saturation (after $N \sim \frac{1}{\rho}$ periods)

$\longleftarrow \ell \longrightarrow$

bunched regions of length

$$l_c \approx \frac{\lambda}{\rho} \approx \lambda N$$

The phases between different bunched regions are random

$$\left| \sum e^{i\theta_i} \right|^2 = \left| \sum_k \sum_{\text{bunch } k} e^{i\theta_i} \right|^2$$

$$= \left(\frac{dN_e}{dz} \frac{\lambda}{\rho} \right)^2 \cdot \frac{\ell}{\frac{\lambda}{\rho}}$$

$$= \left(\frac{dN_e}{dz} \right)^2 \frac{\lambda \ell}{\rho} = N_e \cdot \left(\frac{dN_e}{dz} \frac{\lambda}{\rho} \right)$$

$$= N_e N_{ec}$$

Coherence & phase space

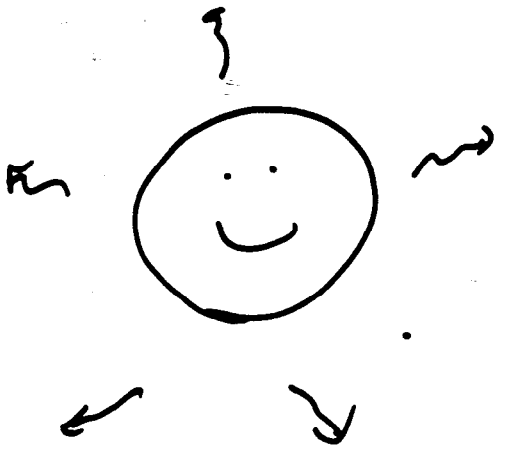

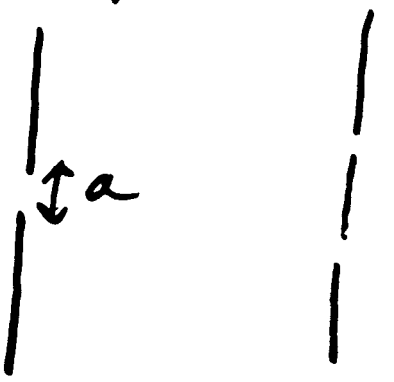

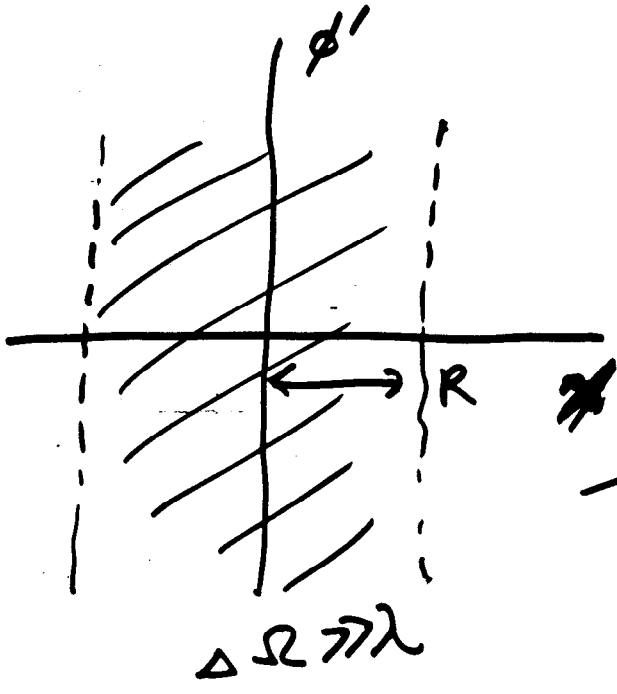

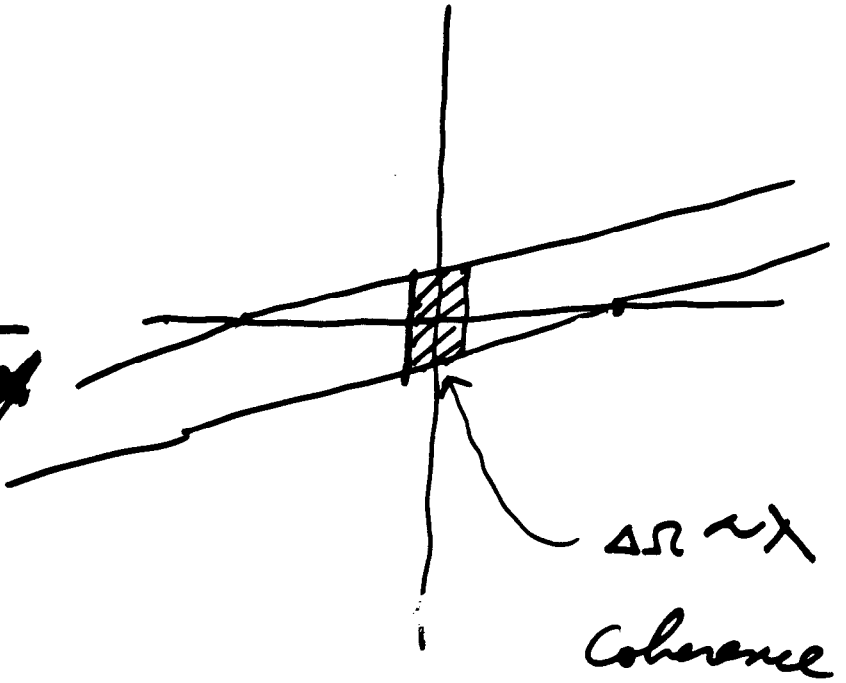

Coherence

Coherence criteria

phase space area $\Omega \lesssim \lambda$

Ming Xie

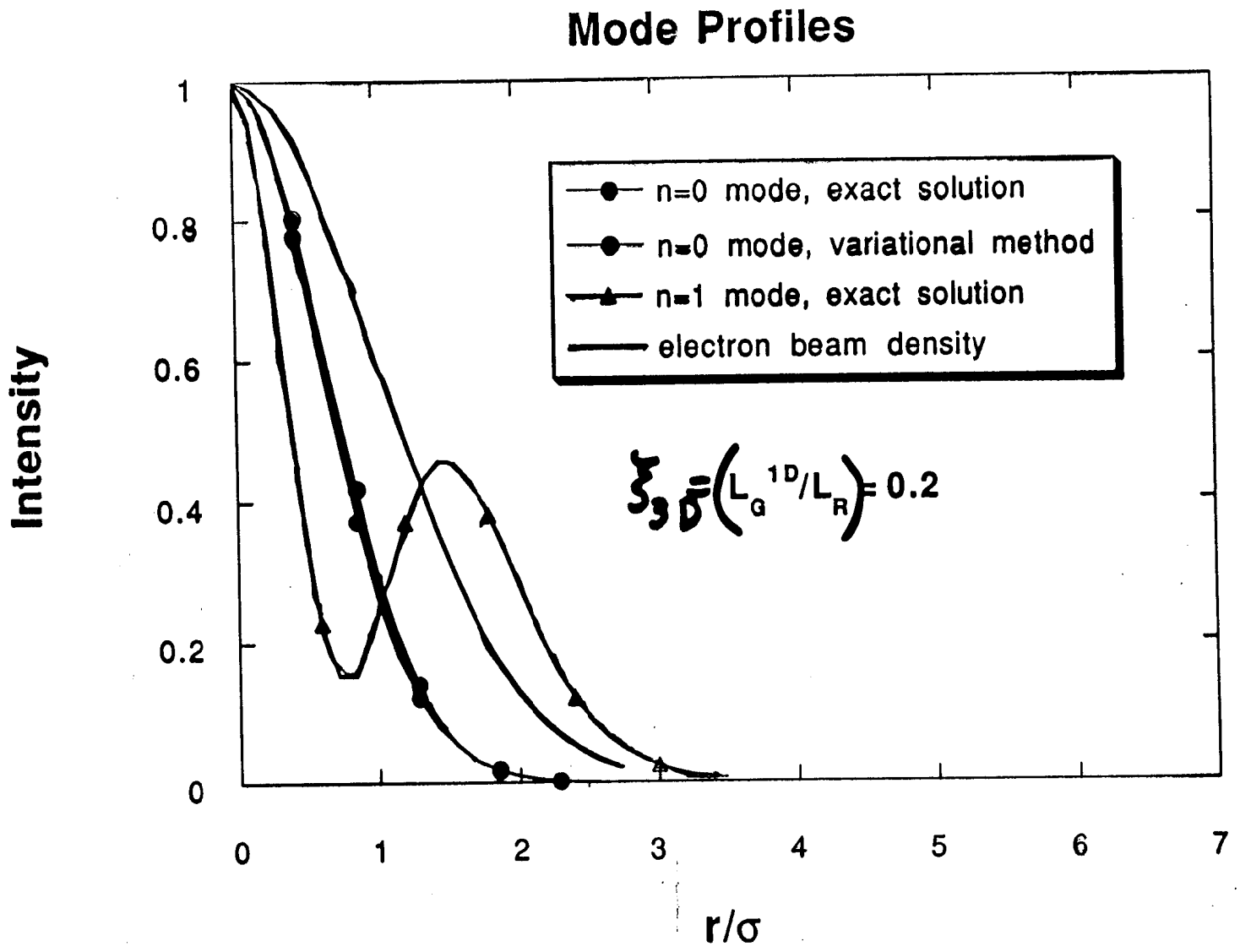
Mode Profiles
Intensity
1
0.8
0.6
0.4
0.2
0
0
1
2
3
4
5
6
7
r/σ
n=0 mode, exact solution
n=0 mode, variational method
n=1 mode, exact solution
electron beam density
$\bar{\xi}_3 \bar{\delta} = (L_G^{1D}/L_R) = 0.2$

Transverse mode profile

- Optical guiding

  Transverse mode is guided by electron beam without diffraction.

- For high gain, generally requires

$$\sigma_x \sigma_{x'} \lesssim \frac{\lambda}{4\pi}$$

$\sigma_x \sigma_{x'}$: electron beam phase space area

$\frac{\lambda}{4\pi}$: radiation beam phase space area

→ **single transverse mode or diffraction limited complete transverse coherence**

- Sometimes high Gain is possible with

$$\sigma_x \sigma_{x'} > \lambda/4\pi \sim 10^{-11}$$

2×10^{-11}

→ several transverse modes are degenerate

partial coherence.

1.85 Å, 25 GeV

Growth Rate for Higher Order Modes

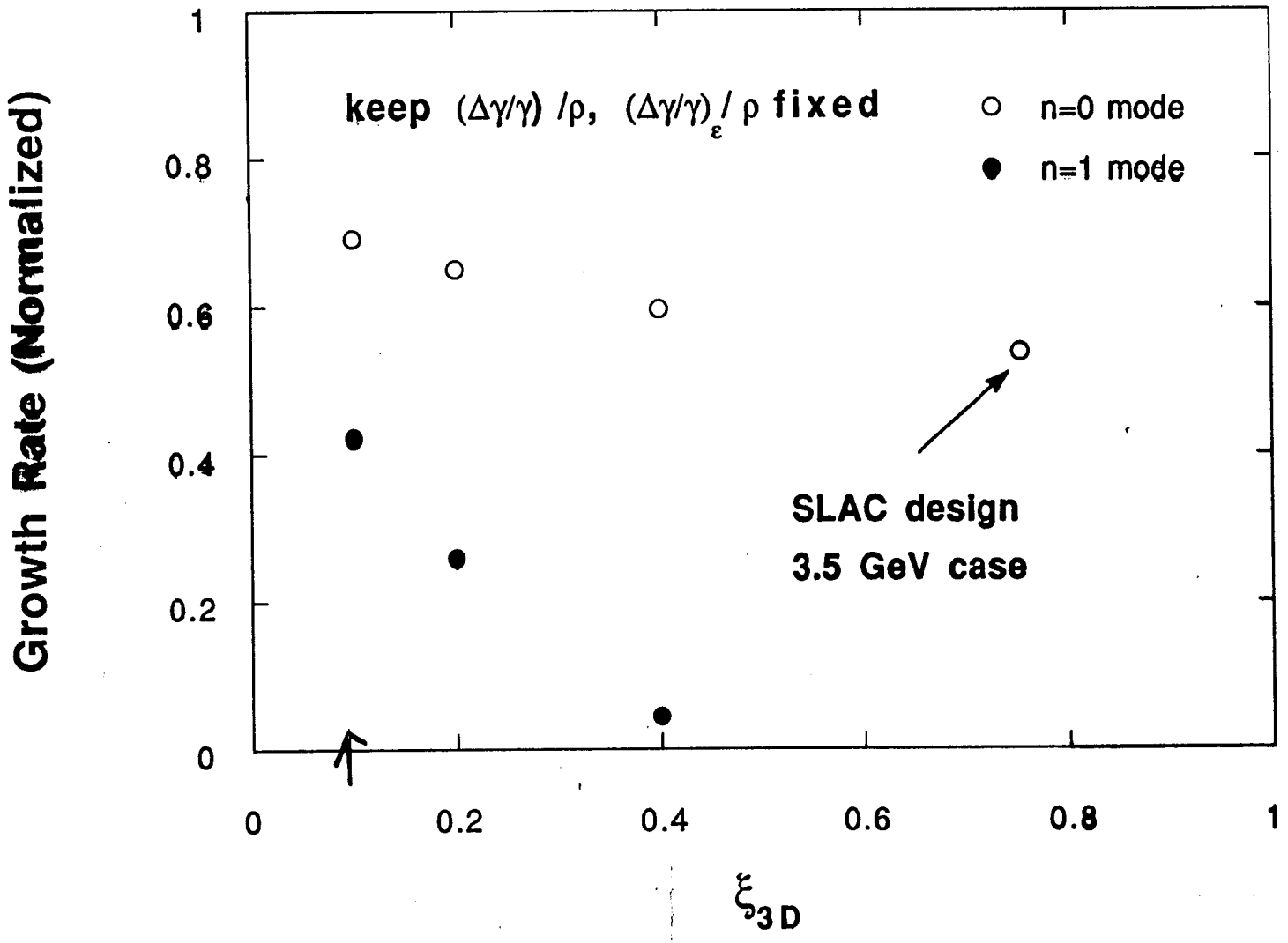

Summary of Discussion

Kim talk:

Chu and others asked about the amounts of FEL radiation occurring in higher order modes, relative to the fundamental mode. Kim and Pellegrini explained that the gain coefficient for the third harmonic is smaller by about a factor of two than the gain coefficient of the fundamental, and that the gain coefficients for higher order modes are much smaller than that. In the SLAC LCLS design, the only modes with appreciable amplification are the fundamental and the third harmonic, and the third harmonic is far from saturation. Therefore the intensity of the third harmonic is less than the fundamental by about a factor of 30.

Time Correlation Spectroscopy with Coherent Hard X-rays

Brian Stephenson, IBM Research Laboratory

Time Correlation Spectroscopy Using Coherent Hard X-rays

G. B. Stephenson
IBM Research Division
Yorktown Heights, NY, 10598-0218, USA

One of the exciting new developments made possible by the high brilliance of undulator x-ray sources is the emergence of techniques using coherent x-rays. The technique of time correlation spectroscopy (TCS) has been widely used with coherent visible light to study the dynamics of processes such as critical fluctuations near phase transitions in fluids and the diffusion of particles in liquids. [1] However, visible light cannot be used to probe processes occurring on length scales smaller than about 100 nm. By employing a high-brilliance x-ray source it should be possible to study atomic-scale dynamics with TCS using coherent x-rays. The development of this technique will provide a powerful new probe which promises to have great impact on many of the most important problems in statistical physics, *e.g.;* liquid crystals, order in alloys, charge density waves, quasicrystals, low-dimensional systems, amorphous systems, diffusion of defects, and dynamic critical phenomena.

To understand the unique nature of the information that can be obtained using TCS with hard x-rays, one must understand the difference between a scattering experiment using a coherent beam and one using an incoherent beam. Under coherent illumination, disorder in the atomic configuration of the sample at any instant gives rise to a random diffraction or "speckle" pattern modulating the far-field diffraction. If the atoms in the scattering volume were strictly stationary, the speckle pattern would, of course, not change with time. In general, however, the atomic configuration will be changing, *e.g.;* due to equilibrium fluctuations in the disorder at finite temperature. One can therefore directly observe the dynamics of such processes by monitoring the resultant changes in the intensity of the speckle pattern as a function of time. The development of TCS using coherent x-rays will make it possible to observe the dynamics of atomic-scale equilibrium thermal fluctuations. In contrast, standard time-resolved scattering techniques using incoherent x-rays are inherently insensitive to the dynamics of such fluctuations, and can only be used to study changes in average properties (such as correlation lengths) in non-equilibrium systems (*e.g.;* following a temperature quench).

In an experiment carried out on the X-25 wiggler beamline at NSLS [2], we demonstrated that it is possible to use pinhole collimation to generate a coherent x-ray beam. This was accomplished by measuring the Fraunhofer diffraction from micron-size pinholes. Using this coherent x-ray beam, we further demonstrated that a speckle pattern can be observed in the diffuse (001) peak from a static anti-phase domain structure in Cu_3Au. Since then, we have begun to attempt x-ray TCS measurements at NSLS and at ESRF. [3] Currently, the major challenges to making such measurements are in obtaining a coherent incident beam of sufficient intensity and in finding a strongly-scattering system with disorder on an appropriate length scale evolving on an appropriate time scale. Although significant progress will be possible when the third-generation x-ray synchrotrons become fully operational, the signal rate will be low enough that the study of time scales as short as milliseconds will only be possible in favorable systems. In contrast, the dramatically (10^5 X) higher coherent flux provided by LCLS will allow study of the systems of greatest interest (*e.g.;* with shortest correlation lengths) on faster time scales. Indeed, the pulsed structure of the LCLS should allow complete speckle patterns to be obtained from the x-rays in a single 100 fs pulse. By developing beam-splitting and path-length-delay techniques, such unprecedented time resolutions should be possible not only for standard time-resolved (incoherent) techniques, but also for TCS using coherent x-rays. This will in principle allow the observation of the dynamics of thermal motion, phonon propagation, etc.

[1] P.N. Pusey, in "Photon Correlation Spectroscopy and Velocimetry", H.Z. Cummins and E.R. Pike eds., Plenum, New York (1977), 45-141.

[2] M. Sutton, S.G.J. Mochrie, T. Greytak, S.E. Nagler, L.E. Berman, G. A. Held, and G.B. Stephenson, "Observation of Speckle by Diffraction with Coherent X-rays," *Nature*: **352** 608 (1991).

[3] G. Gruebel, J. Als-Nielsen, D. Abernathy, G. Vignaud, S. Brauer, G.B. Stephenson, S.G.J. Mochrie, M. Sutton, I.K. Robinson, R. Fleming, R. Pindak, S. Dierker, and J.F. Legrand, "Scattering with Coherent X-rays," *ESRF Newsletter*, January 1994.

Time Correlation Spectroscopy Using Coherent Hard X-rays

Brian Stephenson
IBM Research

Collaborators:

Steve Brauer, Glenn Held, *IBM Research*
Ralf Bruning, Eric Dufresne, Mark Sutton, *McGill Univ.*
Carol Thompson, *Polytechnic Univ.*
Simon Mochrie, *MIT*
Robert Fleming, Ron Pindak, *AT&T Bell Labs*
Ian Robinson, *Univ. of Illinois*
Steve Dierker, *Univ. of Michigan*
Steve Nagler, *Univ. of Florida*
Stuart Brown, *UCLA*
Lonny Berman, *National Synchrotron Light Source*
Randy Headrick, *Cornell High Energy Synchrotron Source*
Brian Rodricks, *Advanced Photon Source*
Jens Als-Nielsen, Gerhart Gruebel, *ESRF*

OUTLINE

- UNIQUE CAPABILITIES OF COHERENT X-RAYS

  Scattering with Coherent Light:

  > *Resolution and Coherence*

  > *Speckle from Disordered Systems*

  X-ray Intensity Fluctuation Spectroscopy:

  > *Dynamics of Atomic-Scale Disorder*

  Example: Equilibrium Fluctuations in Ordered Alloys

  > *Simulation of Dynamics: Real and Reciprocal Space*

- EXPERIMENTAL STATUS

  > *Producing a Coherent X-ray Beam: Source Brilliance*

  > *Studies of Domain Growth in Cu_3Au*

  > *Optics to Tune Coherence Length*

- ADVANTAGES OF LCLS FOR XIFS

  > *Time Resolution > Repetition Rate (10 ms)*

  > *Time Resolution > Pulse Width (100 fs)*

Resolution and Coherence

Scattering with a coherent beam $\Rightarrow$
Coherence length as large as sample size

$$d_{coh} \geq L$$

Equivalent to:
Wavenumber uncertainty small enough to resolve correlations as large as L

$$\Delta q \leq \frac{2\pi}{L}$$

or, high angular resolution

$$\Delta\theta \leq \sim \frac{\lambda}{2L}$$

Scattering from a Disordered System

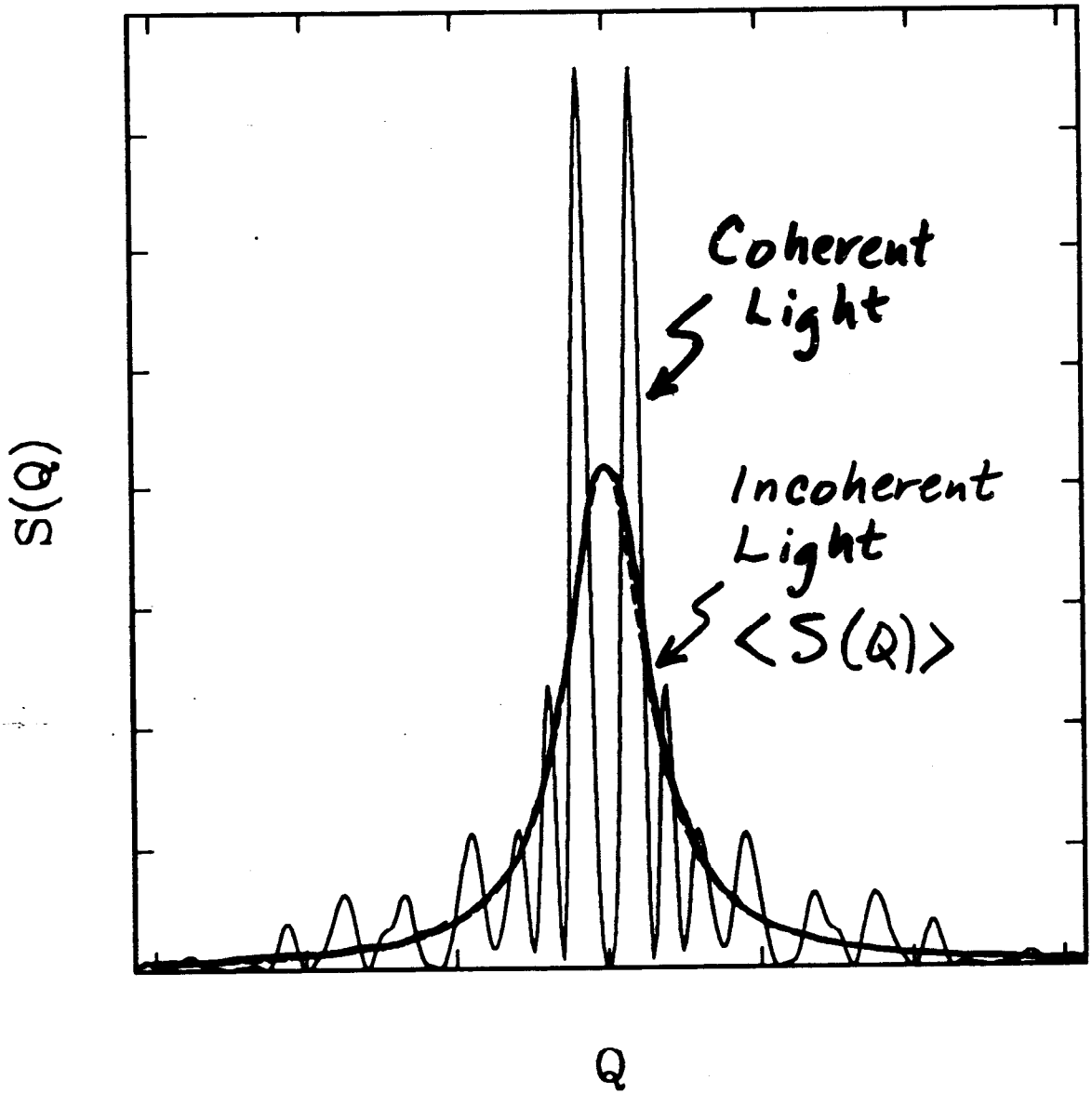

- Speckle pattern depends on exact arrangement of domains, not just domain size distribution
- If incident light is not coherent, resolution is insufficient to observe speckle pattern

Domain Size Distribution:

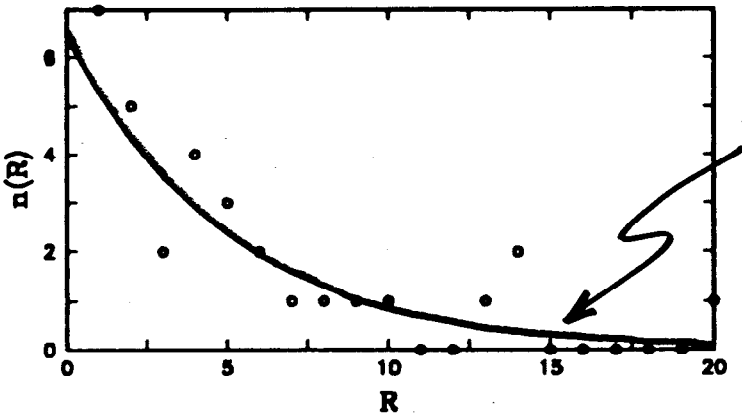

$\langle n(R) \rangle$

An Actual Domain Arrangement:

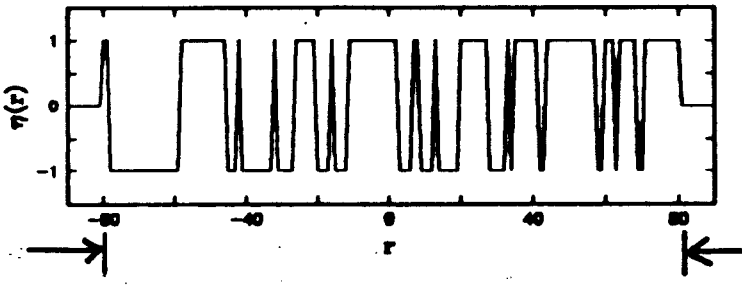

Sample Size
L

Scattering Pattern from Domains:

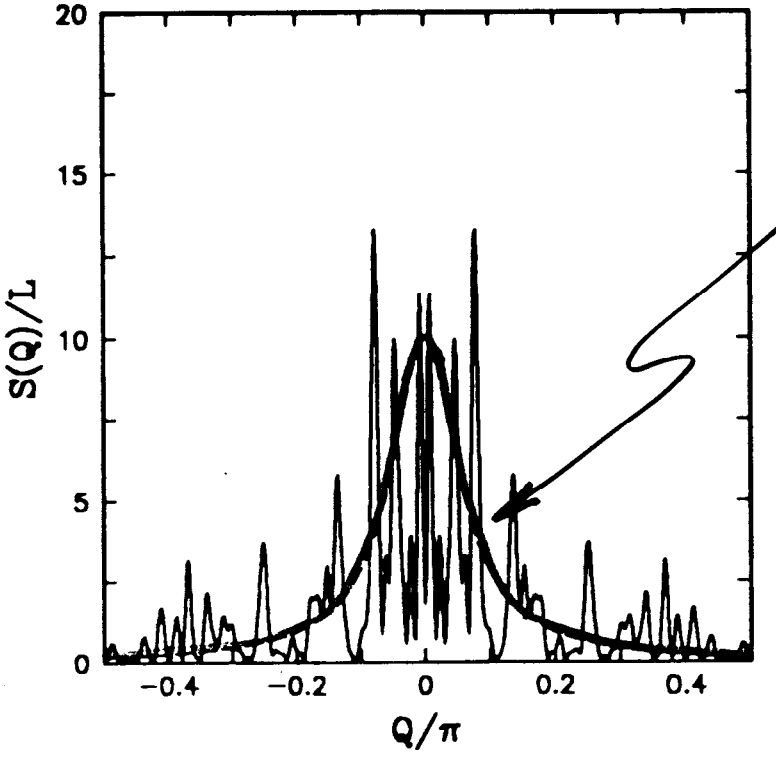

$\langle S(Q) \rangle$

Intensity Fluctuation Spectroscopy

Motion of sample domains

⇒ motion of speckle

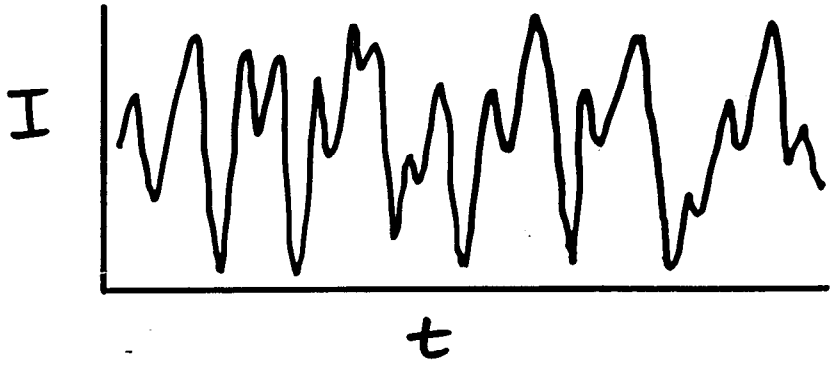

Time autocorrelation function of intensity gives information about <u>equilibrium</u> dynamics

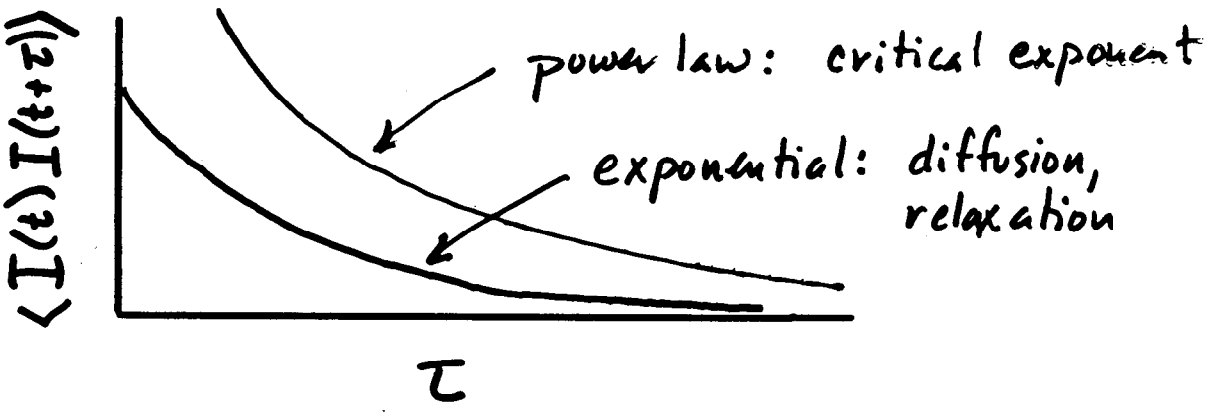

The ability to use X-rays will allow the study of length scales Å → μm

Intensity Fluctuation Spectroscopy

- Well-developed technique using visible light (lasers)
- Used to study dynamics of processes such as
  - density fluctuations near critical points
  - diffusion of particles in fluids
- Visible light ($\lambda = 4000\mathring{A}$)
  cannot be used for length scales smaller than 2000 Å
- Use of x-rays ($\lambda = 1\mathring{A}$) would allow study of dynamics of atomic-scale fluctuations
- Potentially of great impact on many of the most important problems in statistical physics:
  - order in alloys, liquid crystals, etc.
  - charge density waves
  - quasicrystals
  - low-dimensional systems
  - amorphous systems
  - diffusion of defects
  - dynamic critical phenomena
- Such dynamics can not be studied by conventional time-resolved scattering with incoherent x-rays, which is sensitive only to the ensemble average

Producing a Coherent Hard X-ray Beam

Longitudinal coherence length:

$$\ell_{coh} = \frac{\lambda}{2} \frac{\lambda}{\Delta\lambda}$$

Determined by monochromator; typically 0.5 μm

Transverse coherence length:

$$d_{coh} = \frac{\lambda}{2} \frac{R_{source}}{d_{source}}$$

Determined by collimation; typically 10 μm

Transversely coherent flux: $F_{coh} = \left(\frac{\lambda}{2}\right)^2 \times$ *Brilliance*

1.24 Å (10 keV) X-ray Source:	NSLS Wiggler	APS Undulator	LCLS Undulator
Brilliance (ph/s/mm^2 /mrad^2/10$^{-4}\Delta\lambda/\lambda$)	3×10^{14}	1.5×10^{17}	10^{22}
F_{coh} (ph/s/10$^{-4}\Delta\lambda/\lambda$)	1.2×10^{6}	6×10^{8}	4×10^{13}

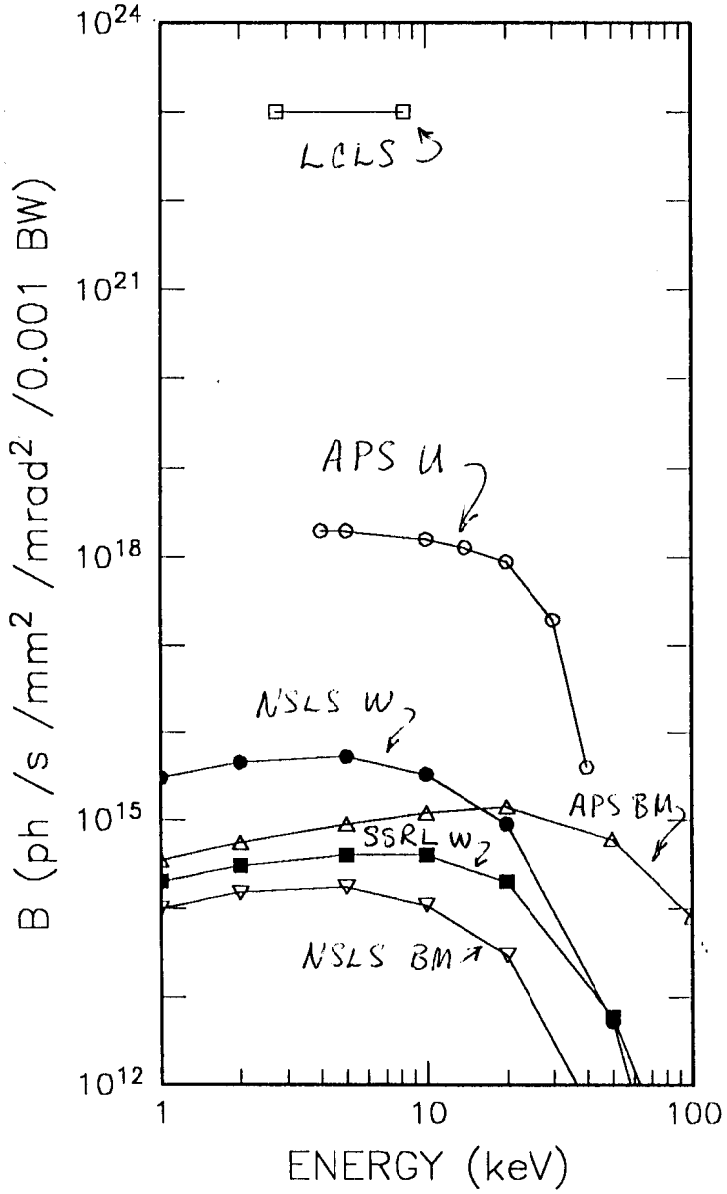
10^{24}
10^{21}
10^{18}
10^{15}
10^{12}
B (ph /s /mm^2 /mrad^2 /0.001 BW)
LCLS
APS U
NSLS W
SSRL W
APS BM
NSLS BM
1
10
100
ENERGY (keV)

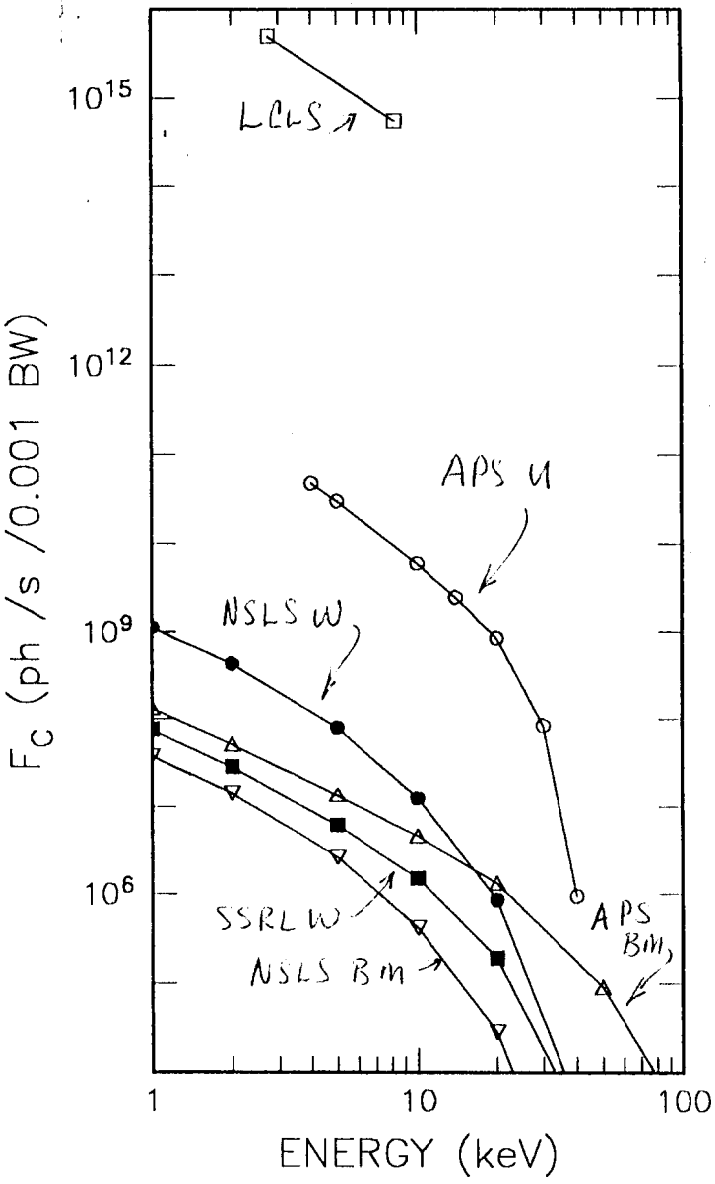
10^{15}
10^{12}
10^{9}
10^{6}
F_c (ph /s /0.001 BW)
LCLS
APS U
NSLS W
SSRL W
NSLS BM
APS BM
1
10
100
ENERGY (keV)

Use of Incoherent X-ray Source:

Resolution / Coherence Requirements for Incident Beam

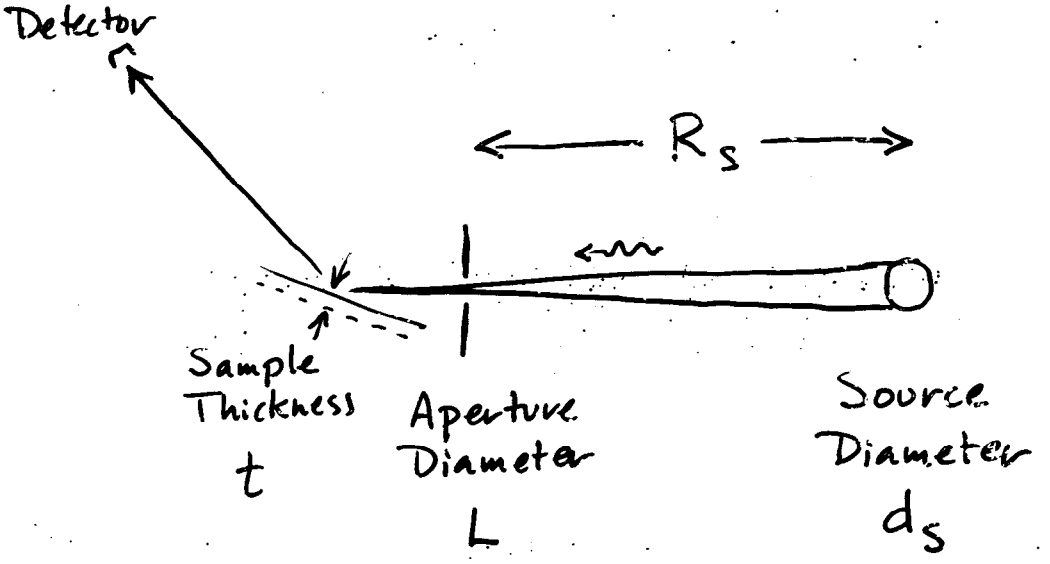

$$L \leq d_{coh} \equiv \frac{\lambda}{2} \frac{R_s}{d_s}$$

$$2t\sin\theta \leq l_{coh} \equiv \frac{\lambda}{2} \frac{\lambda}{\Delta\lambda}$$

Scattering Geometry using micron-sized pinholes

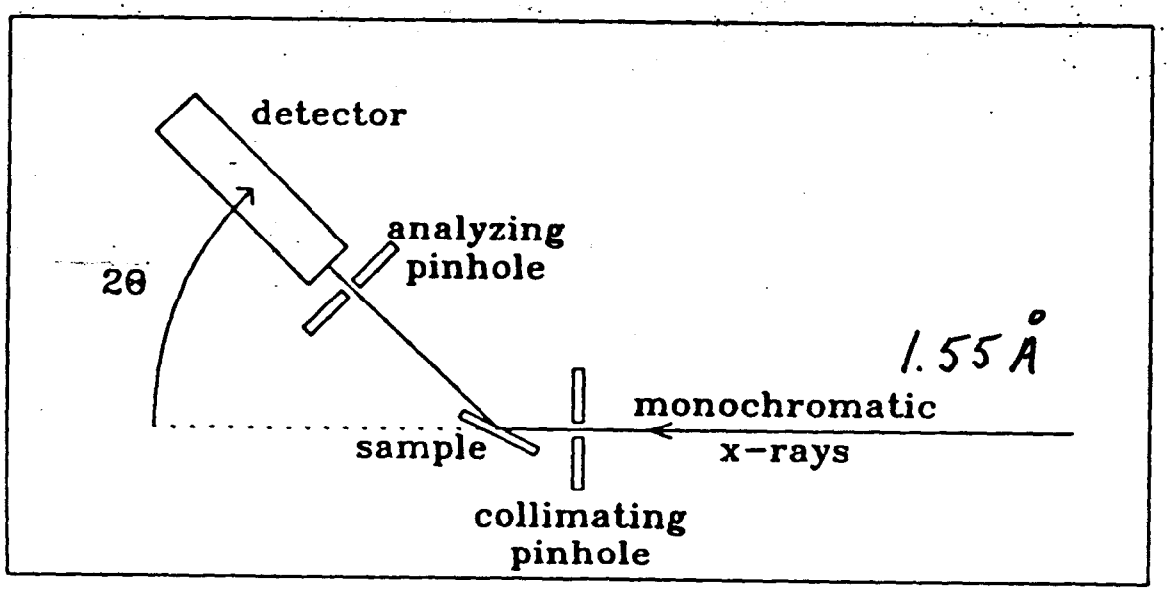

Analyser resolution:

each "speckle" subtends $\Delta(2\theta) \doteq \frac{\lambda/2}{L}$

For $L = 5\,\mu m$, $\Delta(2\theta) = 15\,\mu rad$

Fraunhofer Patterns from Circular Pinholes
demonstrating 10 μm coherence length of undulator x-ray beam
(11.8 keV, horizontal source size apertured to equal vertical, ESRF TROIKA 11/93)

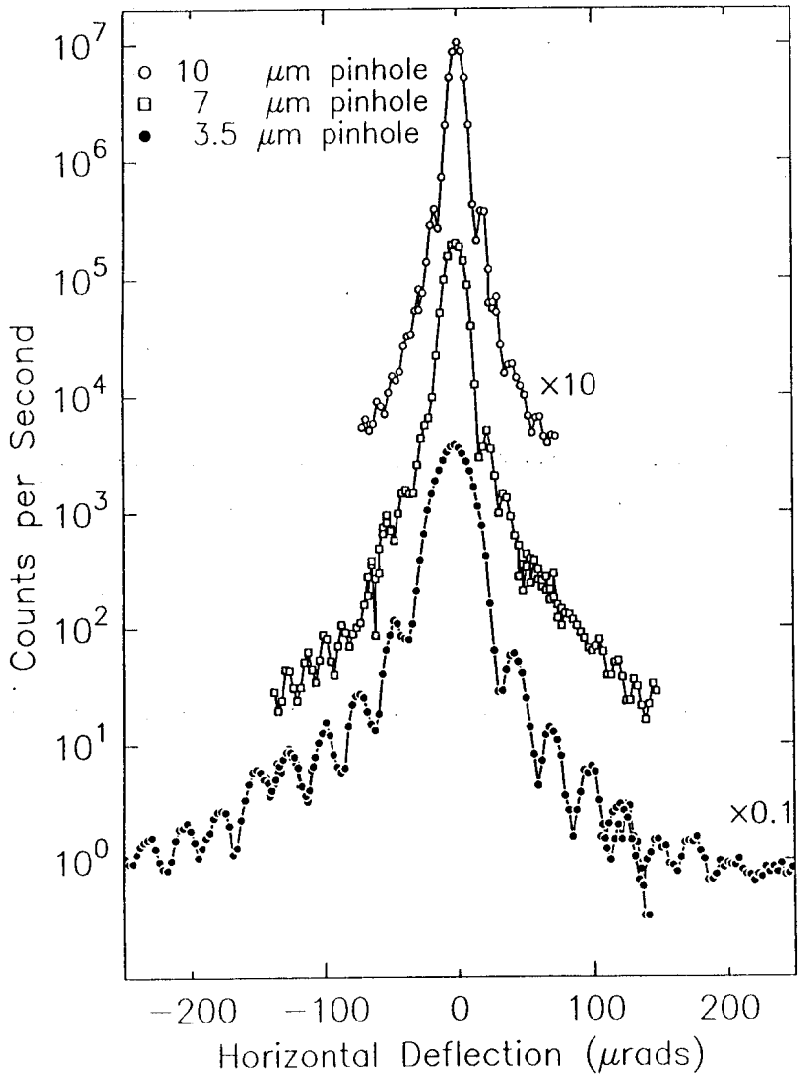

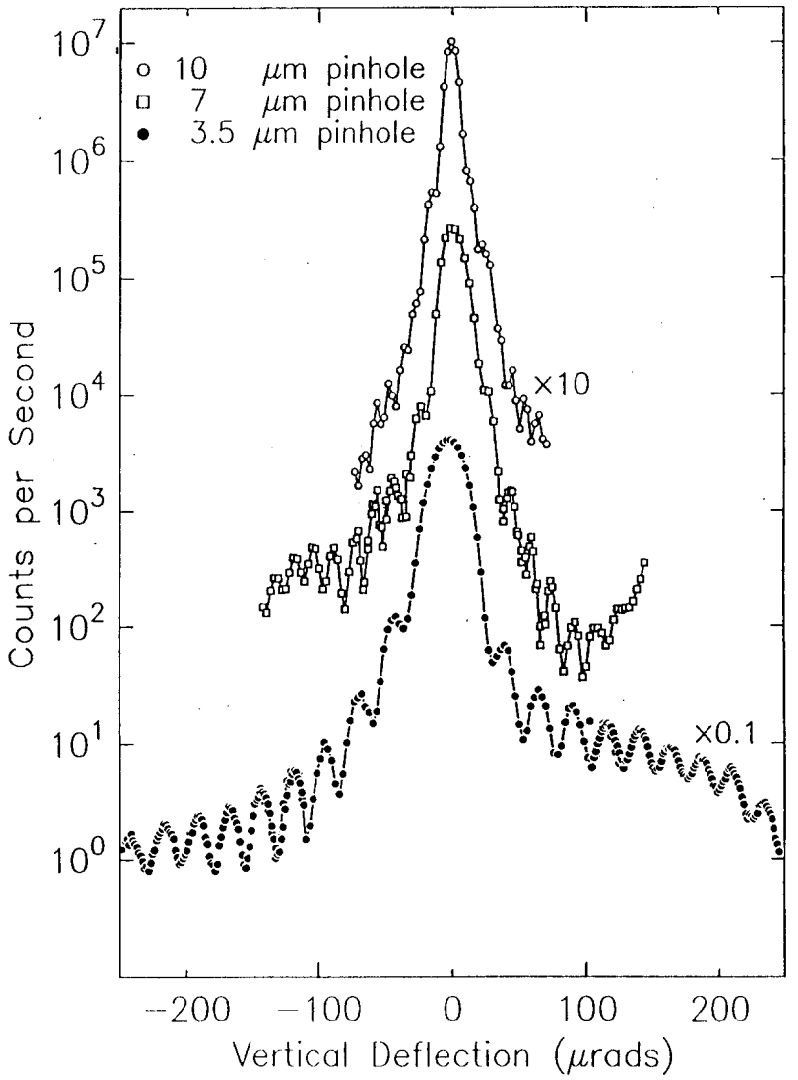

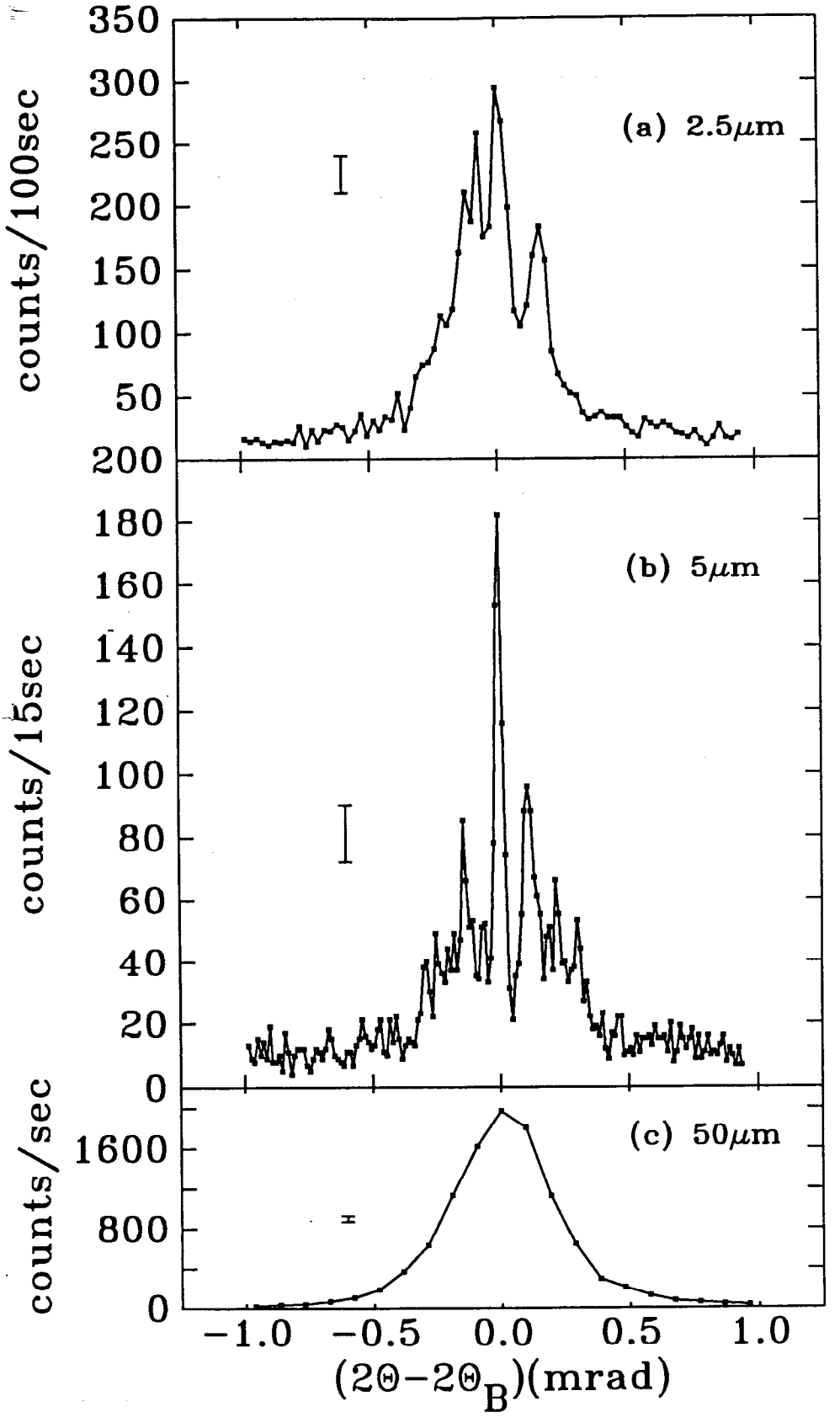

Static Speckle patterns from anti-phase domains in Cu_3Au

Various incident aperture sizes

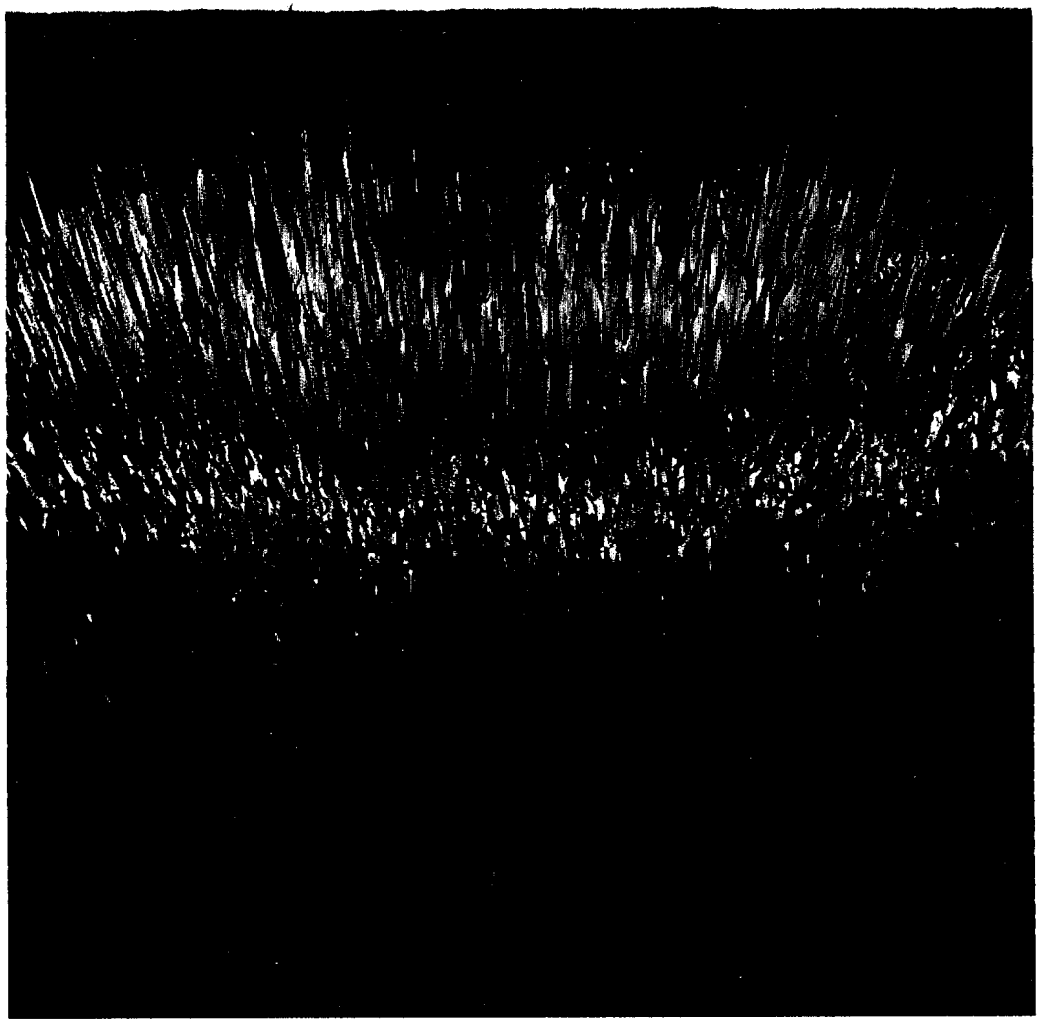

$\Delta 2\theta_{\parallel}$

$\Delta 2\theta_{\perp}$

out of paper = intensity (peak ~10 cps)

Static speckle pattern from anti-phase domains in Cu_3Au

Single diffuse peak resolved into thousands of 'speckles'

obtained using CCD detector

Ising Model Simulation

Evolution of speckle pattern from equilibrium critical fluctuations

($T/T_c = 1.1$)

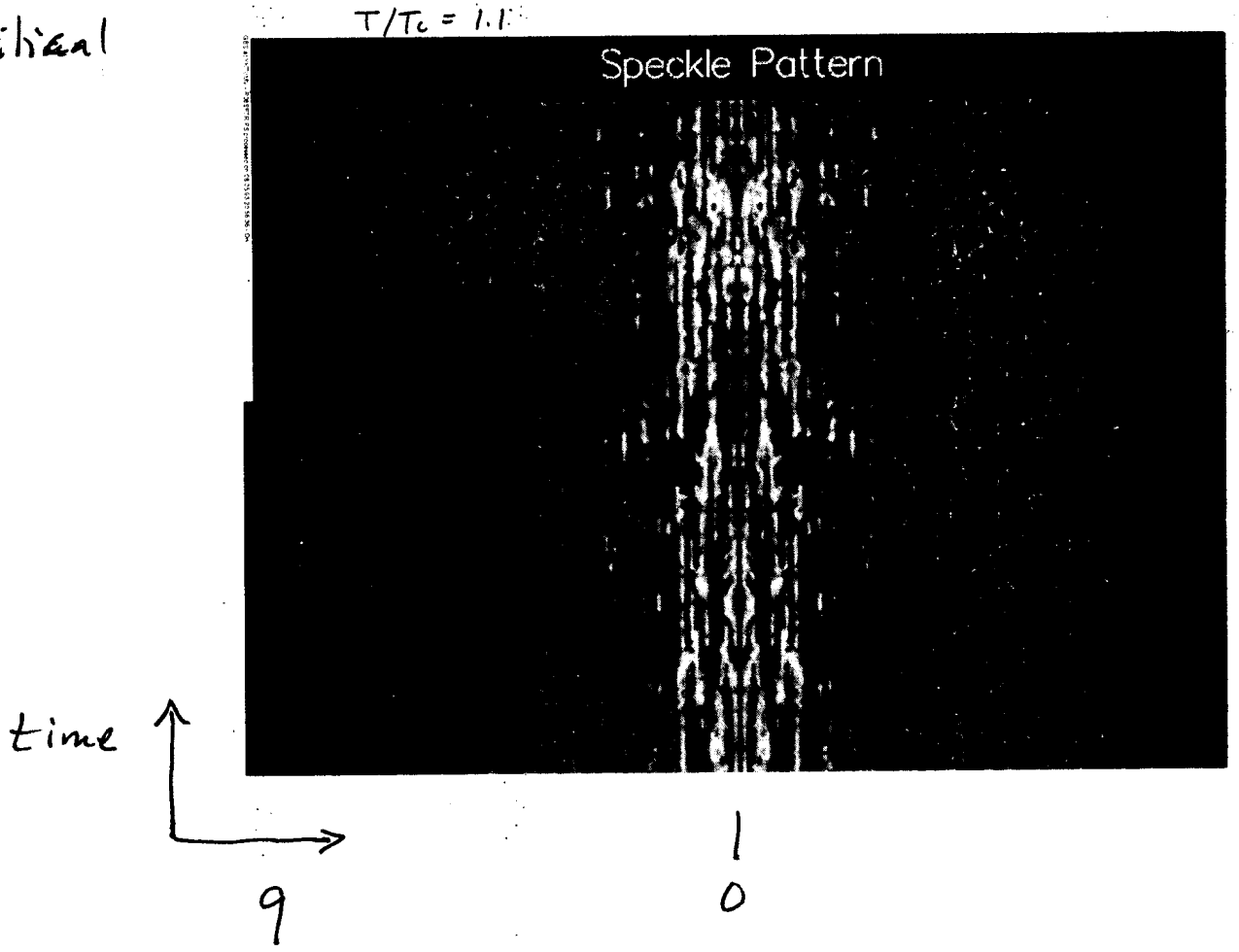

Need Optics to Tailor Coherence Volume

Divergence ↔ Spot Size

Asymmetric Crystal

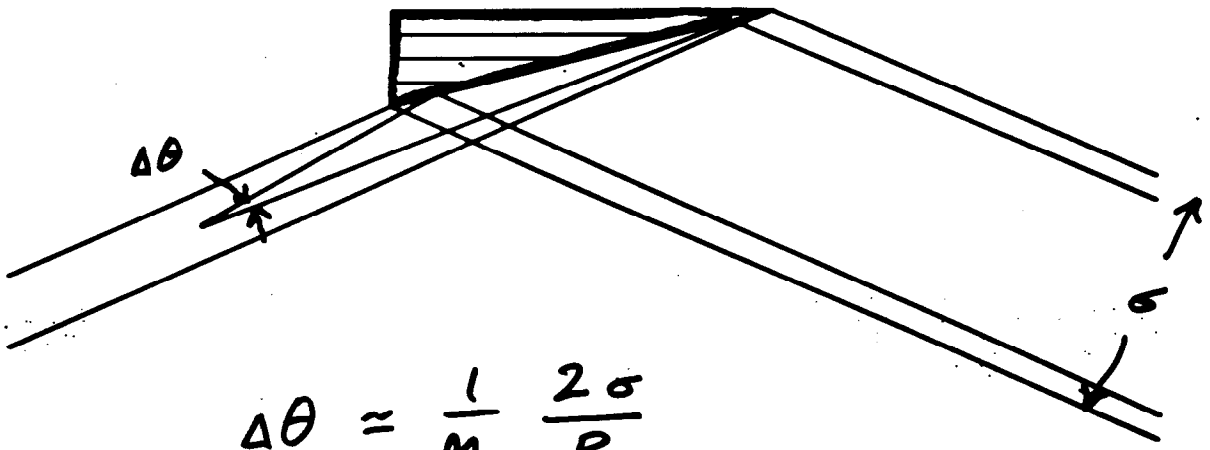

$$\Delta\theta \simeq \frac{1}{M}\,\frac{2\sigma}{R}$$

Focussing Optic (Mirror / Zone Plate)

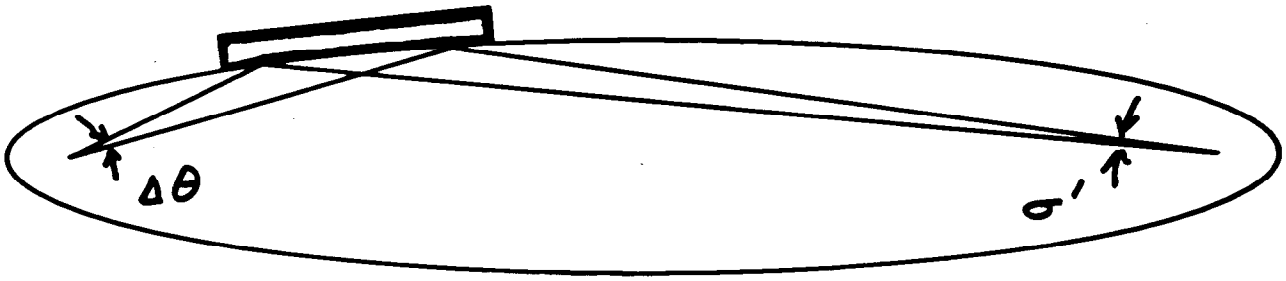

$$\Delta\theta \simeq \frac{1}{M}\,2\sigma'$$

Expected Signal Levels in XIFS Studies as a Function of Sample Type and Source Brilliance

Sample characteristics:

Correlation length	ξ	typ. 10 - 1000 Å
Sample (beam) size	L	typ. 0.1 - 10 μm

Sample Type:	ξ (Å)	L (μm)	Signal Level per 'Speckle': at APS (cps)	at LCLS (cps)
Single Crystal	1000	10	10^3	10^8
	100	1	10^2	10^7
	10	0.1	10	10^6
Amorphous Material	10	0.1	1	10^5

Time Correlation Spectroscopy at LCLS

A) Time Resolution larger than rep. rate (~10ms)

- Much larger coherent flux will allow study of greater variety of systems, in particular those with smaller ~~coherence~~ correlation lengths, using similar XIFS techniques being developed for 3rd-generation undulator sources

B) Time resolution larger than pulse width (~100 fs)

- Unprecedented time resolution could in principle be obtained by "stroboscopic" techniques, using split-beam w/ delay, to study e.g. thermal motion, elastic wave propagation

SUMMARY

- Scattering with coherent x-rays provides unique capabilities
  e.g. observing dynamics of atomic-scale equilibrium fluctuations

- Coherent x-ray beams of sufficient intensity
  to measure speckle patterns in minutes
  have been demonstrated using current synchrotron sources

- Third-generation x-ray undulator sources (e.g. APS)
  will allow x-ray intensity fluctuation spectroscopy
  to be developed on time scales as short as milliseconds
  in favorable systems

- Dramatic (up to 10^5 X) increase in coherent flux
  provided by LCLS will allow study of systems of greatest interest
  (smallest correlation lengths)

- Pulsed nature of LCLS will allow unprecedented time resolution
  (100 fs) not only in standard scattering studies
  but also in techniques using coherent x-rays (e.g. XIFS)

Observation of speckle by diffraction with coherent X-rays

M. Sutton*, S. G. J. Mochrie†, T. Greytak†, S. E. Nagler‡, L. E. Berman§, G. A. Held‖ & G. B. Stephenson‖

* Department of Physics, Centre for the Physics of Materials, McGill University, Montréal, Québec, Canada H3A 2T8
† Department of Physics, Massachusetts Institute of Technology, Cambridge, Massachusetts 02139, USA
‡ Department of Physics, University of Florida, Gainesville, Florida 32611, USA
§ National Synchrotron Light Source, Brookhaven National Laboratory, Upton, New York 11973, USA
‖ IBM Research Division, Thomas J. Watson Research Center, Yorktown Heights, New York 10598, USA

REFLECTED light from a coherent light source such as a laser shows a graininess known as speckle. In general, a speckle pattern is produced whenever randomly distributed regions of a material introduce different phase shifts into the scattering of coherent incident light. If the arrangement of the regions evolves with time, the speckle pattern will also change. Observation of the intensity fluctuations at a single point in the speckle pattern provides a direct measure of the time correlation function of the inhomogeneity. This leads to a technique[1,2], alternatively called light-beating spectroscopy, dynamic light scattering or intensity fluctuation spectroscopy, which has been widely used with visible light to study processes such as critical fluctuations near phase transitions in fluids and the diffusion of particles in liquids. But it is not possible to study processes involving length scales less than about 200 nm, or those in opaque materials, using visible light. If intensity fluctuation spectroscopy could be carried out using coherent X-rays, however, one could probe the dynamics of processes involving atomic length scales in a wide range of materials. Here we show that by using a high-brilliance X-ray source it should be possible to perform this type of measurement using radiation of wavelength ~0.15 nm. Specifically, we have observed a speckle pattern in the diffraction of coherent X-rays from randomly arranged antiphase domains in a single crystal of the binary alloy Cu_3Au.

To obtain a speckle pattern, the incident beam must be sufficiently coherent. With visible light this is typically achieved with a laser source, but it is possible to use an incoherent source, such as a mercury arc lamp[2] or, as in our case, an X-ray wiggler, provided that it is suitably collimated and monochromatic. The coherent intensity so obtained depends directly on the brilliance of the source. To resolve speckle, the difference in the path lengths of rays scattered by different parts of the sample must not be much greater than the longitudinal coherence length of the incident beam. This is equal to $\lambda^2/2\delta\lambda$, where λ is the wavelength and $\delta\lambda$ is the distribution of wavelengths. In addition, the incident beam size must not be much greater than the transverse coherence length[3], given by $\lambda R_s/2d_s$, where R_s is the distance from the source and d_s is the source size. For a typical X-ray wavelength, $\lambda = 0.15$ nm, a silicon (111) monochromator gives $\delta\lambda/\lambda \approx 1.4 \times 10^{-4}$, which results in a longitudinal coherence length of ~0.5 μm. For a 0.3-mm-diameter synchrotron source at $R_s = 30$ m, the transverse coherence length is ~7 μm. Thus an X-ray wiggler source with a brilliance of 10^{15} photons s^{-1} $mrad^{-2}$ mm^{-2} per 0.1% bandwidth, when collimated through a 5 μm pinhole, is expected to deliver a usable coherent beam of $\sim 3 \times 10^5$ photons s^{-1}. As we shall demonstrate, it is possible to obtain sufficient coherent intensity with current wiggler X-ray sources to perform scattering measurements from certain types of samples.

The experiments were performed using the X25 wiggler beamline at the national synchrotron light source (NSLS). Figure 1 shows the scattering geometry. The nominal size of the wiggler source is 0.4 mm in the horizontal and 0.1 mm in the vertical[4]. A wavelength of 0.155 nm was selected by a specially designed double crystal silicon (111) monochromator[5]. A coherent beam of X-rays was obtained by placing either a 2.5-μm or 5 μm nominal diameter pinhole 28 m from the source. The collimated beam was then diffracted by the sample, which was located 40 mm behind the pinhole. A second, analysing pinhole was placed 1 m from the sample and the scattered intensity profile measured by counting the photons that passed through this pinhole as it was scanned in and perpendicular to the scattering plane (the 2θ and α directions, respectively).

To verify that our X-ray source provided the required transverse coherence, we measured the Fraunhofer diffraction pattern of the collimating pinhole by removing the sample and bringing the detector angle, 2θ, to near zero. Figure 2 shows the diffraction patterns in the 2θ direction for the 2.5- and 5-μm pinholes. Diffraction profiles in the α direction are similar. The solid lines are the fits to Fraunhofer diffraction patterns of circular apertures[3] convolved with the acceptance of the analysing pinhole. The fitted aperture diameters of 2.9 and 4.5 μm agree well with the pinhole sizes measured by electron microscopy. The observed shape of the central peak and the positions of the subsidiary minima and maxima of the measured patterns agree well with the theoretical curve, indicating that the transverse coherence length of the source is at least 5 μm in both the horizontal and vertical.

In conventional diffuse X-ray scattering with incoherent light, the angular width of a peak is $\sim\lambda/\xi$ where ξ is the average domain size. Such a diffuse peak results from the incoherent sum of the scattering from different domains. With coherent light, the coherent sum of the scattering from a random array of domains results in a speckle pattern modulating the diffuse peak[6]. The angular extent of each 'speckle' is comparable to the width of the central peak in the Fraunhofer diffraction pattern of the collimating pinhole, as this corresponds to a change of λ in the largest path-length difference. This width is $\sim\lambda/L$, where L is the beam diameter. If, instead of diffuse scattering, we consider Bragg diffraction from a highly ordered sample ($\xi \gtrsim L$), the complete peak is the size of a single speckle. We confirmed this by measuring the (111) peak of a perfect silicon crystal which simply reproduced the Fraunhofer diffraction pattern of the collimating pinhole. Because of the limited intensity of our coherent beam, the optimum condition to observe a speckle pattern is obtained with a diffuse peak not too much broader than λ/L.

We chose to measure the diffuse (001) peak from an ordered single crystal of Cu_3Au. The structure of such a crystal consists of a random arrangement of antiphase domains, which arise because of the four equivalent ways in which the Cu_3Au unit can occupy the underlying crystal lattice[7]. Neighbouring domains differ only by a phase shift in the periodic occupation of lattice sites by this unit. By an appropriate heat treatment, the crystal was prepared with an average domain size of a few

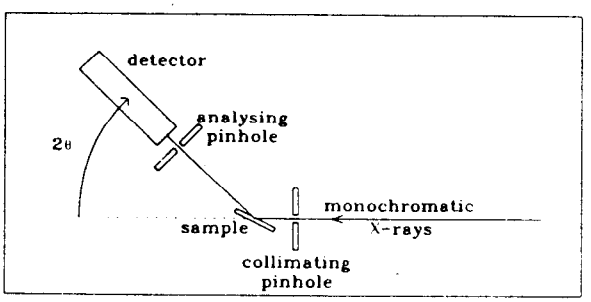

FIG. 1 Schematic representation of the scattering geometry. The angle 2θ is shown; α (not shown) is the corresponding angle in the direction normal to the scattering plane (normal to the page).

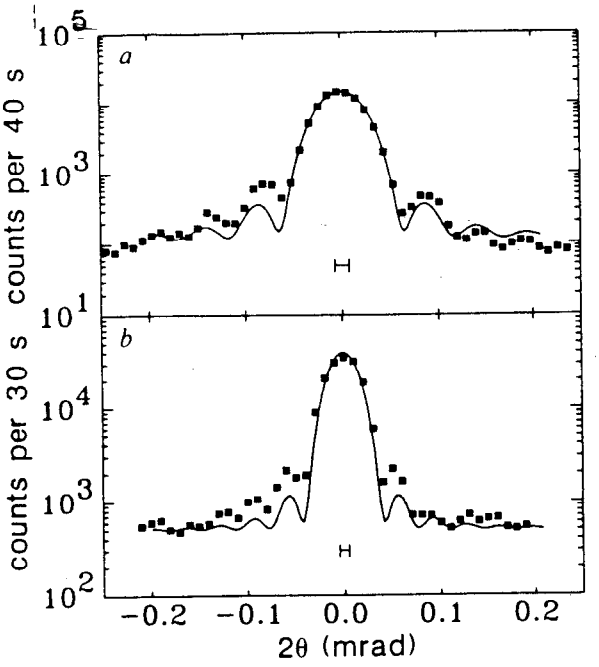

FIG. 2 Fraunhofer diffraction from *a*, 2.5-μm and *b*, 5-μm nominal diameter pinholes. Error bars due to counting statistics are smaller than the symbol size. The solid line represents the calculated diffraction pattern of a circular aperture convolved with the analyser resolution shown by the horizontal bar. A constant background is included in the fit.

hundred nanometers. During our experiment the domain structure was static, as atomic mobility was negligible at room temperature. The (001) peak at $2\theta_B = 23.9°$ had an angular width of 0.3 mrad in 2θ and 0.5 mrad in α. Measurement of the (002) Bragg peak gave widths much sharper than this, confirming that the (001) peak width results from the antiphase domain size rather than from imperfections in the underlying lattice. The scattering path-length differences were smaller than the longitudinal coherence length because of X-ray absorption. In the symmetric reflection geometry, the largest path-length difference is $2L_z \sin\theta$, where L_z is the penetration depth normal to the surface. For Cu_3Au, $L_z \approx 0.6$ μm.

Figure 3 shows a photograph of the speckle pattern observed from this Cu_3Au crystal. It was obtained by placing film (Kodak DEF) at the analyser position. A 2.5-μm collimating pinhole was used. The diffuse peak is seen to be made up of small intense spots. The angular extent of each spot is comparable to that of the central peak of the Fraunhofer diffraction pattern of the pinhole ($\lambda/L \approx 50$ μrad). A more quantitative measurement is presented in Fig. 4, which shows the scattering patterns obtained using 2.5-, 5- and 50-μm collimating pinholes with 50-, 25- and 100-μm analysing pinholes, respectively. For the first two cases, the observed angular sizes of the intense spots are ~50 and 25 μrad, respectively, again in good agreement with λ/L. The measurement using the 50-μm collimating pinhole is included for comparison. It is equivalent to a conventional incoherent X-ray measurement, because 50 μm is larger than the coherence length of the source.

The observed structure in the (001) peak cannot be explained by a topographic imaging effect, where each of the intense spots arises by independent diffraction from a small region of the illuminated area. This is ruled out because diffraction from a region much smaller than L would spread over an angular region much larger than λ/L. As the observed size of the intense spots is comparable to λ/L, they must arise by diffraction from the full illuminated volume.

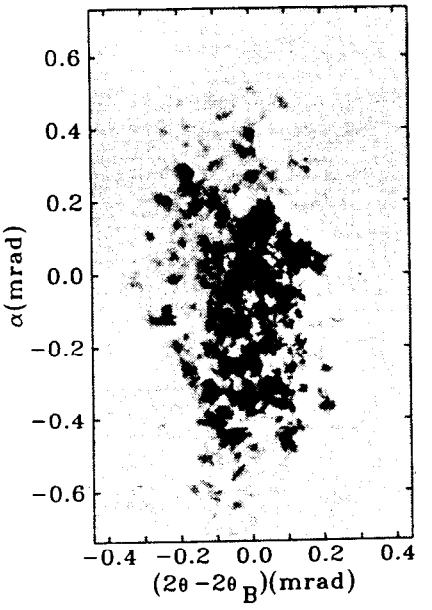

FIG. 3 Photograph of the speckle pattern in the diffuse (001) peak of Cu_3Au. The collimating pinhole is 2.5 μm.

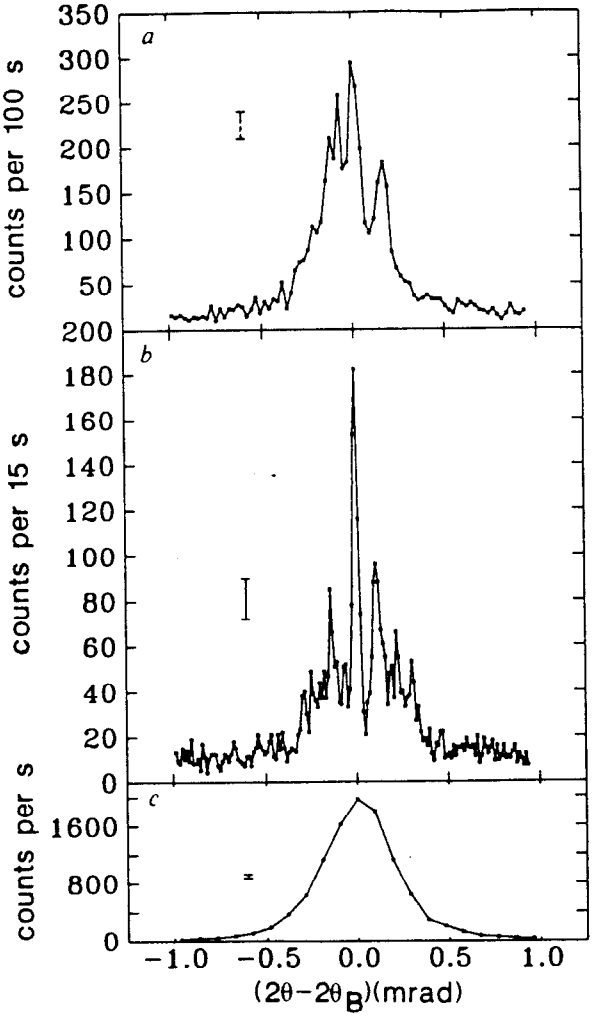

FIG. 4 Speckle patterns measured using *a*, 2.5-μm, *b*, 5 μm and *c*, 50-μm collimating pinholes. The analysing pinholes used were 50, 25 and 100 μm, respectively. Representative error bars are indicated, and the solid lines simply connect the data points. The (001) Bragg angle, $2\theta_B$, is ~23.9°.

The observation of speckle using X-rays opens up many exciting possibilities for future work. In particular, by measuring the evolution of the speckle pattern in time, we can carry out X-ray intensity fluctuation spectroscopy. This technique not only measures the dynamics of nonequilibrium systems but is also one of the few techniques that can directly measure the dynamics of equilibrium systems. One important class of applications is the study of mass-transport mechanisms on length scales of 1–100 nm in materials such as metal alloys and complex fluids[8]. Of immediate interest are critical phenomena in equilibrium dynamics[9] and fluctuations during nonequilibrium domain coarsening[10]. Another class is the study of phason dynamics in materials with an incommensurate modulation, such as charge-density-wave systems and quasicrystals.

The present measurements using X25 at NSLS give a maximum count rate of 10 counts per s, allowing the study of correlation times down to 0.1 s. Such timescales are relevant to mass transport over all distances down to the atomic scale in typical solids at temperatures below about half their melting point. New undulator-based facilities at the European synchrotron radiation facility, the advanced photon source and elsewhere will provide an increase of three orders of magnitude in coherent intensity. This will enable studies probing correlation times in the microsecond range and studies of materials that scatter relatively weakly.

Intensity fluctuation spectroscopy does not make full use of the structural information in the speckle pattern. In principle, the speckle pattern contains complete information on the disordered structure producing it[6]. This structure could be imaged by Fourier inversion. In some cases, such as single grain boundaries or dislocations, the speckle pattern will be relatively simple, and one could use it to determine the atomic structure of these defects. □

Received 25 February; accepted 25 June 1991.

1. Pusey, P. N. in *Photon Correlation Spectroscopy and Velocimetry* (eds Cummins, H. Z. & Pike, E. R.) 45–141 (Plenum, New York, 1977).
2. Jakeman, E., Pusey, P. N. & Vaughan, J. M. *Opt. Commun.* **17**, 305–308 (1976).
3. Born, M. & Wolf, E. *Principles of Optics* 396; 511 (Pergamon, Oxford, 1975).
4. Rarback, H., Jacobsen, C., Kirz, J. & McNulty, I. *Nucl. Instrum. Meth.* **A266**, 96–105 (1988).
5. Berman, L. E. & Hart, M. *Nucl. Instrum. Meth.* **A300**, 415–421 (1991).
6. Ludwig, K. F. Jr. *Phys. Rev. Lett.* **61**, 1526 (1988).
7. Warren, B. E. *X-ray Diffraction*, 206–247 (Dover, Minoela, New York, 1990).
8. Lipowsky, R. *Nature* **349**, 475–481 (1990).
9. Hohenberg, P. C. & Halperin, B. I. *Rev. mod. Phys.* **49**, 435–479 (1977).
10. Roland, C. & Grant, M. *Phys. Rev. Lett.* **63**, 551–554 (1989).

ACKNOWLEDGEMENTS. We thank M. Grant for discussions and R. Sweet, Jia Wang, B. Ocko and R. Shannon for their help.

Non-Linear X-ray Phenomena Using High Intensity Coherent Beams

Peter Eisenberger, Princeton University

Non-Linear X-ray Scattering to Study Microscopic Optical Properties and Other Interesting Phenomena

by
P. Eisenberger
Princeton University

The development of an intense, short pulsed, bright (diffraction limited) X-ray source with parameters similar to the Stanford XFEL will make it possible to study the interaction of light with crystals on the sub-atomic scale. It will be possible to explore the microscopic features of both linear and non-linear optical phenomena. The same basic approach can be used to study local relaxation effects, energy transfer phenomena, breakdown phenomena, and the production of intense femto-second X-ray beams. Extensions of the basic idea to other types of excitations like acoustic waves offers the possibility of studying their microscopic effects.

In the early seventies, the basic formalism for non-linear X-ray phenomena, specifically the mixing of X-rays with light was worked out.[1, 2] As stated in one of those papers[1] "Direct observation of sum-frequency mixing of a laser and a source of X-rays is unattractive because of the low spectral brightness of available spontaneous-emission X-ray devices." Because of this the phenomena studied was parametric down conversion (one X-ray splits into two) and was actually observed confirming the basic mechanisms.[3] With an XFEL one can not only capture the promise that light-X-ray mixing has for studying the microscopic aspects of linear optical phenomena but calculations show that the study of optical non-linear phenomena is also possible.

The basic idea is very simple. The light beam creates an oscillating charge at each atom at the frequency of light with the spatial periodicity of the light wavelength in the medium. Even though the light wavelength is much greater than interatomic spacing at each atom there is a microscopic electric field ("local field") causing a microscopic fluctuating charge at the light frequency which is related to microscopic polarizability of the medium. In a periodic crystal the oscillating charge will have Fourier components at $\bar{G} \pm \bar{q}_L$ where $\bar{G}$ are the reciprocal lattice vectors of the crystal and $\bar{q}_L$ is the wavelength of the light in the medium. By satisfying the phase matching conditions (k and ω are the x-ray momentum and frequency)

$$\omega_{out} = \omega_{in} \pm \omega_L$$

$$\bar{k}_{out} = \bar{k}_{in} + \bar{G} \pm \bar{q}_L$$

at various reciprocal lattice vectors one can in complete analogy with Bragg crystallography determine the charge distribution associated with the induced polarization. As the light frequency approaches a resonance one can

use this approach to study polaritons (excitonic or optical modes). At resonance one of course produces a finite population on the excited state which represents other opportunities for the XFEL (see Coppens).

Straightforward but detailed calculation show that with intense pulsed lasers ~10^{10} watts/cm^2 and a source with the properties of the proposed XFEL at Stanford the probability of scattering is very large 6_{NL}~10^{-5} of the incident beam. With pulsed incident X-ray beams with 10^{14} photons/sec. ev. the signal rates can be as high as 10^9 photons/sec. In fact, the signal is so strong that some limited experiments can be carried out at the new Advanced Photon Source at Argonne. The signal rates there would be at best 10^4 photon/sec. reflecting its lower brightness and poorly matched time structure to powerful lasers. Since each higher order optical phenomena (e.g. second harmonic, sum frequency generation) produces an oscillating charge reduced by 10^{-5} to 10^{-6} with intense fields (10^{10} watts/cm^2) it is also possible with XFEL to study the microscopic charge associated with non-linear optical phenomena with signal rates as high as 10^3 to 10^4 photons/sec. Signal rates for non-linear phenomena at APS would be 10^{-4} to 10^{-5} per second. With the brightness of XFEL one can also use lower frequency laser light to study the displacive contributions to polarizablity.

With such large signals one can contemplate various other kinds of additional studies. By delaying the X-ray beam on the picosecond time scale relative to the light beam one can study local relaxation effects. One can even contemplate the observing of the microscopic aspects of the development of gain in a crystal. Since in the multiple light beam case one can simultaneously study both the effects of the incident light and the non-linear light generated component (e.g. second harmonic) one can, in principle, observe the transfer of energy from one beam to the other at the microscopic level. One can clearly envision studying the microscopic aspects of the onset of optically induced breakdown. Since the scattered X-ray beam will have the time structure of the light beam this mixing can be used to produce femto-second X-ray beams which could, in turn, be used for other studies. Finally, one can contemplate extending the same approach to mixing an X-ray beam with other types of modulations like acoustic waves.

The author would like to acknowledge stimulating discussions with P. Fenter, D. McClure and S. Mukamel. In fact, S. Mukamel has documented the impact he believes these type of experiments might have in the attached letter.

1. I. Freund and B. Levine, *Physical Review Letters*, **25**, 1241, (1970).

2. P. Eisenberger and S.L. McCall, *Physical Review* ,A, **3,** 1145, (1971).

3. P. Eisenberger and S.L. McCall, *Physical Review Letters*, **26**, 684, (1971).

4. J. Knoester and S. Mukamel, *J. Chem. Phys.*, **91**, 98E, (1989).

UNIVERSITY OF
ROCHESTER

COLLEGE OF ARTS AND SCIENCE
DEPARTMENT OF CHEMISTRY

Phone (716) 275-3080
Fax (716) 473-6889
Email: samu@db1.cc.rochester.edu

February 2, 1994

Professor Peter Eisenberger
Director
Princeton Material Institute
Princeton University
79 Prospect Avenue Room 320
Princeton NJ 08540

Dear Peter:

I am pleased to summarize my thoughts regarding the potential applications of x-ray lasers in nonlinear spectroscopy. Nonlinear optical spectroscopy in the visible and UV can be formulated using multitime correlation functions of the dipole operator. These correlation functions are nonlocal in time and space. The observed single photon and multiphoton resonances are usually related to the *temporal* evolution and provide information about characteristic frequencies (energy levels). The spatial dependence is usually less informative. It yields a phase matching condition that determines e.g. the preferred wavevectors in four wave mixing signals, but contains no useful physical information. The problem is that optical wavelengths are long and the spatial information is highly averaged and purely macroscopic. An experiment such as the transient grating which raised high hopes for measurements of exciton and polaritons coherent motions turned out to be very disappointing. The attainable grating wavelengths cannot be shorter than $\lambda/2$, λ being the optical wavelength. On the length scale of thousands of Å, all information about coherent exciton/polariton motions is lost. Performing the grating experiment with a combination of x-ray and optical beams should provide a direct and unambiguous probe of spatial coherences and motions [1-3]. Another fascinating problem is related to polariton effects. Transient grating measurements provide a circumstantial and indirect evidence for these effects (faster transport than excitons) [4-6]. A mixing of x-rays with optical gratings performed in the stop gap regime should allow a direct look the polariton charge density fluctuations. I envision multiple pulse experiments with phase control, wave mixing, and pump probe. The later should allow to follow charge density changes following an excitation process.

The dipole approximation works very well in the optical regime. Consequently a molecule or a unit cell in a semiconductor can be modelled as a point dipole. This makes the calculation easier and reflects the inability of optical measurements to probe microscopic spatial charge changes. By using the multipolar hamiltonian (which is obtained from the minimal coupling hamiltonian by a gauge transformation) it is possible to formulate nonlinear optical susceptibilities in terms of multi-point correlation functions of the polarization density, without invoking the dipole approximation [7, 8]. x-ray measurements should probe these correlations directly.

University of Rochester
Rochester, New York 14627-0216

Another important aspect of x-ray scattering processes is that they probe directly the charge density rather than oscillator strength. Charge density is more fundamental since it is directly related to chemical bonding and structure. Femtosecond time resolved observation of molecular collisions, and the creation and formation of bonds etc. can be readily monitored. In the optical regime one has to find some specific properties (e.g. an electronic transition wavelength that changes when a particular bond breaks) [9]. This requires a detailed prior knowledge of the system in order to interpret optical "femtochemistry" experiments. This is not the case in x-ray scattering. The indepth understanding of optical nonlinearities should allow a vast number of predictions and experiments to be made for x-ray measurements.

Nonlinear optical experiments performed on nanostructures [10] should be greatly enhanced by x-ray lasers. These are characterized by multiple coherence sizes associated with superradiance, two exciton scattering, biexciton formation, and Wannier excitons. All of these could be probed directly in space [11, 12].

Conjugated polyenes and polyacetylenes, undergo rapid structural changes upon optical excitation leading to the formation of solitons, polarons, etc. The role of these elementary excitations in the mechanism of the optical nonlinearities is a subject of an ongoing controversy. The charge transfer excitons found in these systems could be directly measured by pump probe x-ray techniques, which should resolve many of the outstanding questions [13].

I hope that these comments are helpful to you. Best regards.

Sincerely,

Shaul Mukamel
Professor of Chemistry

SM/jan

[1] H.J. Eichler, P. Gunter, and D.W. Pohl, Laser-induced Dynamic Gratings, (Springer, Berlin) (1986)
[2] T. S. Rose, R. Righini, and M. D. Fayer, Chem. Phys. Lett., **106**, 13 (1984)
[3] J. Knoester and S. Mukamel, Physics, Reports, **205**, 1 (1991)
[4] M. Orrit and P. Kottis, Adv. Chem Phys., **74**, 1 (1988)
[5] G. M. Gale, F. Vallee, and C. Flytzanis, Phys. Rev. Lett., **57**, 1867 (1986)
[6] S. H. Stevenson, M. A. Connolly, and G. J. Small, Chem Phys., **128**, 157 (1988)
[7] D. P. Craig, T. Thirunamachandran, Molecular Quantum Electrodynamics (Academic Press, London) (1984)
[8] J. Jenkins and S. Mukamel, J. Chem Phys., **98**, 7046 (1993).
[9] M. J. Rosker, M. Dantus, and A. H. Zewail, Science, **241**, 1200 (1988); A.H. Zewail, Faraday Discuss. Chem Soc., **91**, 207 (1991), and references therein.
[10] F. F. So and S. R. Forrest, Phys. Rev. Lett., **66**, 2649 (1991)
[11] Molecular Nonlinear Optics, J. Zyss, Editor (Academic Press, New York) (1994).
[12] L. Banyai and S. W. Koch, Semiconductor Quantum Dots (World Scientific, Singapore) (1993)
[13] B. I. Greene, J. Orenstein, and S. Schmitt-Rink, Science, **247**, 679 (1990)

Non-Linear X-ray Scattering

to

Study Microscopic Optical Properties

and

Other Interesting Phenomena

by

P. Eisenberger
Princeton University

Non-Linear X-ray Phenomena
Light X-ray Mixing

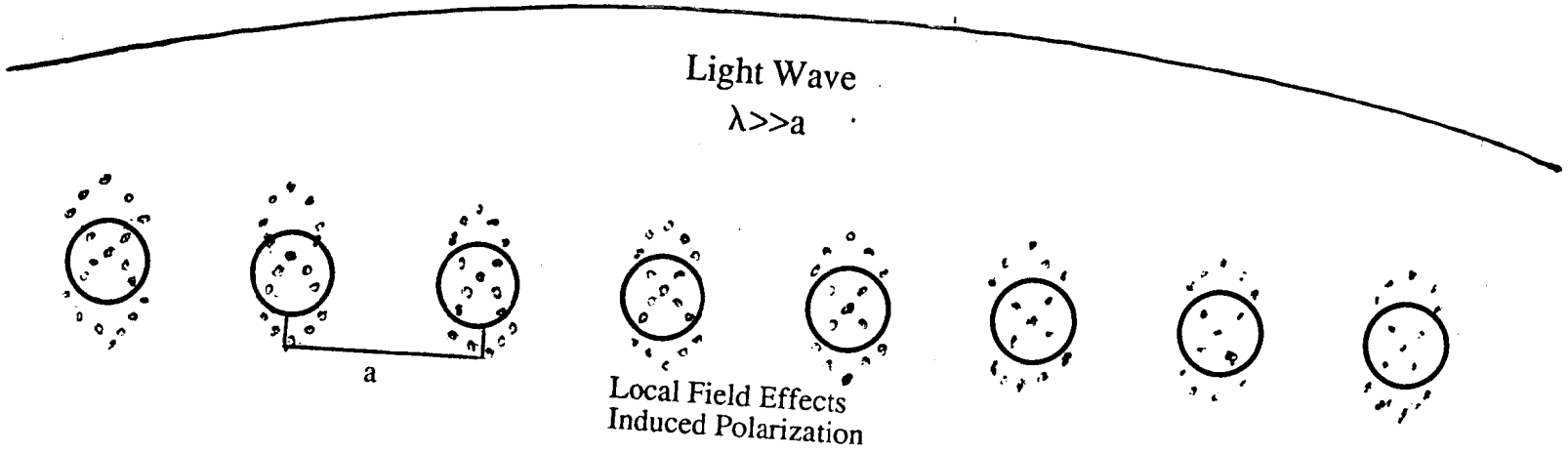

$\bar{k}_{in} - \bar{k}_{out} = \bar{G} \pm \bar{q}_L$

$\omega_{in} - \omega_{out} = \pm \omega_L$

By doing crystallography on phase matched component
- local induced polarization can be determined

Can Extend to study various non-linear phenomena
- second harmonic
- stimulated Raman
- stimulated Brillouin

X-RAY LIGHT MIXING BASIC APPROACH
Linear Polarization

$$\vec{E}_L(\vec{r}, t) = \vec{E}_L \cos(\omega_L t - \vec{q}_L \cdot \vec{r})$$

$$H_0 + H^1 = H_0 - \frac{e}{mc} \vec{P} \cdot \vec{A} + \frac{e^2}{2mc^2} A^2$$

For electric dipole transitions

$H^1 = -\vec{p} \cdot \vec{E}$ $\quad$ $\vec{p}$ = electric dipole operator

$\phi_q^{(i)}(\vec{r})$ $\quad$ ground state wave functions

Using First order steady - state time dependent perturbation theory

$$\psi^i(\vec{r}, t) = \phi_q^{(i)}(\vec{r}) + 1/2\, \vec{E}_L \cdot \hbar^{-1} \Sigma\, \vec{p}_j\, \phi_j^{(i)}(\vec{r})$$

$$X\left(\frac{e^{i(\vec{q}_L \cdot \vec{r} - \omega_L t)}}{\omega_j - \omega_L} + \frac{e^{-i(\vec{q}_L \cdot \vec{r} - \omega_L t)}}{\omega_j + \omega_L} \right)$$

New electron density in presence of the laser field

$$\rho(\vec{r}, t) = \sum_i |\psi^i(\vec{r}, t)|^2$$

$$= \rho(\vec{r}) + \Delta\rho(\vec{r}, t)$$

where

$$\Delta\rho(\vec{r}, t) = \vec{E}(\vec{r}, t) \cdot \vec{R}(\vec{r})$$

$$R(\vec{r}) = \hbar^{-1} \sum_{ij} \frac{2\omega_j \vec{p}_j}{\omega_j^2 - \omega_L^2} \phi_j^{(i)}(\vec{r})\ \phi_q^{(i)}(\vec{r})$$

$$\int_{uc} \vec{r}\ \vec{R}(\vec{r})\, d^3 r = 1/eN\ \overleftrightarrow{X}$$

N = number of unit cells / cm^3

$\overleftrightarrow{X}$ = optical susceptibility tensor

In a periodic crystal

$$\vec{R}(\vec{r}) = \sum_{\vec{G}} \vec{R}_{\vec{G}} \; e^{i\vec{G}\cdot\vec{r}}$$

$\therefore$ The induced charge has Fourier Components

$$\rho_{\vec{Q}} = e^{\mp i \vec{q}_L \cdot \vec{r}} \; e^{\mp i w_L t} \; e^{i\vec{G}\cdot\vec{r}} \; \rho_L(\pm \vec{q}_L + \vec{G})$$

where

$$\rho_L(\pm \vec{q}_L + \vec{G}) = \vec{R}_{\vec{G}} \cdot \vec{E}_L$$

$$\vec{R}_{\vec{G}} = N \int_{uc} \vec{R}(\vec{r}) \; e^{-i\vec{G}\cdot\vec{r}} \; d^3r$$

If one now scatters an X-ray beam off the induced charge oscillations phase matching occurs when

$$\omega_{out} = \omega_{in} \pm \omega_L$$

$$\vec{k}_{out} - \vec{k}_{in} = \vec{G} \pm \vec{q}_L$$

$\therefore$ **Therefore beam is shifted both in angle and energy from Bragg**

GENERALIZATION AND ADDITIONAL CONSIDERATIONS

- Approach can be used to study higher order interactions

$\vec{P}(\vec{q},\omega)$ = induced polarization by presence of light fields

$= P^1(\vec{q},\omega) + P^2(\vec{q},\omega) + \ldots$

where

$$P^1(\vec{q},\omega) = \overleftrightarrow{X}^1 (-\vec{q}, -\omega ; \vec{k}_i\omega_i) \cdot \vec{E}(\vec{k}_i, \omega_i)$$

$$P^2(\vec{q},\omega) = \overleftrightarrow{X}^2 (-\vec{q}, -\omega ; \vec{k}_i\omega_j \vec{k}_j \omega_j : \vec{E}(\vec{k}_i, \omega_j) \vec{E}(\vec{k}_j, \omega_j)$$

$\overleftrightarrow{X}^N$ N^{th} order susceptibility tensor of rank N+1

For each case one can define an induced charge density

$$e\rho(\vec{q},\omega) \cong \nabla \cdot \overleftrightarrow{X}^N : \vec{E}(\vec{k}_i, \omega_i) \vec{E}(\vec{k}_j, \omega_j) \ldots$$

- Each higher order is down by approximately $\dfrac{E_L^2}{E^2 at}$

- One can extend the same type of approach to study displacive contributions to the polarizability if the laser frequency is low

  p_j – represent dipole created by atomic motion
  ω_j – represent vibrational frequencies

- One can also consider studying microscopic charge induced during stimulated Raman and Brillouin scattering processes

- For both electronic and displacive components one can explore polariton effects by tuning the laser to either an excitonic or optical mode resonance

- At resonance one will establish an equilibrium population of the excited state and one can see at $\vec{G}$ of lattice and $\Delta\omega = 0$ Fourier components of the excited charge which can be measured by comparing Bragg signal with light on and off (Coppens Talk)

PHASE MATCHING CONIDITIONS
(General)

$\vec{k}_{in}$ = input X-ray wave vector

$\vec{k}_{out}$ = outgoing X-ray wave vector

$\vec{G}$ = reciprocal lattice vector

$\vec{q}_{L1}$ = wave vector of laser at ω_{L1}

$\vec{q}_{L2}$ = wave vector of laser at ω_{L2}

$\hbar\,\omega_{in}$ = energy of input X-ray

$\hbar\,\omega_{out}$ = energy of outgoing X-ray

- Three Wave mixing (linear optical polarization)

$$\vec{k}_{out} - \vec{k}_{in} = \vec{G} \pm \vec{q}_{L1}$$

$$\omega_0 = \omega_{in} \pm \omega_{L1}$$

- Three Wave Mixing (non-linear optical polarizability e.g. second harmonic)

$$\vec{q}_{L1} = 2\vec{q}_{L1}$$

› first must satisfy optical phase matching

$$\omega_{L1} = 2\omega_{L1}$$

- Four Wave Mixing (mixing, stimulated Raman or Brillouin, optical gratings)

$$\vec{k}_{out} - \vec{k}_{in} = \vec{G} \pm \vec{q}_{L1} \pm \vec{q}_{L2}$$

$$\omega_0 = \omega_{in} \pm \omega_{L1} \pm \omega_{L2}$$

$\vec{G}$ allows one to always achieve phase matching

SOURCE COMPARISON

	APS	XFEL
T (pulse width seconds)	65×10^{-12}	65×10^{-15}
N_p (number of pulses per second)	10^7	120
TN_p	6.5×10^{-4}	10^{-11}
Average Brightness (photons/s − mm² − mrad² 0.1% BW)	2×10^{18}	10^{23}
Beam Size at Sample (microns) (50 meters from source -no mirror)	1300×450	100 X 100
Beam Divergence (seconds)	4.8×1.8	.4
photons/sec − ev	6.7×10^{13}	6×10^{14}

PULSED LASER & X-RAY EXPERIMENTS

T	=	pulse width (sec)
N_p	=	number of pulses/sec
σ_{NL}	=	cross-section for non-linear component
σ_B	=	cross-section for linear Bragg component
n_o	=	scattered photons/sec (average)
n_{in}	=	incident photons/sec that can be phase matched (average)
n_{op}	=	$\sigma_{NLP}\, n_{inp}$
n_o	=	$\dfrac{\sigma_{NL}\, n_{in}}{N_p T}$

$N_pT = 10^{-11}$ XFEL $N_pT = 6.5 \times 10^{-4}$ APS

$\therefore$ Non-linear experiments are better with high peak power and low duty cycle (for the same average power)

LASER DAMAGE

LPL_p = peak laser power limit
varies with material
varies with pulse width

$\cong$ $10^9 - 10^{11}$ watts/cm^2

$$n_o = \frac{\sigma_{NL}\ n_{in}}{N_p T} \Rightarrow \frac{\sigma_{NL}}{N_p T} \propto \frac{E_L^2}{N_p T} \leq LPL_p$$

$n_o \leq \sigma_{NLmax}\ n_{in}$

N_{LP} = number of laser pulse/sec

T_L = laser pulse width

L_{avg} = average laser power/watts/cm^2

A_L = area of laser beam (cm^2)

LP = average laser power = $L_{avg}\ A_L$

$LP_{max} = LPL_p \times (N_{LP} \times T_L) \times A_L$
$= 10^{10} \times 10^{-11} \times 10^{-4}$
$= 10^{-5}$ watts XFEL
$= 10^{10} \times 6.5 \times 10^{-4} \times 5 \times 10^{-3}$
$= 30 \times 10^3$ watts APS not possible, even with mirror

$\therefore$ LP at APS $\sim 10^{-3}\ LP_{max}$

X-ray Cross-section

- The Fractional Scattered Intensity (symmetric reflections in the plane of polarization)

$$\sigma_B = \frac{\lambda^2 r_0^2 \mid \rho(\vec{G}) \mid^2}{\Delta k^2 + \alpha^2} = \frac{n_{out}}{n_{in}}$$

α^{-1} is the x-ray absorption length

$\mid \rho(\vec{G}) \mid^2$ is the square of the Fourier Transform of the charge density

- If input x-ray beam $\Delta k > \alpha$, then one measures the integrated intensity (no extinction)

$$\sigma_B^I = \frac{n_{out}}{n_{in/rad}} = \frac{\lambda_0^3 r_0^2 \mid \rho(\vec{G}) \mid^2}{4\alpha \sin 2\theta\beta}$$

The Experiment

Linear Case

- Phase Matching Requirements

n	=	index of refraction
$\delta\theta$	=	difference of input from Bragg angle
$\delta\theta^1$	=	difference of output from $2\theta_\beta$ of input
β	=	angle of light beam relative to incident x-ray
$\delta\theta$	=	$\pm\ q_L/G\ \cos\theta_B\ \ (\cos\ (2\theta_B + \beta) - 1/n)$
$\delta\theta^1$	=	$\pm\ (q_L/k_I\ \cos\theta_B)\ (\sin(\theta_B + \beta)\ +\ \sin\theta_B n)$

For the simple case $\vec{q}_L$ opposite to $\vec{G}$ (light normal to the surface)

$$\delta\theta = \mp \frac{q_L}{G\cos\theta_B} (\sin\theta_B + 1/n) \cong \frac{d_{hkl}\, n}{\lambda_L}$$

$$\delta\theta^1 = \mp \frac{q_L\ (1 + \sin\theta_B/N)}{k_{in}\cos\theta_B} \cong \frac{n\lambda_x}{\lambda_L}$$

$\therefore$ electronic $\delta\theta$, $\delta\theta^1 \sim 20$ - 200 seconds
displacive $\delta\theta$, $\delta\theta^1 \sim 2$ - 20 seconds

Can also do energy discrimination on output

Divergence of light beam not critical

Estimate of Signal Strength

Linear case

$$|\rho_L(\pm \vec{q}_L + \vec{G})|^2 = |\vec{R}_G \cdot \vec{E}_L|^2$$

ρ_m = microscopic charge

$\rho_m = [\nabla \cdot \overleftrightarrow{X}_m \cdot \vec{E}_m] / e$ Maxwell's Equation Fourier component ∇ multiplies X_m E_m by G

$$|\vec{R}_G \cdot \vec{E}_L|^2 = |S(\vec{G}, \omega_L)|^2 \frac{|GXE_L|^2}{e}$$

$\vec{P}(r)$ = polarization density = $X \cdot \vec{E} = \frac{e\langle r \rangle}{v}$ v = volume of unit cell

$$|\rho_L(\pm q_L + G)|^2 = [G\langle r \rangle]^2 \; 1/v^2 \; |S(G,\omega_L)|^2$$

$$|\rho(\vec{G})|^2_B = 1/v^2 \; |F(\vec{G})|^2$$

$|S(\vec{G}, \omega_L)|^2$ form factor for induced charges at ω_L

- contains microscopic information
- in general a fourth rank tensor
- valence electrons - S large for small $\vec{G}$ (electronic)
- Displacive Polarization - S similar to F

Signal Strength

$$|S(\vec{G}, \omega_L)|^2 \frac{G^2X^2E_L^2}{e^2} = |S(\vec{G}, \omega_L)|^2 \, 10^{16} G^2 X^2 LP_p$$

$|S(G, \vec{\omega}_L)|$ varies from $1 \rightarrow 0$ as G increases

$LPp \leq LPLp \sim 10^{10}$ watts/cm^2 XFEL

G varies from $.3 \rightarrow 10 \times 10^8$

X varies from $1/4\pi \rightarrow 3/4\pi$

For $S^2 = .1$, $G = .5 \times 10^8$, $X = .1$ $LP_p = LPL_p = 10^{10}$

$|\rho(\vec{G} + \vec{q}_L|^2 = 2.5 \times 10^{38}$ cm^{-6}

$\Delta k < \alpha$ $\alpha^{-1} = 1$ mm $\lambda = 1.5$ Å

$\mathcal{G}_{NL} = 4 \times 10^{-44} \times 2.5 \times 10^{38} = 10^{-5}$ but $\Delta\theta = .05$ seconds

$\Delta k > \alpha$ $\mathcal{G}^1 = 6 \times 10^{-50} \times 2.5 \times 10^{38} \cong 10^{-11}$ (XFEL)

$\cong 10^{-14}$ (APS)

Signal Rates

Linear Case

	XFEL	APS	
$n_{in/rad\ (1\ ev)}$	3×10^{20}	10^{19}	
$n_{out\ (photons/sec)}$	3×10^{9}	10^{5}	electronic
$n_{in/rad\ (.1\ ev)}$	3×10^{19}	10^{18}	
$n_{out\ photon/sec}$	3×10^{8}	10^{4}	displacive

2nd Order

Each higher order scales roughly as

$$\frac{|E_{Lp}|^2}{|E_{atomic}|^2} \propto \frac{|eEa|^2}{|\hbar\omega j - \hbar\omega g|^7} \cong 4 \times 10^{-6} \text{ XFEL} \cong \mathcal{G}_{NL}$$
$$4 \times 10^{-9} \text{ APS}$$

$E_{atomic} \cong 3 \times 10^{8}$ v/cm

$E_{Lp} = 6 \times 10^{5}$ v/cm XFEL

$E_{Lp} \cong 2 \times 10^{4}$ v/cm APS

	XFEL	APS
n_{out} (photon/sec) (1 ev)	10^{4}	$\sim 10^{-4}$
n_{out} (photon/sec) (.1ev)	10^{3}	$\sim 10^{-5}$

General Conclusion

- The microscopic aspects of the interaction of light with crystals can be readily studied

  - Both linear optical and non-linear optical phenomena with XFEL

  - Includes polariton effects

  - Only linear at Argonne (even that limited)
    + small values of S cannot be explored
    + only crystals with relatively small x-ray absorption

Other Interesting Possibilites

- Time dependence

  - By delaying X-ray pulse relative to optical pulse can probe local relaxation phenomena

  - Can study development of gain (crystal in a cavity)

- Energy Transfer

  - With two light beams can simultaneously measure incident light fields effects and non-linear signal effects

- Produce Femtosecond X-ray beams
  - Use Femtosecond laser (higher LPLp possible)

- Other modulations
  - acoustic waves, electron waves etc.

Summary of Discussion

Eisenberger talk:

Several questioners asked for clarification of Eisenberger's assertion that in experiments looking for nonlinear interactions between x-rays and optical-wavelength radiation in a sample, the data rate is limited by the rate at which the optical-wavelength power (from a high-power laser) can be dissipated. Eisenberger explained that in general the average power of the x-ray source is much less than that of the high-power optical laser. He pointed out that for pulsed x-ray and optical sources the data rate depends on the peak power, while the sample dissipation limit depends on average power, so that pulsed x-ray and optical sources with matching cycle times would be best for these experiments. However, existing pulsed x-ray sources such as synchrotron beam lines have cycle times much shorter than those available from high-power optical lasers. In contrast, the LCLS design, with its pulse rate of 120 Hz, would be a much better match for a high-power pulsed optical laser.

X-ray Parametric Scattering Stimulated by an Intense Laser Field

Kazumichi Namikawa, Tokyo Gakugei University

X-ray Parametric Scattering Stimulated by an Intense Laser Field

K. Namikawa[A,B], H. K. Uematsu[A], M. Ohi[A], X. W. Zhang[B], M. Ando[B] and S. Itoh[C]

A)Department of Physics, Tokyo gakugei University, Koganei, Tokyo 184, Japan.
B)Photon Factory, KEK, Tsukuba, Ibaraki 305, Japan.
C)Tokyo Institute of Politechnics, Atsugi, Kanagawa 243, Japan.

X-ray spontaneous parametric scattering[1] is a well known quantum optical phenomenon; an incident x-ray field couples with a field due to the vacuum fluctuation through a higher order susceptibility of the material and results in a two photon scattering. These phenomena that both scattered photons are in x-ray region[2] or one photon is in x-ray region and the other photon is in VUV region[3] are observed already. However, the case where one of the two photon is in the optical region is not observed yet because of its small scattering probability; it is an order of 10^{-9} compared to the one photon scattering[4]. We can expect the emission of the optical photon to occur as an induced process provided an intense laser field exists. In this case, scattering probability of the x-ray parametric scattering can be enhanced enormously. Estimated from the laser assisted x-ray absorption under 10^7 W/cm^2 laser field[5], scattering probability of the x-ray parametric scattering amounts to 10^{-2} of the one photon scattering.

Adopting a GGG single crystal as a sample, we presume such resonance scattering process that 2p electron in Gd is excited into empty 5d band, then an intra-band transition takes place by the stimulated emission of two optical photons, finally an emission of x-ray photon takes place. These process occurs effectively under so-called phase matching conditions as follows are fulfiled.

$$\omega_{X'} = \omega_X - 2\omega_l, \tag{1}$$

$$k_{X'} = k_X - 2k_l + G, \tag{2}$$

where, x and x' mean the incident and scattered x-rays, respectively, l means the optical photon and G is a reciprocal lattice vector. From the eqs (1) and (2), we can expect a satellite to take place at the tail of higher angle side of the Bragg scattering.

Experiment has been performed at an undulator beam line AR NE-3 in KEK, which is operated in a single-bunch mode. Incident x-ray has been monochromated by Si(111) double crystal monochromator within resolution 2eV to the energy 4.66eV, double energy of the optical photon, higher than the energy of Gd L2 absorption maximum. Second higher harmonics of pulsed Nd-YAG laser 50 Hz in repetition and 2 nsec in width has been utilized as the laser beam. Under the condition descrived above, the satellite has been expected to appear at 268" higher angle side of the 444 Bragg reflection. Simultaneous iradiation of x-ray beam and laser beam has been performed by refering to the ring control timing signal. Intensity profile has been measured with respect to the rotation of the crystal. Two kind of the profiles have been measured simultaneously; one is gated by the laser Q-switch trigger, the other is ungated.

The gated profile normalized by ungated profile exhibits an intensity enhancement at the region expected by the phase matching conditions. The profile of the satellite enhancement consisting of two peaks agrees well with that of the 444 Bragg reflection consisting of two peaks due to the domain structure accidentally. The enhancement amounts to about 1.3 % of the background intensity in this region. This value corresponds to 1×10^{-5} of the intensity of the 444 Bragg reflection. Scattering probability of the relevant phenomenon amounts to 10^{-3} of that of a normal one photon scattering if the effective number of atoms contributing to the relevant structure factor is taken into consideration. These results strongly suggest that the observed intensity enhancement is due to the x-ray parametric scattering induced by a strong laser field.

1) I. Freund and B. F. Levine, Phys. Rev. Lett. **23** (1969) 854.
2) P. Eisenberger and S. L. McCall, Phys. Rev. Lett. **26** (1971) 684.
3) H. Danino and I. Freund, Phys. Rev. Lett. **46** (1981) 1127.
4) I. Freund, Phys. Rev. **A7** (1973) 1849.
5) I. Freund, Opt. Commun., **8** (1973) 401.

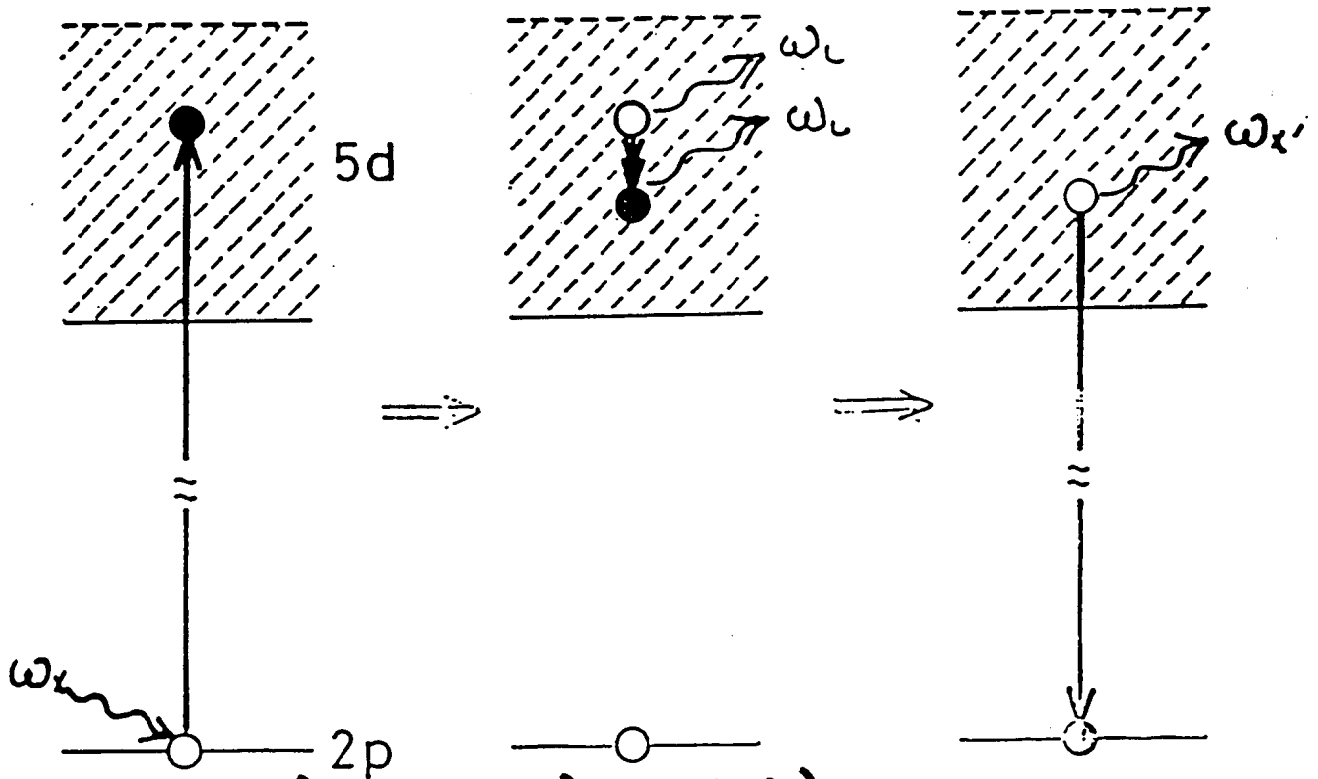

$$\omega_{x'} = \omega_x - 2\omega_L$$

$$K' = K - 2K_L + G$$

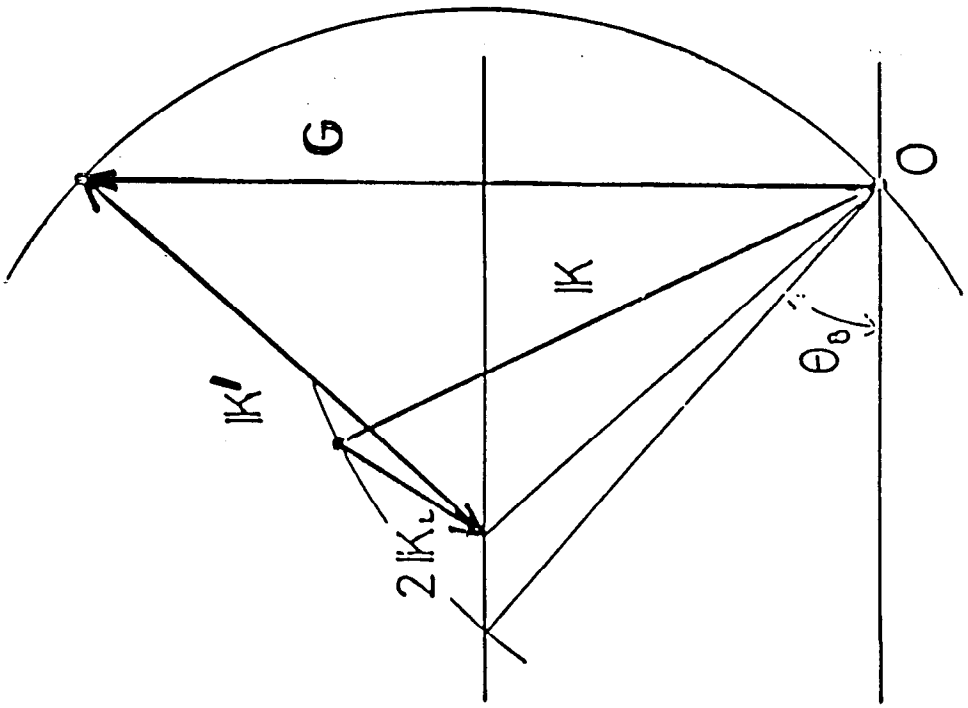
G
O
|K
|K'
2|K_c
θ_0

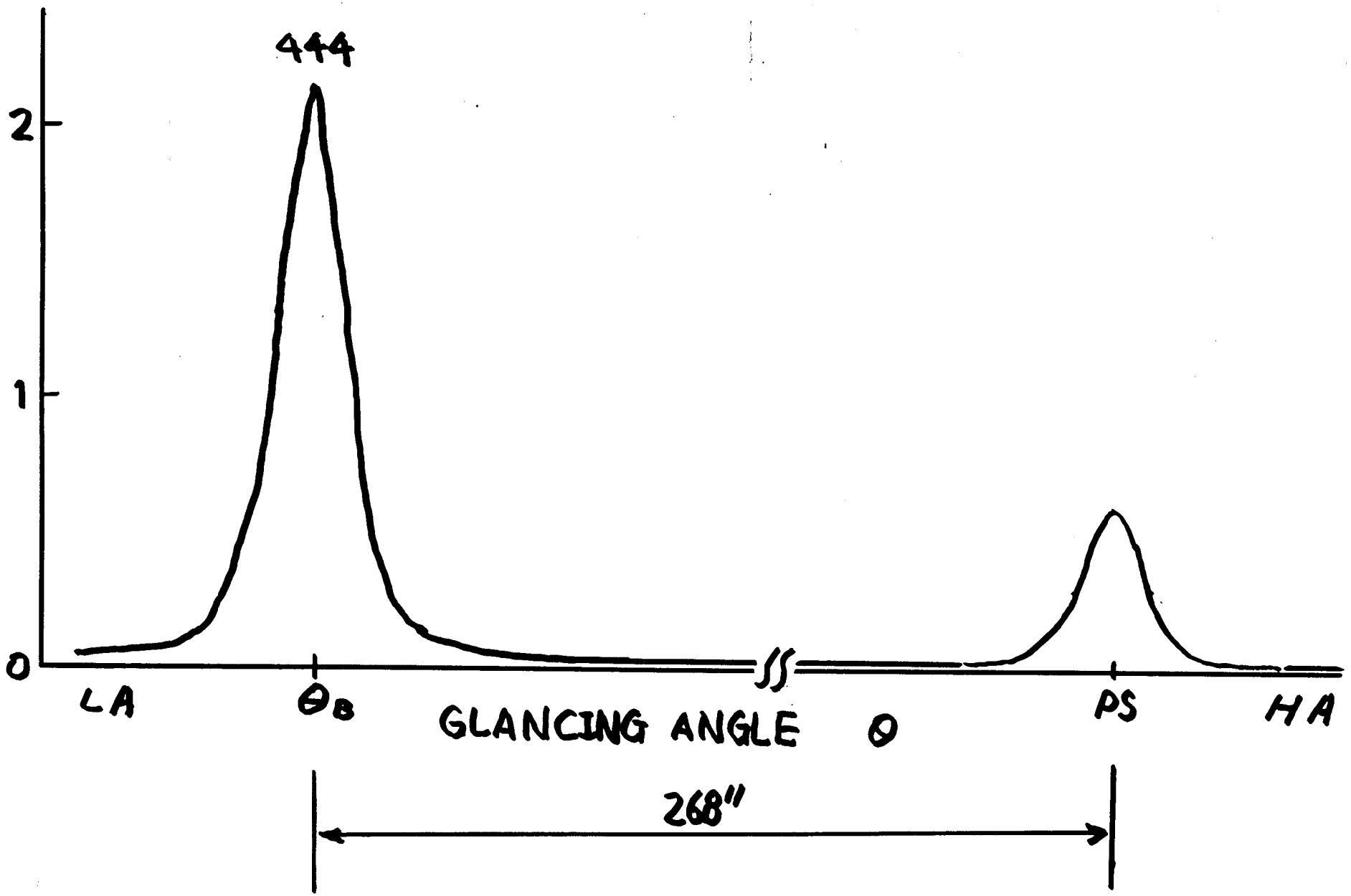
444
2
1
0
LA
θ_B
GLANCING ANGLE θ
PS
HA
268"

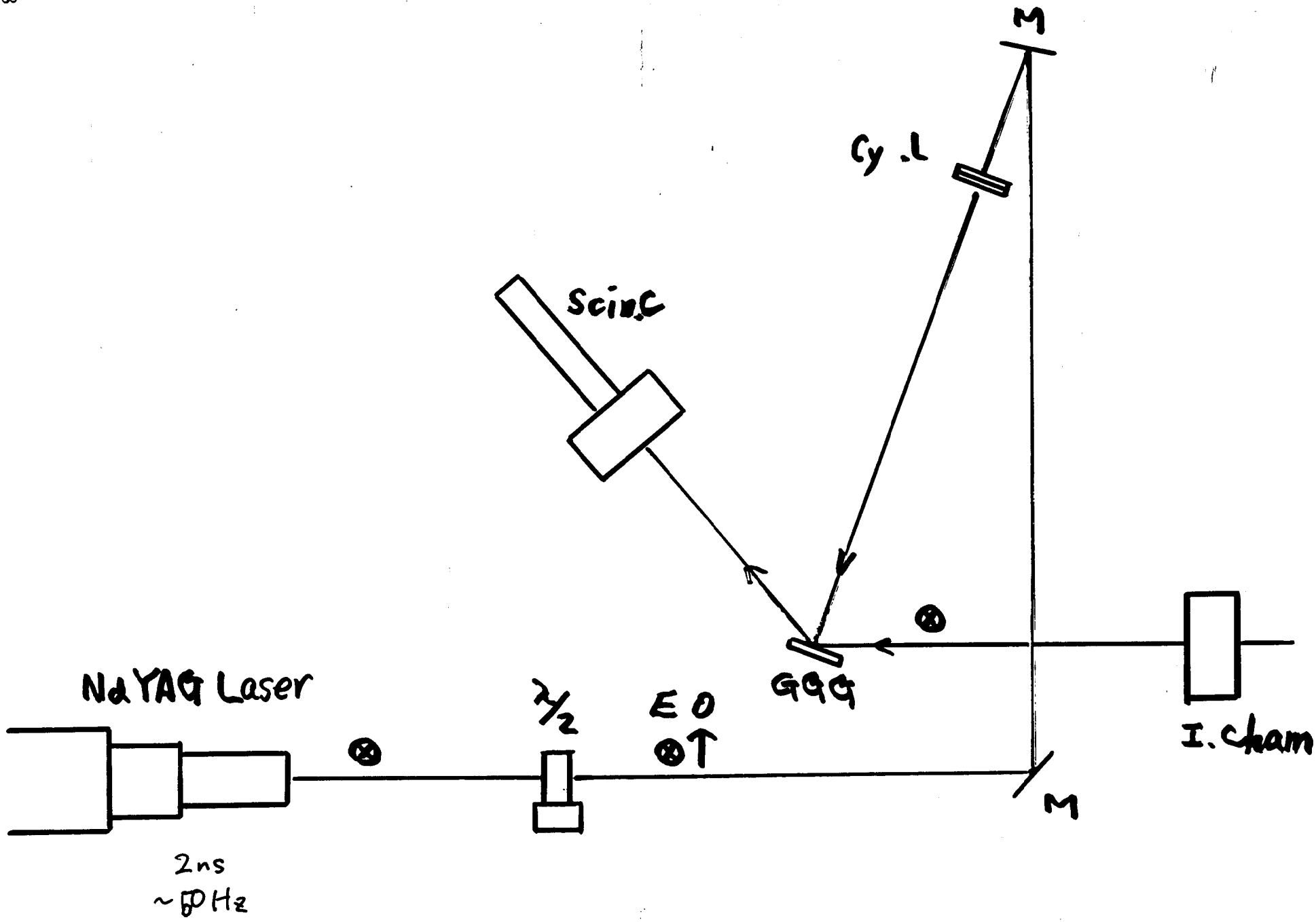
M
Cy .L
Scint
GGG
I. cham
NdYAG Laser
λ/2
EO
M
2ns
~10Hz

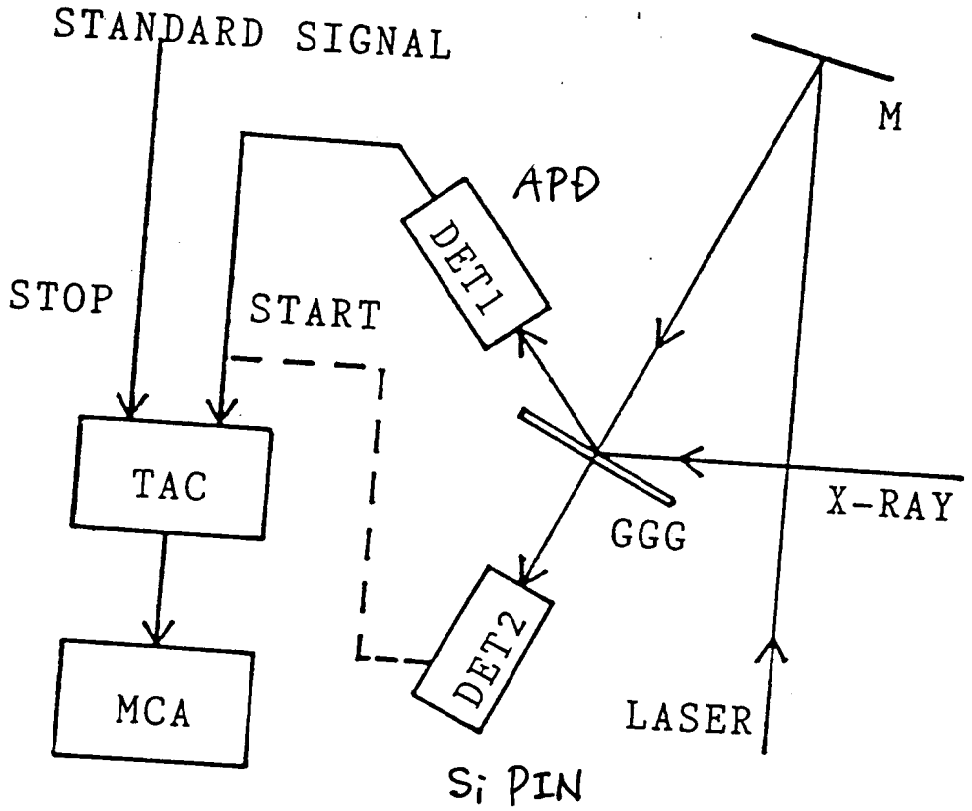
STANDARD SIGNAL
M
APD
DET1
STOP
START
TAC
X-RAY
GGG
DET2
MCA
LASER
Si PIN

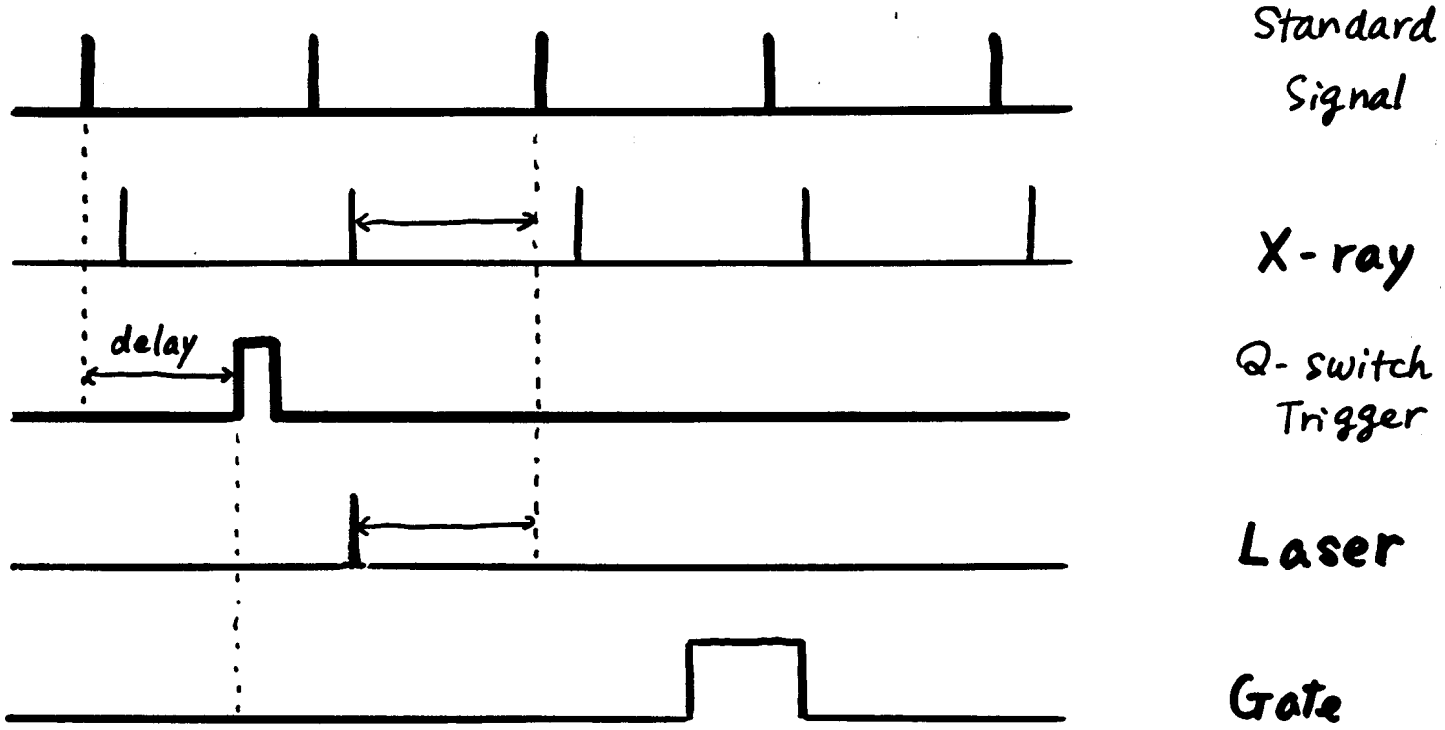
Standard
Signal
X-ray
delay
Q-switch
Trigger
Laser
Gate

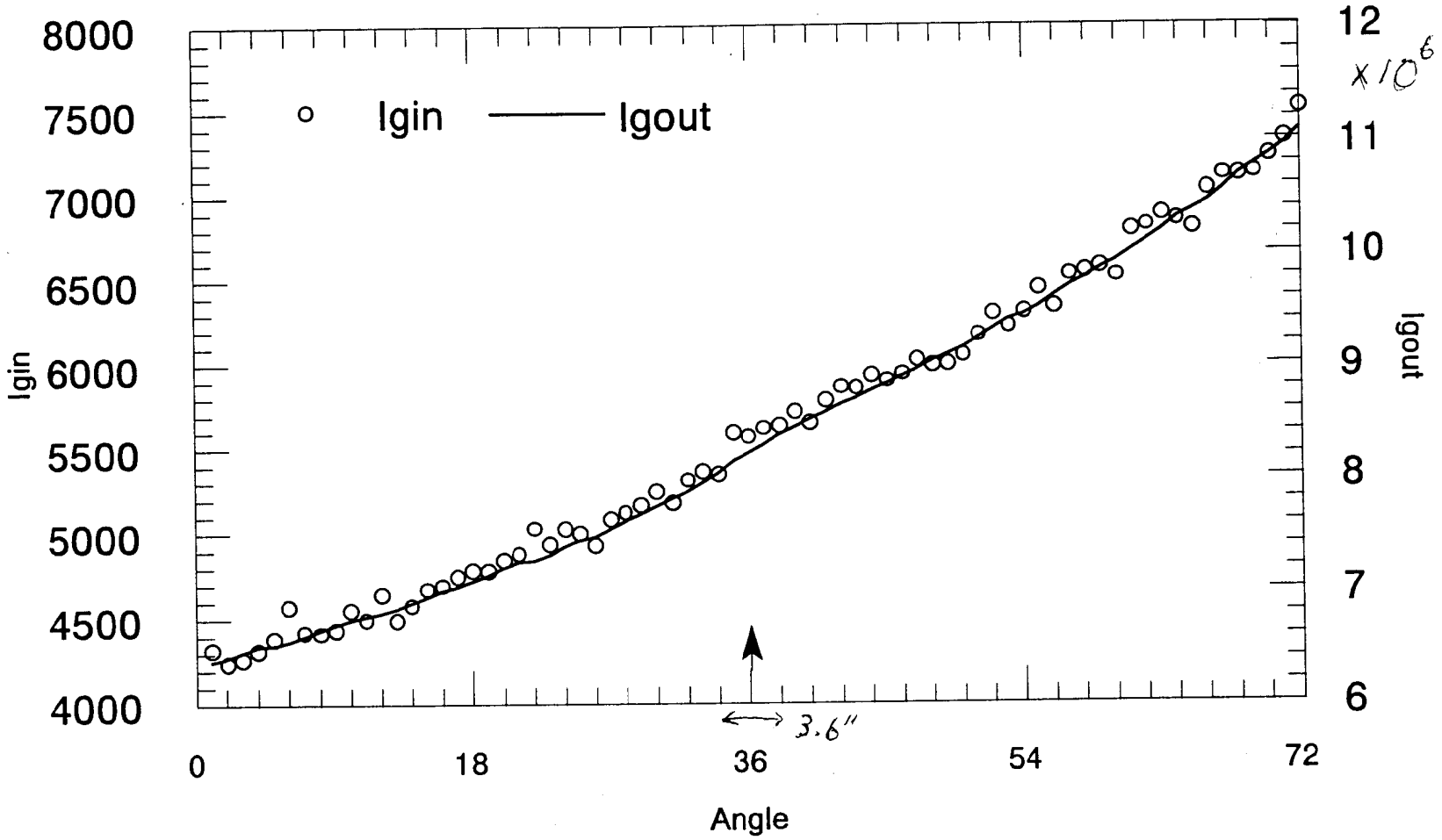
8000
7500
7000
6500
6000
5500
5000
4500
4000
Igin
12
x10^6
11
10
9
8
7
6
Igout
Igin
Igout
3.6"
0
18
36
54
72
Angle

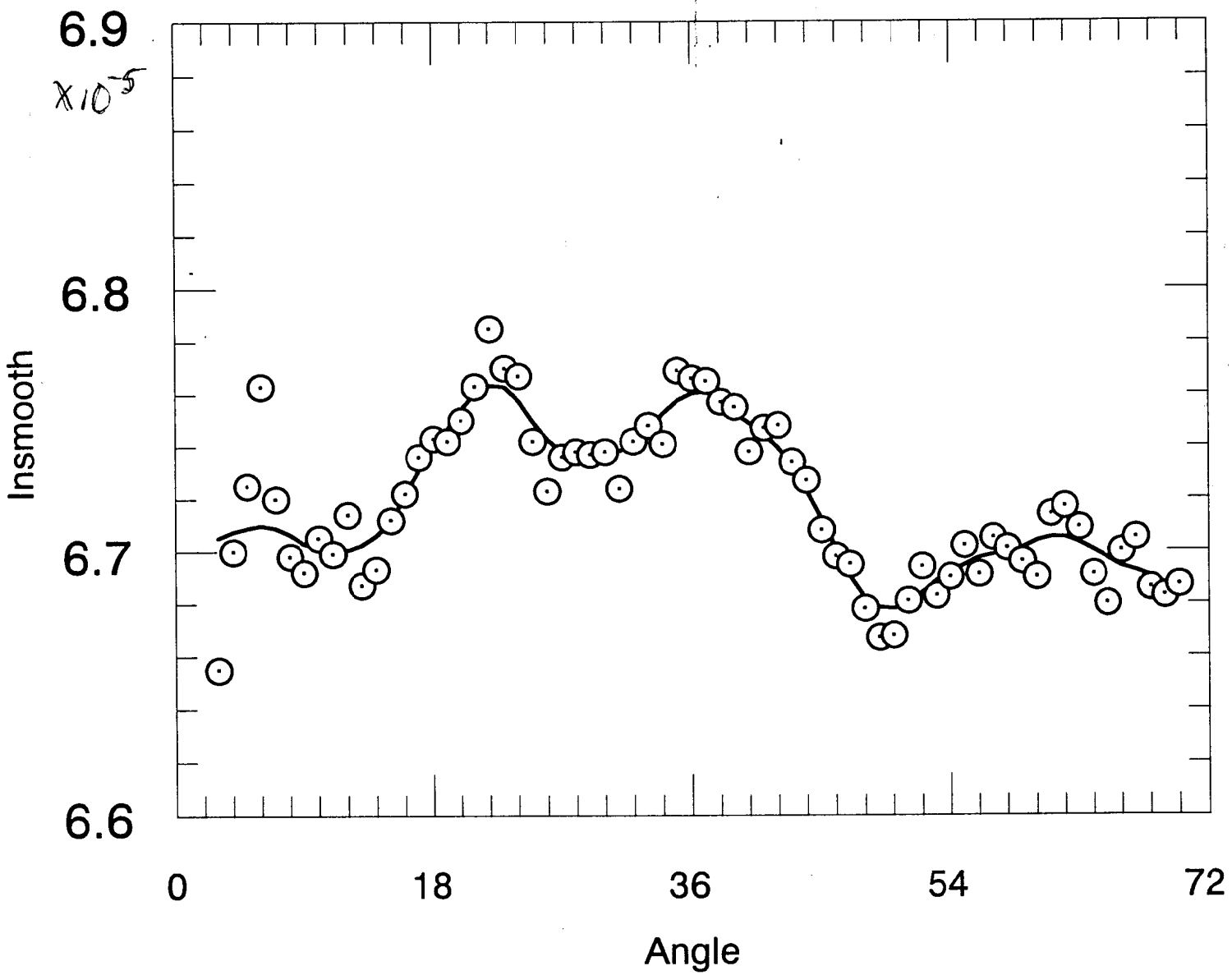
6.9
X10-5
6.8
6.7
6.6
Insmooth
0
18
36
54
72
Angle

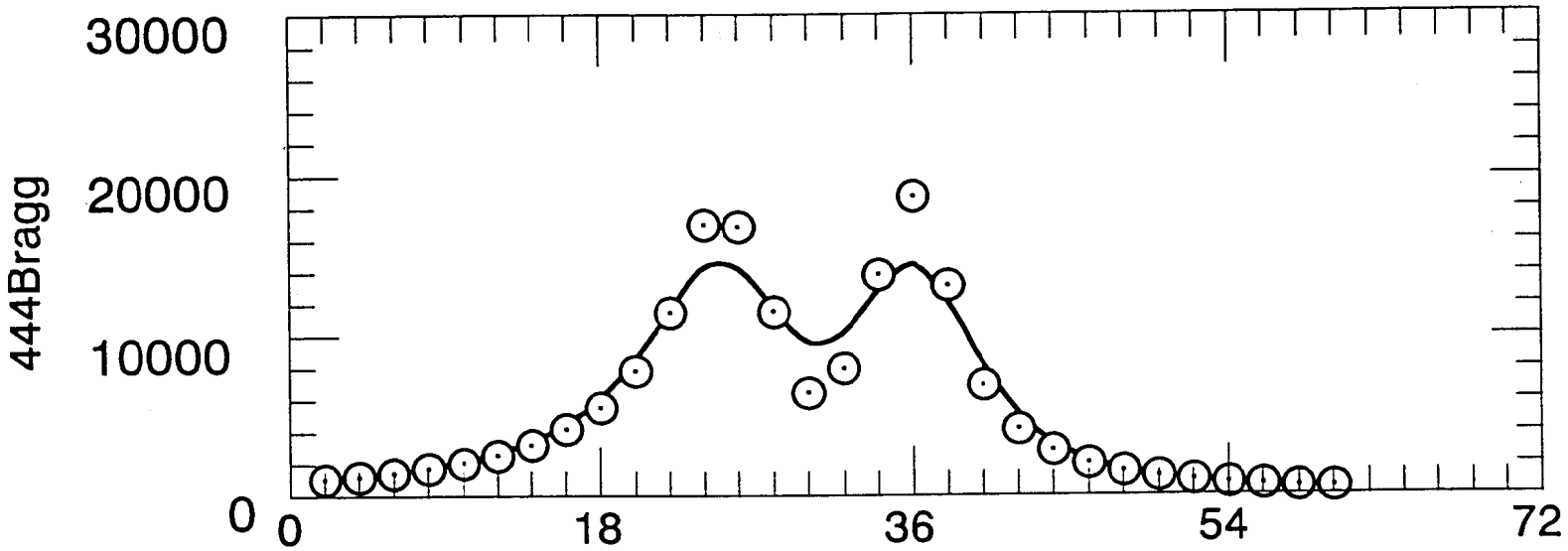
30000
20000
10000
0
444Bragg
0
18
36
54
72

Imaging with Soft & Hard X-rays

Janos Kirz, SUNY Stony Brook

MICROSCOPY WITH SOFT AND HARD X-RAYS

Janos Kirz
Physics Department, SUNY, Stony Brook, NY 11794

The unique characteristics of the source (intense, short pulses of coherent, narrow band radiation) should make it possible to perform single shot imaging of biological specimens. These images would be obtained fast enough so that neither motion, nor the consequences of radiation damage will corrupt the results. It should be therefore possible to consider initially live specimens, and use the timing characteristics to study the response to stimuli as in the case of muscle, nerve, etc.

Using the technique of rapid freezing, other forms of microscopy may make it possible to immobilize initially live material, but would have difficulty in competing with the precise timing possibilities of this source in clarifying the action of light and sound receptors, or the sequence of the events taking place at the neuromuscular junction.

The anticipated transverse resolution would be about 30 nm. To extend this resolution to the depth dimension, it would be necessary to make multiple simultaneous exposures from several directions, and to perform diffraction tomography, as discussed at this workshop by Howells and by Haddad.

Imaging could be via holography, or dark field microscopy.

Tuneability of the source is particularly important as it can be used to maximize contrast, or to use XANES resonances to highlight a particular chemical state.

Within the "water window", between the carbon and oxygen absorption edges, amplitude contrast is optimal for wet specimens up to about 5μm thick. Thicker specimens are best imaged using phase contrast in holography at shorter wavelengths. As the wavelength goes down, so does the cross section. As a result the signal from single small features becomes weaker, and hard x-rays are therefore not attractive for high resolution imaging. They may still find important use for the study of opaque dynamical systems, such as buried circuits and micromachines in operation.

Why is the proposed source so exciting for microscopy?

- **Fast** ↘ Single shot imaging possible before motion or damage corrupts
- **Intense** ↗
- **Narrow band** → Can use zone plates w/o monochromator
- **Spatially Coherent** ↘ Suitable for holography
- **Tuneable** Elemental or chemical mapping

GOAL:

- 3D imaging of whole (initially) live cells
- Study response to stimuli
  - muscle
  - nerve
  - receptors
- resolution ~30 nm

SOFT X-RAYS: 250 eV - 600 eV

- water window: good amplitude and phase contrast.
  (wet specimens 0.5μm - 5μm)
- efficient, high resolution detectors,
  zone plates and microstuctures
- C, N, O K absorption edges, XANES contast
  Cl, K, Ca L " "

SOFT X-RAYS: 600 eV - 5 KeV

- Good phase contrast (wet specimens 5μm - 50μm)
- Efficient, high resolution detectors
- F, Na, P, S, Cl, K, Ca K absorption edges, XANES
  Mn - Ba L " "

STXM image of a JU56 (Wallaby) fibroblast

V. Oehler *et al.*, Stony Brook Physics

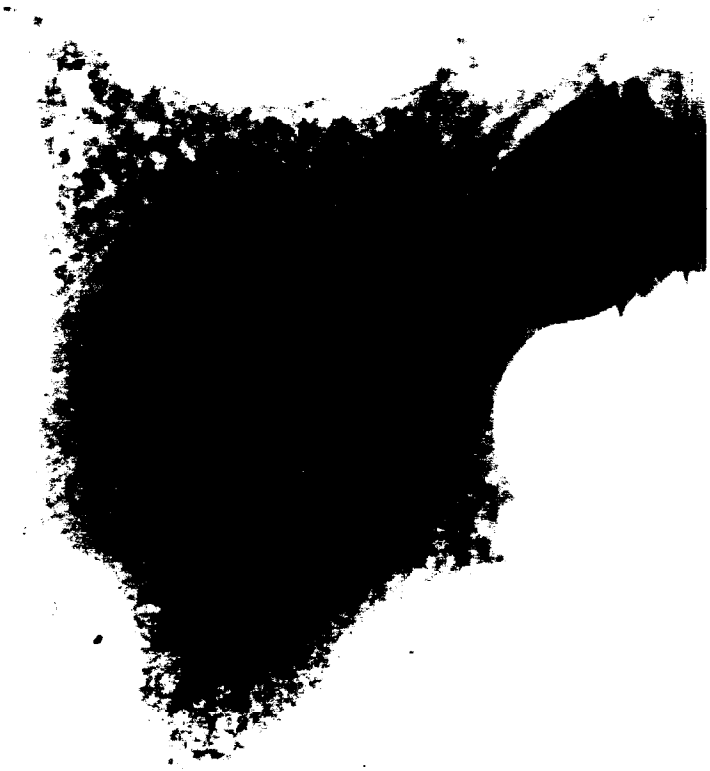

X-1A scanning transmission x-ray microscope image of a fixed, wet, whole JU56 (Wallaby cell line) fibroblast, acquired using a 45 nm zone plate fabricated by E. Anderson, LBL, using e-beam lithography facilities at IBM Yorktown Heights.

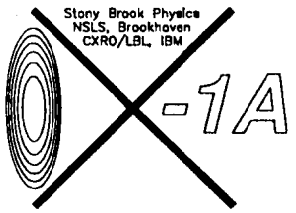

SOFT X-RAY MICROGRAPH OF WET, INITIALLY "LIVE" RABBIT MYOFIBRIL.
(NSLS X1A SCANNING MICROSCOPE)
COURTESY OF C. BUCKLEY, KING'S COLLEGE, LONDON.

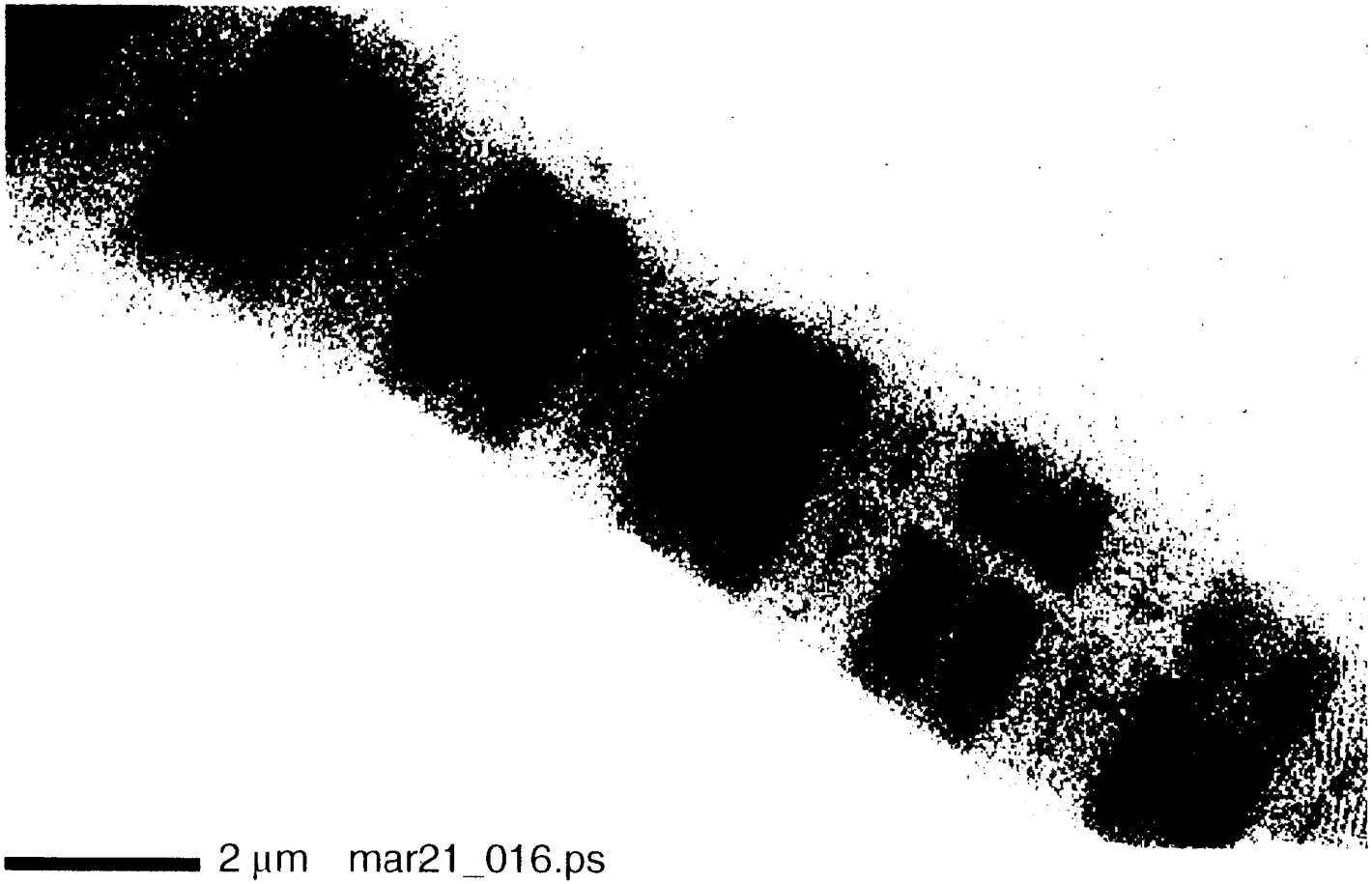

Wet chromosome series at the carbon edge

S. Williams, Brookhaven Biology

X. Zhang, C. Jacobsen, and J. Kirz, Stony Brook Physics

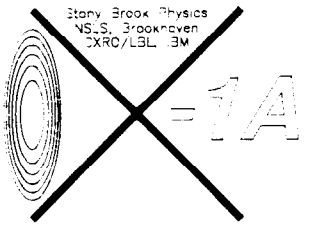

Series of images of a wet, fixed *v. faba* chromosome taken at the indicated photon energies. The contrast variations are due to x-ray absorption near-edge differences in carbon absorption cross-sections as affected by the chemical bonding of carbon. The image at 288.93 eV is taken at the large absorption peak of protein, while the one at 286.53 eV is taken at the absorption peak of DNA. The image taken at 281.77 eV shows the good inorganic (silicon residue) and poor organic (chromosome) image contrast expected for viewing wet biological specimens with photon energies below that of the carbon absorption edge (i.e., outside the "water window"). The final image indicates that the chromosome suffered limited mass loss after a cumulative dose of about 2.5×10^6 Gray=250 MRad.

Hard X-RAYS: > 5 KeV

- X-rays see individual atoms
- Highly penetrating
- Microtomography of microcircuits
  or buried micro-actuators in operation
- Out of my league
  (fluorescence analysis not well matched)

THE COMPETITION

1/ Confocal:
- Can do a lot!
- Limited resolution
- Cannot do flash

2/ Scanning probes
- Surfaces or very thin layers
- Cannot do flash

3/ Electron Microscopy
- Can do a lot!
- Cannot do flash
- Thin specimens only.
  - (multiple scattering)
  - Response to stimuli hard

4/ X-rays at Synchrotron Radiation Sources
- Can do a lot!
- Cannot do flash
- Need cryo to stop motion
- Response to stimuli hard

5/ X-ray lasers (atomic systems)
- Potentially a major competitor!
- Not continuously tuneable
- Longer pulse could be a problem

Resolution: confocal versus x-ray

See e.g., C. Jacobsen, J. Kirz, and S. Williams, "Resolution in soft x-ray microscopes", *Ultramicroscopy* **47**, 55–79 (1992).

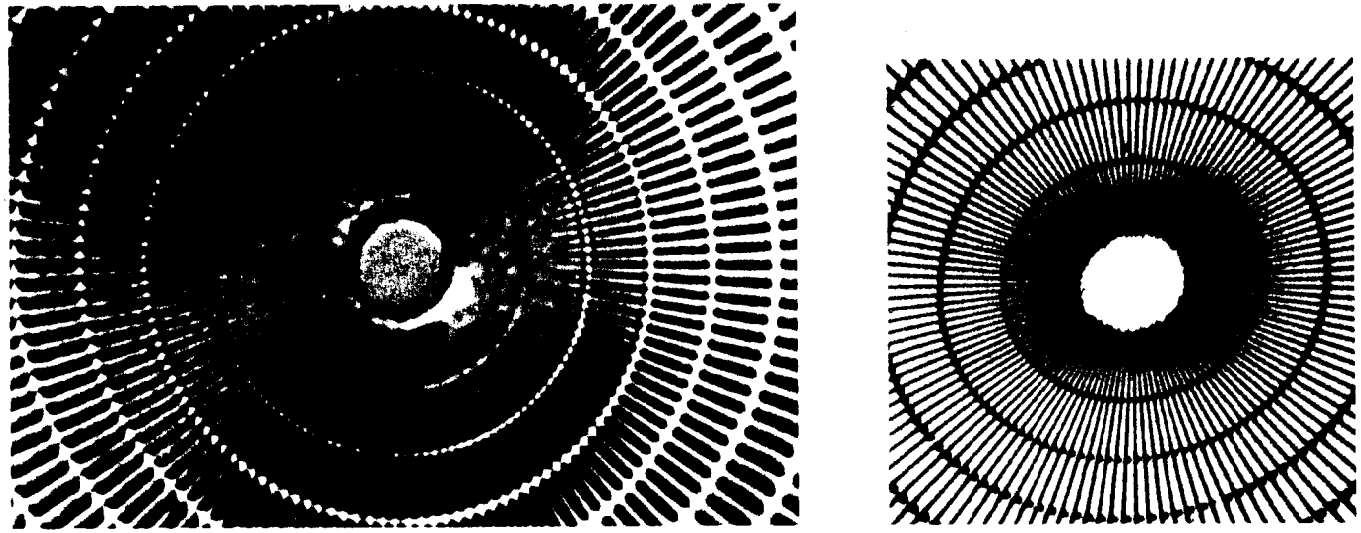

2.0 microns

Confocal: Zeiss N.A.=1.2 objective
(features to ~0.15 microns)

X-1A STXM: 45 nm zone plate
(features to ~0.03 microns)

Microfabricated test pattern viewed in reflection mode in a confocal microscope and in transmission mode using a scanning transmission x-ray microscope. The x-ray microscope is able to resolve $\sim 5\times$ smaller features.

Confocal image courtesy Barry Burbach, Stony Brook Neurobiology. Test pattern and zone plate fabricated by Erik Anderson, Center for X-ray Optics, Lawrence Berkeley Laboratory, using e-beam lithography facilities at IBM Yorktown Heights.

CONCLUSION:

Flash imaging of unsectioned cells at high resolution and 3D is an exciting prospect.

Summary of Discussion

Kirz talk, given by Howells:

Materlik asked whether it was possible to produce circular-polarized FEL radiation. Pellegrini and Kim agreed that this would be possible, and that a good way to do it would be to rotate the final section (about one gain length) of the undulator (where the FEL gain is approaching saturation) so that its field is perpendicular to the field in the earlier undulator sections. The FEL radiation would then consist of two linear, phase-related perpendicularly-polarized components, or, equivalently, elliptical polarization. The length of the crossed section would need to be adjusted carefully to produce circular rather than elliptical polarization. This will be studied in the future.

Diffraction Studies of Excited States of Molecules in Crystals - Present Experiments and Prospects for Studies of Very Short Lifetime Excited States Using Pulsed X-ray Sources

Phil Coppens, University of Buffalo

FEL'S AND EXCITED STATE MOLECULAR STRUCTURE

Philip Coppens
Chemistry Department
State University of New York at Buffalo
Buffalo, New York 14214

Thought X-ray diffraction is the standard technique for the determination of the structure of molecules in their ground state, parallel information on excited state structure has not been available, but is of crucial importance for the understanding of chemical and biological processes. We have recently been able to determine the structure and electron density of an extremely long-lived excited metastable state of sodium nitroprusside directly from the diffraction measurements.[1]

The experimental approach for excited state studies must be lifetime-dependent. For long lifetimes, excitation and diffraction are sequential. For intermediate lifetimes of the order of msecs, a modulation technique can be used in which 'on' and 'off' periods alternate, and the diffraction signal is gated to different channels in synchronization with the laser pulses. However, the more interesting study of short-lived species and kinetics of rapid processes requires a pulsed source of low repeat rate, to allow synchronization with intense laser pump pulses, and very high intensity per probing X-ray pulse. Free Electron Lasers are eminently suited for this purpose.

Fast electron transfer processes are part of the mechanism of photosynthesis,[2] are being explored extensively for molecular storage and switching devices in molecular computing,[3] and can be used in molecular sensors.

A Free Electron Laser with the proposed parameters, capable of producing ≈ 10 keV photons, would allow dramatically new experiments. A small area of a thin crystalline sample is to be excited by an intense laser pulse, and the diffraction intensity of the central area (≈ 10 x 10 μm) recorded at a variable time delay. The stroboscopic experiment can use narrow wavelength radiation from the main pulse, in which case reflections will be recorded sequentially, or a broader band from the intense background radiation, in which case a Laue technique can be applied. Since data collection will be rapid because of the extremely high X-ray intensity, the more accurate sequential technique may be preferable.

1 Pressprich, M.R., White, M.A. and P. Coppens, *J. Am. Chem. Soc.*, **15**, 6444-6445 (1993).

2 Deisenhofer, J., Epp, O., Miki, K., Huber, R. and Michel, H., *J. Mol. Biol.*, **180**, 38 (1984).

3 Mirkin, C.A. and Ratner, M.A., *Ann. Rev. Phys. Chem.* **43**, 719 (1992).

BOND LENGTH CHANGES ON MOLECULAR EXCITATION

Spectroscopic techniques: Franck-Condon Analysis of Vibrational Fine Structure

Examples

$W(CO)_5$ piperidine[1]
$^3E \Rightarrow {}^1A_1$, d_z^2 to (d_{xz}, d_{yz}),

Δ (trans W-C)= 0.25 Å

trans-dibromotetrakis(d^5-pyridine) rhodium(III) bromide hexadeuterate
$[RhBr_2(d\text{-}py)_4]$[2,3,4]
$^1A_1 \Rightarrow {}^3T_1$; $\pi \Rightarrow \pi^*$ transition

Δ(Rh-Br) ≈ 0.3Å

1 Zink, J. I., *Coord. Chem. Rev.*, **64**, 93 (1985).
2 Thomas, T. R., Watts, R. J. and Crosby, G. A., *J. Chem. Phys.*, **59**(4), 2123–2131 (1972).
3 Carstens, D. H. W. and Crosby, G. A., *J. Molec. Spectr.*, **34**, 113–135 (1970).
4 McClure, L. J. and Ford, P. C., *J. Phys. Chem.*, **96**, 6640–6650 (1992).

LIFETIME-DEPENDENCE OF EXPERIMENTAL APPROACH

A) Long lifetimes (seconds to hours): diffraction after excitation

B) Intermediate lifetimes (msecs): Use of modulation techniques with alternating 'on' and 'off' periods

C) Short lifetimes (μsecs, nsecs and less): Stroboscopic experiments using pulsed sources

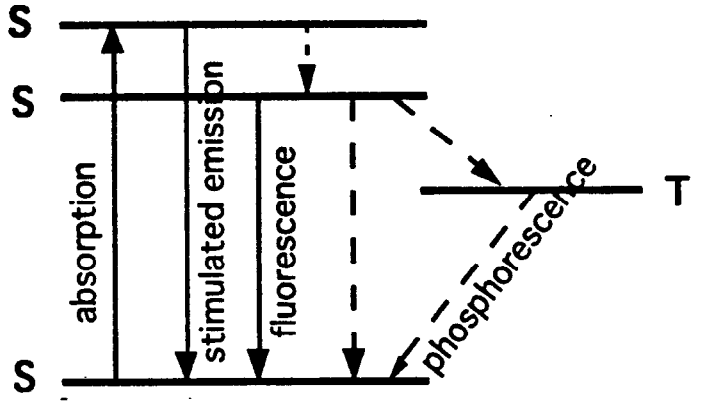

Photophysical processes. S, singlet state; T, triplet state. The dashed lines represent radiationless transitions. The two excited singlet levels may be different vibrational levels of one electronic state.

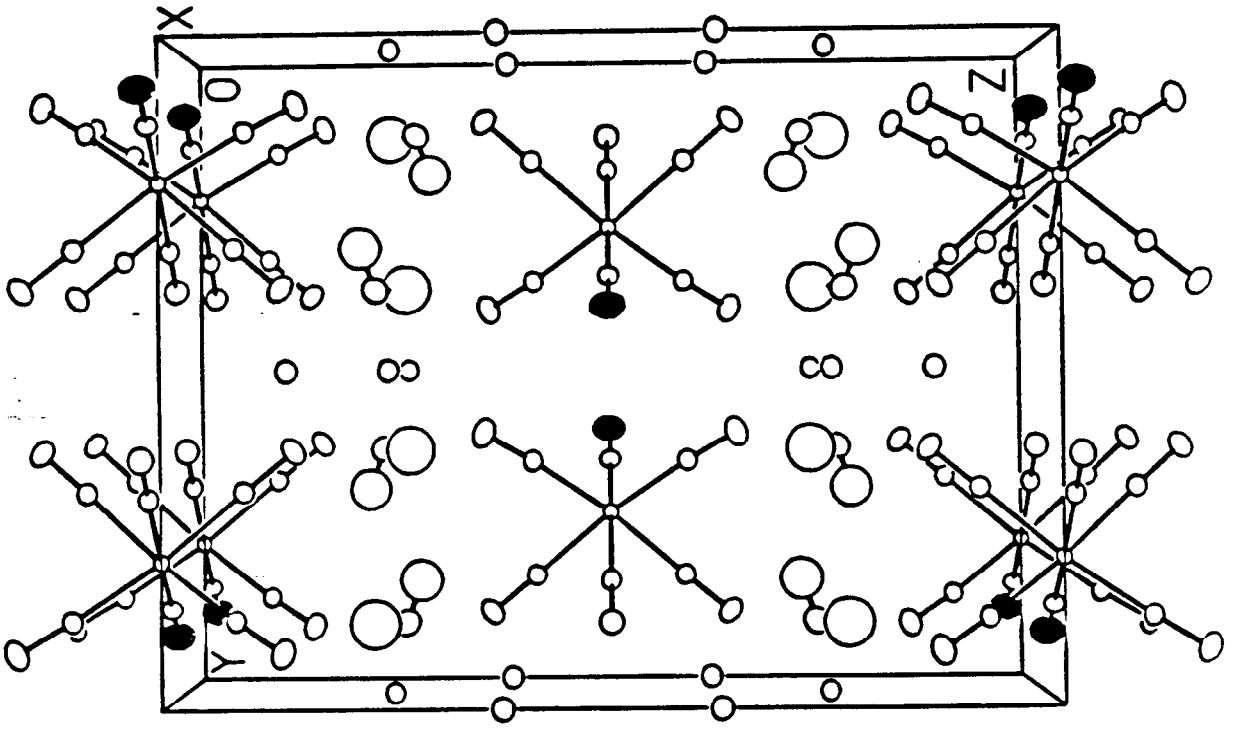
X
O
Z
Y

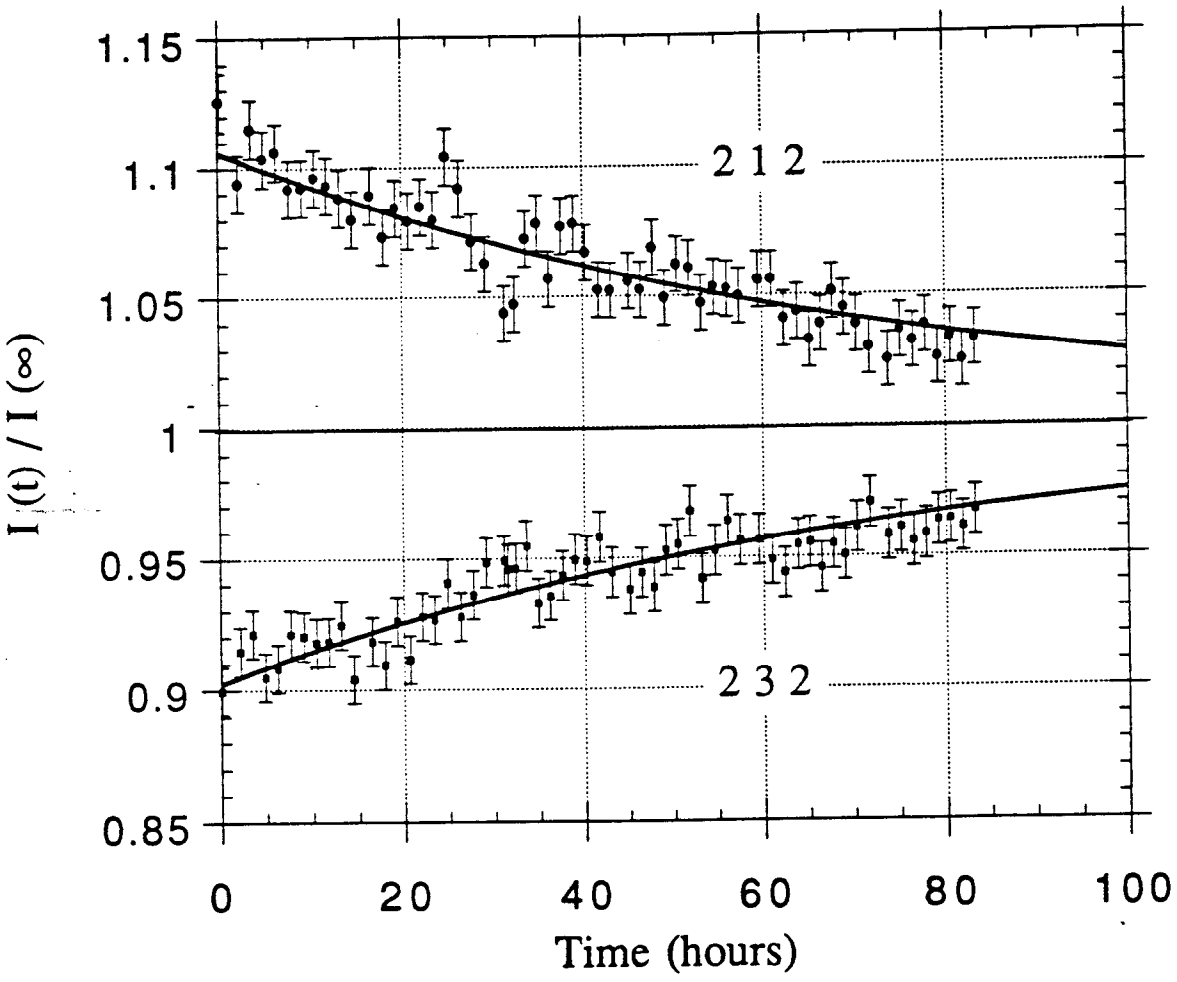
1.15
1.1
1.05
1
0.95
0.9
0.85
I (t) / I (∞)
212
232
0
20
40
60
80
100
Time (hours)

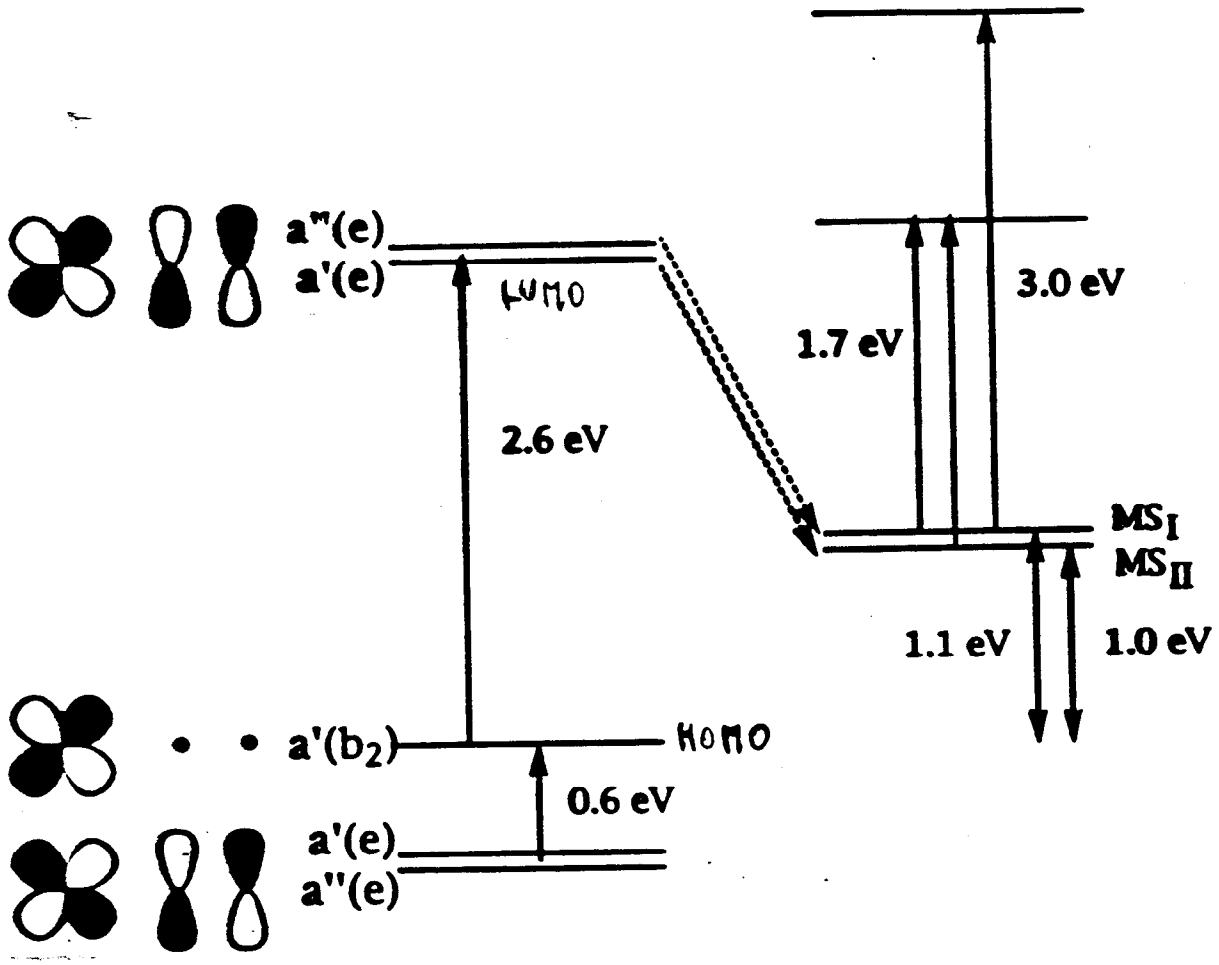
a"(e)
a'(e)
LUMO
2.6 eV
1.7 eV
3.0 eV
MS$_I$
MS$_{II}$
1.1 eV
1.0 eV
a'(b$_2$)
HOMO
0.6 eV
a'(e)
a"(e)

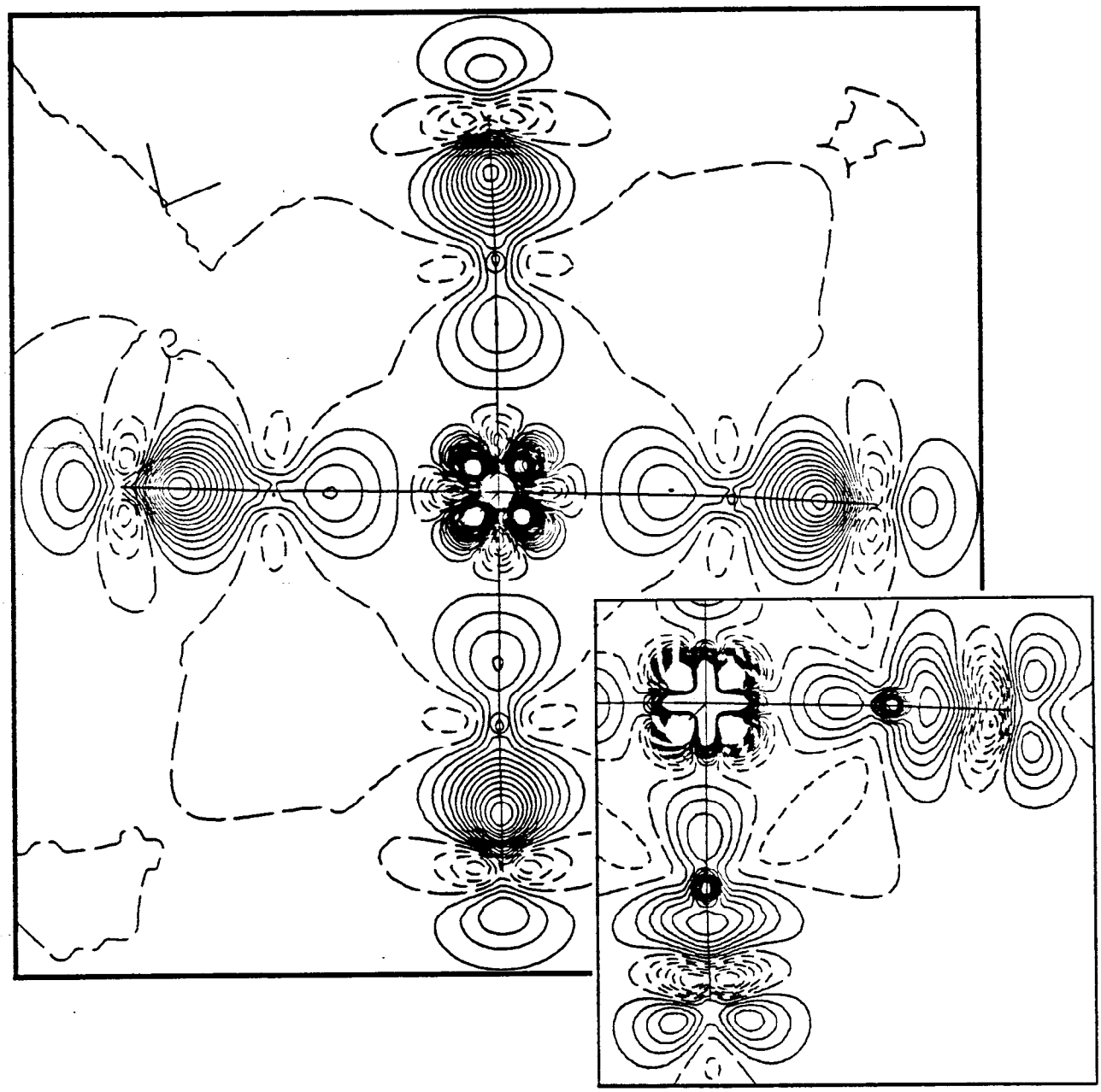

For first-order decay kinetics:

$$N^*/N = I_0 \sigma \Phi_{S \rightarrow T} \tau_e$$

Intensity needed

$$I_0 = N^*/(N \sigma \Phi_{S \rightarrow T} \tau)$$

With $\mu = 10$ cm^{-1} and N (the number of absorbing molecules per cm^{-3}) = 10^{21} ($V_{mol} = 10^3$ Å^3), the molecular cross-section σ, given by $\sigma = \mu/N$, equals 10^{-20} cm^2. So, (with $\Phi_{S \rightarrow T} = 1$), for a 1% steady state concentration ($N^*/N = 0.01$),
I_0 must be of order $10^{18}/\tau$ photons cm^{-2} s^{-1}.

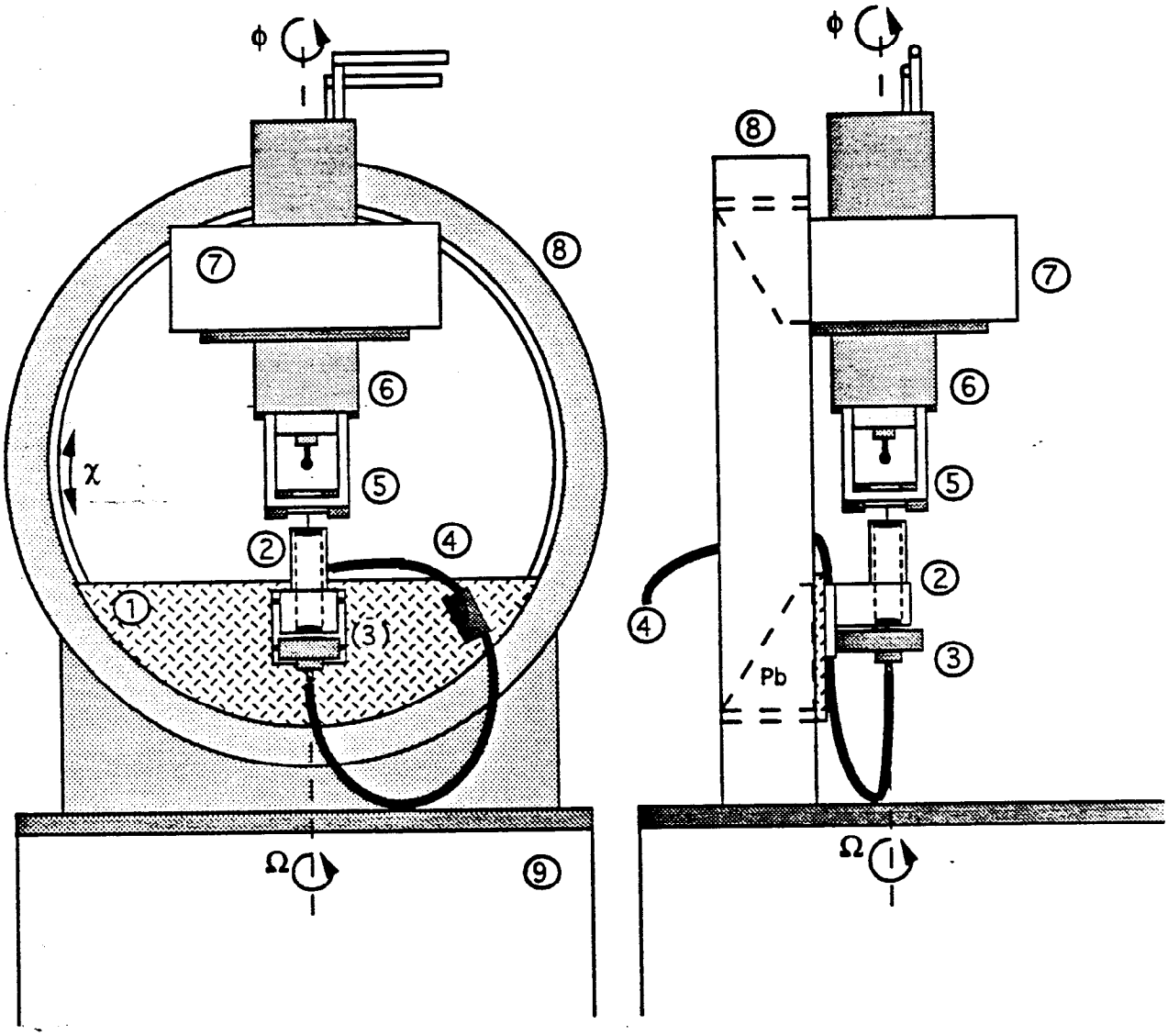
φ
χ
Ω
Pb
1
2
3
4
5
6
7
8
9

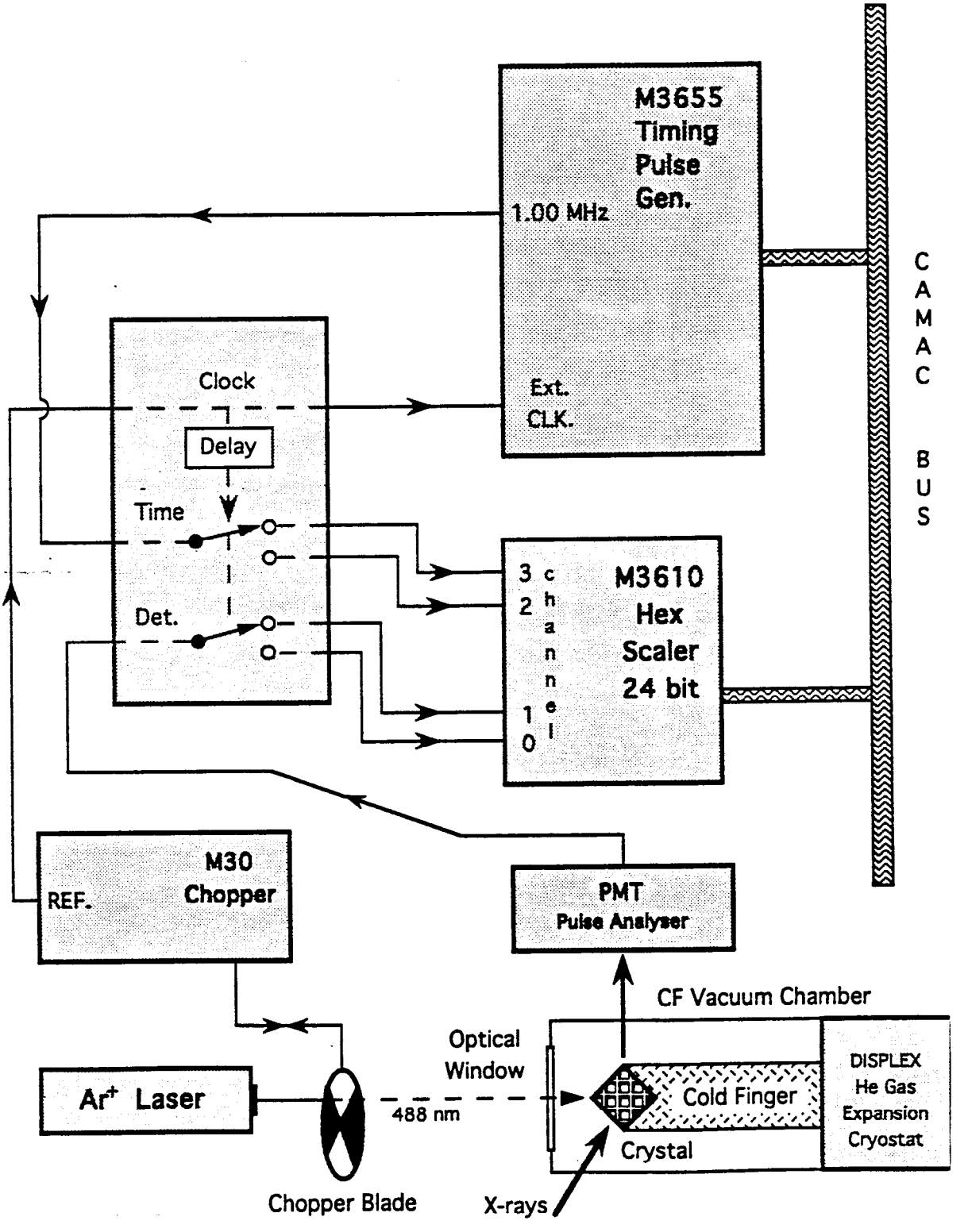
M3655
Timing
Pulse
Gen.
1.00 MHz
Ext.
CLK.
CAMAC
BUS
Clock
Delay
Time
Det.
32 channel
M3610
Hex
Scaler
24 bit
10
M30
Chopper
REF.
PMT
Pulse Analyser
CF Vacuum Chamber
Optical
Window
Ar+ Laser
488 nm
Cold Finger
Crystal
DISPLEX
He Gas
Expansion
Cryostat
Chopper Blade
X-rays

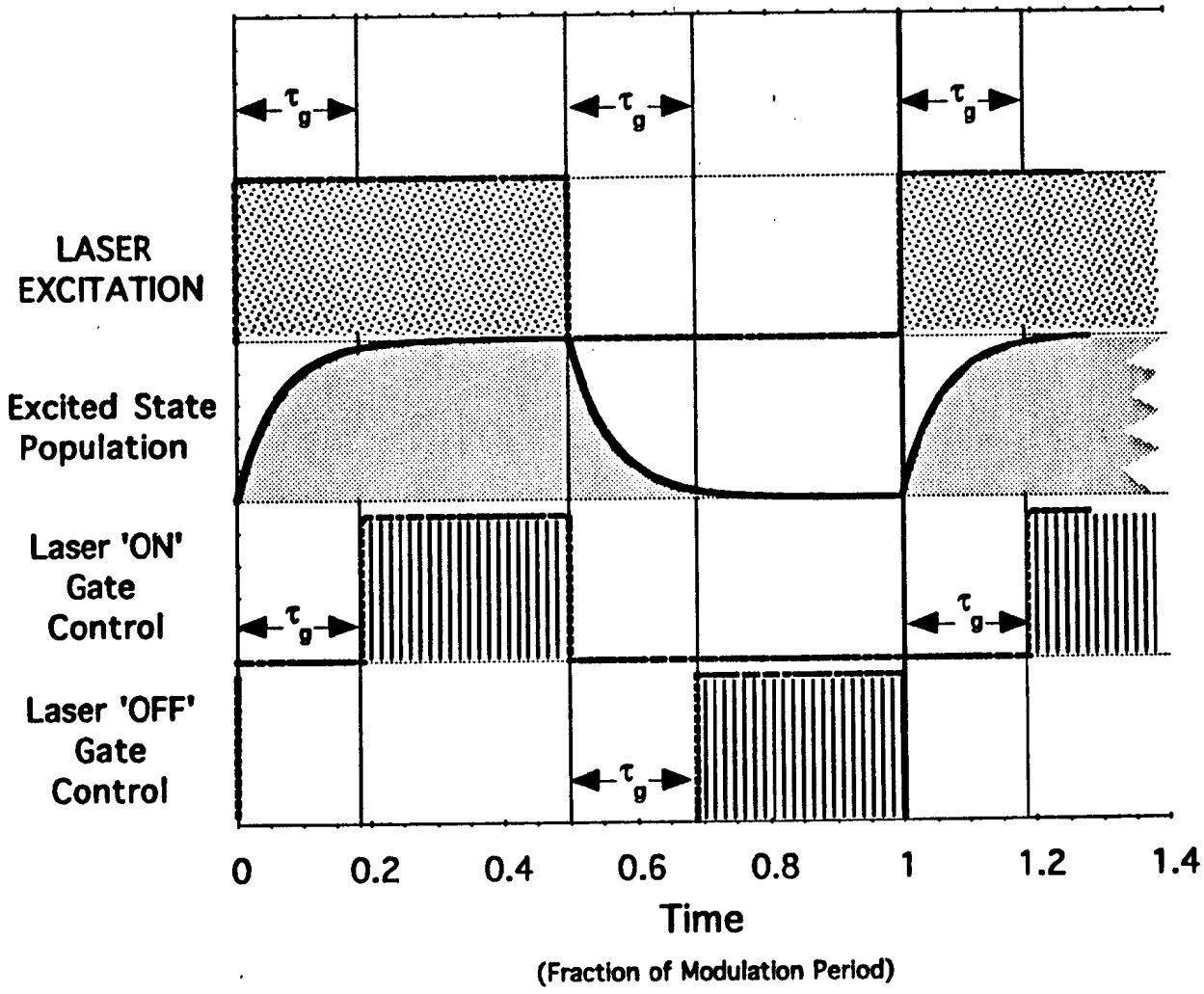
LASER EXCITATION
Excited State Population
Laser 'ON' Gate Control
Laser 'OFF' Gate Control
τ_g
τ_g
τ_g
τ_g
τ_g
0
0.2
0.4
0.6
0.8
1
1.2
1.4
Time
(Fraction of Modulation Period)

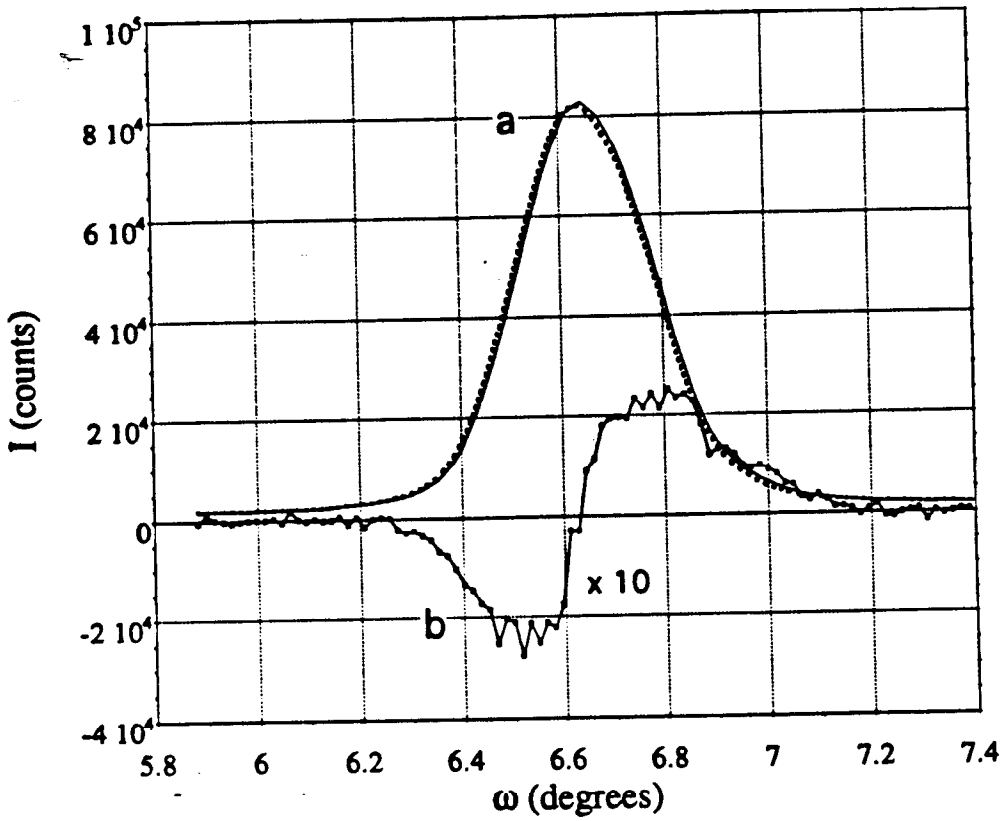
1 10^5
8 10^4
6 10^4
4 10^4
2 10^4
0
-2 10^4
-4 10^4
I (counts)
a
b
x 10
5.8
6
6.2
6.4
6.6
6.8
7
7.2
7.4
ω (degrees)

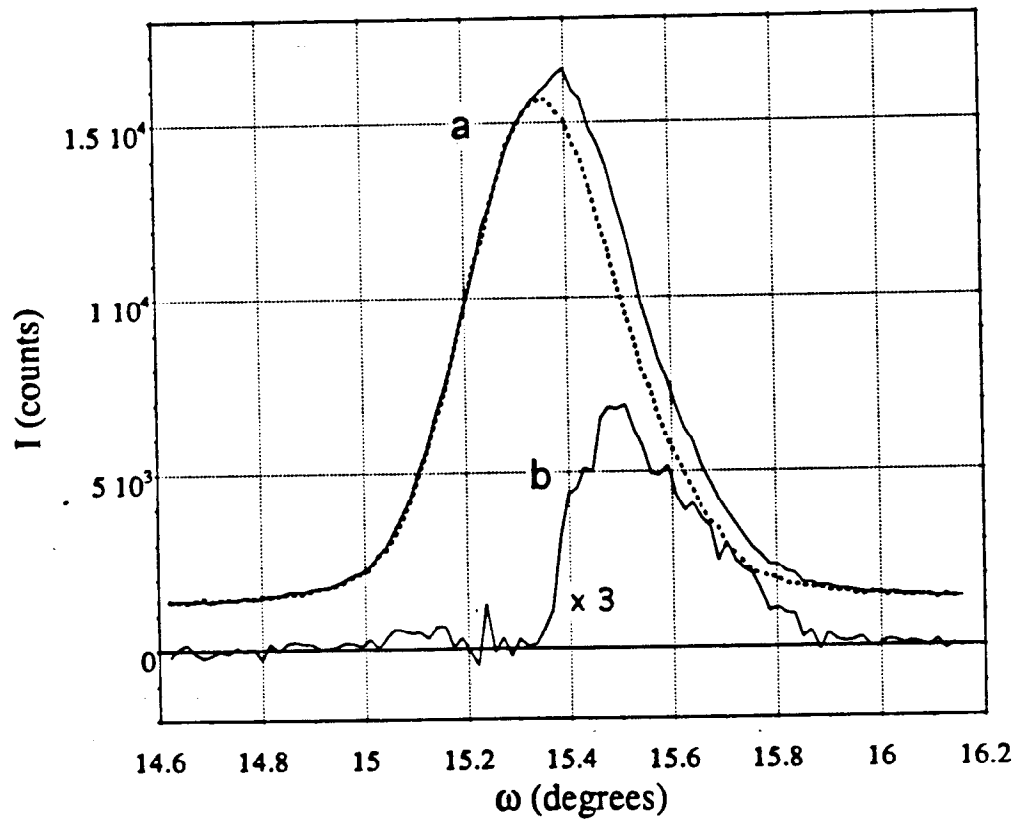
1.5 10^4
1 10^4
5 10^3
0
I (counts)
a
b
x 3
14.6
14.8
15
15.2
15.4
15.6
15.8
16
16.2
ω (degrees)

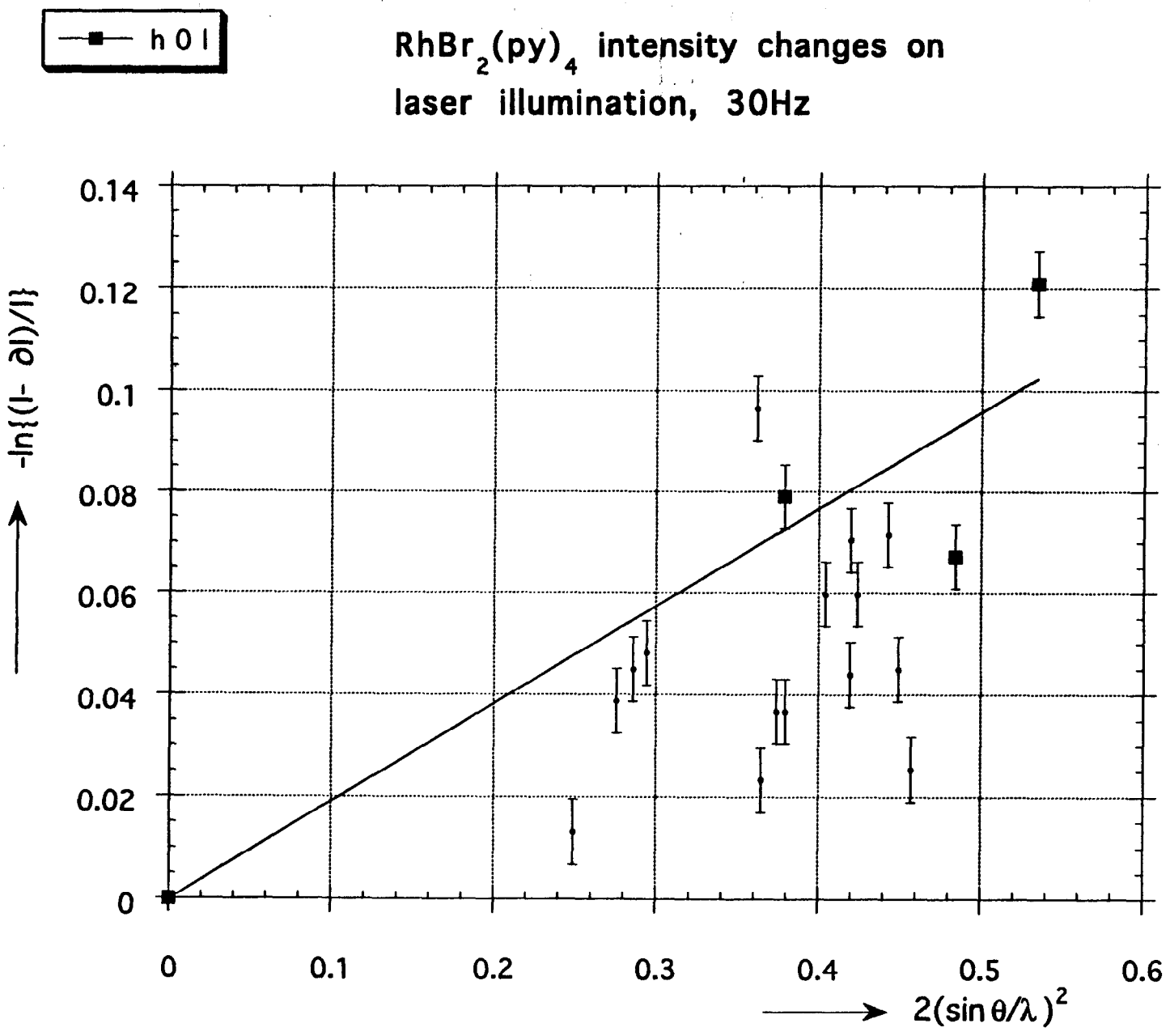
h 0 l
RhBr2(py)4 intensity changes on
laser illumination, 30Hz
0.14
0.12
0.1
0.08
0.06
0.04
0.02
0
-ln{(I/I0 -1)}
0
0.1
0.2
0.3
0.4
0.5
0.6
2(sin θ/λ)2

SYNCHROTRON STORAGE RING FREQUENCIES

NSLS: 52.8 MHz with 28-bunches, and proportionally less in 5- and 1-bunch operational periods, pulse duration 170 ps.

APS: 351.9 MHz with all buckets filled, pulse duration 10–100 ps.

LCLS	***Comments***
wavelength: 1.5Å	shorter may be preferable
repetition rate: 120 Hz	suitable
coherent photons/pulse: 0.5×10^{13}	$\approx 5 \times 10^{12}$
beam cross section: $\approx 10\mu$	molecules in 50μ thickness
$\sigma(E)/E : 2 \times 10^{-4}$	suitable for resonance experiments

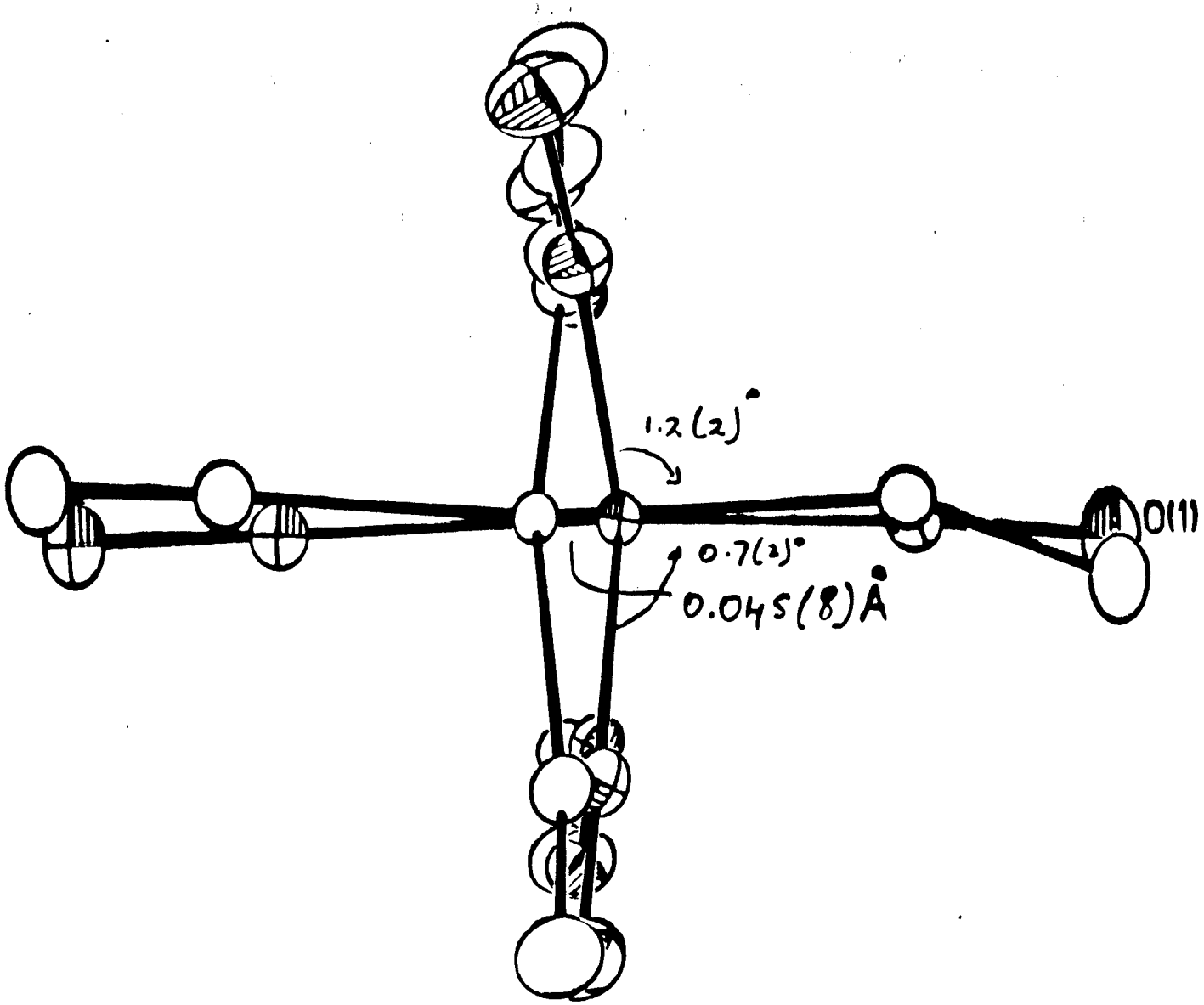
1.2(2)°
O(11)
0.7(2)°
0.045(8)Å

Possibilities for One-Shot Soft X-ray Tomographic Imaging

Malcolm Howells, ALS/LBL

Possibility for one-shot tomography using a high-gain free-electron laser

M. R. Howells*, C. J. Jacobsen**, S. Lindaas**

*The Advanced Light Source, Lawrence Berkeley Laboratory, Berkeley, CA 94720 USA

**Department Physics State University of New York, Stony Brook, NY 11794 USA

Background

Although x-ray holography has a long history, it is only in recent years that the technologies needed for it to be successful have begun to be available. The advent of undulators and x-ray lasers and the prospect of even more advanced pulsed sources such as high-gain free-electron lasers [Winick 1993] have led to an increase in the level of interest and activity in x-ray holography at several centers around the world. This is based in part on the high interest in three-dimensional imaging experiments and the realization that diffraction-tomography experiments in the x-ray region can *only* be done via a holographic type of recording because that is the only known way to record the x-ray phases.

Given that true three-dimensional imaging will require a diffraction tomography experiment [Spiller, 1987; Devaney, 1986] and that x-ray holography is the right way to record each view [Howells, 1990], we are faced with the challenge of recording experimentally the many views, probably dozens, that will be required. Moreover, it appears as though such a sequence will not be possible for unfrozen biological material without alteration of the sample during data collection. The traditional response to the damage problem in x-ray imaging is to propose a flash experiment. One of the advantages of holographic imaging is compatibility with this type of exposure. However, there is still a problem in acquiring a *sequence* of flash images because the first one or first few may still change the sample. There are two ways out of the dilemma. One is to argue that there is no dilemma. Given that the data from each view will be combined in forming the final three-dimensional image, we might argue that the total counts needed (and hence the total dose) may not be much greater than for a single high-quality two-dimensional image [Nugent 1993]. The second way is to perform a flash experiment where *all* the views are taken simultaneously [Trebes 1990]. The latter is the option we want to explore in this presentation.

Possibility for One-shot Flash Tomography

In order to illuminate a sample with a considerable number of beams with different directions at the same time we need a device that can receive a single coherent beam as input and deliver a multiplicity of similarly coherent beams in a variety of directions as output. The setup could be as

shown in Fig. 1 with the "beam splitter" mounted on the upstream side of a thin membrane and the sample on the downstream.

For the beam splitter to work it would have to be thin enough to transmit a major fraction of a soft x-ray beam. This suggests a two-dimensional crystal-like structure. The advantage of this would be that the spots in the reciprocal lattice of a three-dimensional crystal become rods for a two-dimensional one. This means that they would be *certain* to make a hit with the Ewald sphere and thus would always represent an observable reflection.. In other words we would switch from the Bragg equation to the grating equation.

Diffracting structures to realize the beam-splitter concept

Ordinarily, we think of a transmission grating as having a square-wave transmission function with a bar-to-period ratio of about 1:2. This does what we usually want which is to concentrate as much diffracted light as possible into the +1 and −1 orders. However we can produce the opposite effect by making the bar-to-period ratio either close to zero or to one. This means that either the bars would change into narrow walls or the gaps would change into narrow trenches either of which would distribute the diffracted intensity over many orders. We can do the same in two dimensions in which case the walls or trenches would be replaced by an array of either towers or holes. The diffraction pattern is the same (by Babinet's principle) for both towers and holes (the sizes being taken as equal) anywhere outside of the footprint of the incident beam. As an example, an array of 10nm holes on a 50nm grid would give 4% transmission which would be divided among 49 beams on a square grid with the orders m, n such that $-3 < m < 3$, $-3 < n < 3$ having significant relative strength. If such a system were used to disperse 3nm radiation then a set of 48 holograms with numerical aperture of 1/20 (resolution 30nm) and a maximum angle of over 30° between illumination directions, could in principle be recorded. The low efficiency of such a system based on holes in an opaque background can be improved by a factor four by using π-phase-shifting towers on a transparent background or holes on a π-phase-shifting background. Further details of projected efficiencies are given in the presentation.

Proposed scheme to do a complete tomography experiment using one pulse of the high gain free-electron laser

The layout of the proposed experiment is shown in Fig. 1, to which should be added some focusing of the beam and a beam-defining aperture upstream of the sample. To get a rough idea of the amount of light we need consider the following

- coherent energy per pulse of LCLS = 3mJ
- fluence needed to expose PMMA at 30Å= 0.5 J/cm^2

- therefore energy needed for a 20×20 μm^2 hologram = 2μJ

Thus without accounting for any losses we would have enough energy to make 1500 holograms. For a useful reconstruction we would need at least 30 views so we would need to maintain an x-ray exploitation efficiency of about 2% which does not seem unreasonable.

Caution

Successful x-ray diffraction tomography experiments will deliver a value for the complex refractive index as a function of position. This quantity is meaningful because the complex refractive index of all well-defined materials is known and tabulated in the Henke tables [Henke 1993]. However if the materials are driven nonlinear by strong fields as one gets from a strong pulsed source then resulting refractive indices which are derived will not be intelligible in the usual sense. The x-ray imaging community has not needed to address this matter up till now and it may turn out that it poses no difficulties at the Stanford LCLS. However the issue should be examined in future studies of applications of the LCLS.

Acknowledgments

This research is supported by the following United States agencies: the NSF under Grant No. DIR-9006893 (SL and CJJ) and Presidential Faculty Fellow Award RCD 92-53618 (CJJ) and The Office of Health and Environmental Research of the Department of Energy under Subcontract No. 431-3378A of Grant No. DE-FG02-89ER60858 (MRH).

References

Devaney, A. J., "Reconstructive Tomography with Diffracting Wavefields", *Inverse Problems*, **2**, 161-183 (1986).

Howells, M., Jacobsen, C., Kirz, J., McQuaid, K., Rothman, S., "Progress and Prospects in Soft X-ray Holographic Microscopy", *Modern Microscopies: Techniques and Applications*, Duke, P., Michette, A. G., 132-119, Plenum, New York (1990).

Nugent, K. A., J. Trebes, "Signal-to-Noise Ratio and Image Quality for 3D Multiple-View X-ray Microscopy", *Technical Report*, **UM-P-93/59** , University of Melbourne (1993).

Spiller, E., "X-ray microholography-exciting possibility or impossible dream", *X-ray Microscopy: Instrumentation and Biological Applications*, P. C. Cheng and G. J. Jan, 224-230, Springer-Verlag, Berlin (1987).

Trebes, J., J. Brase, J. Gray, R. London, D. Mathews, D. Peters, D. Pinkel, G. Stone, M. Rosen, T. Yorkey, "X-ray Laser Holography of biological microstructures", *X-ray Lasers 1990*, G. Tallents, 279-287, Institute of Physics Conference Series No. 116, Institute of Physics, Bristol (1990).

Winick, H., K. Bane, R. Boyce, J. Cobb, G. Loew, P. Morton, H.-D.Nuhn, J. Paterson, P. Pianetta, T. Raubenheimer, J. Seeman, R. Thatchyn, "V. Vylet, C. Pellegrini, J. Rosenzweig, G. Travish, D. Prosnitz, E. T. Scharleman, K. Halbach, K.-J. Kim, R. Schlueter, M. Xie, R. Bonifacio, L. De Salvo, P. Pierini", *Short-Wavelength FEL's Using the SLAC Linac* , US Conference on Synchrotron Radiation Instrumentation, Gaithersburg (1993).

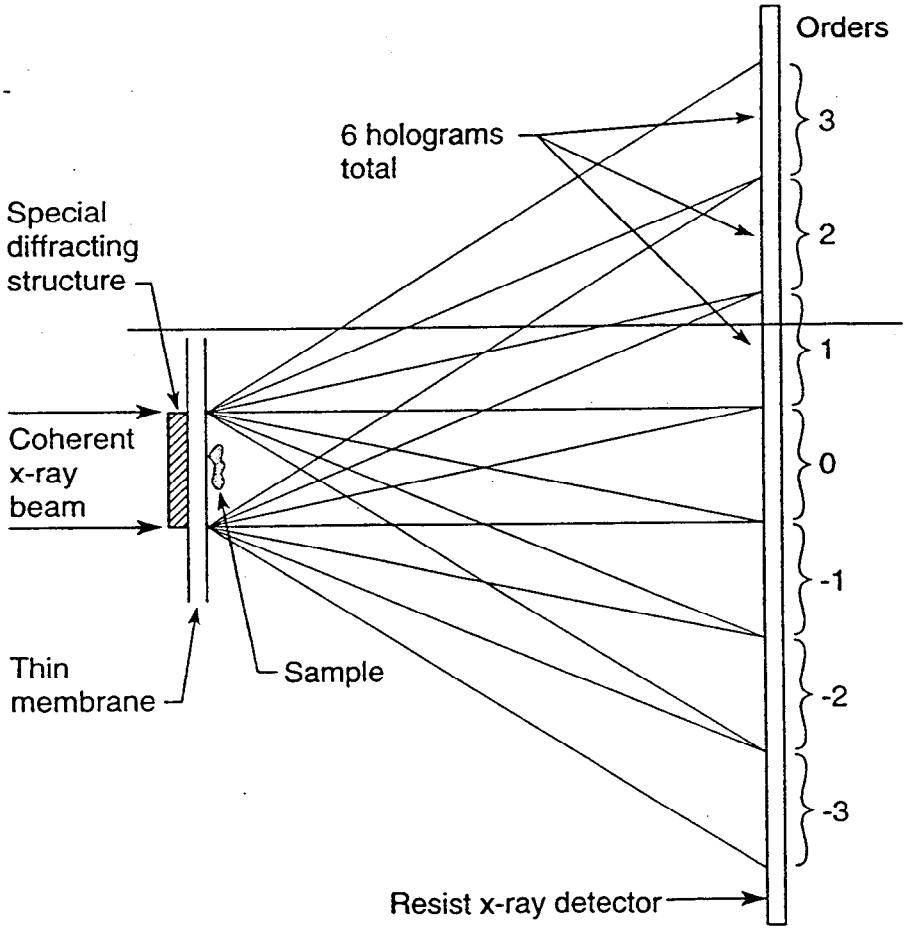

Fig. 1. Principles of a possible method of one-shot flash tomography. A total of six holograms are shown but they are part of a two-dimensional array of 7x7-1=48

X-RAY HOLOGRAPHIC MICROSCOPY WITH THE ATOMIC FORCE MICROSCOPE

PARTICIPANTS:

S. Lindaas	SUNY, Stony Brook
C. J. Jacobsen	SUNY, Stony Brook
S. Spector	SUNY, Stony Brook
M. R. Howells	Lawrence Berkeley
K. Frank	Lawrence Berkeley

SUMMARY:

Previous work

Present status

- What barriers remain?
- Tomography and the dose per view
- One-shot flash tomography?

Resist read out by atomic force microscope

- Microscope design
- Achievement of a linear scale
- Results and performance

Discussion and future prospects

X-RAY MICROSCOPY BY IN-LINE HOLOGRAPHY

PRINCIPLES:

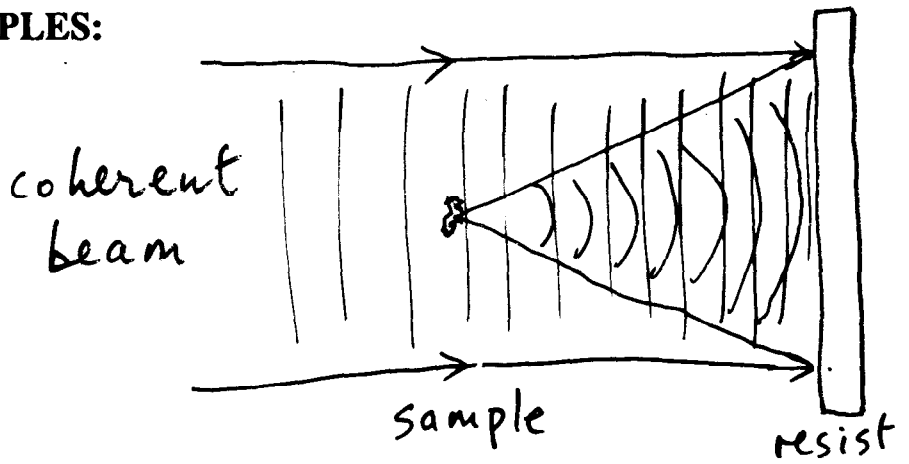

- **Expose the resist *through* the sample with a coherent beam**
- **Develop and read the resist recording into the computer**
- **Calculate the image and try to remove the twin image**

FEATURES:

- **No optics**
- **No focusing**
- **Large fields**
- **Can use flash**
- **Resolution depends on resist read/write**
- **One view does not give 3-D**
- **Twin-image artefact [Koren 1993]**
- **Doses are high ($\gtrsim 10^2$ Mrad) →flash**

- Phase + amplitude contrast

High resolution hologram of biological sample

By: Lawrence Berkeley Laboratory (CXRO)
SUNY Stony Brook

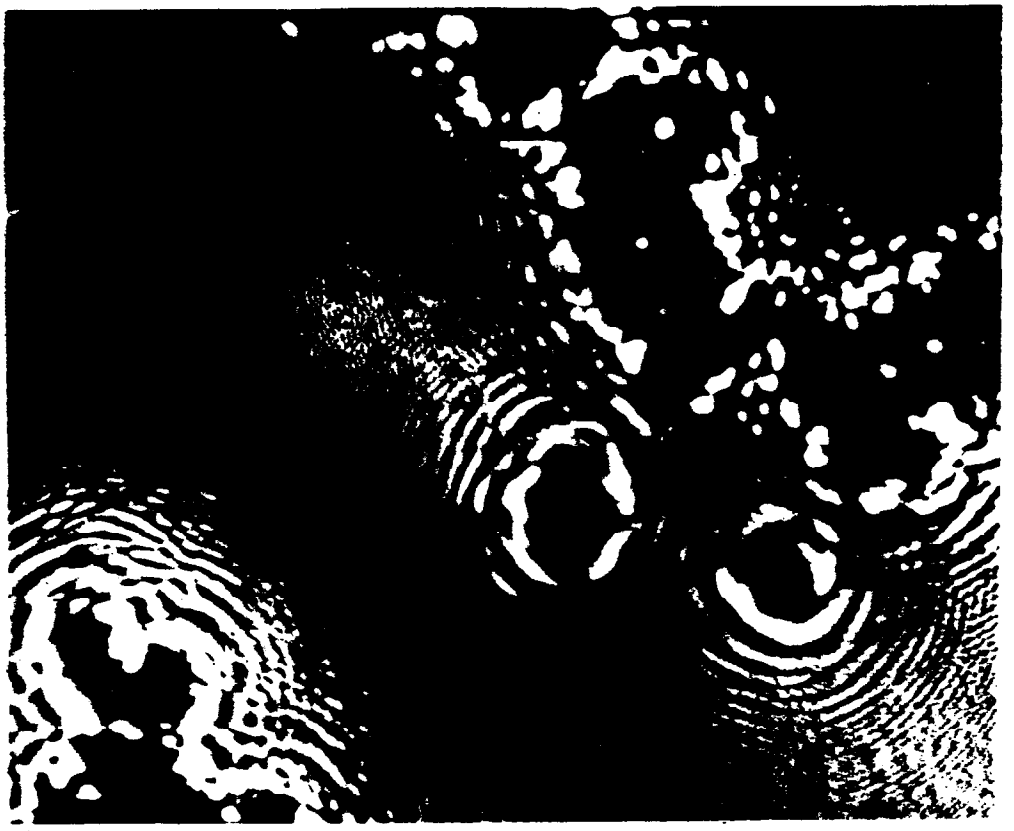

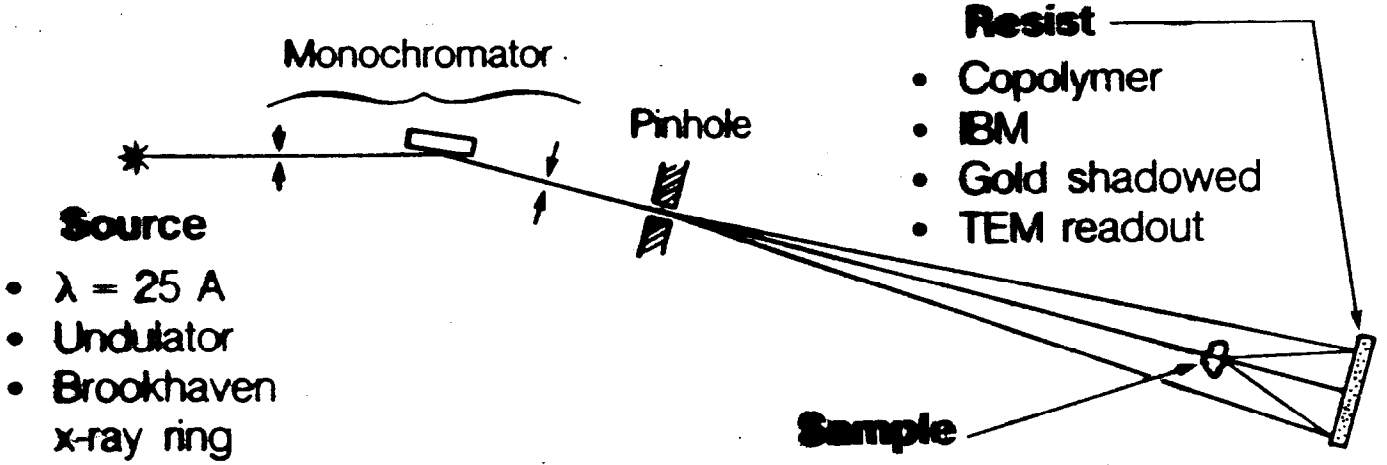

XBB 871-421

X-Ray Gabor (in-line) Holography

M. Howells[†], S. Lindaas[‡], and C. Jacobsen[‡] († LBL, ‡ Stony Brook)

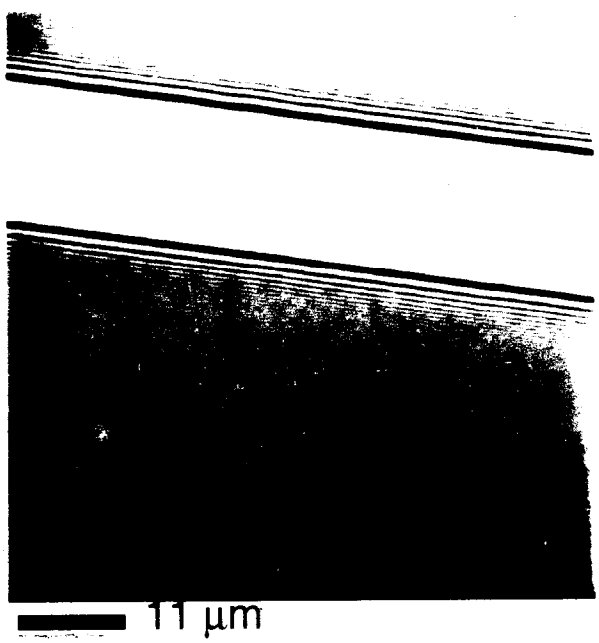

(400 pixels × $0.15\mu m)^2$

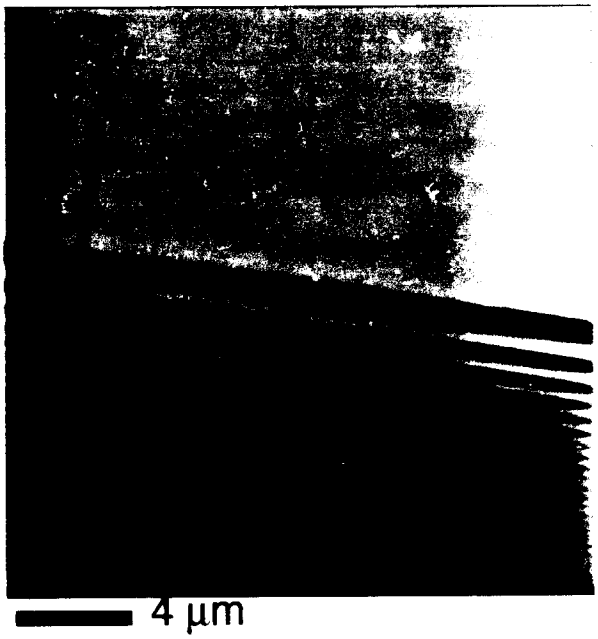

(512 pixels × $0.04\mu m)^2$

Gold wire (diameter = $12\mu m$) exposed on PMMA using $\lambda = 1.89$ nm x-rays.

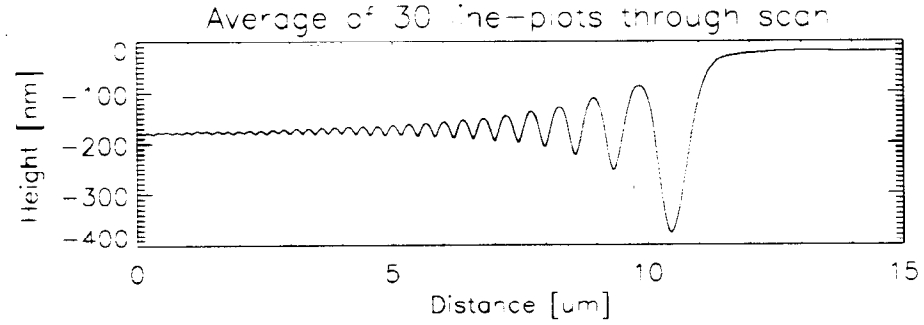

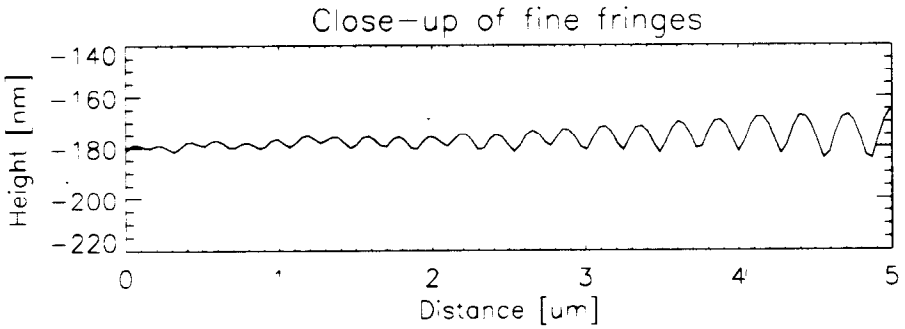

A METHOD FOR FLASH TOMOGRAPHY

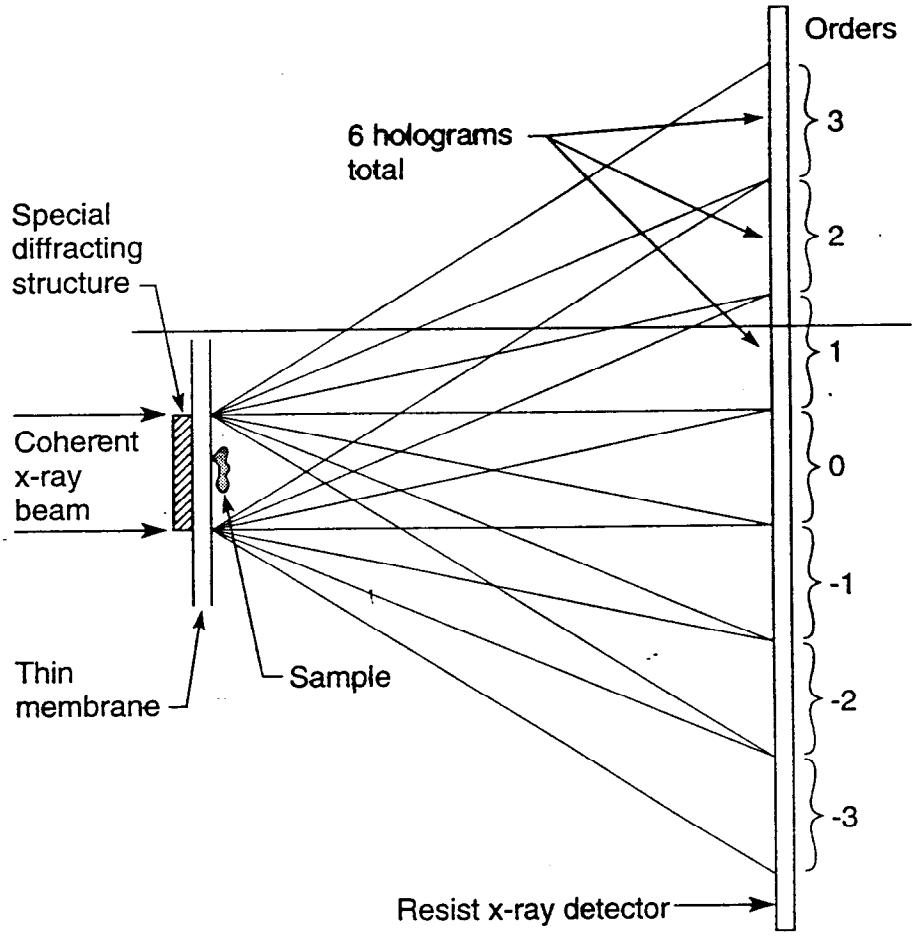

XBL 939-4838

LAMINA AMPLITUDE GRATING

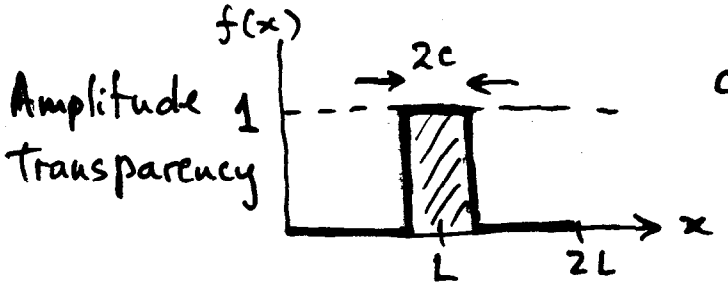

$c/L \equiv p$

periodic with period 2L

$$f(x) = \sum_{-\infty}^{+\infty} (-1)^n p \, \mathrm{sinc}(np) \exp\left(\frac{in\pi x}{L}\right)$$

$$|c_0|^2 = p^2 \qquad |c_1|^2 = p^2 \mathrm{sinc}^2 p$$

$\boxed{p = 0.5}$ $\quad |c_0|^2 = \frac{1}{4} \quad |c_1|^2 = \frac{1}{\pi^2} \quad 2\sum_{1}^{\infty} |c_n|^2 = \frac{1}{4}$

$|c_{-1}|^2 = \frac{1}{\pi^2}$

optimum light into ± 1 orders.

$p \to 0$, $p \to 1$ } a lot of light into higher orders.

Lamina phase grating.

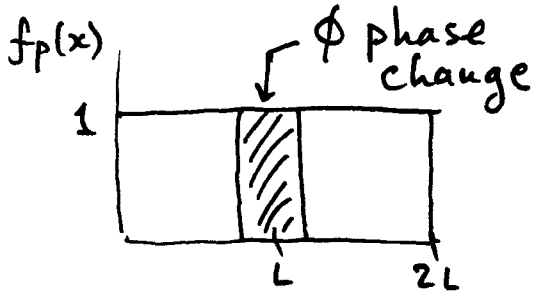

$$f_p(x) = 1 + (e^{i\phi} - 1) f(x)$$

$$f_p(x) = 1 + (e^{i\phi} - 1) \sum_{-\infty}^{+\infty} (-1)^n p \, \mathrm{sinc}\, np \exp \frac{in\pi x}{L}$$

$$|c_0|^2 = |1 + p(e^{i\phi} - 1)|^2 \qquad |c_1|^2 = |(e^{i\phi} - 1)p|^2 \mathrm{sinc}^2 np$$

$\phi = \pi \quad p = 0.5 \quad |c_0|^2 = 0 \quad |c_1|^2 = \frac{4}{\pi^2}$

$|c_{-1}|^2 = \frac{4}{\pi^2}$

TWO-DIMENSIONAL STRUCTURES

SHADING = OPAQUE

SHADING = π PHASE SHIFT

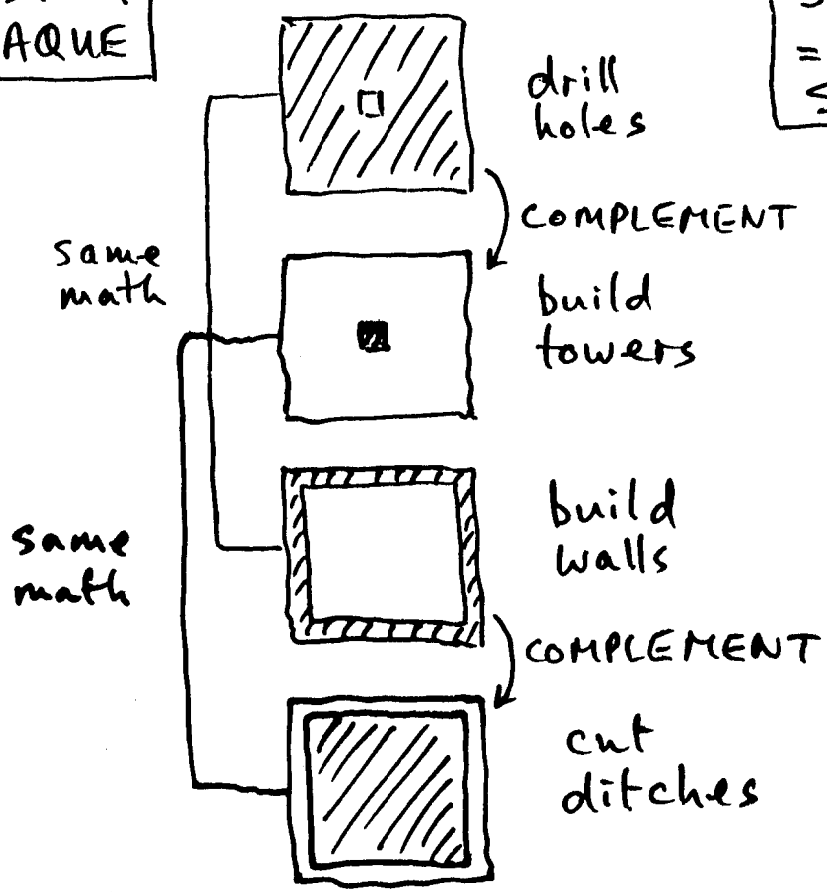

same math

same math

— ditto —

— ditto —

— ditto —

— ditto —

$$f(x,y) = \sum_{m,n=-\infty}^{+\infty} c_{mn} \exp \frac{i\pi}{L}(mx+ny)$$

$$|c_{mn}|^2 = p^4 \operatorname{sinc}^2 mp \operatorname{sinc}^2 np$$

$$|c_{mn}|^2 = p^4 \operatorname{sinc}^2 mp \operatorname{sinc}^2 np\,(1+r)$$

amplitude

transmis

STRENGTH OF ORDERS

Principles:

Babinet's principle:

complementary screens have the same diffraction pattern outside the incident beam

$$\left|(1-p)\,\mathrm{sinc}\,m(1-p)\right|^2 \equiv \left|p\,\mathrm{sinc}\,mp\right|^2 \quad (m \neq 0)$$

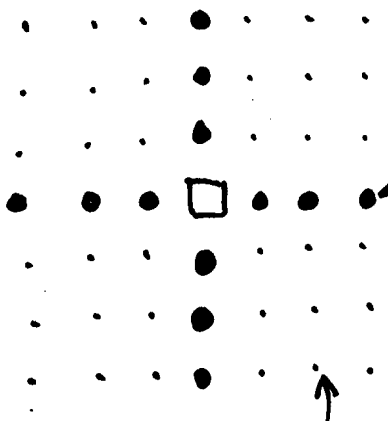

$|c_{10}|^2$, $|c_{20}|^2$ etc much stronger for walls & ditches

$m \neq 0$
$n \neq 0$
} equally weak for all four types

π phase shifters always 4 times more efficient

Diffraction efficiency for the n0 order in two dimensions

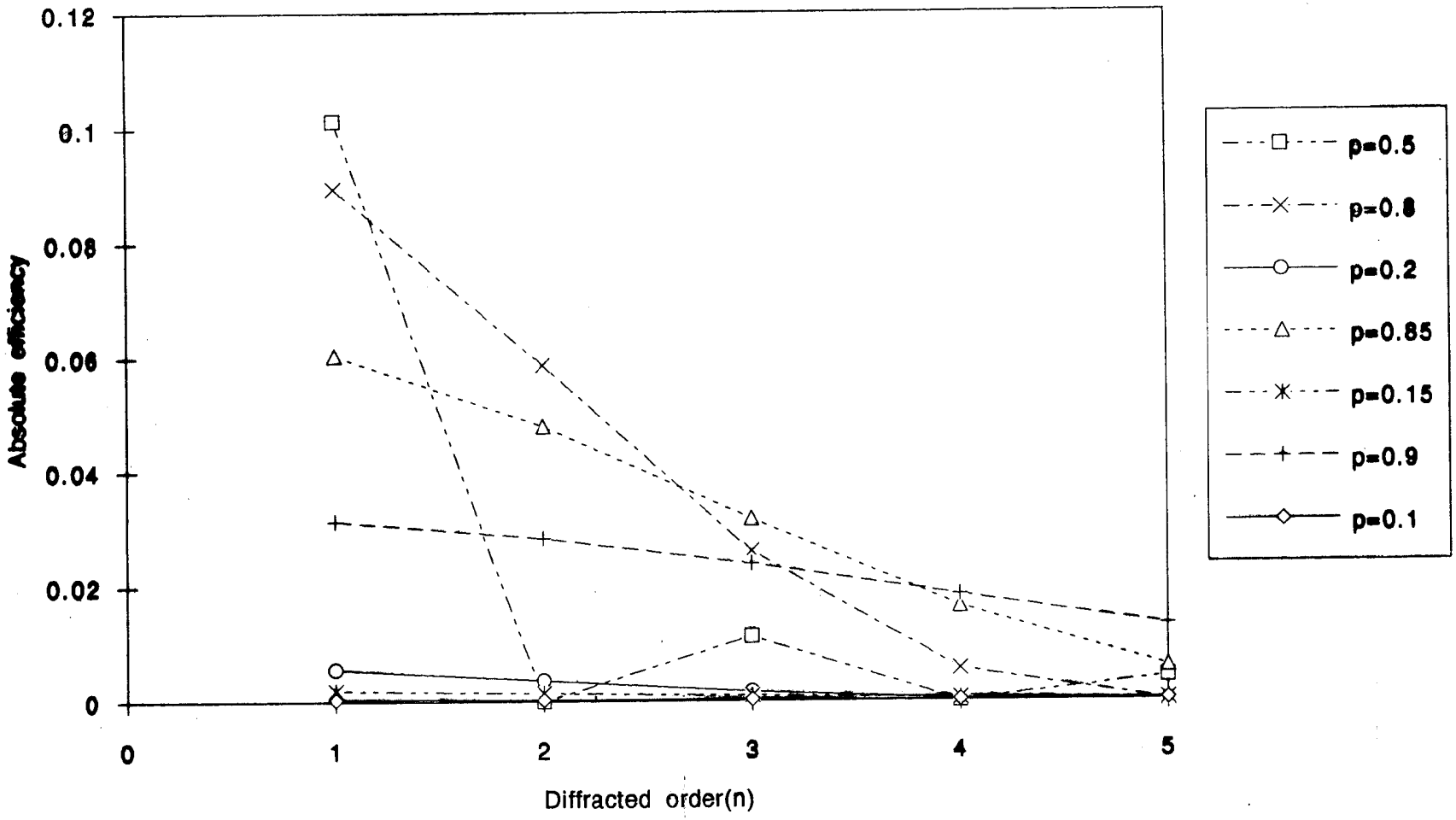

Diffraction efficiency for the n3 order in two dimensions

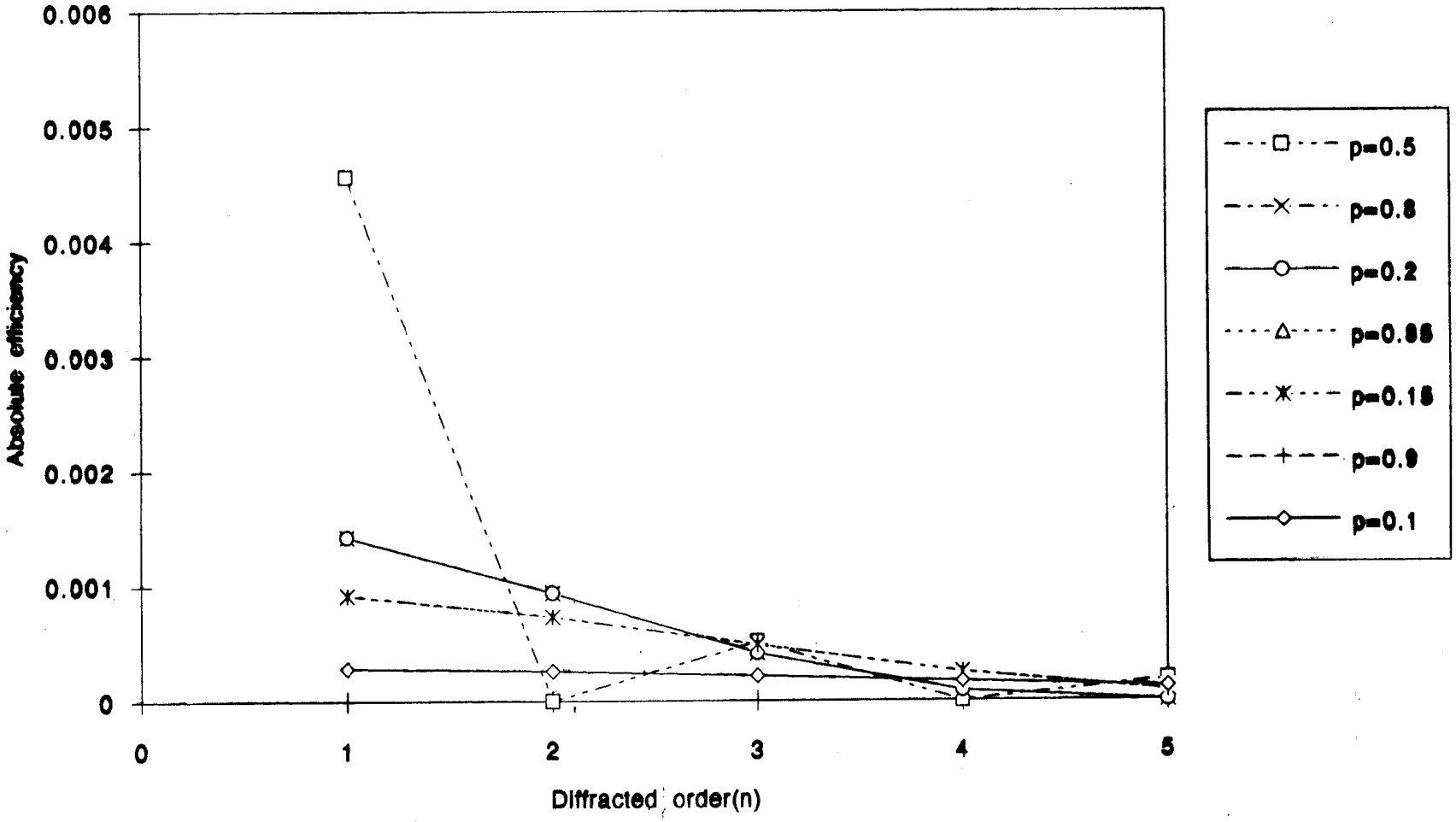

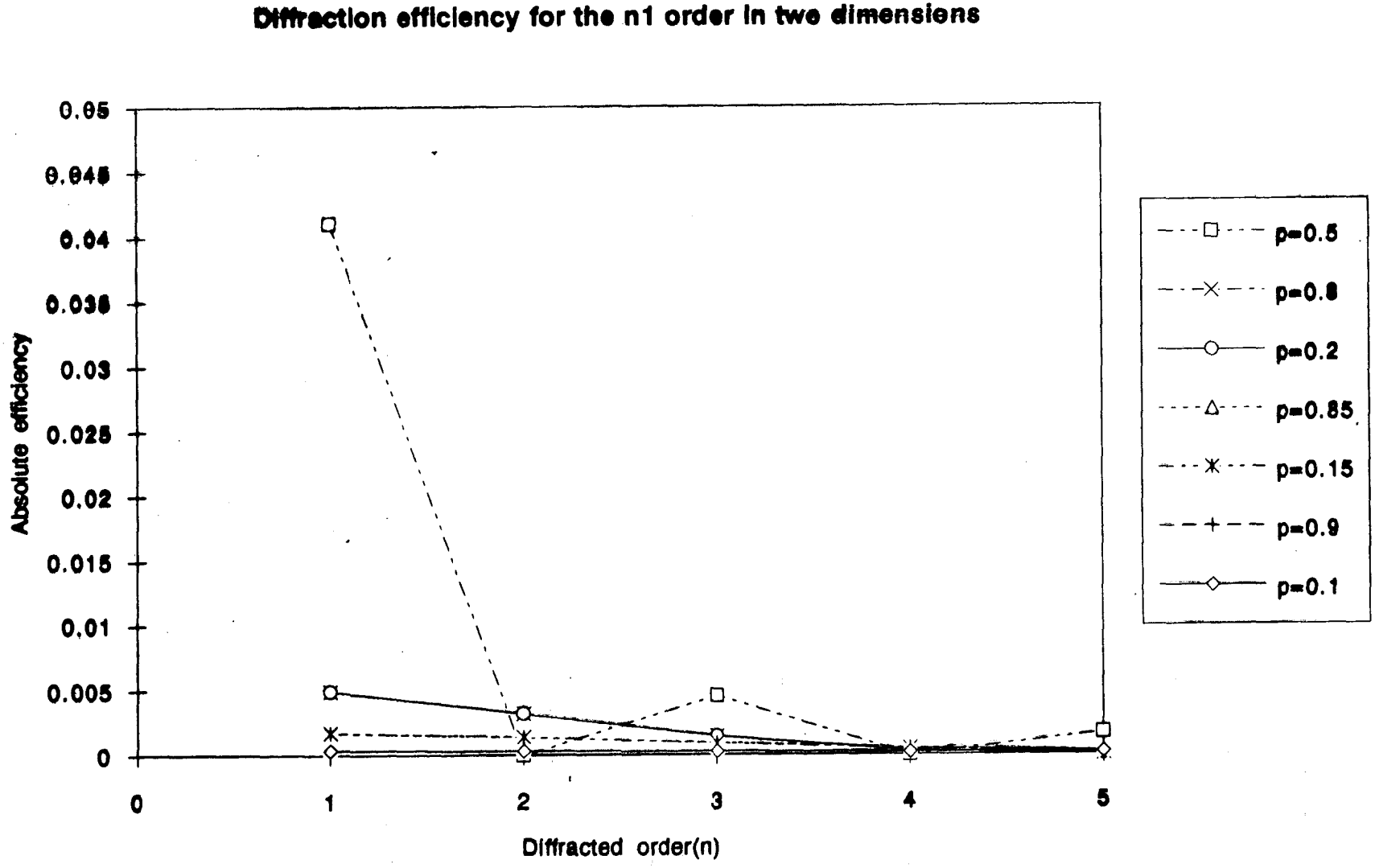
Diffraction efficiency for the n1 order in two dimensions
Absolute efficiency
0.05
0.045
0.04
0.035
0.03
0.025
0.02
0.015
0.01
0.005
0
0
1
2
3
4
5
Diffracted order(n)
p=0.5
p=0.8
p=0.2
p=0.85
p=0.15
p=0.9
p=0.1

THE LINAC COHERENT LIGHT SOURCE (LCLS) AT STANFORD

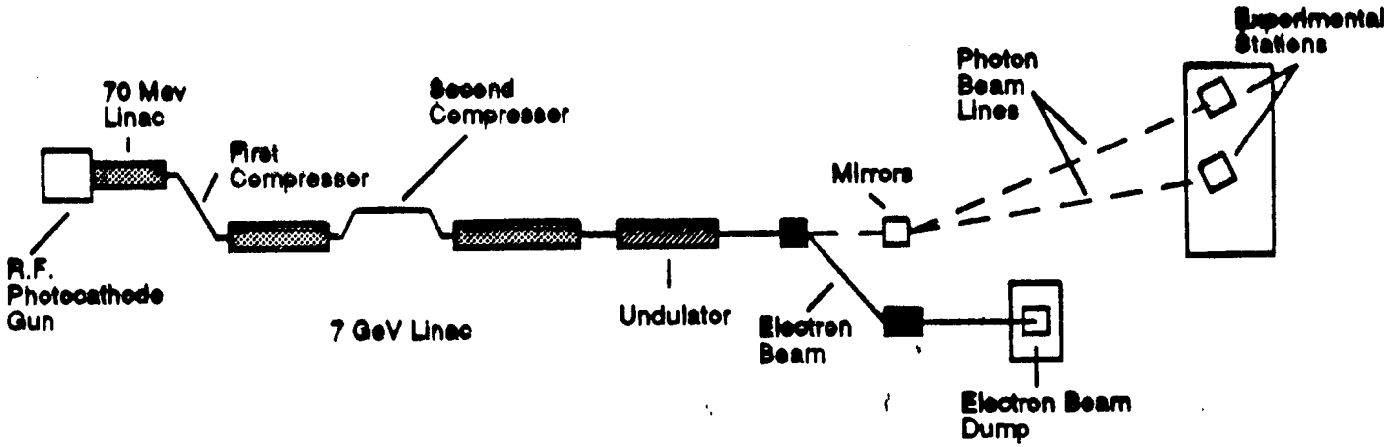

Coherent energy per pulse ~ 3mJ

PMMA @ 25Å needs ~ .5 J/cm²

~ 2μJ / hologram of 20×20μ²

1500 holograms per pulse

SOME ROUGH NUMBERS

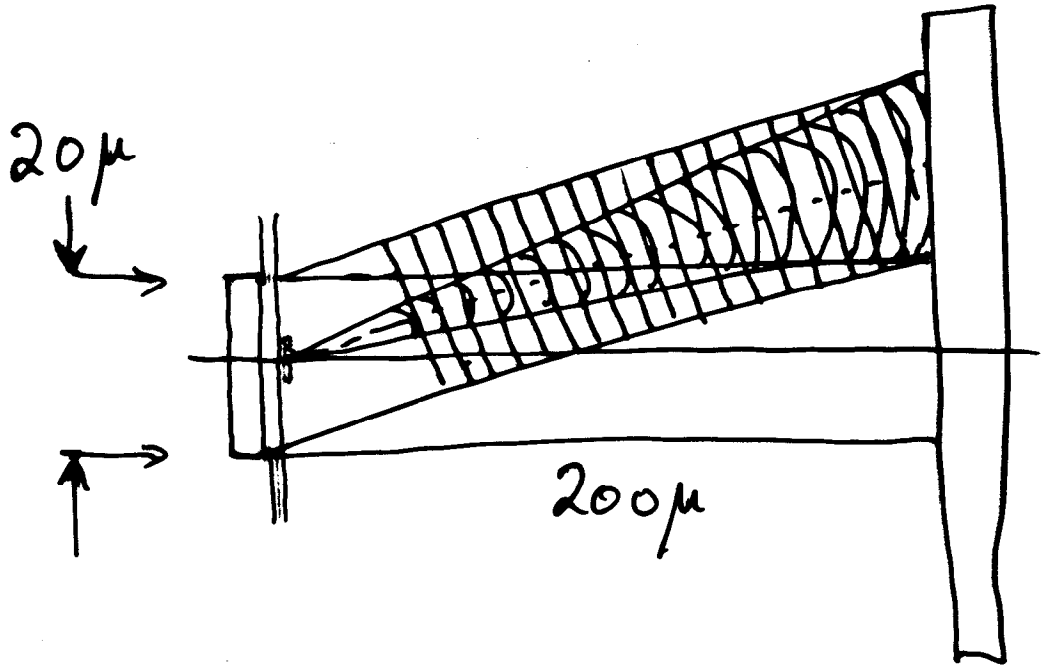

$\lambda = 30\,\text{Å}$ $\quad p = .8$

Res'n = 300 Å $\quad$ "ditch" width = 100 Å

$NA = \frac{1}{20}$ $\quad$ period = 500 Å

Max angle between beams $\cong 20°$

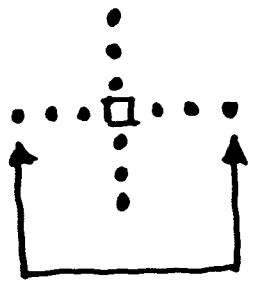

Summary of Discussion

Howells talk:

Coppens asked whether the beam splitter would be destroyed by the FEL pulse. Howells replied that both beam splitter and sample would likely be destroyed, but that the beam splitter should be easy to replicate.

Chu asked what limits the resolution in a flash hologram. Howells replied that the resolution is determined by the size of the narrowest discernible fringes in the interference pattern, which in turn is generally determined by photon statistics or noise in the detector.

Demonstration of Ultra High Resolution Soft X-ray Tomographic Imaging

Lee Haddad, LLNL

Demonstration of Ultra High Resolution Soft X-Ray Tomography

W. S. Haddad*, I. McNulty, J. E. Trebes,
E. H. Anderson, L. Yang, J. M. Brase

Extended Abstract for the SSRL FEL Workshop, 2/12/1994

X-ray microscopy has been an active area of research for many years, but it is now beginning to emerge as a viable imaging tool for microbiologists and materials scientists. Several groups have developed x-ray microscopes of various types. The most productive systems have been the scanning transmission x-ray microscopes (STXM). Near diffraction limited performance can be achieved with such instruments. There are however no x-ray optics having sufficiently high numerical aperture (NA) to achieve resolution in depth that is comparable with the transverse resolution. Currently the best x-ray zone plates have a NA < 0.1 for radiation in the water window. The ratio of depth resolution to transverse resolution $\partial l/\partial_t \approx 2/NA > 20$ for present state-of-the-art zone plates.

In order to improve the depth resolution, it is necessary to effectively increase the NA of the imaging system. This can be done by recording several views of the object over a large angular range. If each of the views is taken with low NA optics such that the longitudinal extent of the object is less than the depth resolution of the imaging system, then each view will be a 2-D projection of the object. It is then possible to reconstruct a 3-D image of the object using the principles of tomography with the set of 2-D projections as raw data. We have implemented this approach in conjunction with the STXM on the X1A undulator beamline at the National Synchrotron Light Source in Brookhaven National Laboratory. This was done by modifying the STXM to allow the sample to be rotated about an axis perpendicular to the x-ray beam. This modified STXM was then used to make a high resolution 3-D image of a phantom test object.

The phantom consisted of two unique patterns of 600 Å thick gold bars written onto silicon nitride windows which were separated by ~5μm. The 2 μm x 2 μm patterns contained bar features in the size range between 1000 Å and 5000 Å. Thus the overall dimensions of the phantom were approximately 2 μm x 2 μm x 5 μm. The STXM forms high transverse resolution 2-D images using coherent x-radiation from the undulator. The x-rays are focused to a nearly diffraction limited spot using an x-ray zone plate lens. 2-D images are formed by raster scanning the object through the focus of the zone plate and measuring the transmission. For this experiment the undulator was operated at a wavelength of 36 Å and a spectral width of 1%. Physical limitations of the instrument allowed only a small number of projection images to be taken. In addition, only a limited angular range was available over which to record the projections. A total of nine 2-D images of the object were recorded at angles between -50 to +55 degrees with respect to the beam axis. Since the images were recorded incoherently, diffraction was not a factor and the system was then effectively a first generation tomographic imaging system, i.e.. diffractionless straight-ray tomography. The projections were reconstructed into a 3-D image using an algebraic reconstruction technique (ART) algorithm which is an iterative method of optimization. This was necessary because of the limited projection data, especially the restricted angular range, which make backprojection undesirable as a reconstruction technique.

We observe transverse resolution of ~750 Å in the 2-D projections. Artifacts due to the limited angular range, errors in projection alignment and angle and the ART algorithm limit the depth resolution and produce a loss of transverse resolution in the 3-D reconstruction. The resulting transverse resolution in the 3-D reconstruction is found to be ~1000 Å. The overall depth resolution is ~6000 Å., however some features are clearly reconstructed with a depth resolution of ~1000 Å. Our current efforts include improving the methods for projection alignment and measurement of projection angles, and developing better reconstruction algorithms.

Demonstration of Ultra High Resolution Soft X-Ray Tomography

LLNL

W. S. Haddad
J. E. Trebes
J. M. Brase

ANL

I. McNulty
L. Yang

LBL

E. H. Anderson

Ultra High Resolution 3-D imaging with Soft X-Rays: Basic Plan

Current state of the art x-ray microscopes have good transverse resolution, but poor depth (longitudinal) resolution.

$$\partial_l / \partial_t \approx 2/NA$$

$$= 40 \quad \text{with best zone plates}$$

Basic plan for 3-D imaging:

- use scanning transmission x-ray microscope (STXM) to record high ∂_t 2-D images.
- modify STXM for rotatable sample
- record 2-D images of the sample (projections) at several angles
- reconstruct 3-D image tomographicaly

STXM Geometry with Modification for Rotating Target

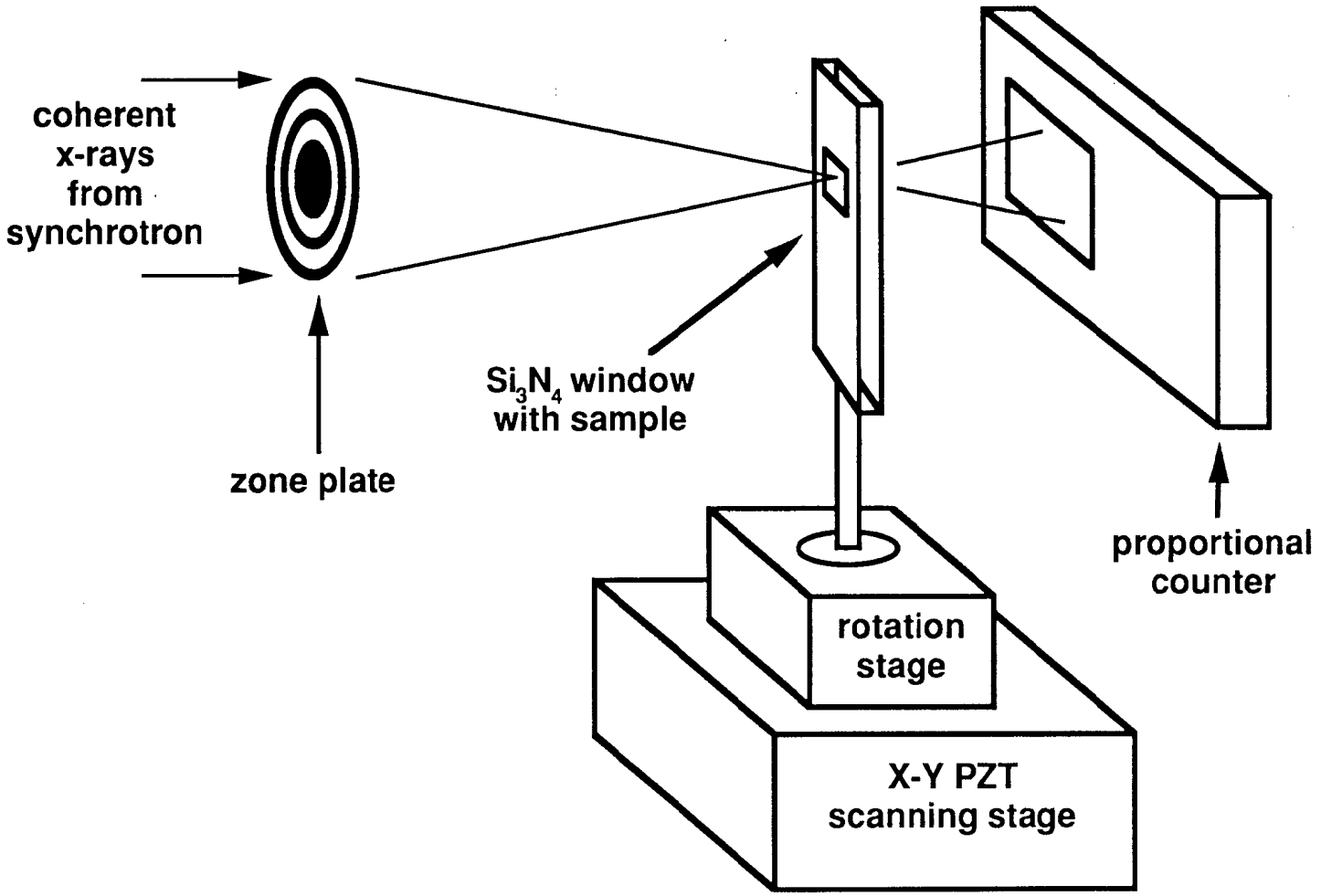

3D-1 Phantom Layout and Dimensions

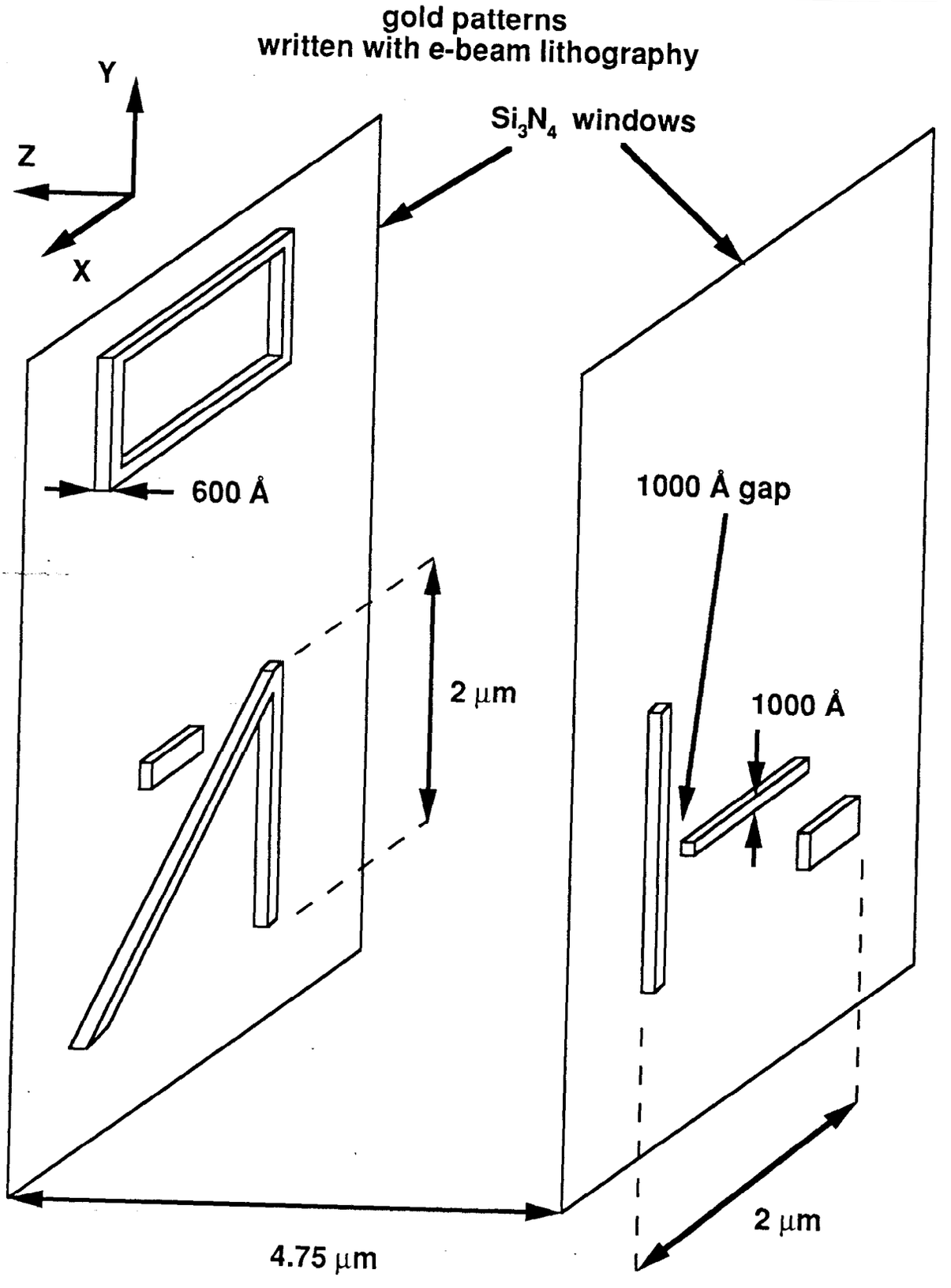

- Physical limitations of the instrument restrict both the number and the angular range of the projections.

- We took nine 2-D projections at angles: -50°, -45°, -30°, -15°, 30°, 45°, 55°

- This presents a challenging reconstruction problem -- special inversion methods required

  - iterative optimization algorithms

    - Algebraic Reconstruction Technique (ART)

    - Maximum Entropy

    - global minimizers

  - other techniques ?

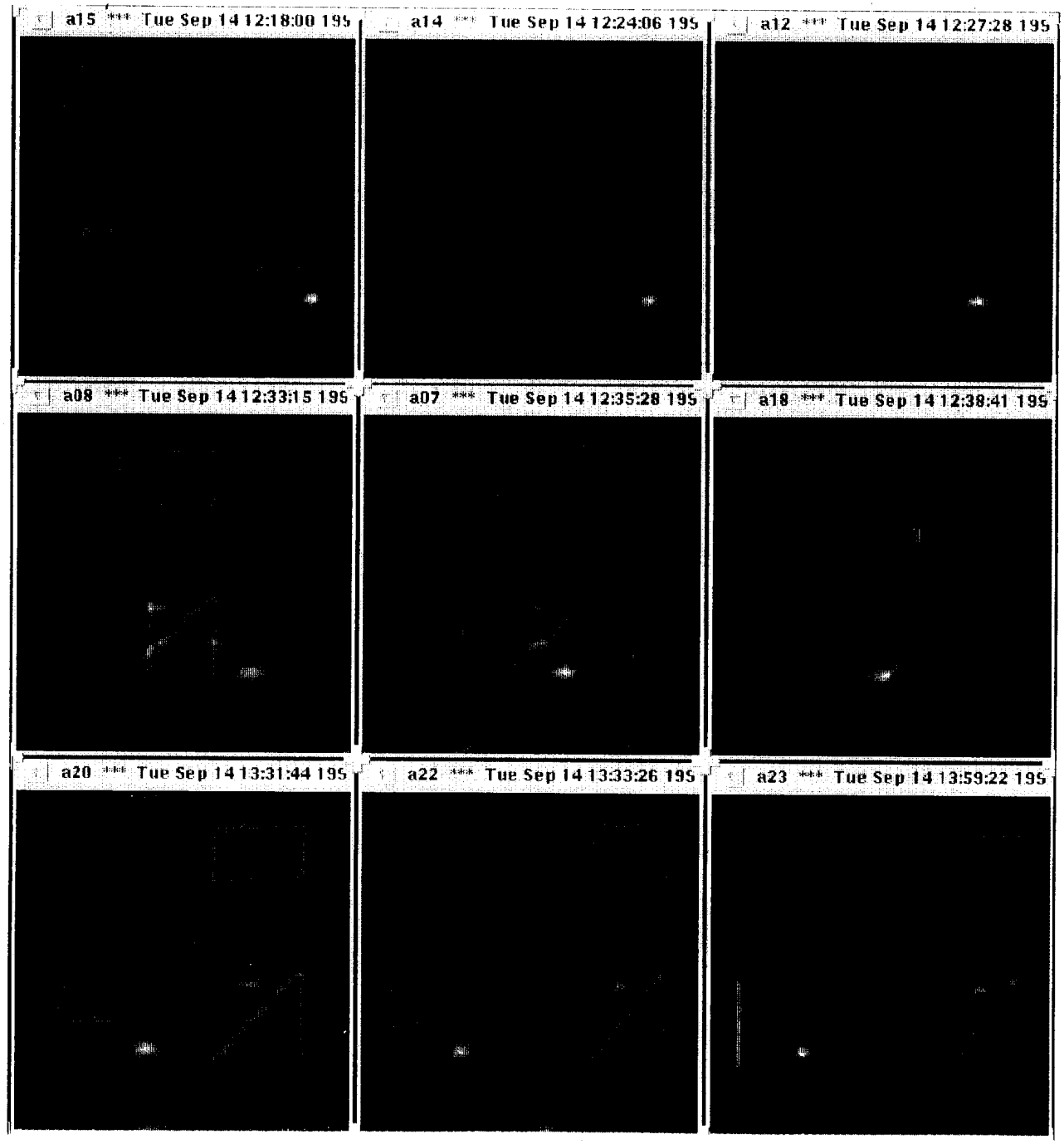
a15 *** Tue Sep 14 12:18:00 195
a14 *** Tue Sep 14 12:24:06 195
a12 *** Tue Sep 14 12:27:28 195
a08 *** Tue Sep 14 12:33:15 195
a07 *** Tue Sep 14 12:35:28 195
a18 *** Tue Sep 14 12:38:41 195
a20 *** Tue Sep 14 13:31:44 195
a22 *** Tue Sep 14 13:33:26 195
a23 *** Tue Sep 14 13:59:22 195

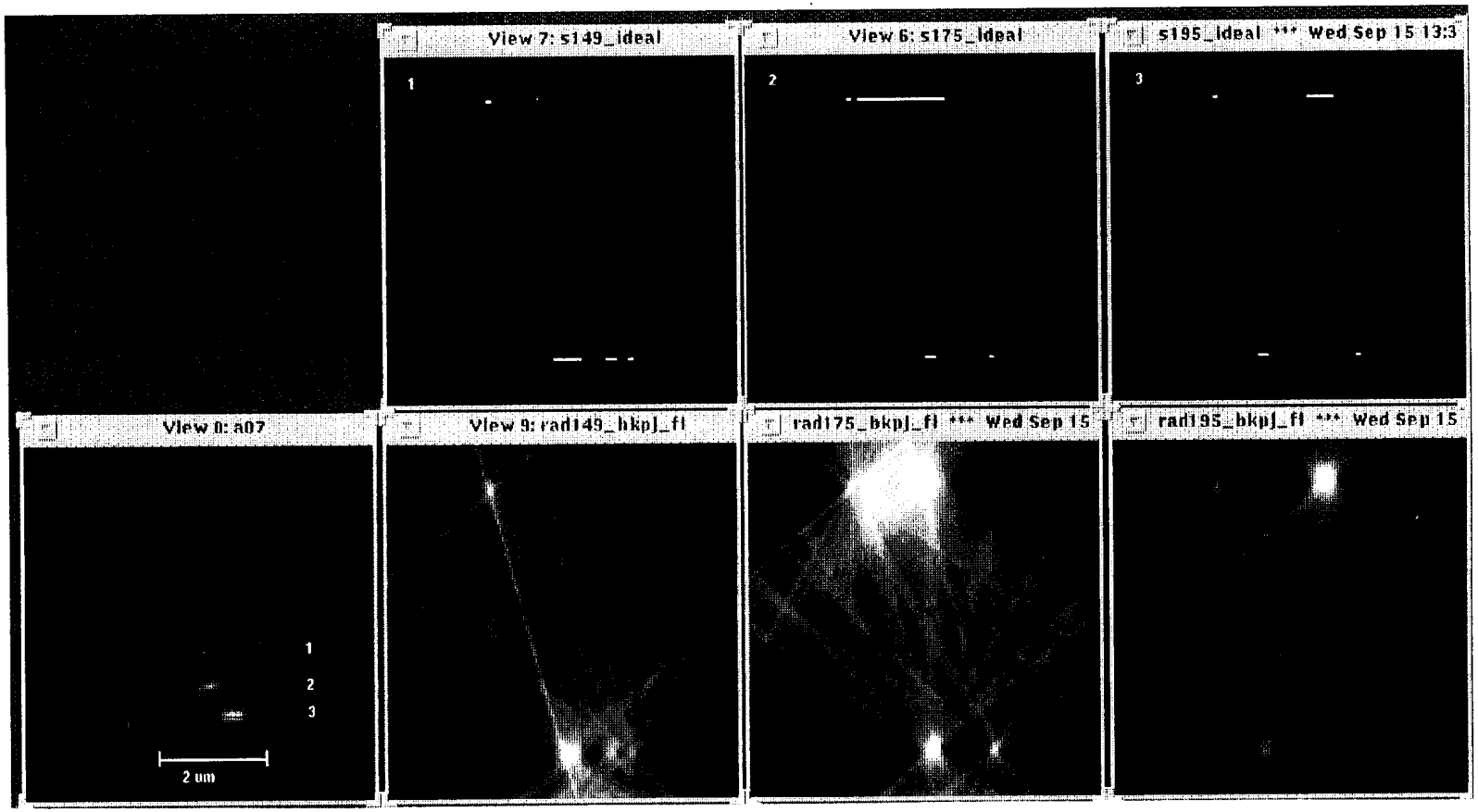
View 7: s149_ideal
View 6: s175_ideal
s195_ideal *** Wed Sep 15 13:3
1
2
3
View 8: a07
View 9: rad149_bkpJ_fl
rad175_bkpJ_fl *** Wed Sep 15
rad195_bkpJ_fl *** Wed Sep 15
1
2
3
2 um

Optimization algorithms solve the inverse problem by iteratively modeling the forward problem

1. guess at the object
2. calculate projections of the guess
3. compare with the real projection data
4. if Error < ß then stop
5. formulate a new guess at the object
6. goto 2

- Can apply constraints during iterations

Image quality depends on:

- accuracy in model of projection operation
- angular range and number of projections
- 'noise' in the projection data

The effects noise in projection data on the reconstructed image increase rapidly with reduction in angular range of projections.

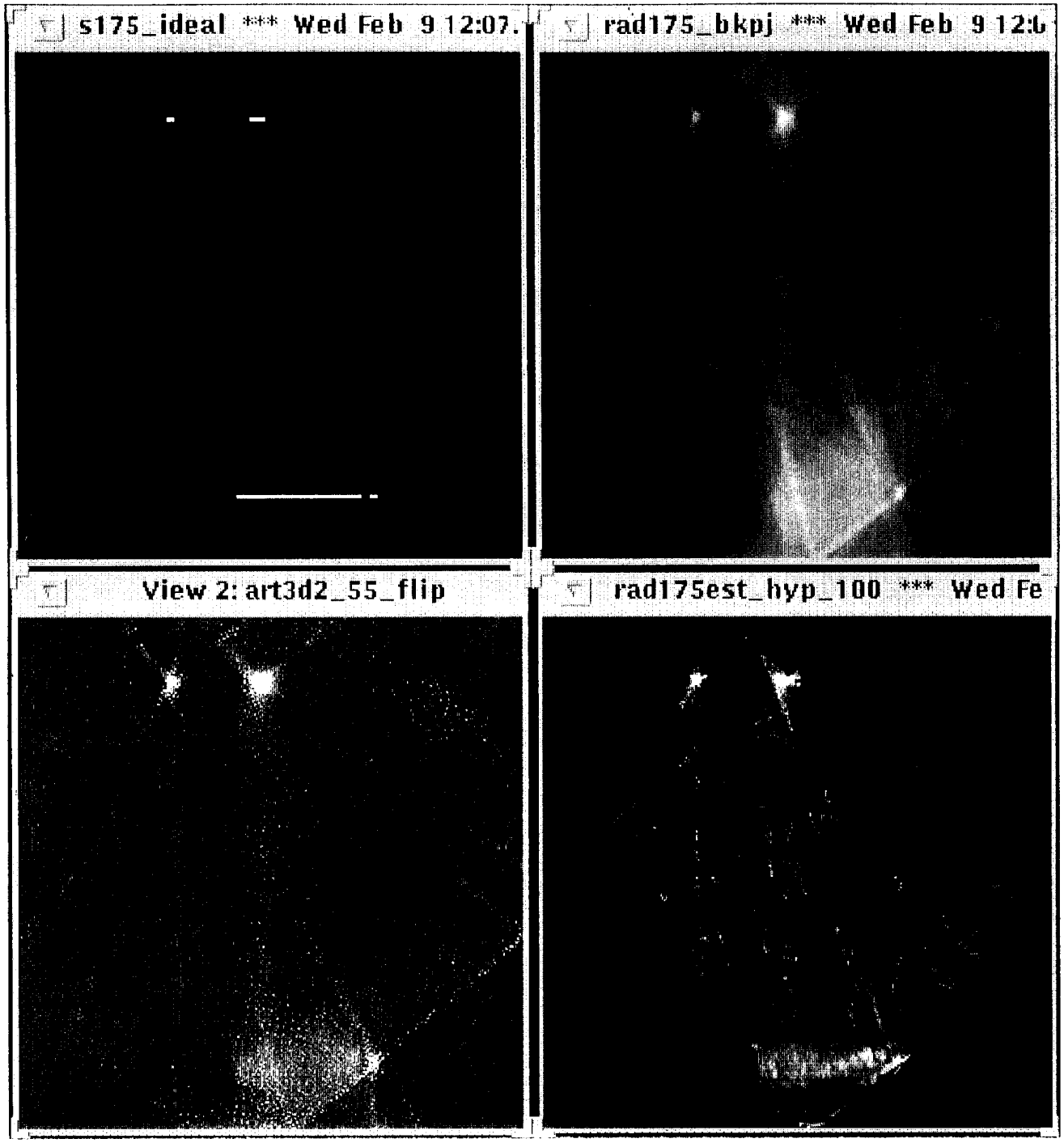
s175_ideal *** Wed Feb 9 12:07.
rad175_bkpj *** Wed Feb 9 12:0
View 2: art3d2_55_flip
rad175est_hyp_100 *** Wed Fe

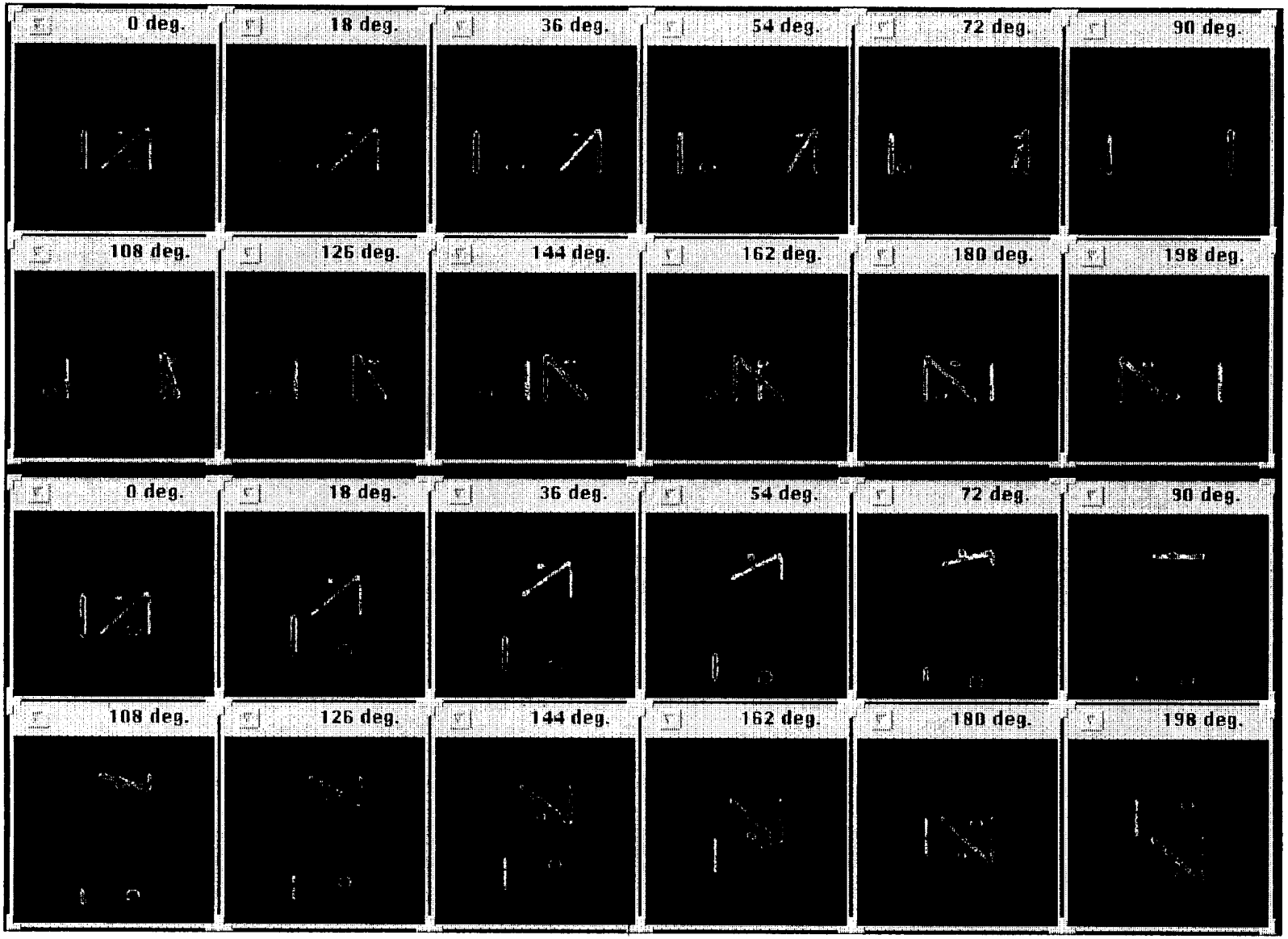
0 deg.
18 deg.
36 deg.
54 deg.
72 deg.
90 deg.
108 deg.
126 deg.
144 deg.
162 deg.
180 deg.
198 deg.
0 deg.
18 deg.
36 deg.
54 deg.
72 deg.
90 deg.
108 deg.
126 deg.
144 deg.
162 deg.
180 deg.
198 deg.

Summary

We have demonstrated ultra high resolution tomography of a 3-D phantom (test object) with 36 Å radiation using STXM.

- raw data was 9 projections over the angular range -50° to +55°
- 3-D image reconstructed using algebraic reconstruction technique (ART)
- $\partial_t \approx 1000$ Å
- $1000 \text{ Å} \leq \partial_l \leq 6000 \text{ Å}$

Current efforts include:

- reduce 'noise' in raw data especially in the angular measurements and position (alignment) of the projections
- develop better reconstruction algorithms

Coherent Optical Spectroscopy Throughout the Brillouin Zone

Keith Nelson, MIT

WORKSHOP ON SCIENTIFIC APPLICATIONS OF COHERENT X-RAYS
SSRL/SLAC - February 12, 1994

Coherent Spectroscopy Throughout the Brillouin Zone

Keith A. Nelson, Department of Chemistry, MIT

Ultrafast x-ray pulse can be used to record time-resolved "snapshots" of coherently vibrating crystals, observed at various stages of distortion along a selected lattice vibrational coordinate. With x-ray excitation pulses, collective vibrational modes with wavevectors throughout the Brillouin zone could be excited and monitored, providing direct access to structural change on the mesoscopic distance scale. Finally, multiple excitation pulses could be used to extensively manipulate, as well as characterize, material structure.

Extended Abstract

Techniques in time-resolved optical spectroscopy have evolved which permit direct observation of coherent phonon oscillations and decay. Optical properties which are influenced by lattice vibrational motion, such as birefringence or absorption frequencies, have been measured following pulsed excitation to monitor the lattice vibrations. This has permitted substantial progress in understanding structural rearrangements such as structural phase transitions which are driven by instabilities in zone-center phonons. In such cases, it would be of great interest to determine transient crystal structures reached as a function of distortion along a lattice vibrational coordinate. Essentially, time-resolved "snapshots" of a coherently vibrating crystal lattice could be recorded by using an ultrashort visible pulse to initiate the vibrational motion and ultrashort x-ray probe pulses to monitor it. This would be especially interesting for "soft" optic phonons in crystals near structural phase transitions, in which the vibrational displacements move ions or molecules from their initial positions in the lattice along a well defined microscopic pathway toward the positions occupied in an incipient crystalline phase.

The next step would be to use ultrashort x-ray pulses for initiation as well as probing of coherent vibrational motion. The advantage would be that modes with large wavevectors $q >> 0$ could be excited. With current time-resolved spectroscopies in the visible-UV range, it is possible to gain access to phonon wavevectors in only the first percent or less of the Brillouin zone (i.e. in the zone center) for most materials. For characterization of acoustic phonons, this limits the frequency range to about 10 GHz depending on the stiffness of the sample. Many structural changes involve acoustic or optic phonon modes at wavevectors far from the zone center. Inelastic neutron scattering can be used to characterize high-q modes, but those which are most involved in mediating structural change are often too strongly damped to be studied this way. Zone-boundary structural phase transitions, incommensurate transitions (in which soft modes occur at various points in the Brillouin zone) and dynamical relaxation of correlated structures on mesoscopic distance scale in a wide range of disordered and partially ordered materials (glass-forming liquids and polymers, charge-density waves and other incommensurates, relaxor ferroelectrics and spin glasses, etc.) could be observed directly.

Finally, by using multiple pulses it may become possible to manipulate coherent lattice motion to an extent sufficient to drive selected structural rearrangements. Such experiments are currently attempted in the visible regime, and would have a wide range of new possibilities with x-ray wavelengths.

COHERENT TIME-RESOLVED SPECTROSCOPY THROUGHOUT THE BRILLOUIN ZONE

AND SPECULATION ON MULTIPLE-PULSE FEMTOSECOND SPECTROSCOPY WITH X-RAYS

KEITH A. NELSON
DEPARTMENT OF CHEMISTRY
MIT

Sources of support:
ONR
NSF

OUTLINE

I. Watching Crystals and Molecules Vibrate
- **Current Optical Experiments**
- **Future X-ray Experiments**

II. Making Crystals and Molecules Vibrate
- **Current Optical Experiments**
- **Future X-ray Experiments**

III. Throughout the Brillouin Zone
- ~~**Optical Experiments**~~ ***IMPOSSIBLE!***
- **X-ray Experiments**

IV. Multiple-pulse Spectroscopy
- **Current Optical Experiments**
- **Future X-ray Experiments?**

MOTIVATIONS

Direct x-ray characterization of distorted crystal lattices

Characterize crystal structures in nonequilibrium configurations
Determine "normal" lattice modes
Examine lattices during rearrangement

Study of high-q optic phonons

Examine lattice instabilities at $q > 0$, i.e. Brillouin zone boundary phase transitions, incommensurate transitions, etc.

Study of high-q acoustic phonons

100 GHz - 10 THz frequency range
Important in liquid-glass transitions, other structural relaxation dynamics
1000 - 10 A wavelength range
Important in mesoscopic ordering of partially ordered materials

Study of high-q thermal modes

Nondiffusive heat transport over 10-1000 A distances

Manipulation of material structure

Current Experiments: Optical Initiation/Optical Probe

Direct time-resolved observation of elementary collective and molecular vibrations is routinely possible

Ultrashort excitation pulse exerts a sudden driving force on vibrational modes through "impulsive" stimulated scattering or "impulsive" absorption

Ultrashort probe pulses monitor vibrational oscillations and decay

We "watch" molecular and collective vibrations through their effects on refractive index or optical absorption - we don't directly measure the vibrational displacements.

X-rays could!

We determine vibrational wavevectors by crossing two excitation pulses to form an interference pattern. (See Fig. 1.) The wavevector is limited by the long optical wavelength to the first 1% or less of the Brillouin zone.

X-rays could be used to access the entire Brillouin zone!

Current Experiments:
Optical Initiation/Optical Probe

Typical applications (See Figs. 2-7)

Excite and monitor molecular vibrations whose motions lead to chemical reactions, e.g. bond breakage or formation. The vibrational coordinate corresponds to a chemical reaction coordinate. The motion involved in reaction is observed and unstable molecular structures intermediate between reactant and product are characterized spectroscopically.

Excite and monitor "soft" phonons in crystals near structural phase transitions. The vibrations move ions or molecules from their initial lattice positions toward the positions they occupy in an incipient crystalline phase. We observe time-dependent motion along the collective "reaction" coordinate that leads to structural rearrangement.

Excite and monitor acoustic modes in glass-forming liquids and polymers. In this case the longitudinal and shear acoustic vibrational coordinates are the collective "reaction" coordinates leading to structural relaxation. Relaxation on time scales of 1 ns is mediated by acoustic modes with frequencies around 1 GHz. Relaxation of ordered structures on 100 A size scales is mediated by acoustic modes with comparable wavelengths. Since relaxation in complex materials occurs on a very wide range of time and distance scales, a very wide range of acoustic frequencies/wavevectors is needed for its characterization.

Excite and monitor thermal modes in liquids and solids. Thermal transport across short distances is nondiffusive, and this could be observed at wavevectors accessible with x-rays.

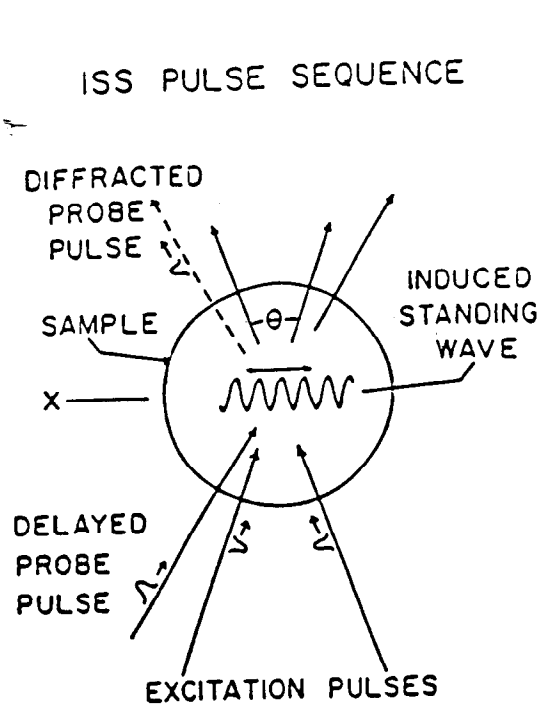

Fig. 1. Impulsive stimulated scattering (ISS) experiment conducted with crossed excitation pulses. The crossed pulses form an interference pattern whose spatial period defines the excitation wavevector. The spatial period depends on the angle between and wavelength of the excitation pulses. For pulses in the near-IR through near-UV wavelength range, the spatial period may range from about 0.1 - 100 μm. With coherent x-ray pulses, spatial periods in the 10-1000A range could be reached.

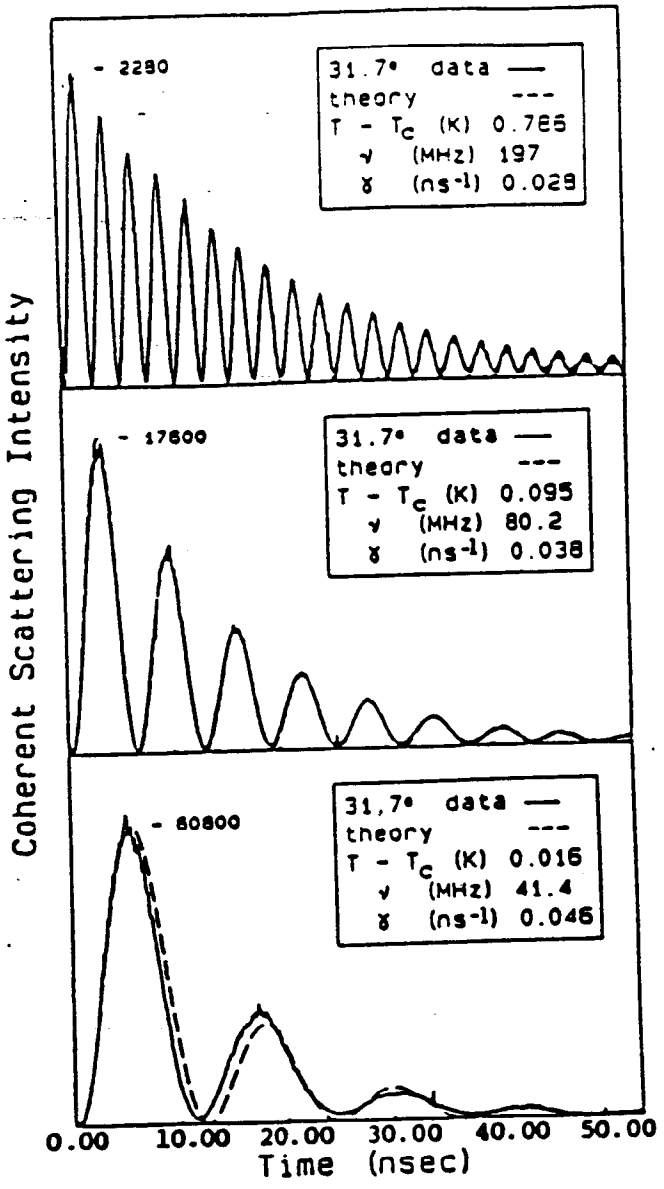

Fig. 2. Impulsive stimulated scattering data from "soft" transverse acoustic phonons in rubidium dihydrogen phosphate (RDP), an inorganic hydrogen-bonded crystal, at three temperatures approaching the ferroelectric phase transition temperature T_c from above. Visible excitation pulses were crossed at a 31.7^o angle to initiate the coherent acoustic waves whose oscillations and decay are observed through diffraction of a variably delayed probe pulse. Below the transition temperature, shear distortion of the crystal occurs spontaneously. As the transition temperature is approached, the crystal's resistance to shearing is reduced dramatically and so is the transverse acoustic frequency, as observed in the data.

In this crystal the lattice instability occurs at $q = 0$, i.e. the shear strain which occurs below T_c is uniform throughout the crystal. In other phase transitions, the instability occurs at high wavevectors and no unusual phonon responses are observed at the small wavevectors accessible to visible light. X-ray pulses will permit access to the high wavevectors of interest.

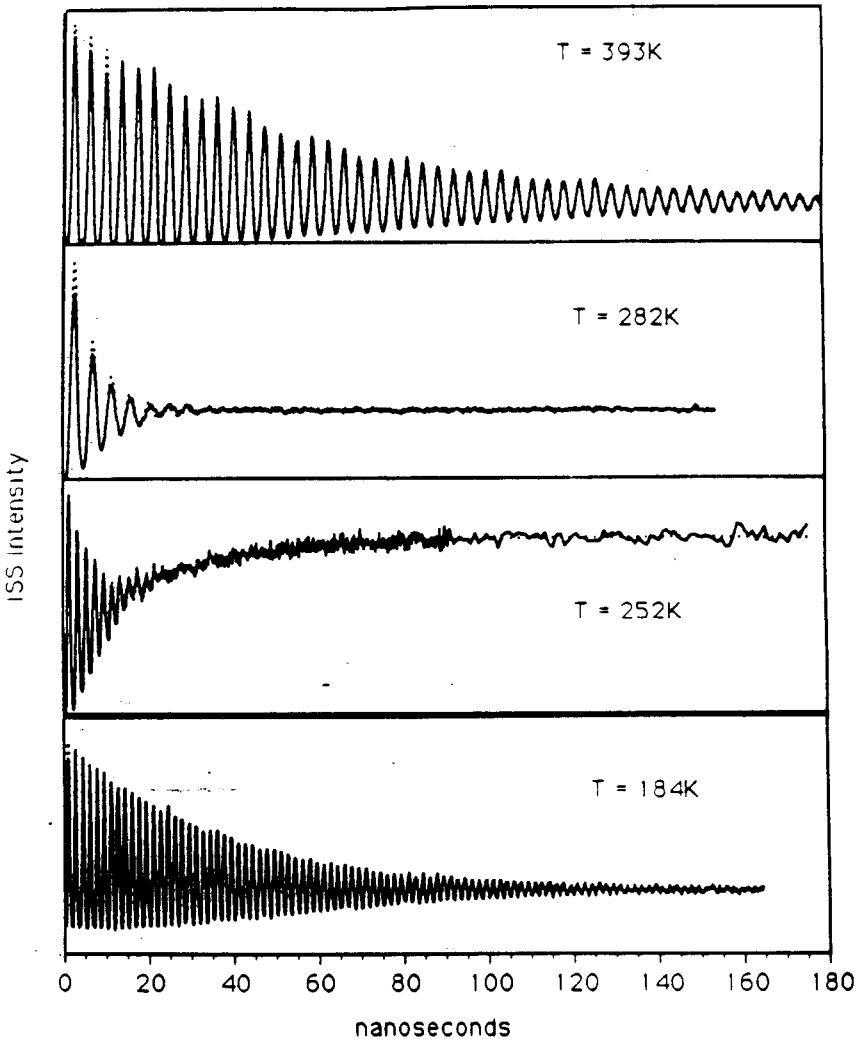

Fig. 3. Impulsive stimulated scattering data from longitudinal acoustic waves in polypropylene glycol (PPG). At high temperatures the sample is liquid-like, i.e. structural relaxation occurs on fast (ps) time scales. As the temperature is reduced, the viscosity increases and eventually glassy behavior is observed, i.e. structural relaxation dynamics become slower and eventually too slow to measure. The acoustic attenuation reaches a maximum when the structural relaxation dynamics are comparable to the acoustic oscillation period, i.e. when the relaxation spectrum overlaps the acoustic frequency. With visible wavelengths, acoustic frequencies of about 10 MHz - 10 GHz can be reached by varying the acoustic wavevector (the excitation angle and wavelength). X-rays will provide access to far higher wavevectors and therefore to higher acoustic frequencies in the GHz-THz range. This will permit characterization of relaxation dynamics in glass-forming liquids at temperatures well above the glass transition temperature, where the onset of nonergodic behavior occurs. Other rapid relaxation processes in a wide range of partially ordered materials will also become accessible.

Acoustic signatures similar to those observed here will also occur when the acoustic wavelength coincides with the correlation length of short-range ordering in samples such as glass-forming liquids, spin glasses, etc. X-rays will permit determination of correlation lengths in this manner.

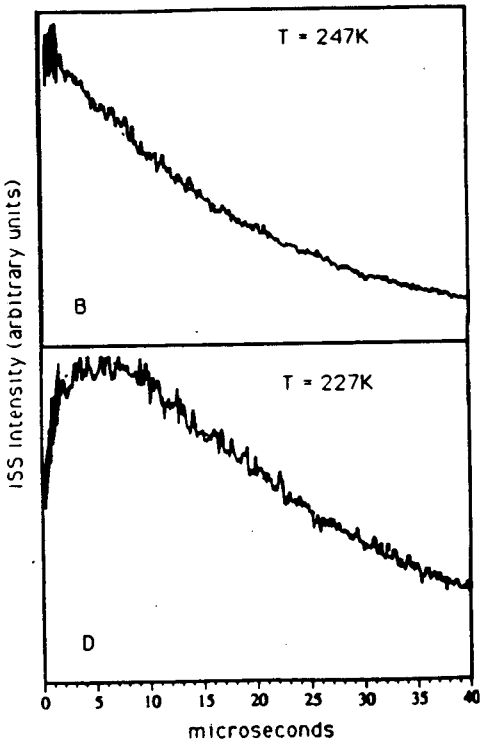

Fig. 4. ISS data from PPG on slower time scales showing the thermal response (thermal expansion and diffusion). With x-rays, heat transport in the nondiffusive regime could be observed in many materials. This is only possible if the spatial period over which heat travels (i.e. the ISS grating period) is short compared to high-q phonon mean free paths.

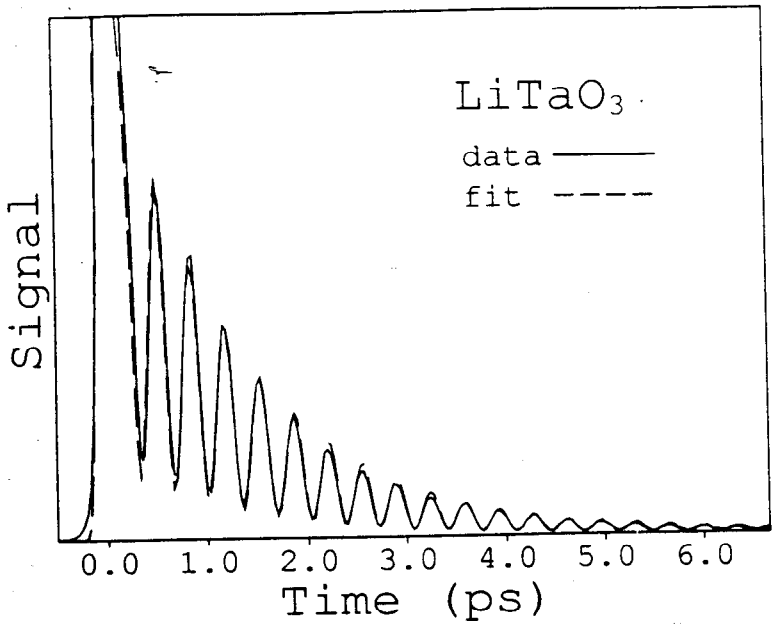

Fig. 5. ISS data from optic phonons in a crystal of lithium tantalate. Crossed visible excitation pulses were used to generate the phonon response, and the coherent lattice oscillations and decay were observed with variably delayed probe pulses. The observations are possible because the lattice vibrations lead to refractive index changes which are detectable with visible light. Birefringence and other optical observables can also be measured.

With x-rays, crystallographic measurements of the actual lattice geometry at various stages of vibrational distortion could be made. This corresponds to recording "snapshots" of distorted microscopic structures.

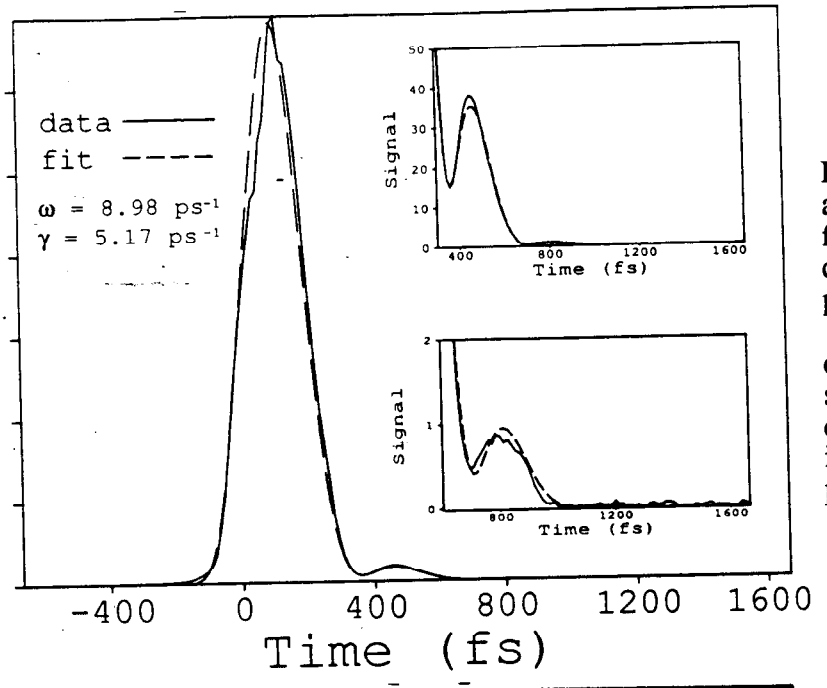

Fig. 6. ISS data from soft optic phonons in a crystal of potassium niobate. The low frequency and strong damping are characteristic of soft modes near structural phase transitions.

X-ray crystallographic measurements of crystal lattice structures assumed during soft mode distortions would provide detailed information about the mode-mode interactions which drive many structural phase transitions.

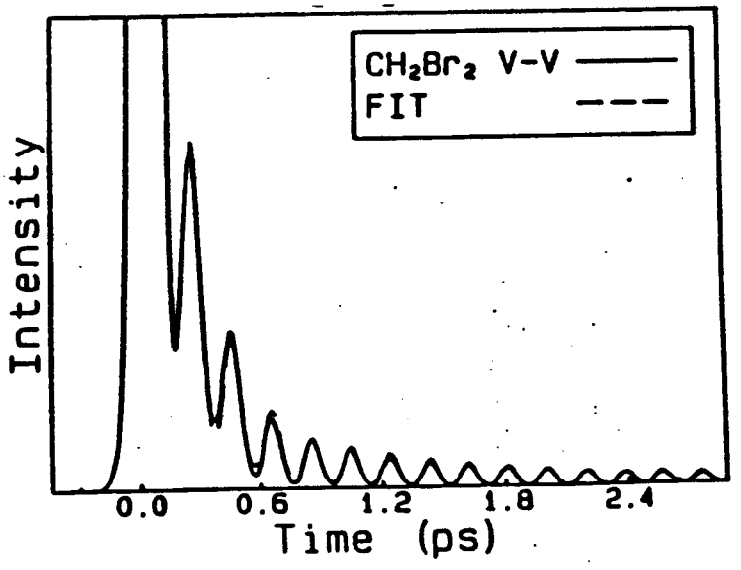

Fig. 7. ISS data from molecular vibrations in dibromomethane liquid. With x-rays, it may be possible to characterize distorted molecular structures assumed at various stages in vibrational cycles.

Future Experiments: Optical Excitation/X-ray Probe

Same "impulsive" excitation mechanism, but probe is now x-ray diffraction instead of optical measurement

Direct measurement of lattice or molecular displacements at various stages of vibrational distortion

Permits determination of lattice or molecular vibrational coordinate

For large amplitudes, permits determination of mode-mode interactions

Permits direct characterization of unstable structures formed during chemical or structural change

Future Experiments: X-ray Excitation/X-ray Probe

X-ray excitation pulses are crossed to form interference patterns with very short wavelengths (high wavevectors)

Excitation of high-q optic phonons

High-q "soft" modes involved in structural phase transitions
High-q phonons coupled to mesoscopic ordering, e.g. in spin glasses, incommensurate phases, relaxor ferroelectrics, and other systems with short-range order
In these cases, the lattice modes involved in structural rearrangement are not at wavevectors accessible optically but rather at high wavevectors accessible with coherent x-rays.

Excitation of high-q acoustic phonons

Acoustic wavelenths in 10-1000 A range, acoustic frequencies in GHz-Thz range
Examine complex structural relaxation on ps time scales and mesoscopic distance scales in glass-forming liquids and polymers, spin glasses, relaxor ferroelectrics, etc.

Excitation of high-q thermal modes

Observation of nondiffusive (ballistic) thermal transport

Outperforms inelastic neutron scattering

Far better wavevector and frequency/time resolution, far better ability to characterize heavily damped or overdamped modes.

Multiple-pulse femtosecond spectroscopy with x-rays?

Current Experiments: Multiple-pulse Optical Excitation

Femtosecond pulse shaping used to generate complex femtosecond waveforms with controlled amplitude and phase profiles (Fig. 8)

Waveforms are used to manipulate molecular or collective electronic, vibrational responses

Example: Multiple-pulse excitation of lattice vibrational modes (Figs. 9-10)

Objective: Extensive optical control over molecular and material behavior and structure

Future Experiments: Multiple-pulse X-ray Excitation?

X-ray pulse shaping methods needed

Could permit fine control over high-q phonons, high-energy electronic coherences

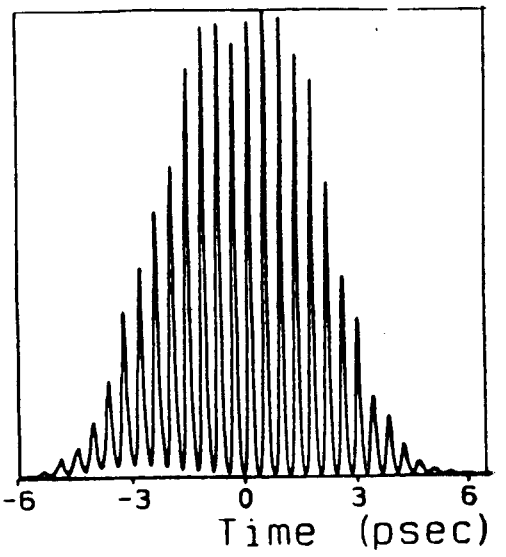

Fig. 8. Sequence of femtosecond pulses produced by pulse-shaping methods. The intensity profile is shown, but the optical phase profile is also under experimental control.

Femtosecond pulse-shaping in the optical regime is now rather well developed, and can be done on a routine and automated basis. As coherent x-ray "optics" become better developed, it is likely that pulse-shaping methods for x-rays will be developed.

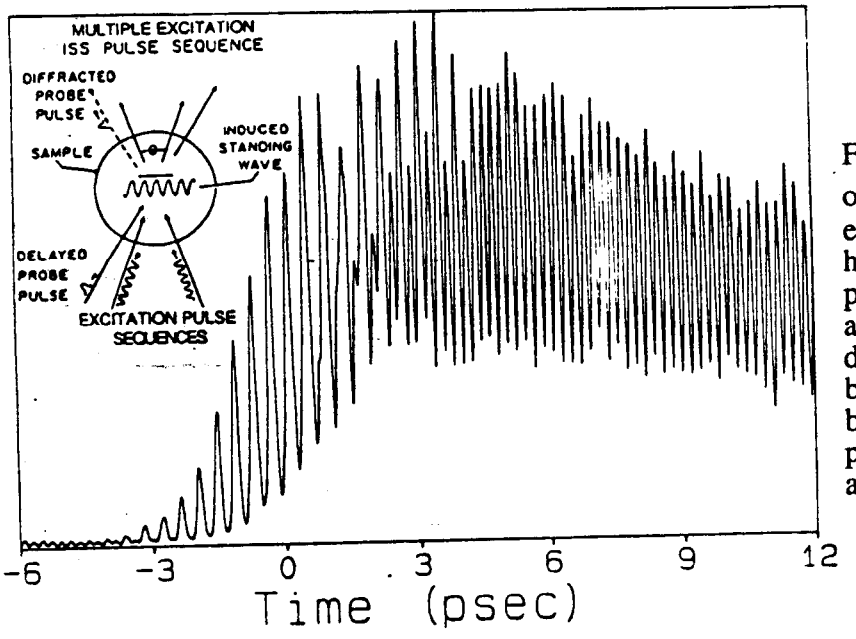

Fig. 9. Multiple-pulse ISS data from an organic molecular crystal, α-perylene. The excitation pulse sequence (shown in Fig. 8) has been timed to match a selected optic phonon frequency. The phonon response is amplified by each successive pulse. The data show the coherent vibrational response building up during the pulse sequence (first becoming apparent in the data after about 1 ps) and persisting for many picoseconds after the pulse sequence is finished.

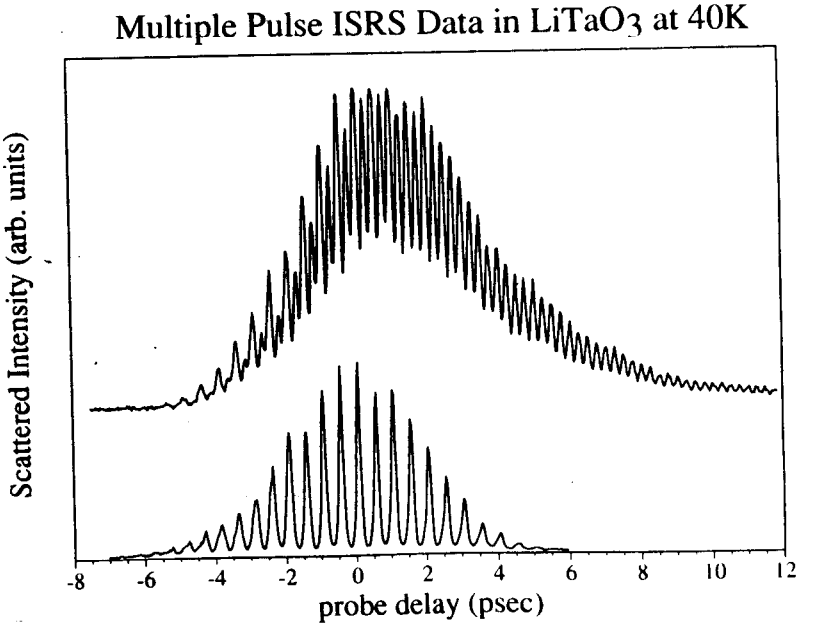

Fig. 10. Excitation pulse sequence (bottom) and multiple-pulse ISS data from lithium tantalate crystal at 40K. The optic phonon mode is amplified by the properly timed pulse sequence.

SUMMARY

X-ray probing will permit direct characterization of nonequilibrium lattice, molecular structures

X-ray excitation will provide access to high-wavevector modes of special importance in structural phase transitions, liquid-glass transitions, materials with mesoscopic order

High-q acoustic phonons throughout the Brillouin zone, with GHz-THz frequencies, will be observed

High-q thermal modes will show nondiffusive heat flow

Coherent x-ray spectroscopy will outperform and completely replace inelastic neutron scattering for characterization of high-q modes

Multiple x-ray pulses could yield improved capabilities for "optical" (i.e. x-ray) manipulation of matter

Time Resolved Structural Studies on Biological Macromolecules in the Sub-nanosecond Time Domain

Keith Moffat, University of Chicago

TIME-RESOLVED STRUCTURAL STUDIES ON BIOLOGICAL MACROMOLECULES IN THE SUB-NANOSECOND TIME DOMAIN

Keith Moffat
Department of Biochemistry and Molecular Biology
The University of Chicago

In contemplating time-resolved x-ray crystallographic studies in the 100 fs time scale on molecules of biological interest, two main questions arise: Is there anything to be seen on that time scale? Can such experiments in fact be carried out and their results interpreted? The answer to the first is a resounding yes. Several systems (heme proteins such as myoglobin and hemoglobin as well as bacterial photosynthetic reaction centers) exhibit spectroscopic changes when probed on time scales down to a few fs by an array of techniques. These systems have already been studied by high-resolution crystallographic techniques; other systems (cytochrome oxidase, bacteriorhodopsin, rhodopsin) show these spectroscopic changes but have not yet yielded suitable three-dimensional crystals though these are a reasonable prospect; and yet other systems (e.g., photoactive yellow protein) have not yet been studied by fs spectroscopies but are light-sensitive and form excellent crystals. Note that all contain naturally occurring chromophores; in all but the heme proteins, light absorption is their key initial biological role. Femtosecond biochemistry and biophysics have been reviewed recently by Martin and Vos[1].

The answer to the second question is also yes, but more qualified. Fs crystallography is only worthwhile if conducted in a time-resolved mode, which means that all experiments will be of the pump-probe form where an optical fs pump pulse is followed, after a suitable, adjustable time delay, by the probe x-ray pulse. This combines a still heroic spectroscopic experiment with an even more heroic x-ray experiment; but such heroism can be realistically contemplated. Snags to be overcome include the relative timing of the pump and probe pulses, the extent of heating by the pump pulse, and the rate of vibrational cooling of the chromophore, the extent of crystal damage by the probe pulse, and (above all) the limitations of a strategy for collecting integrated intensities over the unique volume in reciprocal space, at many different time delays, which must illuminate a stationary crystal with nearly monochromatic radiation of bandpass $\Delta\lambda/\lambda \sim 10^{-3}$. Hard x-rays with $\lambda < 2$ Å are (nearly) essential; absorption at longer wavelengths

[1]Martin, J.-L. and Vos, M. H. *Ann. Rev. Biophys. Biomol. Struct.* **21**, 199-222 (1992).

is a very severe problem, even for crystals <50 μm in dimension. The third harmonic of an undulator, whose fundamental lies at 4.5 Å, might suffice. The continuum radiation, which underlies the brilliant harmonics, might also be useful.

The above experiments utilize the exceptionally short pulses and the very large flux per pulse, but they do not explicitly utilize the spatial or temporal coherence of the beam. It is not at all clear what will happen when a highly coherent beam falls on a perfect single crystal or an ideally imperfect crystal. Might phase information be directly derivable via a form of Gabor holography? Simple calculation suggests the coherence length $\lambda^2/\Delta\lambda$ is too short. It could, of course, be enlarged by adding a narrow bandpass monochromator, but then the reflections from a stationary crystal are no longer integrated intensities. This area bears further study as (if successful) it would revolutionize crystallography.

3 POINTS:

1. Is there anything to be seen in ~100 fs?

2. Can such an experiment be carried out and interpreted?

COHERENCE:

3. What happens if a spatially - and temporally coherent - x-ray beam falls on a single crystal?

Assuming enough hard x-ray photons can be delivered to the crystal to record a good diffraction pattern in 65 fs*, then . . . .

- Is there any interesting biochemistry to be seen?

- What evidence is there for structural changes:
  - -- on this time scale?
  - -- on which systems?

---

*Beam is <u>small</u> (~50 μm at 10n) and quite monochromatic ($\Delta\lambda/\lambda \sim 10^{-3}$)

OPTICAL CHANGES IN THE fs → fs DOMAIN HAVE BEEN OBSERVED BY:

- Transient absorption spectroscopy
- Transient raman spectroscopy
- Transient IR spectroscopy
- Fluorescence depolarization
- Photon echo spectroscopy
- Coherent anti-stokes raman spectroscopy

BUT: PHOTONS HEAT THE CHROMOPHORE!

eg, 585 nm ≡ 49 kcal/mole

Fe-CO energy ~22 kcal/mole

$\therefore$ 27 kcal/mole excess $\Rightarrow$ ΔT ~200°K

HEME cooling in <10 fs?

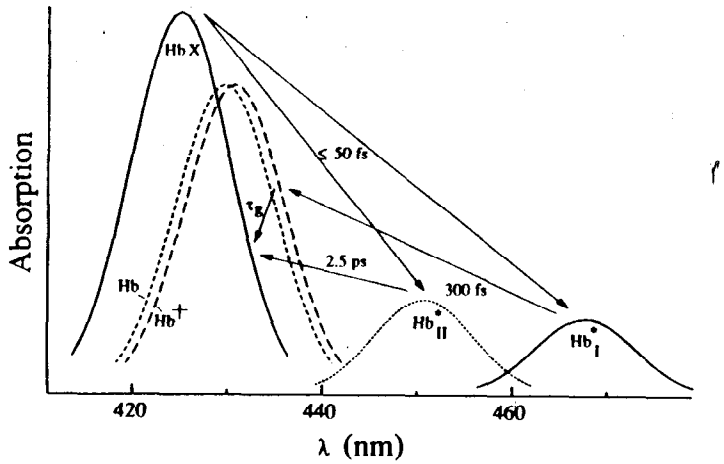

Figure 2 Generalized absorption spectra of heme proteins and their photoproducts. The diagram is labeled for hemoglobin, but is equally applicable to myoglobin and protoheme, provided that the associated shapes and positions of the deoxy-like species (+) are taken into account. X denotes the ligand (O_2, CO, or NO). The excited-state unligated species Hb^*_I and Hb^*_{II} are formed in less than 50 fs from the photoexcited HbX; their relative amounts depend on X. The deoxy-like species is formed from Hb^*_I in 300 fs; Hb^*_{II} decays to the ground state in 2.5 ps. The term τ_g reflects the time constant(s) for geminate recombination.

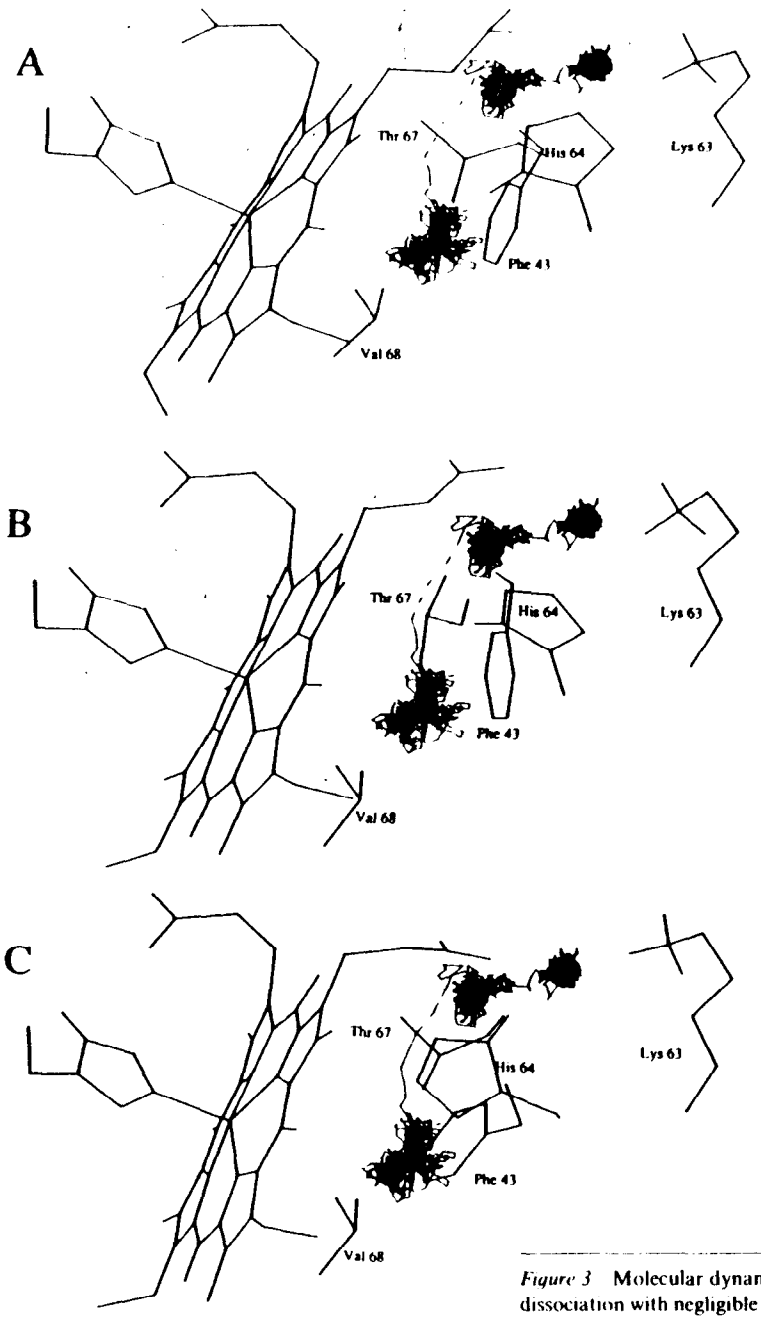

Figure 3 Molecular dynamics simulation of the pathway of CO in myoglobin after photodissociation with negligible excess energy. Each drawn step is 50 fs; the total trajectory is 100 ps. The CO ligand clearly resides in three distinct intermediate states during this trajectory. In this specific simulation, the transitions from the first to the second state and from the second to the third state take place after, respectively, 36 ps and 65 ps. Each figure shows the entire trajectory; the position of the nearest amino acid residues is averaged over the residence time in the first (*A*), second (*B*), and third (*C*) state.

Ann. Re. Biophys. Biomolec. Struc. **21**, 199-222 (1992)

Structural Dynamics Of Heme Proteins

e g , Fe motion
HEME "doming"
Histidine relaxation

Ligand Dynamics: Geminate
Recombination

CO ≥ ns; NO, O_2 ~fs

Photosynthetic Reaction Center

Primary electron transport from

Bacteriochlorophylls →

Bacteriopheophytins →

Quinones → fe

Get a charge-separated species p^+I^- in a few fs at 300°K.

Coupling to low-frequency vibrational modes of the protein matrix?

MLCO - ML* 40°K

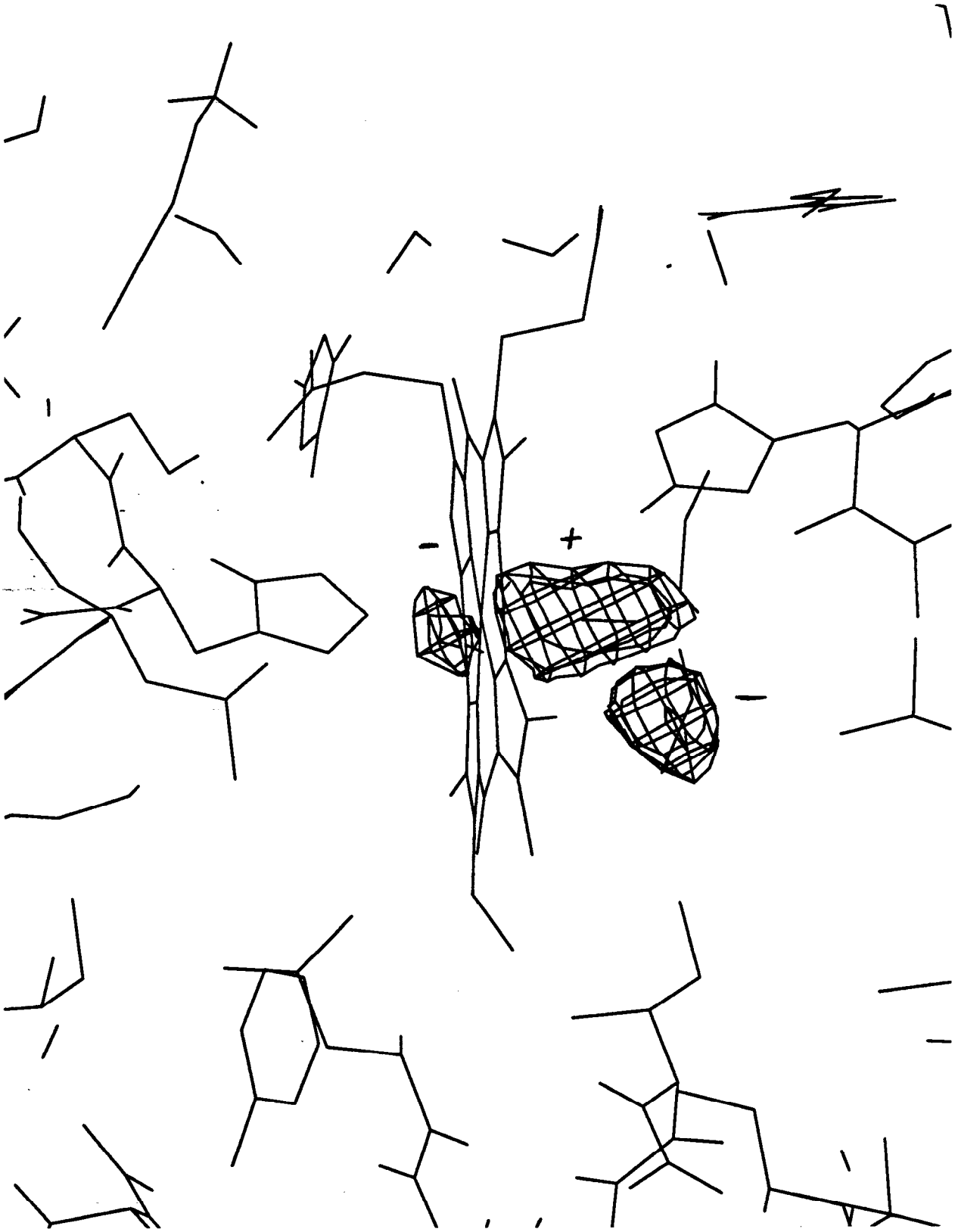

Scripps Xfit/XtalView plot created Fri Feb 11 11:57:21 1994

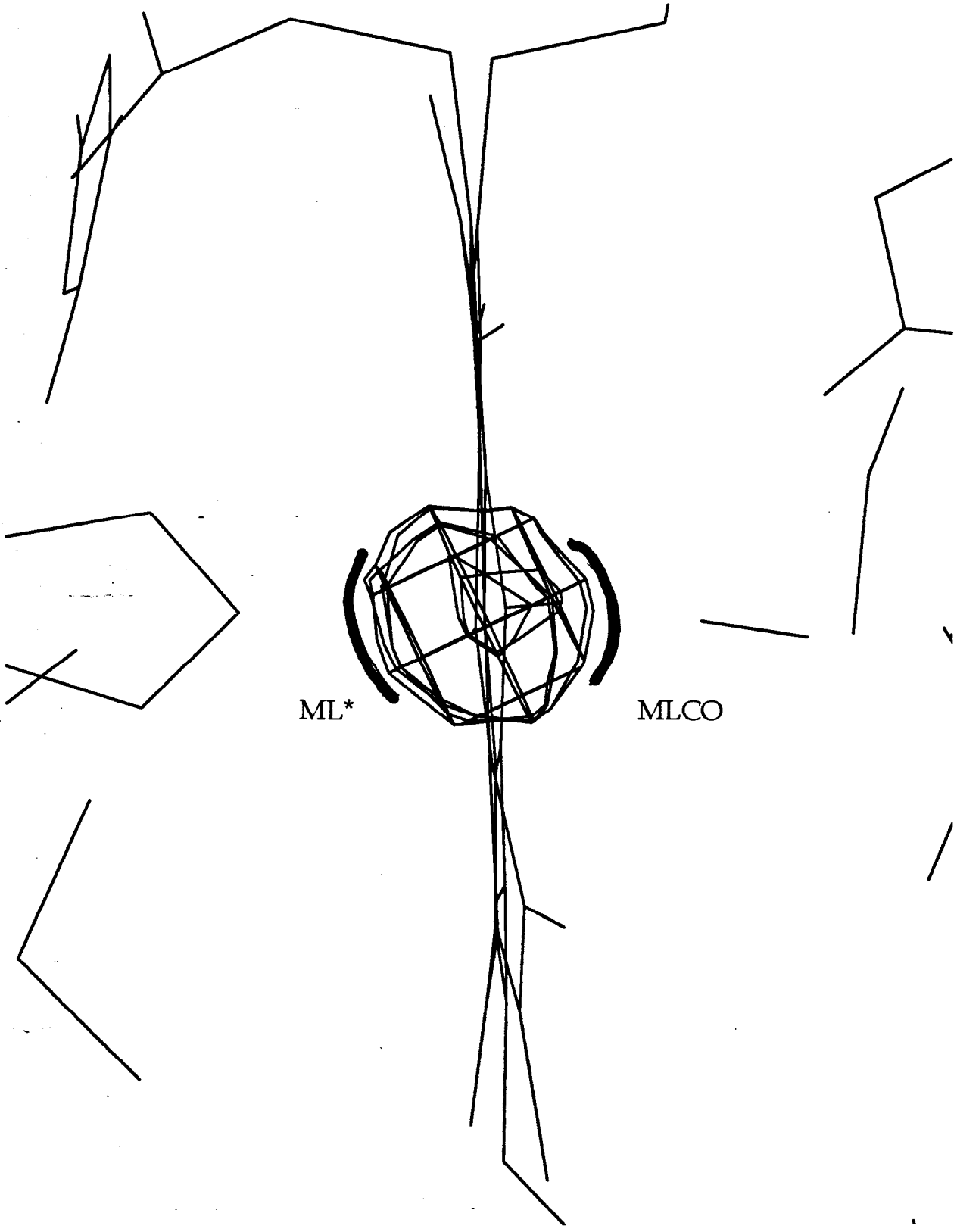

Scripps Xfit/XtalView plot created Fri Feb 11 12:21:15 1994

Bacteriorhodopsin/Rhodopsin: Retinal Isomerization

Structure ? ?

Photoactive yellow protein:

Are there any sub-ns processes?

What damage processes can occur in the time scale of observation?

Can small structural changes be detected?

Is the 0.5 fs synchronization precision a limitation?

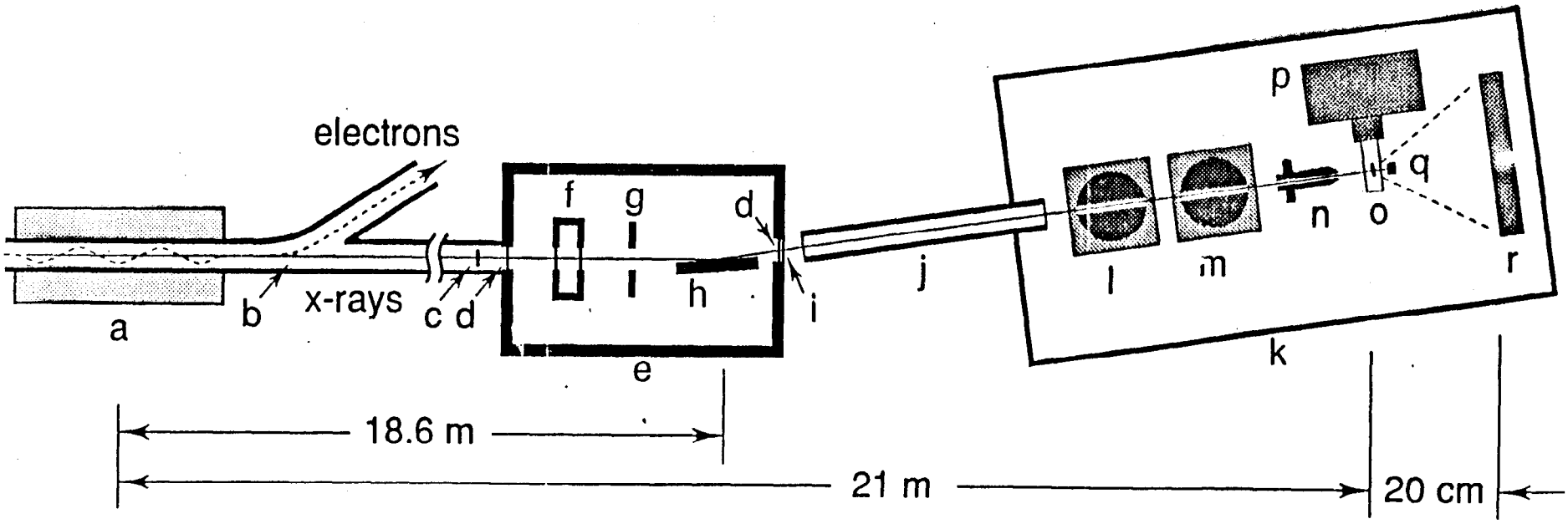
electrons
a
b
x-rays
c d
e
f
g
h
d
i
j
k
l
m
n
o
p
q
r
18.6 m
21 m
20 cm

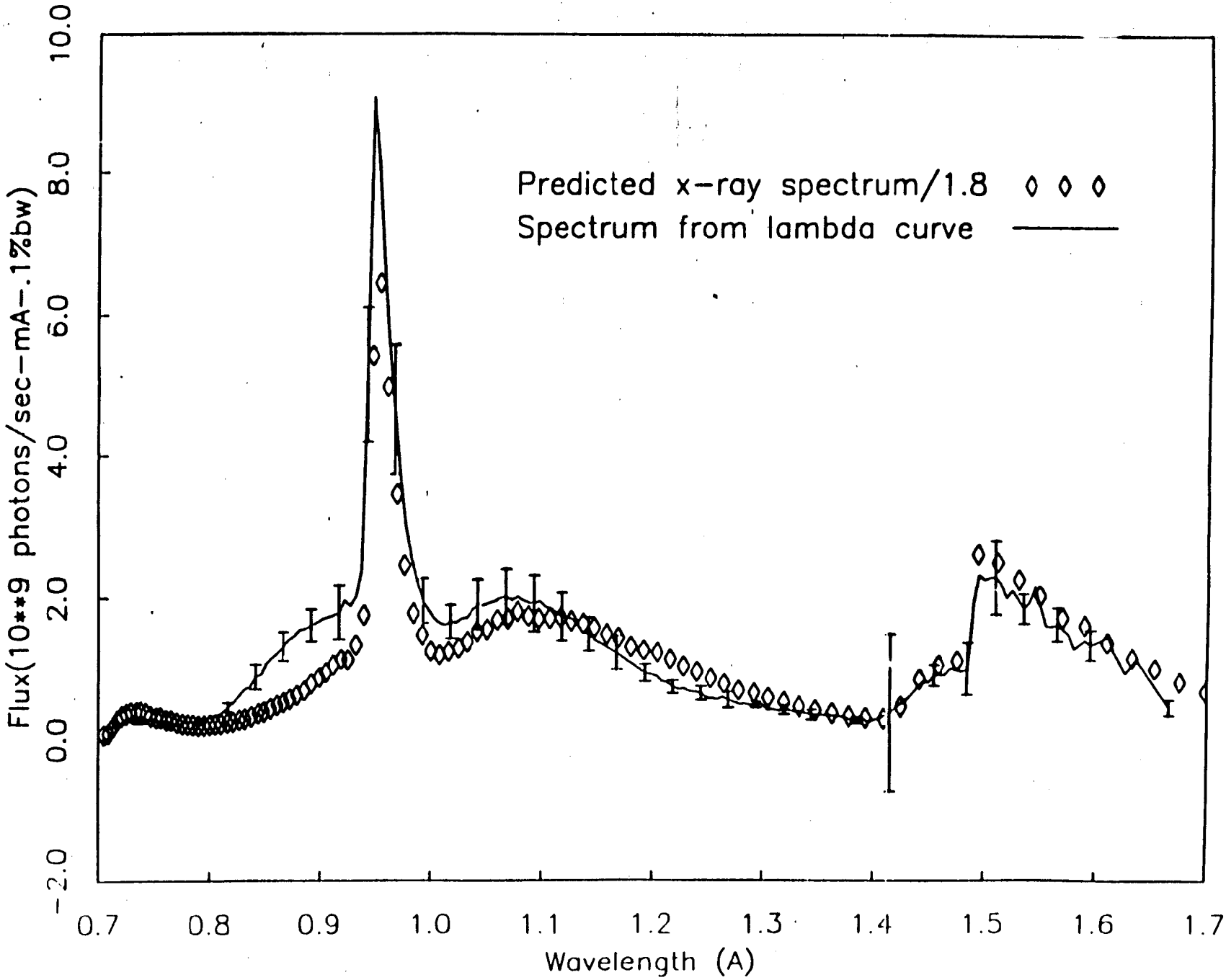

Szebenyl, et al, *J. Appl. Cryst.* **25**, 414-423 (1992)

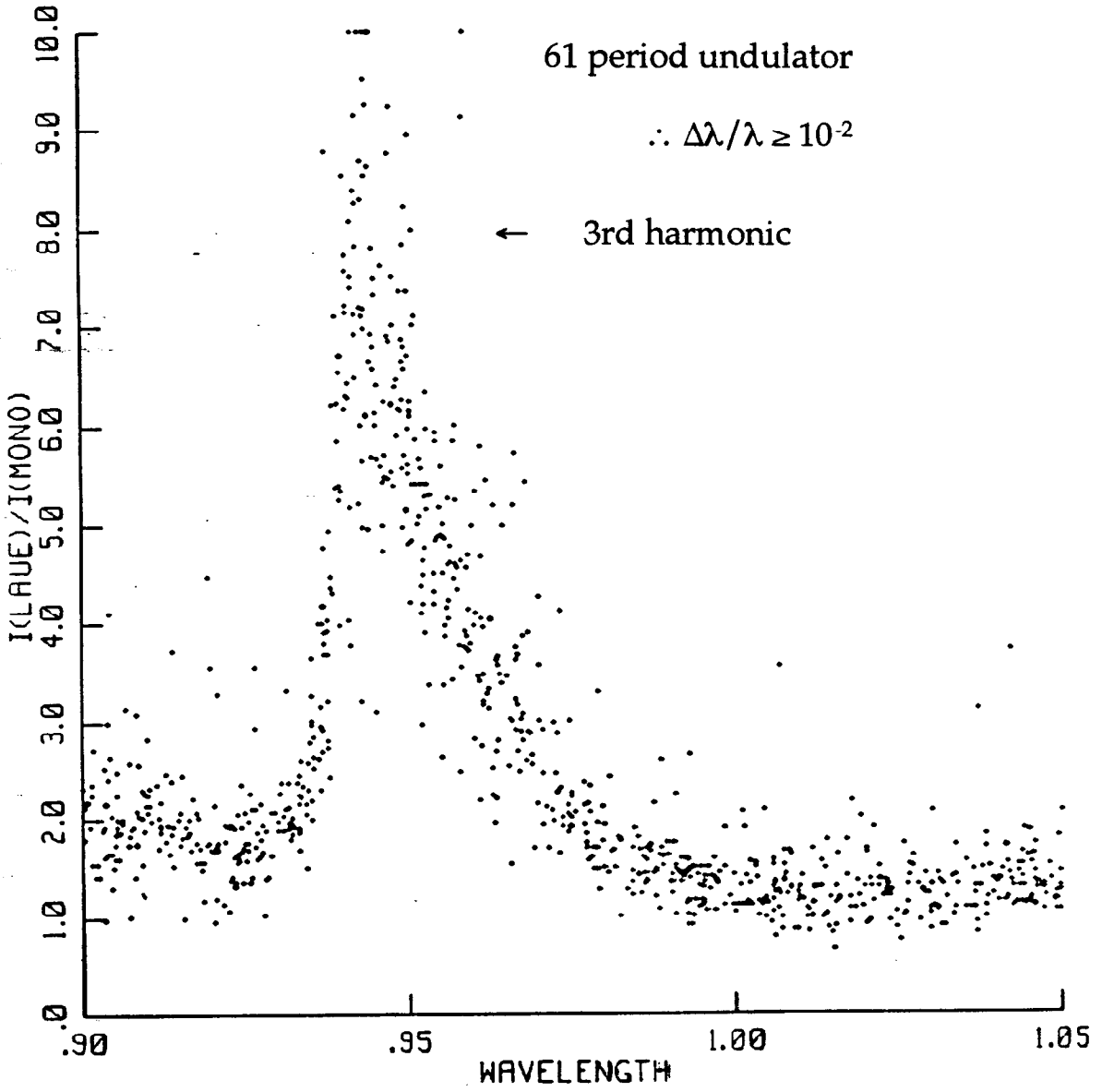

Lyso 5 100-bunch images corrd except I0 vs mono

INTENSITY RANGES 1 THROUGH 5 PLOTTED

Table 1. *Observed and projected spectral intensities for Laue beam lines, near* 1 Å

beam line	source	spectral intensity photons/(s mm^2 0.1 %)	spectral intensity per bunch photons/(mm^2 0.1 %)
Daresbury SRS 9.5	wiggler	2×10^{12} (*a*)	2×10^{4} (*b*)
NSLS X26C	dipole	3×10^{12} (*c*)	5×10^{4} (*d*)
CHESS C2	dipole	1×10^{11} (*e*)	2×10^{5} (*f*)
CHESS A3	undulator	1×10^{13} (*g*)	1×10^{7} (*h*)
APS	undulator A	7×10^{14} (*i*)	1×10^{8} (*j*)
ESRF	wiggler	2×10^{15} (*k*)	4×10^{8} (*l*)

(*a*) 5T. 3 pole wiggler with Pt coated. focusing toroid. Assumes SRS operation at 200 mA. Adapted from table 5.5 of Helliwell (1992). (*b*) As in (*a*): assumes 5 mA operation. (*c*) Dipole with Pt coated. focusing cylinder. Assumes NSLS operation at 200 mA. (*d*) As in (*c*): assumes 5 mA operation. (*e*) Dipole. unfocused. Assumes CESR operation at 80 mA. See fig. 5.2 of Shenoy *et al.* (1988). (*f*) As in (*e*): assumes 32.5 mA operation. (*g*) APS prototype for undulator A. CESR operated in dedicated. low emittance mode. Value is for the peak of the third harmonic at 0.97 Å. Assumes operation at 80 mA. See Bilderback *et al.* (1989) and Szebenyi *et al.* (1992). (*h*) As in (*g*): assumes 32.5 mA operation. (*i*) Projected value: on axis at 50 m with no focusing. Assumes APS operation at 100 mA. See fig. 6.7 of Shenoy *et al.* (1988). (*j*) As in (*i*): assumes 5 mA operation. (*k*) Projected value: 44 pole wiggler source with 1.3 m toroidal focusing mirror. at 20 keV. Assumes ESRF operation at 100 mA. The focal spot size is 0.033 mm^2. Adapted from Wulff (1991). (*l*) As in (*k*): assumes 7.5 mA operation.

Table 1.

	100–bunch lysozyme	single–bunch lysozyme	single–bunch GA381
Crystals:	1	2	1
Images:	5	5	3
Spots per plate – no.:	600–720	45–85,135*	35–55
% of predicted:	16–20	2–5,7*	29–42
Total observations:	3357	359	142
Unique reflections:	833	269	120
% of total:	19 (to 2.5Å)	10 (to 3.0Å)	18 (to 1.5Å)
λ range:	0.7–1.7Å	0.7–1.7Å	0.7–1.7Å
Minimum radius on plate:	35 mm.	5 mm.	5 mm.
Maximum x,y on plate:	100 mm.	80 mm.	120 mm.
Rms error in obsvd vs. calcd spot pos'ns, last refinement cycle:	0.2–0.4 r.u.	0.5–0.8 r.u.	0.2–0.4 r.u.
Minimum I/σ_I	4	6	4–6
Max error in spot pos'n:	Not applied	1.8 r.u.	1.8 r.u.
Minimum peak width at half–maximum:	Not applied	2.1+CxRad (C=0.0036 to 0.0130)	2.1+CxRad (C=0.0036 to 0.0064)
R_{scale} – weighted:	0.0723		
unweighted:	0.1133		
R_{sym}:	0.070–0.086 (140–220 ovlps)	0.042–0.236 (2–13 ovlps)	0.040–0.073 (1–2 ovlps)
R_{merge}:	0.0739 (2275 ovlps)	0.1754 (65 ovlps)	0.0667 (19 ovlps)
R_{mono}:	0.0707 (787 ovlps)	0.0978 (257 ovlps)	0.0775 (117 ovlps)

*Scanned with an extra factor of 3 gain.

7×10^9 photons (s . mA . 0.1% BW)$^{-1}$ at peak of 3rd harmonic

$\approx 6 \times 10^5$ photons (0.1%)$^{-1}$ per 120 ps bunch at 32.5 mA through a 300 μm collimator

Need ~ 500X for good exposure

i.e., 3×10^8 photons (0.1%)$^{-1}$

$\approx 5 \times 10^9$ photons (0.1% BW . mm^2)$^{-1}$

The FEL is a (nearly) monochromatic source: $\Delta\lambda/\lambda \sim 10^{-3}$

This is just large enough to give integrated intensities with a stationary crystal

BUT, not many of them!

$\therefore$ need many crystal orientations

($\geq$100); many time points

($\geq$10)

i.e., $\geq 10^3$ crystals/experiment if this is a destructive exposure!

What happens when a hard x-ray beam with diffraction-limited transverse coherence, but only modest longitudinal coherence, falls on a perfect single crystal? or on an ideally imperfect crystal?

Phase determination of Mössbauer sources?

The beam is very small in spatial extent: ~50μm at 10m

Expand it while retaining coherence?

Holographic-style recording?

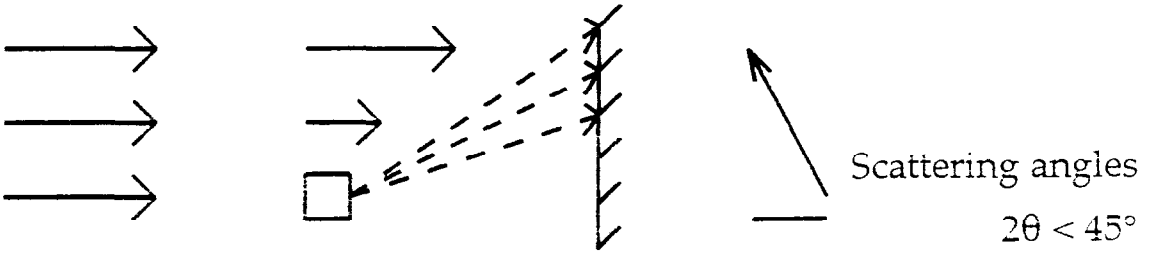

Summary of Discussion

Moffat talk:

Discussion centered around Moffat's assertion that the LCLS had problems as a source for protein crystallography. The beam is too monochromatic and collimated to fully record very many reflections at one orientation. The picosecond pulse length makes the LCLS a stationary crystal system. Pellegrini suggested that the FEL pulse could be split into multiple beams so that multiple orientations of one sample could be observed in a single shot. Materlik suggested that the continuum, spontaneous emission spectrum from the undulator could be used. Winick pointed out that the continuum has a larger divergence and, for the very-short-wavelength FEL designs, has a larger integrated intensity than the amplified peaks.

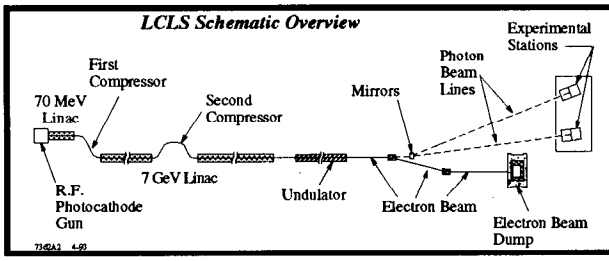

OTHER CONTRIBUTIONS

A Distinguished Feature of SLAC FEL

K. Namikawa[A,B] and S. Yamamoto[B]

A)Department of Physics, Tokyo Gakugei University, Koganei, Tokyo 184, Japan.
B)Photon Factory, KEK, Tsukuba, Ibaraki 305, Japan.

X-ray quantum optics investigates interactions between X-ray quantized photon fields and materials. Although the polarization is one of characteristics of the quantized photon fields, it is an inherent nature from the clasical electromagnetic fields. On the other hand, statistical characters are peculiar to the quantized photon fields. Statistical nature can be recognized even as a new degree of freedom of quantized photon fields.

Commonly, it appears in the zero point motion of the vacuum field, and does also in nonlinear phenomena. Nonlinear interaction between X-ray photon fields and matters changes the statistical characters of the post-interacted X-ray fields. From this change in statistical character we can deduce some information on a statistical response of the materials to the X-ray photon fields. Since the concept of the statistics basically stands upon a single photon mode, that the keyfactor in such phenomena is a degree of Bose degeneracy of the photon fields.

Bose degeneracy δ of the synchrotron radiation is discrived in terms of the peak brilliance and the number of mode in the cavity of undulator as follows,

$$\delta = 6.7 \times 10^{-27} \lambda^3 B_p,$$

where, λ is the wave length given in Å and B_p is the peak brilliance given in photons/s/mm^2/mrad^2/0.1%bw. Using design parameters for individual synchrotron radiation facilities, we can estimate the degree of Bose degeneracy. The value of δ for the 3-rd generation light sources is the order of 10^{-3} to 10^{-1}, while that of the SLAC FEL is 1.2×10^8 at 1.5 Å. From those values we can recognize that the SLAC FEL is distingushed from the 3-rd generation light sources in Bose degeneracy. This fact means feasibility of the quantum optics in X-ray region is confirmed only by the SLAC FEL source.

We are now preparing a preliminary experiment for the 4-th generation synchrotron radiation using the Tristan Main Ring. Since the Bose degeneracy in this case is close to one, we are planning to investigate, through this experiment, possibilities of sciences to be realized by the use

of 4-th generation sourse. the Tristan Main Ring, however, will not be expected to be used as a 4-th generation X-ray source because of the B physics experiment. After our test experiment it will be converted to the B physics machine.

In this situation, because of the beam quality in short wave length and the compatibility with the elementary particle physics, the SLAC FEL is the unique solution all over the world for the X-ray quantum optics. At present, the SLAC FEL is the best candidate for the 4-th generation synchrotron radiation source.

Contributed to the Workshop on Scientific Research Using X-ray Lasers (Stanford, Oct. 1992)

X-ray intensity interferometry with a short-pulse FEL

I. McNulty
Advanced Photon Source
Argonne National Laboratory, Argonne, IL 60439

Intensity interferometry could be used to measure the coherence of an x-ray beam produced by a high brightness short-pulse free-electron laser. Precise knowledge of the source extent and shape on short time scales is vital for characterization of free-electron lasers, storage ring based undulator sources, and the particle beams that drive these sources. Practical considerations are examined for an intensity interferometry experiment that exploits the ultrashort pulse duration of an x-ray FEL such as that proposed for SLAC.

Introduction

Since the seminal demonstrations conducted by Hanbury Brown and Twiss,[1,2] intensity interferometry experiments have been limited to visible light and longer wavelengths. X-ray intensity interferometry was not possible due to the lack of x-ray sources with sufficient coherent power. The coming availability of ultrahigh brightness x-ray laser[3,4] and undulator[5] sources may now make such experiments realizable.

The application of intensity interferometry to the x-ray region for characterization of x-ray sources based at synchrotron storage rings has been considered before.[6-10] Determination of the source extent and shape is of considerable interest for both x-ray and electron beam diagnostics and for coherence-dependent applications such as x-ray holography, microfocusing, and speckle techniques. Of course, the coherence of an x-ray beam could be measured by conventional (amplitude) interferometric methods, for example, by a Young's double slit experiment, given sufficiently well matched path-lengths and monochromatization of the incident beam. In contrast to conventional techniques however, intensity interferometry offers independence from precision optical tolerances, and it does not necessarily require monochromatic illumination. Moreover, though it involves no new physics, intensity interferometry has yet to be demonstrated with photons whose quantum aspects are as pronounced as they are for x-rays.

An intensity interferometer for soft x-ray undulator radiation was described previously.[9] This paper discusses the use of intensity interferometry to measure the spatial coherence of the beam produced by a soft x-ray free-electron laser (FEL) such as has been proposed for SLAC.[3] The extremely high peak brightness and short pulse widths of the radiation from this source make it especially amenable to this technique. Specifically, using an array detector, it may be possible to obtain a coherence measurement of the FEL beam with a single pulse.

Intensity fluctuations and spatial coherence

Intensity interferometry is possible because, in accordance with Bose-Einstein statistics, any number of photons can occupy the same cell of phase space. Spatially coherent photons produce correlated intensity fluctuations due to the beats between their own Fourier components; these fluctuations are slightly in excess of the uncorrelated fluctuations arising from shot noise in the photon stream. An intensity interferometer measures the modulus-squared of the complex degree of coherence μ_{12} of the beam by correlating the intensity fluctuations (or their time average) detected at two spatially separated points. The quantity $|\mu_{12}|$ is given for a source intensity distribution s(x), wavenumber $k = 2\pi/\lambda$ and distance z from the source by the Van Cittert-Zernike theorem[11]

$$|\mu_{12}| = \left| \frac{\int s(x) e^{-ikx\xi/z}\, dx}{\int s(x)\, dx} \right| , \qquad (1)$$

and is proportional to the fringe visibility that would be recorded with a conventional interferometer. Provided that the source is symmetrical, its shape is found by taking the Fourier transform of $|\mu_{12}|$. In the case of a 3-nm FEL source with a 1σ-width of ~100 μm, the coherent radiation is enclosed within an angle $\lambda/\pi\sigma \sim 10$ μrad, corresponding to a spatial coherence width of 0.3 mm at 30 m.

Bright, short pulses

The peak and average spectral brightness of the proposed FEL will exceed that of any exisiting soft x-ray source by roughly nine and three orders of magnitude, respectively. This phenomenal increase in source brightness has significant consequences for intensity interferometry experiments, because the measurement time depends on the inverse-square of the number of available coherent photons per spatial and temporal mode.[12] The degeneracy parameter or photon mode occupancy is given by

$$\delta = B\frac{\lambda^3}{4c} \quad , \tag{2}$$

for the spectral brightness B and velocity of light c. Based on the average design brightness, ~4×10^{20} ph/mm^2/mrad^2/s/0.1% BW at λ = 3 nm (corresponding to 10^{14} coherent photons per pulse), the degeneracy of the SLAC FEL is about 9. The peak degeneracy is an unprecedented 4×10^{11} based on the peak brightness of ~2×10^{31} ph/mm^2/mrad^2/s/0.1% BW.

In addition to its brightness, this x-ray source is remarkable because the extremely short duration (~160 fs) of the radiation pulses begins to approach the coherence time $t_c \sim \lambda^2/c\Delta\lambda$ of the light. At a wavelength of 3 nm, $t_c \approx 5$ fs for an FEL pulse with an intrinsic optical bandwidth of 500. One can probe the photon beam statistics on the temporal scale of its natural fluctuations with a time resolution that is comparable to the coherence time. The signal-to-noise ratio of an ideal intensity interferometer depends on the instrumental time resolution τ_0 according to

$$\frac{S}{N} = \delta\eta\,|\mu_{12}|^2\,\frac{\sqrt{\Delta T T}}{\tau_0} \quad , \tag{3}$$

where η is the detector efficiency, ΔT is the dead time between pulses and T is the total measurement time. The fastest x-ray detectors (except streak cameras) have a minimum τ_0 of ~10^2 ps. But, by using the short FEL pulses to define the time resolution, the interferometer signal-to-noise ratio can be improved by at least an order of magnitude beyond that possible with the fastest detectors. This permits the use of two-dimensional but comparatively slow detectors such as CCDs, and removes the burden of speed from the correlator electronics as well.

How many pulses are necessary to obtain a good measurement of the beam's spatial coherence? Conservatively inserting S/N = 10, δ = 9, η = 1%, $|\mu_{12}|$ = 0.1, τ_0 = 160 fs and ΔT = 8.3 ms for the SLAC FEL into eq. (3) and solving for T gives a rough lower limit of ~1 fs for the required measurement time. Consequently, a single FEL pulse should be sufficient, even allowing for beam transport inefficiencies.

Array detectors and computer correlation

The possibility of using two-dimensional array detectors such as CCDs offers a unique advantage because it permits a direct measure of the correlation between many simultaneous pairs of points in the photon beam, without the use of slits.[7] Given sufficient signal the entire wavefield can, in principle, be analyzed from a single image of the beam. However, the extremely high peak power densities produced by the FEL (~10^{16} W/cm^2 at normal incidence) challenge the power-handling capabilities and dynamic range of the most robust

detectors. For instance, assuming that a 1%-efficient beamline delivers on the order of 10^{12} photons per FEL pulse to a typical CCD detector array of 1024 × 1024 pixels, then each CCD pixel receives ~10^6 photons per pulse. As a result, it will probably be necessary to attenuate the beam, perhaps by as much as a factor of 10^3, in order to avoid detector saturation. The power load could be further alleviated by tilting the detector, thus spreading the beam out over a larger area. This also has the advantage of increasing the effective spatial resolution of the detector perpendicular to the tilt axis. Various configurations are possible; one scheme is shown in fig. 1.

A video-rate CCD camera with its frame rate synchronized to submultiples of the FEL pulse repetition rate (120 Hz) would enable multiple-pulse measurements. The frame data could be recorded with a suitable magnetic or optical medium for later digital processing. Alternatively, the correlation analysis could be performed on a per-pulse basis using a frame grabber and dedicated computer.[7]

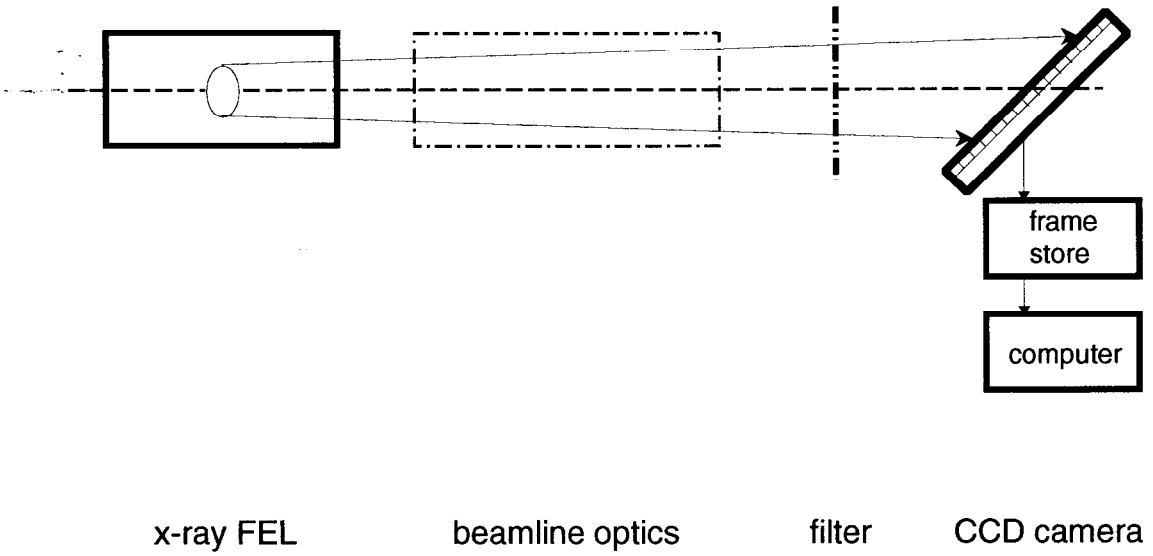

Fig. 1. Measurement of the coherence of an x-ray free-electron laser beam by intensity interferometry. An attenuating filter and tilting the CCD camera with respect to the beam helps to reduce the incident power.

Conclusion

The application of intensity interferometry to the characterization of a high power soft x-ray free-electron laser source has been considered. Intensity interferometry experiments with the proposed SLAC FEL appear promising due to the extreme brightness and pulse

brevity of this source, provided that means are found for handling its enormous peak power. A single-pulse measurement of the beam coherence should be feasible using a CCD detector coupled with computer analysis.

Acknowledgements

I wish to thank M. Howells, E. Gluskin and L. Yang for much stimulating discussion. In particular, the idea of using an array detector in an x-ray intensity interferometer is due to Howells. This work was supported by the U.S. Department of Energy, Office of Basic Energy Sciences, Division of Material Sciences, under contract W-31-109-ENG-38.

References

1. R. Hanbury Brown and R.Q. Twiss, "Correlation Between Photons in Two Coherent Beams of Light," *Nature* **177**, 27 (1956)
2. R.Q. Twiss, A.G. Little, and R. Hanbury Brown, "Correlation Between Photons, in Coherent Beams of Light, Detected by a Coincidence Counting Technique," *Nature* **180**, 324 (1957)
3. C. Pellegrini, et al., "A 2 to 4 nm High Power FEL On the SLAC Linac," 13th International Free-Electron Laser Conference, Kobe, Japan (Aug. 24-28, 1992)
4. *Applications of X-ray Lasers*, R. London, D. Matthews, and S. Suckewer, eds., Lawrence Livermore National Laboratory Report **CONF-9206170** (1992)
5. G.K. Shenoy, P.J. Viccaro, and D.M. Mills, *Characteristics of the 7-GeV Advanced Photon Source: A Guide for Users*, Argonne National Laboratory Report **ANL-88-9**; and *An ALS Handbook*, Lawrence Berkeley Laboratory Report **PUB-643** (1989).
6. E.V. Shuryak, "Two-photon correlations in synchrotron radiation as a method of studying the beam", *Sov. Phys. JETP* **40**, 30 (1975)
7. M.R. Howells, "The X-Ray Hanbury-Brown and Twiss Intensity Interferometer: a New Physics Experiment and a Diagnostic for Both X-Ray and Electron Beams at Light Sources", *ALS Technical Report*, **LSBL 27** (2 February 1989)
8. E. Gluskin, "Intensity Interferometry and its Application to Beam Diagnostics", *1991 IEEE Particle Accel. Conf.* (IEEE, New York, 1991) Vol. 2, p. 1169
9. E. Gluskin, I. McNulty, M.R. Howells, and P.J. Viccaro,*Nucl. Instr. Meth.* **319**, 213 (1992)
10. E. Ikonen, "Interference Effects Between Independent Gamma Rays", *Phys Rev. Lett.* **68**, 2854 (1992)
11. M. Born and E. Wolf, *Principles of Optics*, (Pergamon, Oxford, 1980) pp. 508-513.
12. J.W. Goodman, *Statistical Optics*, (Wiley, New York, 1985) p. 501-510

Towards Femtosecond Time Resolution in a Broad-Band Laue Diffraction Studies - A possibility

Janos Hajdu, Oxford University

TOWARDS FEMTOSECOND TIME RESOLUTION IN BROAD-BAND LAUE DIFFRACTION STUDIES - A POSSIBILITY.

Janos Hajdu

Laboratory of Molecular Biophysics an Oxford Centre of Molecular Sciences, Oxford University,
The Rex Richards Building, South Parks Road, Oxford OX1 3QU, U.K.
Tel: 44-865-275763, Fax: 44-865-510454, E-mail: janos@biop.ox.ac.uk

The fastest exposures in diffraction experiments are limited by the pulse length of X-ray sources (laser plasmas, synchrotrons, free electron lasers) and by the number of X-ray photons delivered by the pulse at the sample. The number of photons required to produce an interpretable Laue photograph on proteins is about 10^{13} on photographic film (Hajdu, 1990; Hajdu & Johnson, 1990). This number can be reduced to about 10^{11} - 10^{12} with low noise detectors (e.g. image plates). Currently, the pulse length within which these photons can be delivered at the sample can be as short as about a picosecond (e.g. with plasma sources, Murnane et al, 1991). Broad band Laue data sets collected near this time scale will probably be available later this year. While picosecond Laue exposures are of considerable importance, the really exciting chemical steps are usually over within a few hundred femtoseconds. Moreover, mechanical perturbations are essentially localised on a time scale of 100 fs within a molecule (see e.g. Martin & Vos, 1992) and so the perturbation of a system can be much better characterized in the femtosecond regime than in picoseconds. A femtosecond UV-VIS laser excitation may, in principle, synchronize molecules within a crystal for a short time, allowing three-dimensional structural studies on excited states and certain photochemical processes.

I. Femtosecond time resolution in picosecond X-ray pulses:

An idea is presented here which may provide near-femtosecond time resolution in Laue diffraction experiments using picosecond X-ray pulses. Note that the physical dimensions of the crystal cannot be ignored when thinking about femtosecond time-resolution in diffraction experiments. Figure 1 shows the proposed experimental arrangement. Consider a 0.3 mm long crystal (most crystals used in X-ray diffraction experiments are about this size) onto which falls a picosecond long X-ray pulse so that the whole body of the crystal is bathed in the X-ray beam. The diffracted beam will produce a topographic image of the crystal. When white X-rays are used in the pulse, the topogram will have reflections arranged in a Laue pattern. From high symmetry crystals, a single exposure like this would be sufficient to obtain about 80% or more of the unique reflection set (Clifton et al., 1991) and obtain a structure (Campbell et al., 1990; Howell et al., 1992). Note that one needs broad band X-rays (0.5 Å - 2.0 Å), i.e. wigglers, to achieve this.

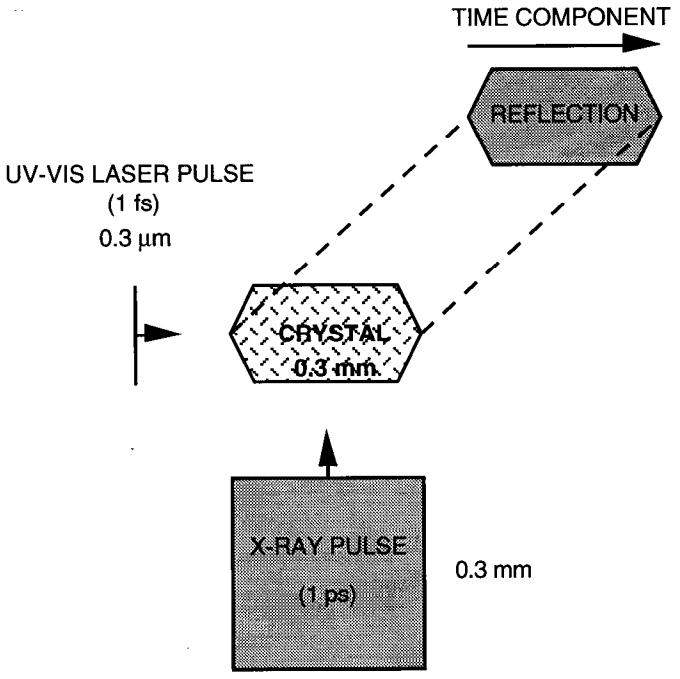

Figure 1: Time resolution in crossed-beam Laue topography

Synchronized with the ps X-ray pulse, a fs long (i.e. 0.3 μm) UV-VIS laser excitation pulse is fired at the crystal so that the direction of the UV-VIS laser pulse is perpendicular to the direction of the X-ray pulse. With crystal dimensions given above, the time required for the UV-VIS laser pulse to pass through the 0.3 mm crystal will be 1 ps. This is also the length of the X-ray pulse. The profile of each reflection recorded by the ps X-ray pulse in the topogram will have a certain time component along the direction of the UV-VIS laser excitation pulse. The analysis of the reflection profiles on the Laue photograph (topogram) along this direction may give a movie with sub-ps time resolution. The case is not as simple as it looks but this possibility is worth of further scrutiny as diffraction experiments on the picosecond-femtosecond time scale could open up a new era in structural biology and chemistry. A few points to consider:

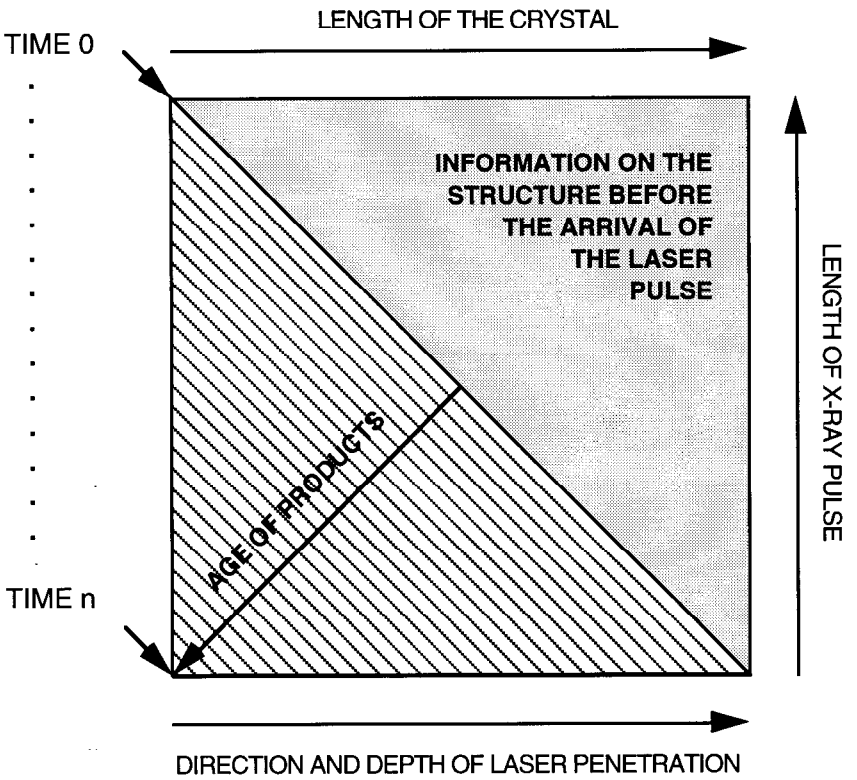

Figure 2: The "in flight" structure of the X-ray reflection (before hitting the detector) in crossed-beam Laue topography. The case of a one-dimensional crystal is considered. Time 0 indicates the arrival of the femtosecond UV-VIS laser pulse.

(i) Each slice of the reflection profiles (sliced perpendicular to the direction of the UV-VIS laser pulse) contains information from a mixture of "old" and "new" structures. The mixing is different from left to right (Figures 2, 3). However, each reflection pulse while "in flight" contains pure and unperturbed temporal information on the crystal (Fig. 2). The averaging of the structures takes place when the reflection hits the detector and the wave fronts reporting from the different time points pile up on the top of each other. If coherent X-rays are used, the coherence of the beam could be used to tackle this problem.

(ii) Apart from averaging, there will be a speed difference between the UV and X-ray pulses due to the difference of the refractive indices for the light and X-ray pulses in the crystal. The Heisenberg principle is lurking in the background, the fs UV-VIS laser pulse will not be monochromatic anymore.

(iii) Currently, the electronic "jitter" in high performance circuits is around 2-0.5 ps. This makes the timing of the arrival of the UV-VIS laser and X-ray pulses difficult but a detector mounted from the Z-direction (X = X-ray, Y = UV-VIS laser, Z = fluorescence detector) could measure the arrival time of the two pulses by measuring scattered radiation (both UV-VIS and X-ray) from the crystal (shoot first, ask questions afterwards).

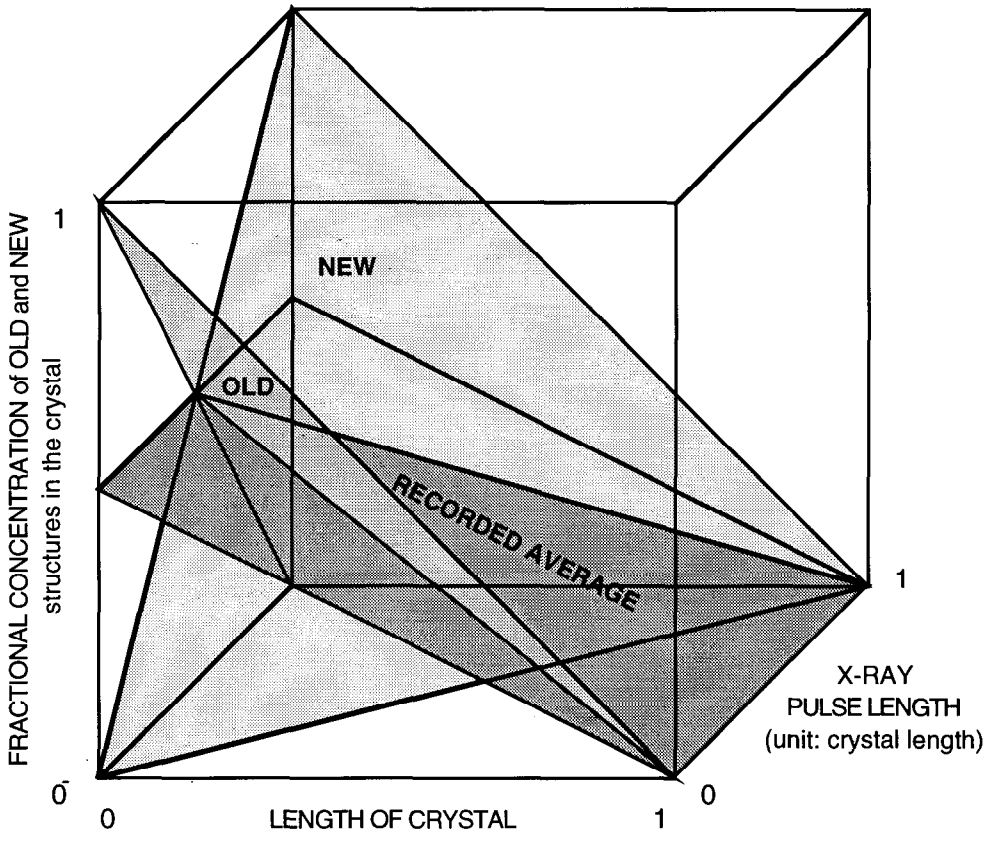

Figure 3: Distribution of structures in the X-ray pulse. The case of a one-dimensional crystal is considered.

II. Femtosecond X-ray pulses:

Two experimental arrangements are considered for broad band Laue experiments: (i) stroboscopic experiments (if the intensity of the X-ray pulse is not strong enough to deliver 10^{12} photons in one pulse), or (ii) parallel beam Laue experiments (if the intensity is strong enough to deliver 10^{12} photons in one pulse). In case (ii), the UV-VIS laser excitation pulse should arrive from the same direction as the X-ray pulse but with a phase shift. Reflections would then contain information on structures whose age is determined by the phase shift between the UV-VIS and X-ray pulses. See comments about refractive indices and Heisenberg.

SUMMARY

The mechanistic interpretation of data on chemical reactions implies a sequence of structural transitions of the components along the reaction coordinate. It seems increasingly likely today that experimental observation of such transitions may be possible with ultra-fast diffraction techniques. Data collection times of minutes to seconds are routinely available at synchrotron sources with monochromatic techniques, and to milliseconds with white radiation techniques (for a review see Hajdu & Andersson, 1993). Attempts have already been made with both monochromatic and Laue techniques to achieve nanosecond-picosecond exposures using flash X-ray tubes or plasma sources (see, e.g. Johnson et al, 1967, 1970; Jamet, 1970; Lunney et al, 1986; Wark et al, 1989, 1992; Woolsey et al, 1990; Murnane et al, 1991) and lately also with synchrotrons (Larson et al, 1983; Szebenyi et al, 1992). It will be exciting to see how much better time resolution can be achieved in diffraction experiments.

REFERENCES:

Campbell, J. W., Clifton, I. J., Greenhough, T. J., Hajdu, J., Harrison, S. C., Liddington, R. C., Shrive, A. K. (1990) *J. Mol. Biol.* **214**, 627-632: Calcium binding sites in tomato bushy stunt virus visualized by Laue crystallography.

Clifton, I. J., Elder, M. & Hajdu J. (1991) *J. Appl. Cryst.*, **24**, 267-277: Experimental strategies in Laue crystallography.

Hajdu, J. (1990) in "*Frontiers in Drug Research*", Alfred Benzon Symposium 28, (eds. B. Jensen, F. S. Joergensen & H. Kofod) Munksgaard Publishing Co., Copenhagen, pp. 375-395: Laue Crystallography of Macromolecules.

Hajdu, J. & L. N. Johnson (1990) *Biochemistry*, **29**, 1669-1678: Progress with Laue diffraction studies on protein and virus crystals.

Hajdu, J. & Andersson, I. (1993a) *Annu. Rev. Biophys. Biomol. Struct.*, vol. **22**, 467-498: Fast crystallography and time-resolved structures.

Howell, P. L., Almo, S. C., Parson, M., Hajdu, J. & Petsko, G. A. (1992) *Acta Cryst.* **B48**, 200-207: Structure determination of turkey egg white lysozyme from Laue diffraction data.

Jamet, F. (1970) *C. R. Acad. Sci. Paris*, Ser. **B271**, 714-717: Laue diffraction movie on an exploding single crystal aluminum with 300 ns X-ray flashes.

Johnson, Q., Keeler, R. N., Lyle, J. W. (1967) *Nature*, **213**, 1114-1115: X-ray diffraction experiments in nanosecond time intervals.

Johnson, Q., Mitchell, A. C., Keeler, R. N., & Evans, L. (1970) *Phys. Rev. Lett.*, **25**, 1099-1101: X-ray diffraction during shock wave compression.

Larson, B. C., White, C. W., Noggle, T. S.,Barhorst, J. F. & Mills, D. (1983) *Appl. Phys. Lett.*, **42**, 282-283: Time-resolved X-ray diffraction measurement of the temperature and temperature gradients in silicon during pulsed laser annealing.

Lunney, J. G., Dobson, P. J., Hares, J. D., Tabatabaei, S. D. & Eason, R. W. (1986) *Opt. Commun.* **58**, 269: Time resolved x-ray diffraction from silicon during pulsed laser annealing.

Martin, J.-P., Vos, M. H. 1992. *Annu. Rev. Biophys. Biomol. Struct.* 21, 199-222: Femtosecond biology.

Murnane, M. M., Kapteyn, H. C., Rosen, M. D., Falcone, R. W. (1991) *Science*, **251**, 531-536: Ultrafast X-ray pulses from laser-induced plasmas.

Szebenyi, D. M. E., Bilderback, D. H., LeGrand, A., Moffat, K., Schieldkamp, W., Smith-Temple, B. & Teng, T. -Y. (1992) *J. Appl. Cryst.* **25**, 414-423: Quantitative analysis of Laue diffraction patterns recorded with a 120 ps exposure from an X-ray undulator.

Wark, J. S., Whitlock, R. R., Hauer, A. A., Swain, J. E. & Solone, P. J. (1989) *Phys. Rev.* **B40**, 5705-5714: Subnanosecond X-ray diffraction from laser-shocked crystals.

Wark, J. S., Woolsey, N. C. & Whitlock, R. R. (1992) *Appl. Phys. Lett.*, **61**, 651-653: Novel measurements of high-dynamic crystal strength by picosecond x-ray diffraction.

Woolsey, N. C., Wark, J. S., & Riley, D. (1990) *J. Appl. Cryst.*, **23**, 441-443: Sub-nanosecond X-ray powder diffraction.

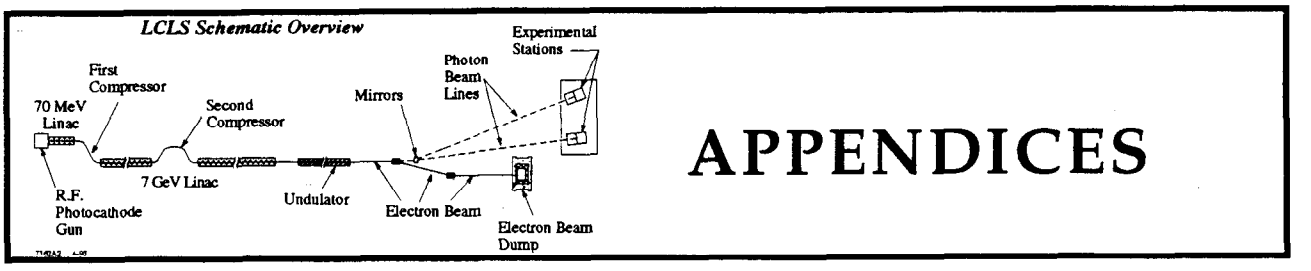
LCLS Schematic Overview
First
Compressor
70 MeV
Linac
Second
Compressor
Mirrors
Photon
Beam
Lines
Experimental
Stations
7 GeV Linac
R.F.
Photocathode
Gun
Undulator
Electron Beam
Electron Beam
Dump

APPENDICES

Scientific Applications of Coherent X-rays

Final Registration List
February 16, 1994

John Arthur
SSRL
PO BOX 4349 MS 69
STANFORD CA 94309
Phone: 415-926-3169
Fax: 415-926-4100
E-Mail: ARTHUR@SLAC.STANFORD.EDU

David Attwood
LBL
CENTER FOR X-RAY OPTICS MS 2-400
BERKELEY CA 94720
Phone: 510-486-4463
Fax: 510-486-4955
E-Mail: ATTWOOD@LBL

Karl Bane
SLAC
PO BOX 4349 MS 26
STANFORD CA 94309
Phone: 415-926-2026
Fax: 415-926-4999
E-Mail: KBANE@SLAC.STANFORD.EDU

Henry Bellamy
SSRL
PO BOX 4349 MS 69
STANFORD CA 94309
Phone: 415-926-3107
Fax: 415-926-4100
E-Mail: BELLAMY@SLAC.STANFORD.EDU

Bob Birgeneau
MIT
PHYSICS ROOM 6-123
CAMBRIDGE MA 02139
Phone: 617-253-8900
Fax: 617-253-8901
E-Mail: ROBERTJB@MIT.EDU

Sean Brennan
SSRL
PO BOX 4349 MS 69
STANFORD CA 94309
Phone: 415-926-3173
Fax: 415-926-4100
E-Mail: BRENNAN@SLAC.STANFORD.EDU

Robert Byer
STANFORD UNIVERSITY
GINZTON LAB MC 4085
STANFORD CA 94305
Phone: 415-723-0226
Fax: 415-723-2666
E-Mail: BYER@SIERRA.STANFORD.EDU

Roger Carr
SSRL
PO BOX 4349 MS 69
STANFORD CA 94309
Phone: 415-926-3965
Fax: 415-926-4100
E-Mail: CARR@SLAC.STANFORD.EDU

John Cerino
SSRL
PO BOX 4349 MS 69
STANFORD CA 94309
Phone: 415-926-2154
Fax: 415-926-4100
E-Mail: CERINO@SLAC.STANFORD.EDU

Steve Chu
STANFORD UNIVERSITY
VARIAN BLDG RM 230
STANFORD CA 94305-4060
Phone: 415-723-3571
Fax:
E-Mail: SCHU@LELAND.STANFORD.EDU

Bill Colson
NAVAL POSTGRAD SCHOOL
PHYSICS DEPT
MONTEREY CA 93943
Phone: 408-656-2896
Fax: 408-656-2834
E-Mail: COLSON@PHYSICS.NPS.NAVY.MIL

Phil Coppens
UNIVERSITY OF BUFFALO
DEPT OF CHEMISTRY
BUFFALO NY 14214
Phone: 716-289-3911
Fax: 716-289-2960
E-Mail: CHE9990@UBVMS

Tony Cox
SSRL
PO BOX 4349 MS 69
STANFORD CA 94309
Phone: 415-926-3105
Fax: 415-926-4100
E-Mail: TCOX@SLAC.STANFORD.EDU

John Edighoffer
LBL
MS B17H
1 CYCLOTRON RD
BERKELEY CA 94720
Phone: 510-486-5107
Fax: 510-486-6485
E-Mail: JEDIG@CSA2.LBL.GOV

Peter Eisenberger
PRINCETON UNIVERSITY
PHYSICS DEPT PO BOX 708
PRINCETON NJ 08544
Phone: 609-258-4762
Fax: 609-258-6878
E-Mail: PETERE@PUCC.PRINCETON.EDU

Charles Fadley
LBL
MATERIAL SCI DIV MS 2-100
BERKELEY CA 94720
Phone: 510-486-5774
Fax: 510-486-5530
E-Mail: FADLEY@LBL.GOV

Roger Falcone
UC BERKELEY
PHYSICS DEPT
BERKELEY CA 94720
Phone: 510-642-8916
Fax: 510-643-8497
E-Mail: RWF@PHYSICS.BERKELEY.EDU

William M. Fawley
LBL
MS 47-112
BERKELEY CA 94720
Phone: 510-486-6229
Fax: 510-486-5392
E-Mail: FAWLEY@LBL.GOV

Efim Gluskin
ANL/APS
BLDG 362
9700 S CASS AVE
ARGONNE IL 60439
Phone: 708-252-4788
Fax: 708-252-3222
E-Mail: GLUSKIN@ANLAPS.APS.ANL.GOV

Lee Haddad
LLNL
PO BOX 808 L-258
LIVERMORE CA 94550
Phone: 510-422-6172
Fax:
E-Mail: HADDAD3@LLNL.GOV

Joseph Hall
NAVAL POSTGRADUATE SCHOOL
PHYSICS DEPT
MONTEREY CA 93943
Phone: 408-656-2116
Fax:
E-Mail: HALL@PHYSICS.NPS.NAVY.MIL

Malcolm Howells
LBL/ALS
BERKELEY CA 94720
Phone: 510-486-4949
Fax: 510-486-7696
E-Mail: MALCOLM_HOWELLS@LBL.Gov

Kwang-Je Kim
LBL
MS 71-259
BERKELEY CA 94720
Phone: 510-486-7224
Fax: 510-486-7981
E-Mail: KWANGJE@LBL.GOV

Brian M. Kincaid
LBL/ALS
1 CYCLOTRON RD
BERKELEY CA 94720
Phone: 510-486-4810
Fax: 510-486-4960
E-Mail: BMK@LUCIFER.LBL.GOV

Janos Kirz*
SUNY
DEPT OF PHYSICS
STONY BROOK NY 11794
Phone: 516-632-8106
Fax: 516-632-8101
E-Mail: KIRZ@SBHEPNY

Norman M. Kroll
UCSD/SLAC
UCSD
SAN DIEGO CA 92110
Phone: 619-534-6695
Fax: 619-534-0174
E-Mail: NKROLL@UCSD.EDU

Hidong Kwak
UC RIVERSIDE
DEPT OF PHYSICS
RIVERSIDE CA 92521
Phone:
Fax:
E-Mail: KWAK@UCRPHO.UCR.EDU

Alexander Lessmann
SSRL
PO BOX 4349 MS 69
STANFORD CA 94309-0210
Phone: 415-926-4893
Fax: 415-926-4100
E-Mail: LESSMANN@SLAC.STANFORD.EDU

Tony Loeser
STANFORD UNIVERSITY
MCCULLOUGH 251
STANFORD CA 94305-4055
Phone: 415-723-3209
Fax: 415-723-4659
E-Mail: LOESER@LELAND.STANFORD.EDU

Hudel Luecke
SSRL
PO BOX 4349 MS 69
STANFORD CA 94309
Phone: 415-926-4944
Fax: 415-926-4100
E-Mail: LUECKE@SLAC.STANFORD.EDU

Gerhard Materlik
SSRL
PO BOX 4349 MS 69
STANFORD CA 94309
Phone: 415-926-3844
Fax: 415-926-4100
E-Mail: MATERLIK@SLAC.STANFORD.EDU
permanent address
HASYLAB/DESY
Notkestrasse 85
D-22603 Hamburg Germany
Phone: 49-40-8998-2484
Fax: 49-40-8998-2787
E-Mail: MATERLIK@VXDESY.DESY.DE

Roger Miller
SLAC
PO BOX 4349 MS 26
STANFORD CA 94309
Phone: 415-926-4457
Fax: 415-926-4999
E-Mail: RHM@SLAC.STANFORD.EDU

Keith Moffat
UNIVERSITY OF CHICAGO
BIOCHEMISTRY & MOLECULAR BIOLOGY
920 E 58TH ST
CHICAGO IL 60637
Phone: 312-702-2116
Fax: 312-702-1896
E-Mail: MOFFAT@CARS1.UCHICAGO.EDU

David Moncton
ANL/APS
BLDG 360
9700 S CASS AVE
ARGONNE IL 60439
Phone: 708-252-7950
Fax: 708-252-4599
E-Mail: DEM@ANLAPS.APS.ANL.GOV

Kazumichi Namikawa
TOKYO GAKUGEI UNIVERSITY
PHYSICS DEPT
4-1-1 NUKUI KITA-MACHI KOGANEI-SHI
TOKYO JAPAN
Phone: 81-423-25-2111
Fax: 81-423-24-9832
E-Mail: NAMIKAWA@KEKVAX.KEK.JP

Keith Nelson*
MIT
RM 6-231
77 MASSACHUSETTS AVE
CAMBRIDGE MA 02139
Phone: 617-253-1423
Fax: 617-253-7030
E-Mail: KANELSON@MIT.EDU

Brian Newnam
LANL
MS J564
LOS ALAMOS NM 87545
Phone: 505-667-7979
Fax: 505-665-2840
E-Mail: BRIAN_NEWNAM@CLS.LANL.GOV *or*
BNEWMAN@LANL.GOV

Heinz-Dieter Nuhn
SSRL
PO BOX 4349 MS 69
STANFORD CA 94309
Phone: 415-926-2275
Fax: 415-926-4100
E-Mail: NUHN@SLAC.STANFORD.EDU

Claudio Pellegrini
UCLA
DEPT OF PHYSICS
LOS ANGELES CA 90024-1547
Phone: 310-206-1677
Fax: 310-206-1091
E-Mail: PELLEGRINI@UCLAHEP

Paul Phizackerley
SSRL
MS 69 PO BOX 4349
STANFORD CA 94309
Phone: 415-926-3431
Fax: 415-926-4100
E-Mail: PHIZ@SLAC.STANFORD.EDU

Zofia Rek
SSRL
PO BOX 4349 MS 69
STANFORD CA 94309
Phone: 415-926-3112
Fax: 415-926-4100
E-Mail: REK@SLAC.STANFORD.EDU

Kem E. Robinson
STI OPTRONICS
2755 NORTHUP WAY
BELLEVUE WA 98004
Phone: 206-827-0460
Fax: 206-828-3517
E-Mail:

Volker Saile
LOUISIANA STATE UNIVERSITY
CAMD
BATON ROUGE LA 70803-2755
Phone: 504-388-8887
Fax: 504-388-6954
E-Mail: ROSAILE@LSUVAX.SNCC.LSU.EDU

Fred Schlachter
LBL/ALS
MS 46-161
BERKELEY CA 94720
Phone: 510-486-4892
Fax: 510-486-7696
E-Mail: FRED@LBL.GOV

Ross Schlueter
LBL/ALS
BLDG 46-161
1 CYCLOTRON RD
BERKELEY CA 94720
Phone: 510-486-7405
Fax: 510-486-4870
E-Mail: ROSS@LBL.BITNET

Z.-X. Shen
STANFORD UNIVERSITY/SSRL
DEPT OF APPLIED PHYSICS
STANFORD CA 94305-4055
Phone: 415-725-8254
Fax: 415-723-4659
E-Mail: SHEN@SIERRA.STANFORD.EDU

Gopal Shenoy
ANL
BLDG 362
9700 S CASS AVE
ARGONNE IL 60439
Phone: 708-252-5537
Fax: 708-252-3222
E-Mail: GKS@ANLAPS.APS.ANL.GOV

Manfred Schuster
SIEMENS
OTTO-HAHN-RING 6
D-81739 MUNICH
GERMANY
Phone: 01149-89-636-44165
Fax: 01149-89-636-42256
E-Mail:

Brian Stephenson*
IBM
20-258 PO BOX 218
YORKTOWN HEIGHTS NY 10598
Phone: 914-945-3008
Fax: 914-945-2141
E-Mail: GBS@WATSON.IBM.COM

Hiroshi Sugiyama
PHOTON FACTORY/KEK
NTL LAB FOR HIGH ENERGY PHYSICS
OHO TSUKUBA IBARAKI 305
JAPAN
Phone: 81-298-64-5678
Fax: 81-298-64-7529
E-Mail: HIROSHIS@JPNKEKVX

Roman Tatchyn
SSRL
PO BOX 4349 MS 69
STANFORD CA 94309
Phone: 415-926-2731
Fax: 415-926-4100
E-Mail: TATCHYN@SLAC.STANFORD.EDU

David Templeton
LBL
BLDG 70A-1150
BERKELEY CA 94720
Phone: 510-486-5615
Fax: 510-486-5596
E-Mail: LILO@CSA3.LBL.GOV

Lieselotte Templeton
LBL
BLDG 70A-1150
BERKELEY CA 94720
Phone: 510-486-5615
Fax: 510-486-5596
E-Mail: LILO@CSA3.LBL.GOV

James Trebes
LLNL
PO BOX 808 L-473
LIVERMORE CA 94550
Phone: 510-423-7423
Fax: 510-422-8395
E-Mail: TREBE1@LLNL.GOV

Hiro Tsuruta
SSRL
PO BOX 4349 MS 69
STANFORD CA 94309
Phone: 415-926-3104
Fax: 415-926-4100
E-Mail: TSURUTA@SLAC.STANFORD.EDU

Chun-Xi Wang
STANFORD UNIVERSITY
APPLIED PHYSICS
STANFORD CA 94305
Phone: 415-325-6505
Fax:
E-Mail: WANGCX@LOKI.STANFORD.EDU

Barry Wells
MIT
DEPT OF PHYSICS 13-2154
CAMBRIDGE MA 02139
Phone: 617-253-1580
Fax:
E-Mail: BWELLS@X-RAY.MIT.EDU

Herman Winick
SSRL
PO BOX 4349 MS 69
STANFORD CA 94309
Phone: 415-926-3155
Fax: 415-926-4100
E-Mail: WINICK@SLAC.STANFORD.EDU

Ming Xie
LBL
MS B71H
BERKELEY CA 94720
Phone: 510-486-5616
Fax: 510-486-7981
E-Mail: MINGXIE@CSA2.LBL.GOV

Li Xu
UC RIVERSIDE
DEPT OF PHYSICS
RIVERSIDE CA 92521
Phone: 909-787-2470
Fax: 909-787-4529
E-Mail: LX@UCRPHO.UCR.EDU

Shigeru Yamamoto
PHOTON FACTORY KEK
NTL LAB FOR HIGH ENERGY PHYSICS
OHO TSUKUBA IBARAKI 305
JAPAN
Phone: 81-298-64-5680
Fax: 81-298-64-7529
E-Mail: SHIGERU@KEKVAX.KEK.JP

Dianne Yeremian
SLAC
PO BOX 4349 MS 55
STANFORD CA 94309
Phone: 415-926-4444
Fax: 415-926-4999
E-Mail: ANAHID@SLAC.STANFORD.EDU

Wenbing Yun
ANL/APS
9700 S CASS AVE
ARGONNE IL 60439
Phone: 708-252-9320
Fax:
E-Mail: YUN@ANLAPS.APS.ANL.GOV

* Invited speakers unable to attend due to severe weather conditions on East Coast.

SCIENTIFIC APPLICATIONS OF COHERENT X-RAYS

SSRL/SLAC
February 12, 1994
Orange room at SLAC

7:45 AM Registration and continental breakfast

Morning Session Chair - ***Gerd Materlik***, SSRL/HASYLAB

8:30 Welcome ***Burt Richter***, Director - SLAC
8:35 Opening Remarks ***John Arthur***, SSRL/SLAC

8:40 Introductory Comments on Spatial and Temporal Coherence
David Attwood, CXRO/LBL
9:10 Discussion

9:30 Properties of short wavelength FELs using the SLAC linac
Claudio Pellegrini, UCLA & ***Herman Winick***, SSRL/SLAC
10:00 Discussion

10:20 Coffee break

10:35 Time Correlation Spectroscopy with Coherent Hard X-rays
Brian Stephenson, IBM
11:05 Discussion

11:25 Non linear X-ray Phenomena using High Intensity Coherent Beams
Peter Eisenberger, Princeton University
11:55 Discussion

12:15 LUNCH

Afternoon Session Chair - ***John Arthur***, SSRL/SLAC

1:00 a. Imaging with Soft & Hard X-rays
Janos Kirz, SUNY Stony Brook,
b. Possibilities for One-shot Soft X-ray Tomographic Imaging
Malcolm Howells, ALS/LBL
c. Demonstration of Ultra High Resolution Soft X-ray Tomography
Lee Haddad, LLNL
1:45 Discussion

2:15 Coherent Optical Spectroscopy throughout the Brilliouin Zone
Keith Nelson, MIT
2:45 Discussion

3:05 Coffee break

3:20 Diffraction Studies of Excited States of Molecules in Crystals - Present experiments and prospects for studies of very short lifetime excited states using pulsed X-ray sources
Phil Coppens, University of Buffalo
3:50 Discussion

4:10 Time Resolved Structural Studies on Biological Macromolecules in the Sub-nanosecond Time Domain
Keith Moffat, University of Chicago
4:40 Discussion

5:00 General discussion and wrap-up
5:20 Closing remarks ***Gerd Materlik***, SSRL/HASYLAB

5:30 Wine and cheese reception on the patio 1/20/94

SCIENTIFIC APPLICATIONS OF COHERENT X RAYS

SSRL/SLAC February 12, 1994

CHARGE TO THE WORKSHOP

1. Examine possible applications for a linac-based X-ray laser, considering the performance parameters that have been distributed. Suggest extensions to present experiments as well as new possibilities offered by the very high levels of coherence, high brightness and peak power, and the short pulse duration.

2. Identify critical issues and possible fundamental limits on the applications of such a source.

3. Identify variations in performance parameters that would extend possible uses (wavelength range, pulse repetition frequency, pulse duration, timing jitter).

4. Consider the need for a pilot project as opposed to a user facility.

PARAMETERS FOR VARIOUS LCLS CASES

Wavelength (Å)	40	40	4.5	1.5
Norm. emittance (mm-mrad)	3.5	1	1	1
Peak current (kA)	2.5	5	5	5
E (GeV)	7	5	15	25
σE/E (%)	0.02	0.02	0.02	0.02
Pulse duration (fs, rms)	130	65	65	65
Repetition rate (Hz)	120	120	120	120
Undulator period (cm)	8.3	4	4	4
Peak field (T)	0.76	1.6	1.6	1.6
Gain length (m)	5.8	1.5	4	7
Saturation length (m)	60	15	40	70
Peak power (GW)	10	40	100	40
Average power (W)	0.4	0.6	1.4	0.6
Energy/pulse (mJ)	3	5	12	5
Coherent Ph/pulse (10^{13})	6.6	13	3.3	0.5
Bandwidth (%)	0.1	0.1	0.1	0.1
Peak Brightness*	5×10^{31}	2×10^{32}	5×10^{33}	5.4×10^{33}
Average Brightness*	2×10^{21}	4×10^{21}	1×10^{23}	1×10^{23}
Trans. Size (microns, rms) **	35	20	12	9
Trans. Diverg. (μrad, rms) **	10	6	4	2

* Photons/s/mm^2/mrad^2/0.1%BW
**at exit of undulator

Approximate values of calculated performance parameters are given for several cases. The first column assumes rather conservative performance of an rf photocathode gun and compression scheme. In this column is included the results of a detailed study of the effects of undulator errors and misalignments, which reduces the output by about a factor of three. These same calculations have not yet been done for the last three columns, which are based on improved guns and stronger compression schemes. In all cases, a third harmonic would also be available, typically with about 1/30 the number of coherent photons/pulse.

The output photon beams could be synchronized with other sources to a precision of about 0.5 ps. This will make it possible to conduct pump-probe experiments with conventional lasers or SSRL synchrotron radiation beams from SPEAR The beams are diffraction limited and hence have full transverse coherence. The longitudinal coherence length is given by the wavelength/bandwidth. Since the bandwidth is about 0.001 in all cases, the longitudinal coherence length is about 1000 times the wavelength.

Peak Power Issues for the SLAC Linac Coherent Light Source (LCLS) in the 4.5Å-1.5Å Wavelength Range*

(R. Tatchyn, Workshop on Science with Coherent X-Rays, SSRL/SLAC, 2/12/94)
Stanford Linear Accelerator Center, Stanford, CA 94305, USA

Abstract

In prior work, LCLS studies at SLAC have concentrated on the 300-400 eV ("water window") range. In that regime, feasible designs for optical components and systems were identified, notwithstanding the unprecedented levels of pulse brevity and peak power [1]. In the past year possibilities for extending the range of linac-driven FEL operation into the 1.5Å-4.5Å regime have been investigated by the LCLS research group, with the tentative conclusion that such an extension may be technically feasible. In this note some of the concerns regarding the capabilities of x-ray optics in handling peak and average powers in this extended energy range are addressed.

I. INTRODUCTION

Most of he basic concerns stem from the extremely high peak power levels associated with the delivery of millijoule-to-decijoule levels of energy within time intervals on the order of 100 fs (rms) in a single pulse. Additional concerns are related to the properties of the spectral-angular distribution of energy radiated by the LCLS. To center the discussion, in Table 1 we list the parameters of the shortest wavelength FEL considered in preparation for this workshop.

Table 1
1.5 Å LCLS Output Parameters

1st Harmonic Wavelength (λ)	1.5 Å
Peak Power (P_{peak})	40 GW
Coh. Beam Diam. (D_W) at 100m from LCLS	0.15mm
Full Pulse Duration ($\sqrt{2\pi}\sigma_\tau$)	0.16ps
Full Pulse Length	50 μ
Pulse Repetition Rate	120Hz
Energy per Pulse	$\approx$ 6.6mJ
Peak Power Density (Norm. Incidence)	$\approx 2\times10^{18}$ W/m^2
Source Emittance (Diffraction Limited)	< 0.75Å-rad

For the undulators considered for the shorter-wavelength LCLS, the K values (K=6) are high enough so that the power radiated by spontaneous emission is comparable to or even greater than the total power in the coherent FEL lines (1st, 3rd, and higher harmonics). A graphical compilation of the total flux vs. photon energy generated by four LCLS undulators spanning the 1.5Å-40Å wavelength range is shown in the figure attached to this note. In general, although the spontaneous vs coherent powers are of the same order, the dominant (peak power) loading of system optics will be by the coherent peaks, as they are angularly more concentrated by factors of the order of $\sqrt{N}$ in comparison to the spontaneous radiation. From the right hand ordinate in the appended figure it is also evident that time-averaged thermal loading of the LCLS optics is not expected to be an issue, a general result of the typically low average currents characteristic of linac electron sources.

* Supported by DOE Offices of Basic Energy Sciences and High Energy and Nuclear Physics and Department of Energy Contract DE-AC03-76SF0015.

II. PEAK POWER DAMAGE LIMITATIONS

From Table 1 it is evident that a photon pulse at normal incidence can deposit of the order of 1-several eV per atom for absorptivities [2] and penetration depths typical of solid state materials in the 100eV-100keV range.. Since this level of energy loading can be shown to lead to the enhanced probability of lattice damage [3,4], an important stratagem for reducing it involves decreasing the angle of incidence, θ_i, on the optical surface in question. As shown in Fig. 1, this leads to the notion of employing multiple reflections at grazing incidence to deflect the LCLS beam into a desired angle θ_T. For

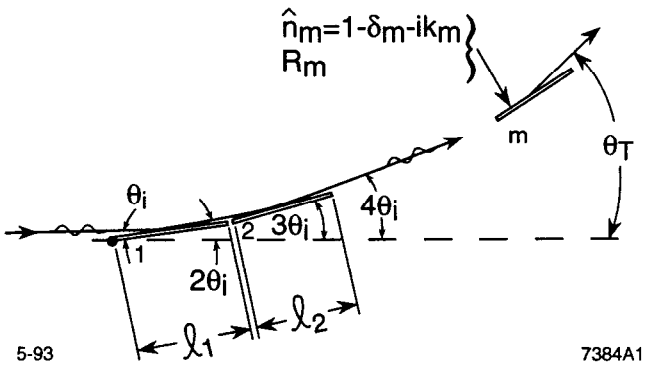

Figure 1. Parameters for multiple grazing-incidence reflection.

reflectors all with equal surface reflectivities R, indices of refraction n=1-δ+ik, atomic densities #[cm^{-3}], and approximate (vertical) penetration depths δ_p ($\delta_p \cong \lambda/4\pi\sqrt{k}$), a useful figure of merit, η_A [eV/atom], can be defined [4] from which practical design parameters can be established:

$$\eta_A = \frac{\bar{P}_{peak}\sqrt{2\pi}\sigma_\tau}{q}\left[\frac{\theta_i}{D_w^{\,2}}\right]\left[\frac{1-R}{\delta_p\#}\right] << 1 . \qquad (1)$$

Selecting $\eta_A \leq 0.01$, a criterion suggested by earlier experimental work at SSRL[5], acceptable grazing-incidence angles for, e.g., Au reflecting surfaces of ≤2mr are arrived at.

Perhaps the greatest concern with the grazing-incidence scheme outlined for 1st harmonic processing lies in the significant absorption of the 3rd and higher FEL (and spontaneous) spectral orders. In the cases represented in the appended figure, however, it can be estimated that the intensity rolloff is sufficiently strong so that even with sizeable absorption the cited energy-loading criterion is not violated. Clearly, the peak power loading of the optics by the spontaneous on-axis orders will be negligible in contrast to the 3rd (and higher) coherent FEL orders.

A second important peak power damage limitation is associated with the intense electrostatic stresses that will be generated by photoemission from the LCLS optical surfaces. Although no definitive experimental studies have been conducted in the present energy ranges, preliminary assessments indicate that care will be necessary in the selection of surface and substrate materials for both mirrors and gratings, (to minimize charge-neutralization time intervals) and in the elimination of sharp-featured grooves or profiles on diffraction grating surfaces (to reduce the generation of peak field stresses).

III. CONCLUSIONS

As was found to be the case in prior studies of the 40Å LCLS, the control of the radiation pulses in the extended 1.5Å-4.5Å regime should also prove to be manageable. The primary basis for optical processing, in both cases, is operation at grazing incidence. A schematic of a configuration capable of diverting 40Å LCLS pulses is shown in Fig. 2. With suitable adjustment of the incidence angles and mirror facet dimensions, the same configuration should also be capable of operation at wavelengths down to 1.5Å and shorter.

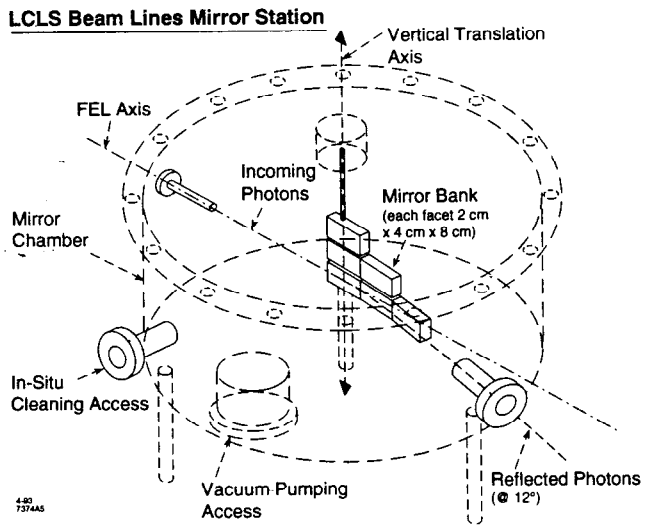

Figure 2. LCLS mirror station tank.

With the advent of FELs with orders-of-magnitude higher peak or average power (e.g., tapered wigglers, enhanced-electron sources), and with operation at wavelengths significantly shorter even than those under discussion at the present workshop, it can be anticipated that a wider range of optical phenomena and elements will become relevant in beam line design (.e.g., diffraction by natural crystals, or the use of "disposable, " or multi-phase optics [4]). In view of this, It is likely that the issue of peak power damage and related high-intensity phenomena in the x-ray range will acquire increasing importance as areas for physical investigation.

IV. ACKNOWLEDGMENTS

Valuable technical support and contributions to this project by David Lunt (Photon Sciences Corp.) and Chris Sheppard and Kent Pflibson (Kaman Aerospace Corporation) are gratefully acknowledged. Thanks are offered to all the members of the LCLS research group for their continuing support and interest in this work.

V. REFERENCES

[1] R. Tatchyn and P. Pianetta, "X-Ray Beam Lines and Beam Line Components for the SLAC Linac Coherent Light Source (LCLS) ," Proceedings of the 1993 IEEE Particle Accelerator Conference, Washington, DC, May 17-20, 1993.

[2] B. L. Henke, P. Lee, T. J. Tanaka, R. L. Shimabukuro, and B. K. Fujikawa, "The Atomic Scattering Factor, f1+if2, for 94 Elements and for the 100 to 2000eV Photon Energy Region," AIP Conference prooceedings No. 75, 340(1982).

[3] R. London, J. E. Trebes, and C. J. Jacobsen, "The Role of X-Ray Induced Damage in Micro-Imaging," in Proceedings of the Workshop on Scientific Applications of Short Wavelength Coherent Light Sources, W. Spicer, J. Arthur, H. Winick, eds., Stanford, CA, October 21, 1992, SLAC-Rep.-414, February 1993, p. 26.

[4] R. Tatchyn, "LCLS Optics: Selected Technological Issues and Scientific Opprtunities," ibid., p.93.

[5] R. Tatchyn, P. Csonka, H. Kilic, H. Watanabe, A. Fuller, M. Beck, A. Toor, J. Underwood, and R. Catura, "Focusing of undulator light at SPEAR with a lacquer-coated mirror to power densities of 10^9 Watts/cm^2," SPIE Proceedings No. 733, 368(1987).

LCLS PEAK AND AVERAGE PHOTON FLUX VS PHOTON ENERGY

(N_i = number of periods (i=1,..,4); K=6 for i=1,..,4; linac pulse frequency 120Hz)

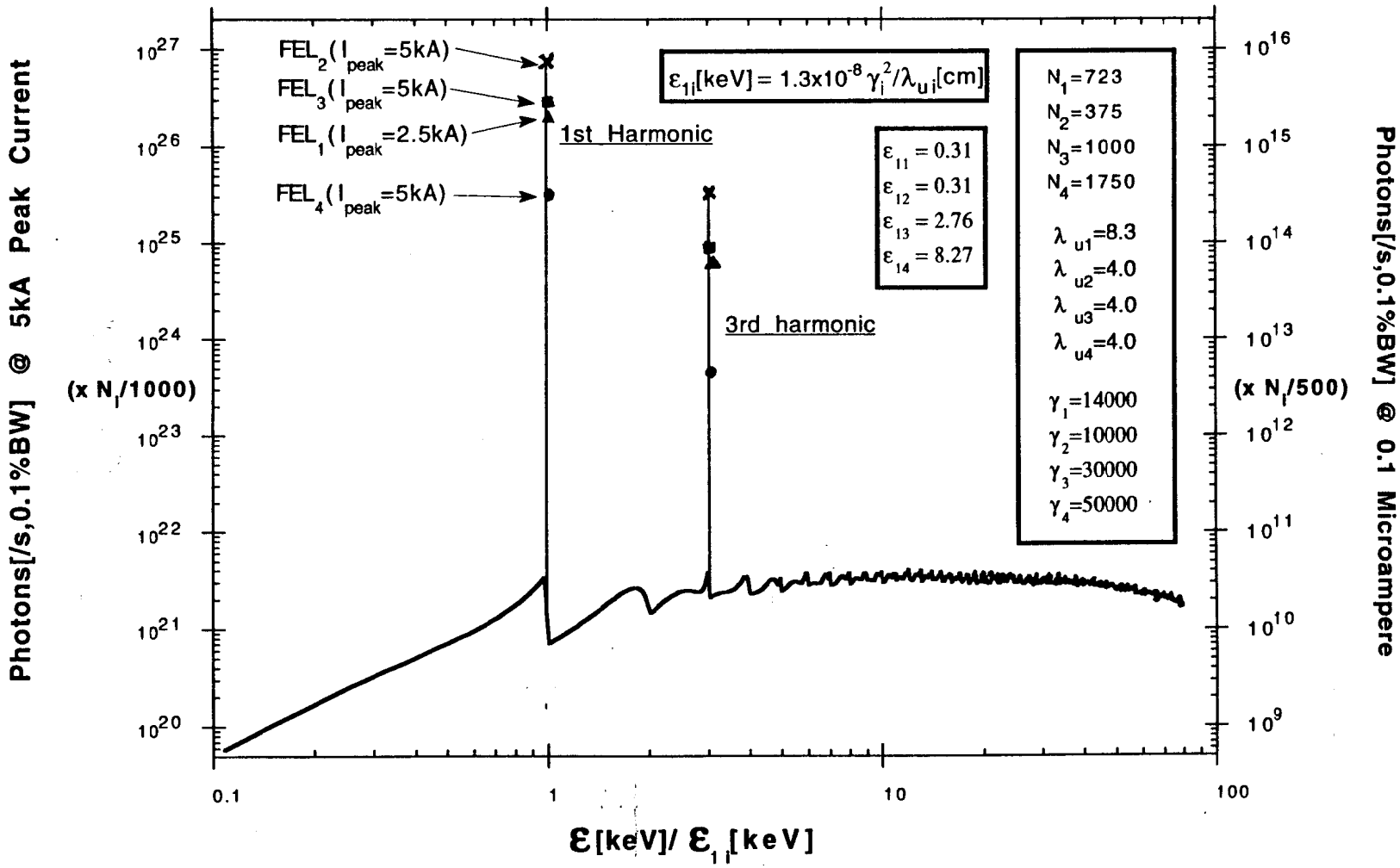

Roman Tatchyn//SSRL//2/11/94

Bremsstrahlung from LCLS Undulator

Observation Point after 60 m